TAILORING PEPTIDE NUCLEIC ACIDS TO ELECTROSTATICALLY MIMIC NATIVE NUCLEIC ACIDS AND TO EXECUTE SINGLE-NUCLEOTIDE TEMPLATED POLYMERIZATION

by

Narahenpitage Tilani Sandamala De Costa

A dissertation submitted to the faculty of
The University of Utah
in partial fulfillment of the requirements for the degree of

Doctor of Philosophy

Department of Chemistry

The University of Utah

December 2014

The University of Utah Graduate School

STATEMENT OF DISSERTATION APPROVAL

The dissertation of

Narahenpitage Tilani Sandamala De Costa

has been approved by the following supervisory committee members:

Jennifer M. Heemstra	, Chair	**08/18/14** Date Approved
Gary E. Keck	, Member	**08/18/14** Date Approved
Cynthia J. Burrows	, Member	**08/18/14** Date Approved
Peter F. Flynn	, Member	**08/18/14** Date Approved
Thomas E. Cheatham, III	, Member	**08/18/14** Date Approved

and by **Cynthia J. Burrows**, Chair of the Department of **Chemistry**

and by David B. Kieda, Dean of The Graduate School.

ABSTRACT

Peptide nucleic acid (PNA) is a nucleic acid mimic that shows tremendous potential for use in therapeutic and biosensing applications due to its high binding affinity for DNA and RNA and its excellent biostability. The therapeutic potential of PNA is hindered, however, by poor cellular uptake, solubility, and bioavailability. Although various approaches have been taken to overcome these critical limitations and realize the full potential of PNA, more efficient solutions are still desired. We hypothesize that negatively charged PNA analogues would electrostatically mimic DNA and RNA, thus overcoming the limitations mentioned above. This dissertation is mainly focused on our initial studies to investigate the tolerance of the PNA structure to the addition of negatively charged side chains.

We explored the effect of ionic strength on binding affinity for modified PNAs having either negatively charged side chains or positively charged side chains (Chapter 2). We observed that as ionic strength is increased, negatively charged PNA increases in affinity for DNA and RNA, whereas positively charged PNA decreases in affinity for DNA and RNA. The point at which these trends intersect hovers near physiological salt concentration. In a simulated physiological buffer, negatively charged PNA shows slightly higher affinity for RNA whereas positively charged PNA shows slightly higher affinity for DNA. Intrigued by the effect of side chain structure and electrostatics on binding affinity, we were also curious to explore the mismatch and orientation selectivity of these γ-substituted PNAs (Chapter 3). We observed that positively charged side chains provide higher selectivity in DNA binding, while negatively charged side chains

provide higher selectivity in RNA binding.

Our results provide insight into the impact of side chain structure and electrostatics on the binding affinity and selectivity with DNA and RNA under physiological conditions. Since PNA can be negatively charged without sacrificing binding affinity and selectivity, we anticipate that these molecules will show promise as therapeutics that take advantage of both the inherent benefits of PNA and the multitude of charge-based delivery technologies currently being developed for DNA and RNA.

PNA also shows promise for use in synthetic biology applications, but the evolution of abiotic polymers such as PNA requires methods for sequence encoding and amplification. Chapter 4 describes our efforts to synthesize a modified PNA monomer that is designed to polymerize using dynamic reaction conditions.

DNA-based micelles have the potential to be used as stimuli-responsive materials due to their ability to undergo programmable assembly and disassembly. Chapter 5 outlines our synthesis of a potential multivalent micellar scaffold.

To the most wonderful people in my life,

my parents, sister, and husband

for their unconditional love and support

TABLE OF CONTENTS

LIST OF ABBREVATIONS

A	adenine
Ac	acetyl
aeg-PNA	aminoethyl glycine PNA
ANA	arabinose nucleic acid
AuNP	gold nanoparticle
BNA	bicyclic nucleic acid
Boc	*t*-butoxycarbonyl
Bu	butyl
C	cytosine
calcd	calculated
CPP	cell penetrating peptides
CTLs	cell targeting ligands
d	doublet (spectral)
DBU	1,8-diazabicyclo[5.4.0]undec-7-ene
DCM	dichloromethane
DCMs	DNA-crosslinked micelles
dd	doublet of doublet (spectral)
DIPEA	diisopropylethylamine
DMAP	4-dimethylaminopyridine
DMF	dimethylformamide
DNA	2'-deoxyribonucleic acid
^{o}C	celsius degrees

EDC	1-ethyl-3-(3-dimethylaminopropyl)-carbodiimide
Et	ethyl
Et_2O	diethyl ether
EtOAc	ethyl acetate
FDA	food and drug administration
Fmoc	fluorenylmethyloxycarbonyl
FT-IR	fourier transform infrared
g	gram(s)
G	guanine
GNA	glycol nucleic acids
GPNA	guanidine-based PNA
h	hour(s)
HATU	1-[bis(dimethylamino)methylene]-1H-1,2,3-triazolo[4,5-b]pyridinium 3-oxid hexafluorophosphate
HOBt	1-hydroxybenzotriazole
HPLC	high performance liquid chromatography
HypNA-pPNA	*trans*-4-hydroxy-L-proline/phosphonate PNA
IBCF	isobutyl chloroformate
*i*Bu	iso-butyl
LDA	lithium diisopropylamide
LNA	locked nucleic acid
LRMS (ESI)	low resolution mass spectroscopy (electrospray ionization)
m	multiplet (spectral)
MALDI-TOF	matrix-assisted laser desorption/ionization
Me	methyl
MeOH	methanol

min	minute(s)
MO	morpholino phosphorodiamidate
MOE	2'-*O*-methoxyethyl
mol	mole(s)
MOM	methoxymethyl
mp	melting point
MS	molecular sieves
MsCl	methanesulfonyl chloride
NMM	N-methylmorpholine
NMR	nuclear magnetic resonance
OD	optical density
p	pentet (spectral)
PCR	polymerase chain reaction
pHypNA	hydroxyproline-based phosphono PNA
PNA **1Me/3Me**	peptide nucleic acid having methyl substituents one/three
PNA **1neg/3neg**	peptide nucleic acid having negative charges one/three
PNA **1pos/3pos**	peptide nucleic acid having positive charges one/three
PNA **nf**	non functionalized peptide nucleic acid
PNA	peptide nucleic acid
ppm	parts per million
pPNA	phosphonate PNA
PS	phosphorothioate
pyr	pyridine
q	quartet (spectral)
quant.	quantitative yield
R_f	retention factor (chromatography)

RNA	ribonucleic acid
RNAi	RNA interference
rt	room temperature
s	singlet (spectral)
SELEX	systematic evolution of ligands by exponential enrichment
siRNA	small interfering RNA
SNP	single-nucleotide polymorphism
t	triplet (spectral)
T	thymine
TBAF	tetra-*n*-butylammonium fluoride
TBAI	tetra-*n*-butylammonium iodide
TBTA	tris[(1-benzyl-1H-1,2,3-triazol-4-yl)methyl]amine
*t*Bu	*tert*-butyl
TFA	trifluoroacetic acid
THF	tetrahydrofuran
TIPS	triisopropylsilyl
TLC	thin layer chromatography
TMS	trimethylsilyl
TNA	threose nucleic acid
TOTU	O-[(ethoxycarbonyl)cyanomethylenamino]-N,N,N',N'-tetra methyluronium tetrafluoroborate
Ts	p-toluene sulfonyl
U	uracil
UNA	unlocked nucleic acid
UV	ultraviolet spectroscopy

ACKNOWLEDGEMENTS

I am indebted to my research advisor Prof. Jennifer M. Heemstra for her guidance, support, encouragement, and inspiration I gained from her great enthusiasm for chemistry and life. In particular, I am thankful to her for introducing me to the field of bioorganic chemistry.

I would like to express my gratitude to my committee members Prof. Gary E. Keck, Prof. Cynthia J. Burrows, Prof. Peter F. Flynn, and Prof. Thomas E. Cheatham, III for their time, support, and guidance during my graduate career. I am grateful to Prof. Gary Keck for his strong influence to become successful in my graduate career. Also, I would like to express my sincere gratitude to Prof. Peter Flynn for his encouragement, availability, and positive influence to reach my best.

I am grateful to the past and current members of the Heemstra group, Dr. Ashwani Sharma, April Anamisis, Trevor Feagin, Zach Headman, Alexandra Kent, Kirsten Meek, Evelyn Kimbrough, David Olsen, Amberlyn Peterson, Alex Rangel, Nick Spiropulos, and Zhesen Tan for their many forms of friendly assistance. Especially, I am thankful to Ashwani for sharing his PNA experience with me. Also, I am thankful to rotation students Julia Schneider and Kyle Trettin for working on my project.

I would like to acknowledge Prof. Jon D. Rainier and his group members, Jin Wang, Dr. Vinson Espejo, Dr. Yuan Zhang, Dr. John Rohanna, Dr. Vyacheslav Boyarskikh, Dr. Jie Zhou, Dr. Xin Hao, and Dr. Clement Osei Akoto for their friendly support in gaining synthetic experience. Also, I would like to thank past and present group members of Keck, Burrows, Louie, Looper, Sigman, Buck-Koehntop, Woycechowsky, Flynn, and Stang groups for their friendly support. Especially, thanks to

Tom Cummins, Sharon Kirk, Dr. Aaron Fleming, Dr. Pranjali Ghude, Dr. Puneet Kumar, Ashish Thakur, Cathy Serrano, Dr. Ryan De Luca, Tommy Terooatea, and Dr. Hsiao-Nung Chen.

I am grateful to Prof. Henry White, Prof. Michael Morse, Prof. Janis Louie, Prof. Ryan Looper, and Prof. Laya Kesner for their kindly assistance. In addition, I am indebted to the Department of Chemistry and the University of Utah for giving me the offer and providing financial assistance. I am grateful to the friendly assistance of the staff members in the Department, especially, Jo Hoovey, Debbie Olson, Tomissa Nielson, and Katie Shelton for their generous assistance. I am thankful to Dr. James Muller, Adam Hollerbach, and George Russell for friendly assistance in obtaining mass spectral data. Also, I am thankful to Dr. Atta Aarif for his kind assistance in NMR troubleshooting. I am grateful to Dr. Anita Orendt and Dr. Tim Cook for their assistance in obtaining computational data for my research proposal.

I would like to acknowledge the faculty of the Department of Chemistry of the University of Colombo for their guidance and inspiration to pursue my PhD, especially, Prof. Dayal De Costa, Prof. Rohan Perera, Prof. Dilip De Silva, Prof. Sujatha Hewage, and Prof. Thusitha Abeytunga.

I am grateful to all my dear friends, in particular, Needra and family, Dr. Mahika, Manik and Anura, Rukshan, Lalindra and Wathsala, Sharmaine and Kalyan, Dennisia and family, Triston, Melanie and Scott, and Dr. Anoka for their friendship and assistance while in Utah. I am indebted to my family members, my in-laws, and relatives for their numerous support and encouragement. Especially, I would like to express my heartfelt thanks to my parents Pushpa and Tilak De Costa, and my sister Dilani for their unconditional love, endless support, and well wishes. Last but not least, I'm extremely grateful to my loving husband and best friend, Aravinda Wijesinghe, for always being there for me.

CHAPTER 1

PEPTIDE NUCLEIC ACID: A VERSATILE NUCLEIC ACID ANALOGUE

"Molecular recognition between nucleic acids via nucleobase complementarity is probably the most elegant molecular recognition system in nature. It is beautifully simple, yet very powerful."

- Peter E. Nielsen[1]

Nucleic acids, together with this powerful molecular recognition system, provide high fidelity information transfer via the processes of replication, transcription, and translation, and this system is the key to our existence. Naturally occurring nucleic acids, 2'-deoxyribonucleic acid (DNA) and ribonucleic acid (RNA), are polymers of nucleotides, and contain a phosphate group, a sugar moiety, and a nucleobase. The molecular recognition between nucleic acids predominantly occurs via "Watson-Crick base-pairs" (Figure 1.1, 1.2), which consist of noncovalent hydrogen bonds between two complementary purine-pyrimidine base-pairs (adenine–thymine/uracil and guanine–cytosine).[2] In addition, non-Watson-Crick base pairing modes such as Hoogsteen[3] and wobble[4] are also possible (Figure 1.3). In Hoogsteen mode, thymine pairs with an adenine, which is already involved in Watson-Crick A:T base pair, and protonated cytosine pairs with guanine of a Watson-Crick C:G base pair, and thus enable formation of triplexes. In wobble base pairing, purine bases recognize noncomplementary pyrimidine bases.

The potential of nucleic acids is not just limited to bioevolution, but they also play a diverse role in numerous disciplines, including therapeutics, diagnostics, research, and

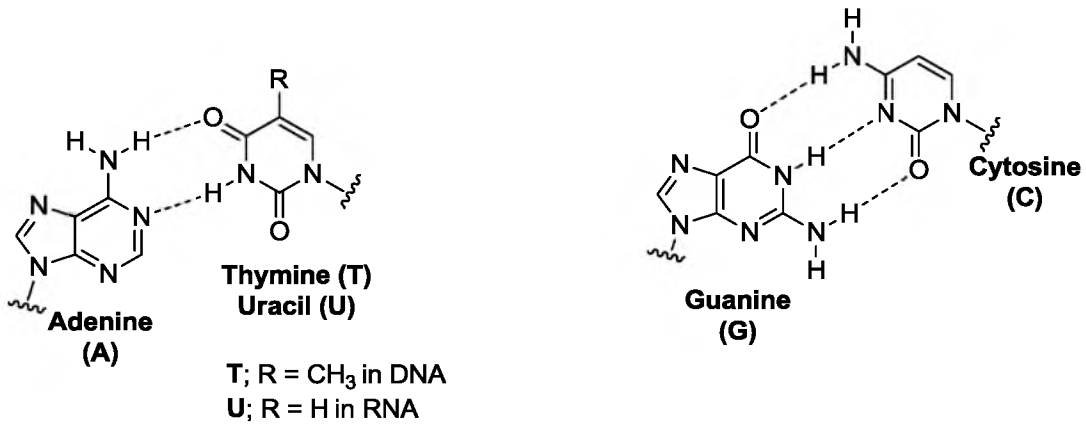

Figure 1.1. Watson-Crick complementary nucleobase pairs.

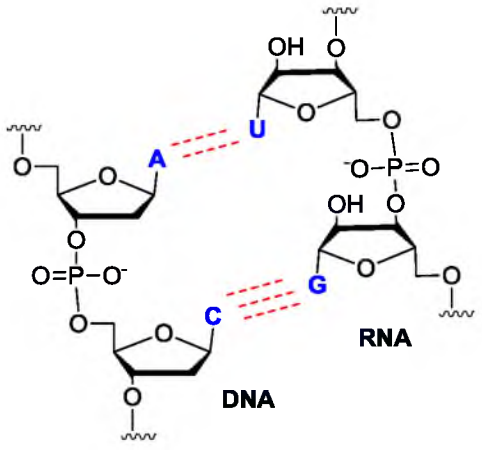

Figure 1.2. Schematic representation of DNA:RNA duplex.

nanotechnology. In particular, nucleic acids have shown great promise for the treatment of various conditions, including cancer, diabetes, cystic fibrosis, and other genetic disorders.[5] One therapeutic approach to treat these diseases is known as the 'antisense strategy', in which gene expression is silenced by binding complementary oligonucleotides (AON) to the disease-causing mRNA sequence. This prevents the translation of proteins either by sterically blocking translation or recruiting RNase H enzyme to degrade the RNA strand in the mRNA-AON duplex (Figure 1.4).[6] In the 'antigene strategy', transcription or replication processes are interrupted by binding of the AON to DNA.[7]

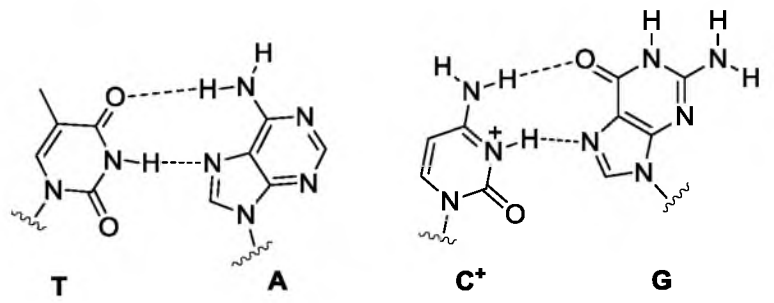

a) Hoogsteen base pairs

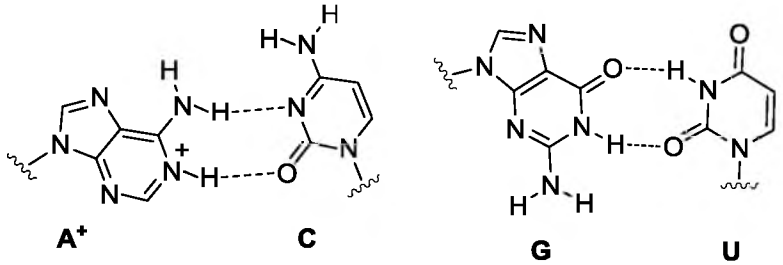

b) Wobble base pairs

Figure 1.3. Non-Watson-Crick base pairing modes a) Hoogsteen base pairing for A:T and G:C base pairs and (b) representative wobble base pairs.

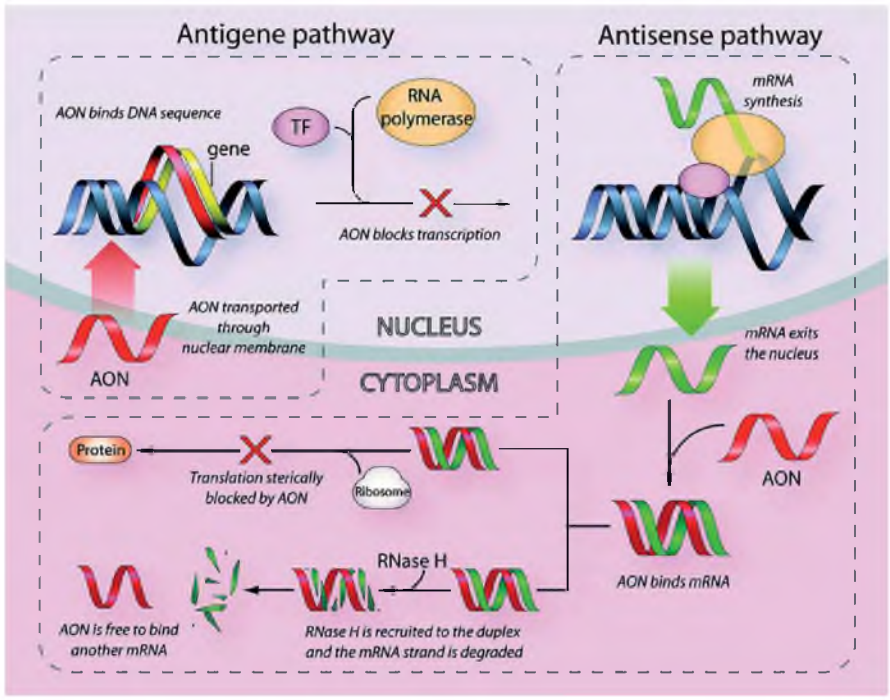

Figure 1.4. Antisense and antigene pathways [reprinted with permission from (Jain, M. L.; Bruice, P. Y.; Szabó, I. E.; Bruice, T. C. *Chem. Rev.* **2011**, *112*, 1284-1309).[8] Copyright (2012) American Chemical Society].

Nucleic Acid Analogues

The use of native nucleic acids for therapeutic applications comes with specific obstacles, including degradation by endogenous enzymes, poor pharmacokinetics, and low intrinsic binding affinity.[9] However, modified nucleic acid analogues have the potential to overcome these challenges. Nucleic acids can be modified at the backbone, sugar, or nucleobase; and these nucleic acid analogues have gained widespread use in therapeutic and diagnostic applications (Figure 1.5).[10]

Synthetic oligonucleotides having modified backbones have been extensively studied in antisense and numerous other biological applications (Figure 1.6). Phosphorothioate (PS) oligonucleotides are one example of 'first generation' antisense oligonucleotides; these are synthesized by replacing one of the nonbridging phosphate oxygen atoms with a sulfur atom, thus improving enzymatic stability and pharmacokinetics. The first PS-based antisense drug, Vitravene™ (ISIS-2922), was approved by the FDA in 1998 to treat cytomegalovirus retinitis in immunocompromised patients.[11] Although PS has remained the most successful and widely used oligonucleotide analogue until now, it does have disadvantages, such as lowered duplex stability, existence of diastereomeric mixtures, and toxicity induced by nonspecific protein binding.[12] Similarly, phosphoramidates are synthesized by replacing the 3'-hydroxyl of the backbone with an amine.[13] Phosphoramidates show increased duplex stability and nuclease resistance but they do not induce RNase H-dependent degradation of the complementary RNA strand in a duplex.[9] Phosphoramidates have been further modified by replacing one of the nonbridging phosphate oxygen atoms with a sulfur atom, providing acid-stable thiophosphoramidates, which have exhibited anticancer activity.[14,15]

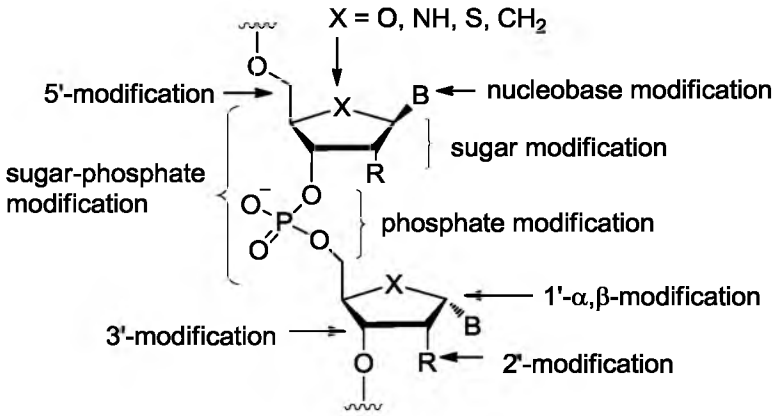

Figure 1.5. Potential sites of modification of nucleic acids [adapted from (Sharma, V. K.; Rungta, P.; Prasad, A. K. *RSC Adv.* **2014**, *4*, 16618-16631) with permission of The Royal Society of Chemistry].

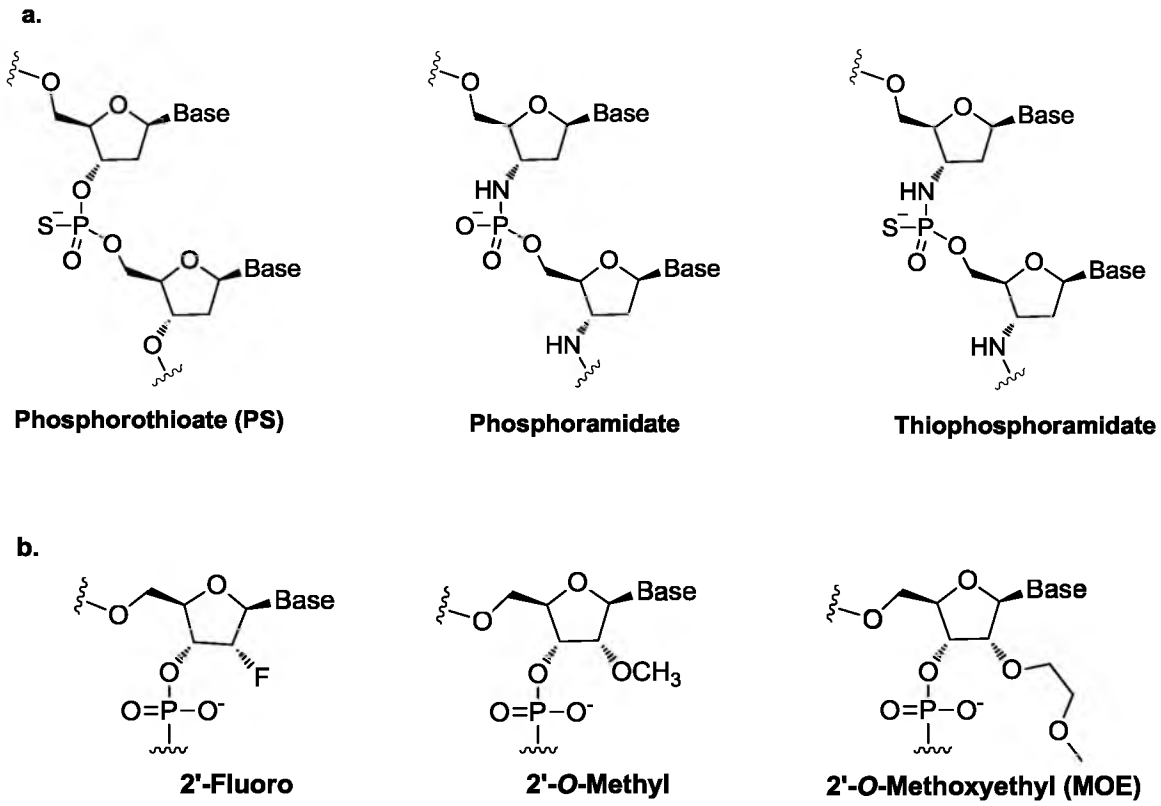

Figure 1.6. Chemical structures of a selection of nucleic acid analogues having modifications in the (a) phosphate backbone or (b) 2′-position of ribose sugar moiety.

Modification of the 2′-position of the ribose sugar moiety to give analogues such as 2′-fluoro and 2′-*O*-alkyl nucleotides has also gained success in therapeutic applications (Figure 1.6). Among these 'second generation' antisense oligonucleotides, 2′-*O*-methoxyethyl (MOE) was the most successful candidate in terms of affinity, stability, and entering into clinical trials.[9] In 2013, the FDA approved the second antisense drug, Mipomersen (Kynamro), to treat homozygous familial hypercholesterolemia in patients with high levels of low-density lipoprotein cholesterol.[16] This drug also contains a PS oligonucleotide sequence, where each end of the sequence contains five nucleotides with 2′-MOE modifications.

In addition to 2′-substitution of ribose, the ribose sugar moiety itself can be replaced by various nonnatural sugar or cyclic structures to obtain nucleic acid analogues (Figure 1.7). Among these 'third generation' antisense oligonucleotides are arabinose nucleic acid (ANA) consisting of an inverted 2′-configuration compared to native RNA,[17] hexitol nucleic acid (HNA) containing a pyranose moiety, and cyclohexene nucleic acid (CeNA) containing a cyclohexene ring instead of the furanose sugar moiety of native nucleic acids.[12,18] ANA exhibits higher affinity to RNA than DNA, but overall lower affinity relative to PS oligonucleotides.[12] Similarly, HNA shows increased nuclease resistance and higher affinity to RNA than DNA. Both ANA and CeNA can induce RNase H-dependent degradation of the complementary RNA strand in antisense therapy.

In an attempt to reduce the entropic cost of duplex formation, and thus increase binding affinity, structurally constrained, bicyclic nucleic acid analogues, such as locked nucleic acid (LNA) were developed (Figure 1.7).[19,20] LNA and LNA analogues have shown great promise in numerous biomedical and nanotechnology applications, including antisense therapy, due to their higher binding affinity, selectivity, and stability.[21] In contrast to locking the backbone, the C2′-C3′ bond of ribose can be cleaved to give a

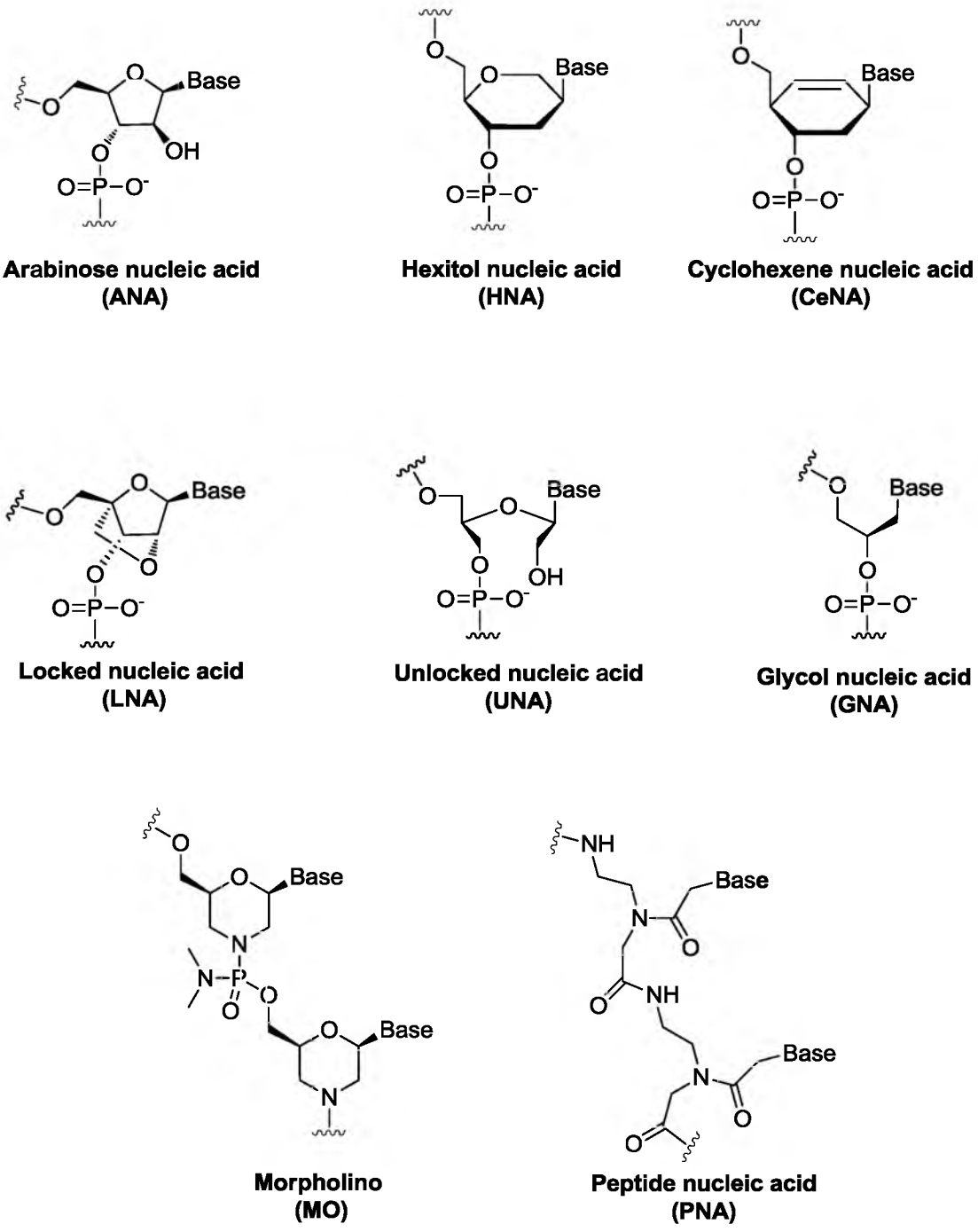

Figure 1.7. Chemical structures of a selection of nucleic acid analogues (continued).

flexible nucleic acid analogue, unlocked nucleic acid (UNA). Although UNA reduces duplex stability, conjugates of UNA with other antisense oligonucleotides have been investigated to achieve flexibility in binding and enhance stability.[22] Another simply-structured nucleic acid analogue, glycol nucleic acid (GNA), has shown promise for biotechnology applications due to its higher duplex stability with DNA and RNA, in contrast to UNA (Figure 1.7).[23]

All of the aforementioned nucleic acid analogues retain either the phosphate group or ribose sugar moiety. In contrast, replacement of the sugar-phosphate backbone with an isostere gives rise to morpholino phosphorodiamidate (MO) and peptide nucleic acid (PNA), which are both neutrally charged due to the lack of a phosphate group (Figure 1.7).[9] Both PNA and MO are promising antisense agents and are stable to nucleases, but PNA shows much higher affinity to DNA and RNA than MO.[24,25]

Peptide Nucleic Acid (PNA)

PNA was first reported by Peter E. Nielsen, Michael Egholm, Rolf H. Berg, and Ole Buchardt in 1991,[26] and was originally designed as a triplex-forming oligonucleotide mimic to bind double-stranded DNA in the major groove via Hoogsteen base pairing.[26,27] However, it was later realized that PNA can also bind to single-stranded nucleic acids.[28] The unique physicochemical properties of PNA can largely be attributed to its achiral, neutral, peptide-like *N*-(2-aminoethyl)glycine backbone in place of the sugar-phosphate backbone found in DNA and RNA (Figure 1.8). The nucleobases are linked to secondary amines in the PNA backbone via methylene carbonyl linkages.[26] PNA is neither a protein nor a nucleic acid and has thus become a promising biomolecular tool with an enhanced lifetime for *in vivo* and *in vitro* applications, such as molecular diagnostics and antisense therapeutics, as it can withstand both nucleases and proteases.[24,29-31]

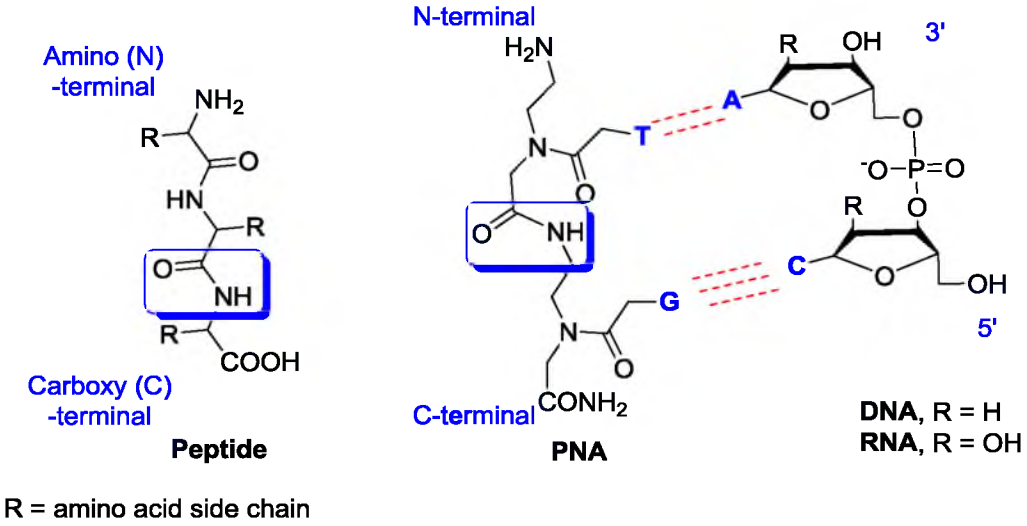

Figure 1.8. Chemical structures of peptides and base pairing between PNA and DNA/RNA. The characteristic amide (peptide) bond of both PNA and peptide is highlighted. PNA is depicted as a peptide having N-terminus and C-terminus. Alignment of the N-terminus of PNA with the 3'-end of DNA/RNA is known as the antiparallel orientation. [Adapted with permission from (Nielsen, P. E. *Acc. Chem. Res.* **1999**, *32*, 624-630). Copyright (1999) American Chemical Society.]

In addition to high affinity, PNA shows high selectivity in binding to DNA and RNA. PNA is more vulnerable to base mismatches than are native nucleic acids, due to the constrained flexibility of the PNA backbone and the inherent asymmetry in PNA:DNA/RNA duplexes.[32] PNA can bind to complementary nucleic acids in both parallel and antiparallel orientations because of its achiral backbone, but generally prefers the antiparallel orientation in binding with nucleic acids (Figure 1.8). The potential of PNA to hybridize with complementary DNA/RNA with high affinity and selectivity following Watson-Crick rules,[28] and also the ability to invade double stranded-DNA,[33,34] has even led to the speculation that PNA may have been a prebiotic material.[35] This interest in finding the relationship of PNA to the origin of life has inspired the recent discovery of PNA-like materials in cyanobacteria.[36]

Structures of PNA in complex with PNA and nucleic acids

Structural information has been obtained for duplexes of PNA:DNA[37] and PNA:RNA[38] using NMR, while structures of PNA_2:DNA triplex[39] and PNA:PNA[40] duplexes were solved by using X-ray crystallography (Figure 1.9). According to these data, PNA:RNA duplexes adopt the A-form structure preferred by RNA,[38] whereas PNA:DNA duplexes adopt an intermediate structure between A- and B-form, in which the base stacking is more A-like.[37,41,42] PNA:PNA duplexes[40] and $(PNA)_2$-DNA triplexes[39] adopt a P-form structure preferred by PNA, which is different from both A- and B-form but more like A-form. Consequently, PNA:RNA duplexes generally show a higher thermal stability relative to analogous PNA:DNA duplexes. These data provide evidence that the backbone geometry and constrained flexible structure of PNA could be the major factors that facilitate stronger affinity with nucleic acids, as PNAs can easily adopt the desired geometries of DNA or RNA by enthalpy-entropy compensation.[1]

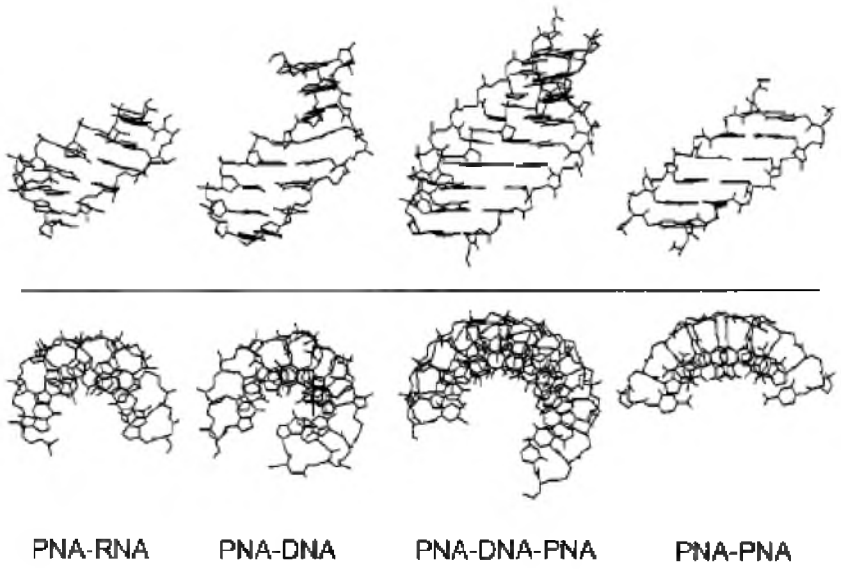

Figure 1.9. Structures of PNA complexes: side view (top) and upper view (bottom). [Reprinted with permission from (Nielsen, P. E. *Acc. Chem. Res.* **1999**, *32*, 624-630; Copyright (1999) American Chemical Society) and (Eriksson, M.; Nielsen, P. E. *Q. Rev. Biophys.* **1996**, *29*, 369-394; Copyright (1996) Cambridge University Press)].

PNA backbone modifications

The ease of altering the PNA backbone has encouraged synthetic organic chemists to develop various PNA analogues to enhance properties such as binding affinity with nucleic acids and cellular delivery (Figure 1.10).[30] Consequently, PNA has been modified by the introduction of conformationally constrained cyclic backbones, different substituents, or modified nucleobases.[1] For example, when the amide group in the backbone is replaced with an amine to remove the rigidity imposed by the amide, this results in reduced binding affinity. This illustrates the significance of the "constrained flexibility" of the PNA backbone. To enhance the rigidity, a cyclic group such as cyclohexyl has been incorporated in the ethylene diamine portion of the PNA backbone, but results in a decrease in binding affinity.[43] However, the introduction of cyclopentyl[44] and proline[45] groups into the backbone has improved binding affinity. Moreover, in an effort to enhance the solubility and cellular delivery of PNA, charged PNA has been developed by incorporating functional groups such as phosphates in PNA backbone.[30]

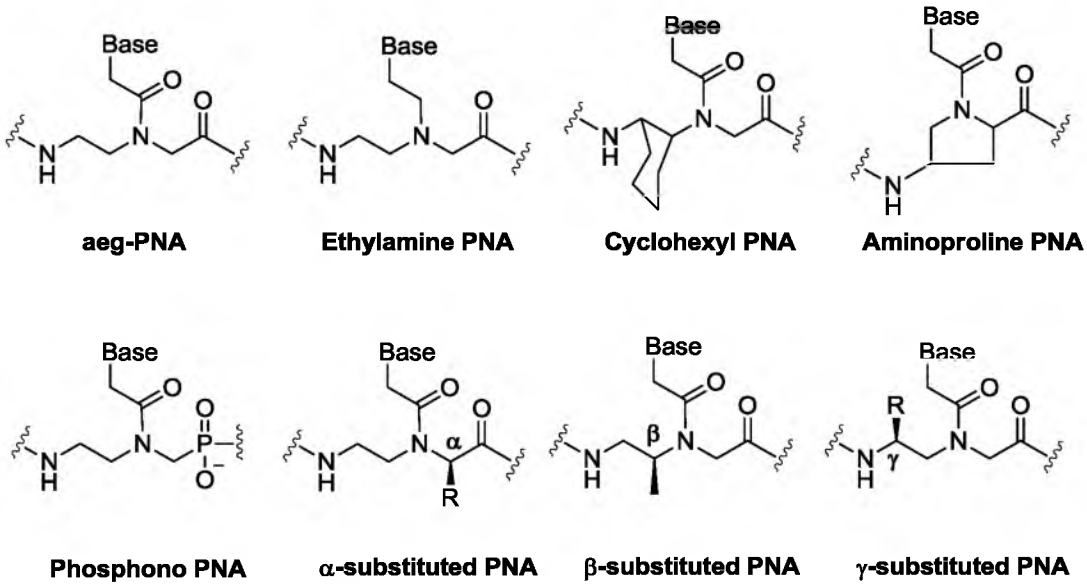

Figure 1.10. Chemical structures of a selection of modified PNAs.

Among PNA modifications, the use of various amino acids for the synthesis of PNA provides a facile way to incorporate diverse substituents with different chirality at the α, β, or γ-positions of PNA. Installation of L-amino acids at the α-position and D-amino acids at the γ-position is detrimental to PNA binding, but L-amino acids at the γ-position and D-amino acids at the α-position enhance binding affinity. Further, substitution at the γ-position is known to be advantageous over substitution at the α-position, with regard to binding affinity, unambiguous antiparallel binding, and helical induction.[41,46-51] β-substituents have only been investigated recently, but exhibited reduced affinity.[52] Specifically, a (*S*)-stereocenter at the γ-position (from L-amino acids) conformationally preorganizes the PNA backbone into a right-handed helix, which is favorable for binding to DNA and RNA.[51] This stereoinduction is unidirectional from the C- to N-terminus, resulting in an antiparallel sequence alignment, and projects the γ-substituents away from the backbone. This ease of modifying the PNA backbone with amino acids allows incorporation of different functional groups to enhance properties such as stronger binding, intercalation, enhanced solubility, and cellular delivery.[47,53]

PNA nucleobase modifications

In addition to backbone modifications, PNA has also been synthesized using "non-Watson-Crick" nucleobases to achieve higher duplex/triplex stabilities (Figure 1.11).[30] For instance, replacement of adenine by diaminopurine increases the melting temperature (T_m) of PNA with nucleic acids by ~4 ^{o}C per substitution. In addition, PNA modified with diaminopurine and thiouracil can invade double-stranded DNA in antigene applications. Similarly, cytosine has been replaced with pseudoisocytosine, which can bind with guanine irrespective of the surrounding pH via Hoogsteen base pairing in triplex-forming PNAs. Additionally, incorporation of a tricyclic G-clamp modified nucleo-

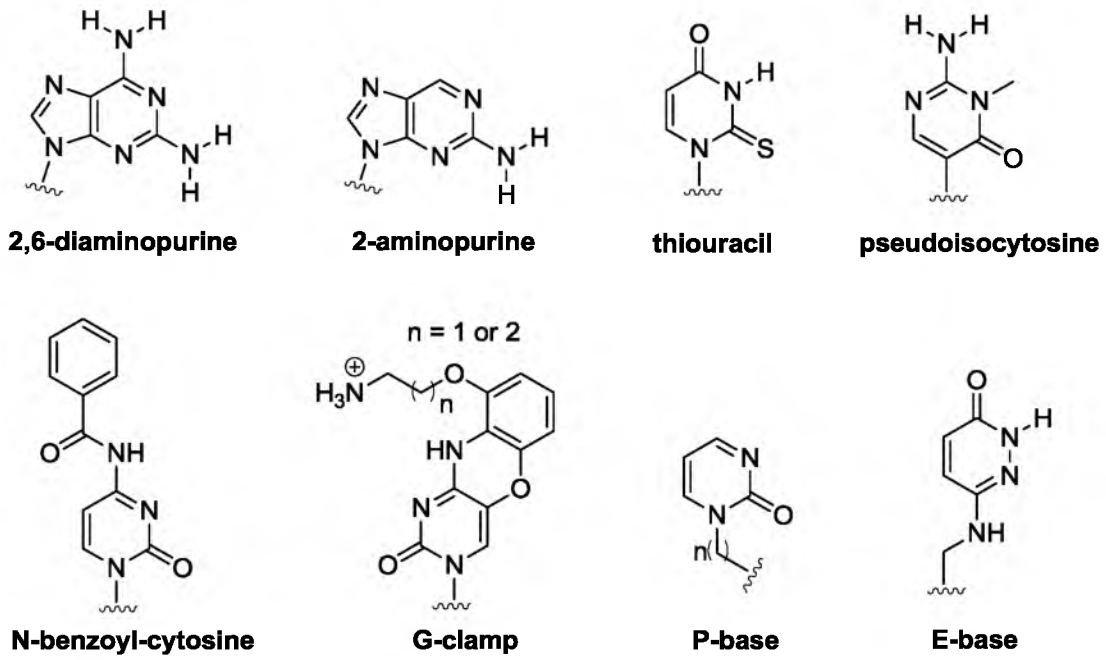

Figure 1.11. Chemical structures of a selection of modified nucleobases.

base has increased duplex stability via both base pairing and base stacking, while enhancing the solubility due to positively charged side chains.[54] Recently, Rozners and coworkers have reported that PNA monomers modified with P and E nucleobases were able to isolate pyrimidine interruptions in polypurine tracts of double helical RNA.[55,56]

Applications of PNA

PNA has been utilized in a diverse range of applications, including therapeutics, diagnostics, molecular biology, and nanotechnology, due to its unique physicochemical properties. For example, PNA is effective in antisense and antigene applications, where stronger binding of PNA to mRNA and DNA inhibits the processes of translation, transcription, and replication.[57] Since RNase H does not recognize the PNA:RNA duplex as a substrate, antisense activity occurs via sterically blocking mRNA translation rather than degradation of RNA strand.[24] Similarly, PNA displays antigene properties by

binding to single-stranded DNA (during replication)[58] and double-stranded DNA (Figure 1.12).[1]

The antisense and antigene potential of PNA has been explored to develop anticancer and antimicrobial PNAs. For example, PNA has shown anticancer effects by suppressing telomerase activity,[59] c-*myc* oncogene,[60] and T antigen[61] expression. PNA has exhibited antimicrobial properties by silencing gene expression in bacteria, viruses, and amoebae.[62] For instance, PNA has inhibited bacterial translation *in vitro* with an efficiency comparable to tetracycline.[24,63] However, the *in vivo* performance was severely hindered by poor cellular uptake of PNA.[24]

The detection of single nucleotide polymorphisms (SNPs) facilitates the diagnosis of genetic diseases, as these slight changes in DNA sequences lead to drastic changes in gene expression or protein function. The highly sequence-specific binding of PNA has been utilized to develop biosensors for SNP detection. For instance, immobilization of PNA into a synthetic ion channel has facilitated the discrimination between complementary DNA and mismatched sequences.[64] Moreover, efficient and sensitive PNA fluorescence *in situ* hybridization (FISH) techniques have been developed for quantitative telomere analyses, chromosome painting, and genotyping of viruses and bacteria (Figure 1.13).[24]

Cellular delivery of PNA

Oligonucleotides are not cell permeable by simple diffusion due to the hydrophobic nature of the membrane lipid bilayer. For instance, negatively charged siRNAs or antisense moieties, as well as charge neutral methylphosphonates, PNAs,[65] or MOs are not cell permeable. Despite the uncharged nature of PNA, its large size (>2000 Da) prevents eukaryotic and prokaryotic cell permeability.[24,25] However, in some cell lines, antisense effects have been observed when PNA was used in fairly high

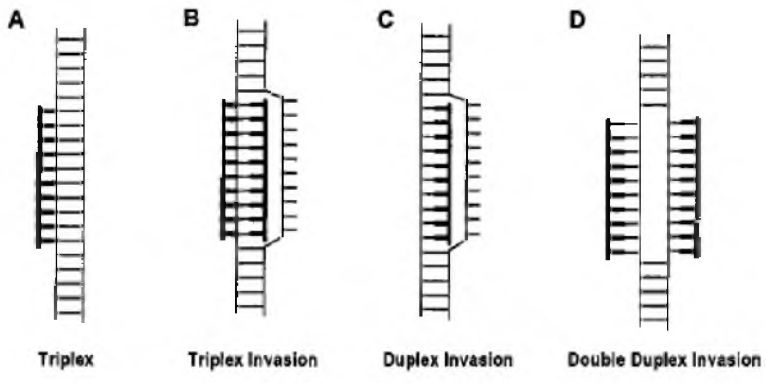

Figure 1.12. PNA binding modes to target double stranded DNA (A) triplex, (B) triplex invasion, (C) duplex invasion, and (D) double duplex invasion (thick structures indicate PNA). [Reprinted with permission from (Nielsen, P. E. *Acc. Chem. Res.* **1999**, *32*, 624-630). Copyright (1999) American Chemical Society].

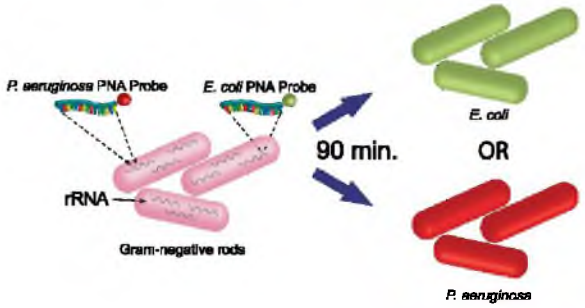

Figure 1.13. PNA-fluorescence *in situ* hybridization (FISH) technique (reproduced with permission from reference 66).

concentrations (10-100 μM).[30] Several methods have been introduced to overcome this critical delivery issue of PNA, ranging from physical or electrical disruption of the cell membrane to chemical complexation, conjugation, or modification of PNA.[24] Temporary disruption of cell membranes by electroporation, pore-forming agents, and physical scrape loading have been successful in some systems; for instance, a 20mer PNA microinjected into cells has reduced T antigen expression.[61] However, due to the stress applied by these methods, they are mainly limited to cultured cells.[24]

Great efforts have been taken to modify PNA to enable effective cellular

penetration. As an example, conjugating fatty acid chains or adamantyl moieties increases the lipophilicity of PNA, enabling its cellular uptake.[24] Additionally, conjugation of PNA to cell penetrating peptides (CPPs), including Tat and penetratin, is a popular method of PNA cellular delivery.[56] PNA is rapidly excreted by the kidneys, thus limiting its bioavailability, but chemical conjugation to cationic peptides may increase its circulation time.[30] However, the bioavailability of PNA delivered via CPP is controlled by endosomal release. As a consequence, endosomal disruption methods, such as photochemical internalization, Ca^{2+} treatment, or chloroquine treatment, have been reported to enhance the efficacy of PNA delivered via CPP.[67] Unfortunately, CPPs are relatively large peptides, making synthesis complicated and also leading to nonspecific toxic effects.[56]

Interest was instead drawn towards using short sequences of cationic peptides such as oligolysine and oligoarginine. For example, PNA covalently linked to a peptide (PKKKRKV) has down-regulated c-*myc* oncogene expression.[60] Covalently linking PNA to cationic shell-cross-linked knedel-like nanoparticles, lipophilic triphenylphosphonium cations, and polyethylenimine have also enhanced cellular delivery.[56]

The use of amino acids to introduce positively charged side chains at the α- or γ-position of PNA is more promising than conjugation to cationic peptides or CPP in terms of low cytotoxicity and convenience in synthesis. Accordingly, Ly and colleagues introduced GPNA (guanidine-based PNA),[68] inspired by the remarkable cellular uptake properties and activity of the human HIV-1 Tat transduction domain (YGRKKRRQRRR)[69] and the homoarginine peptoid[70] (Figure 1.14). Similarly, Ganesh and coworkers reported cationic PNA having aminomethylene side chains.[50,71] Of the cationic modifications investigated by the Ly and Ganesh research groups, γ-GPNA[48] and γ-aminomethylene PNA[50,71] have demonstrated the most promising results in terms of binding, cellular uptake, and antisense activity. PNAs having positively charged side chains, however,

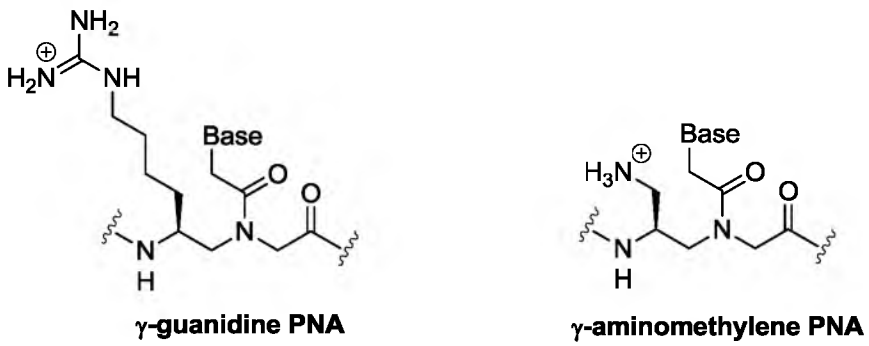

Figure 1.14. Chemical structures of γ-PNA having cationic side chains.

can lead to nonspecific binding due to electrostatic interactions with negatively charged nucleic acids.[72]

Negatively charged PNA: an attempt to enhance cellular delivery

The development of methods to enhance the circulation lifetime and cell permeability of nucleic acids *in vivo* is an ongoing area of research. In particular, the success and widespread application of RNA interference (RNAi) and numerous gene manipulation applications rely on the discovery of clinically suitable, safe, and effective delivery methods.[73,74] Anionic oligonucleotides are efficiently delivered into cells by cell-targeting ligands and nanocarriers, including cationic polymer complexes and polymeric nanoparticles.[74] However, nearly all of these technologies function on the basis of the negatively charged backbone found in native nucleic acids.

Although the inherent neutral charge of PNA limits the use of these methods, complexation with partially complementary oligonucleotide has facilitated the delivery of PNA into cells via cationic liposomes.[24] But some optimization of the carrier oligonucleotide is required to ensure that PNA is released once inside cells. Furthermore, PNA-DNA chimeras were introduced to take advantage of the aforementioned delivery methods and to increase solubility (Figure 1.15).[75] Although

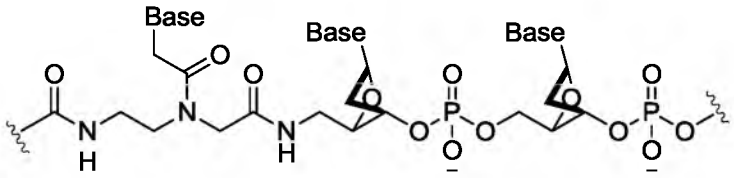

PNA/DNA chimeras

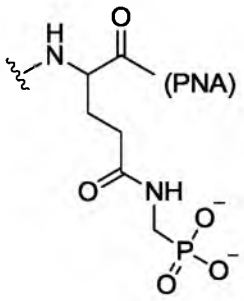

glutamine phosphonate

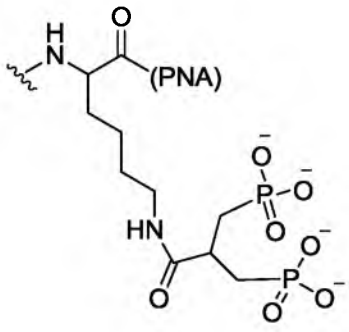

lysine bis-phosphonate

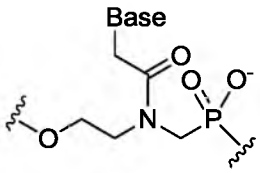

phosphonoPNA (pPNA)

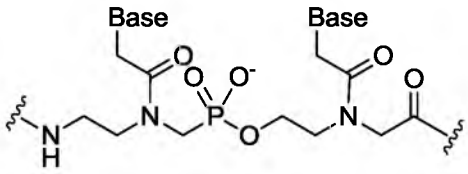

pPNA-PNA hybrid

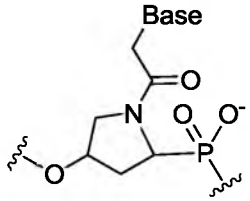

hydroxyproline-based phosphono PNA (pHypNA)

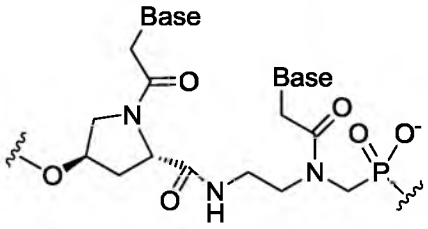

pHypNA-PNA hybrid

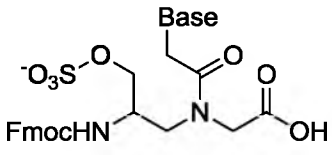

γ-suifate PNA monomer

Figure 1.15. Negatively charged PNA analogues.

PNA-DNA chimeras have been taken up by cells and demonstrated antisense properties, synthesis of these chimeras is challenging due to the requirement for orthogonal protecting groups to ensure stability of DNA.[76]

The abovementioned limitations can be overcome when PNAs having negatively charged groups are synthesized. Nielsen and coworkers investigated phosphonate-peptide nucleic acid conjugates containing twelve phosphonate moieties per PNA oligomer, which were derived from phosphonate modified glutamine or lysine (Figure 1.15). These negatively charged PNAs have been delivered to HeLa cells by cationic lipids and exhibited dose-dependent antisense activity in the nanomolar range.[77]

Taking a different approach to charge incorporation, the research groups of Peyman and Efimov independently synthesized and studied phosphono PNA (pPNA/PHONA), having a negatively charged phosphate group inserted into the PNA backbone (Figure 1.15).[78-80] Efimov and colleagues have also investigated conformationally constrained chiral phosphono-PNA analogues based on 4-hydroxyproline (pHypNAs). Although negatively charged, these analogues have been delivered into cells mostly via microinjection;[81-83] and selective regulation of developmentally important genes was achieved using caged PNA,[81] HypNA-pPNA,[82] and phosphonic ester PNA[83] in fish embryos. However, these modifications often affected the binding affinity of PNA with DNA and RNA. Moreover, synthesis of these negatively charged PNA analogues is more challenging than the incorporation of negatively charged side chains into PNA using amino acids.

Accordingly, incorporation of negatively charged side chains from amino acids (D-Glu, L-Asp) at the α-position of PNA has been investigated, but resulted in reduced binding affinity with DNA.[68,84,85] As the introduction of side chains at the γ-position of PNA enhances its binding properties, we hypothesized that negatively charged γ-side chains would overcome the aforementioned limitations, thus facilitating the use of delivery

vehicles currently being developed for DNA and RNA. This hypothesis is further supported by recent work providing the evidence that negatively charged side chains (L-Glu, sulfate) are tolerated at the γ-position (Figure 1.15).[46,86]

Objectives of this Dissertation

Ever since the DNA double helix structure was elucidated by Watson and Crick in 1953,[2] tremendous strides have been made toward understanding the structure and function of nucleic acids, as well as the use of nucleic acid analogues in biomedical applications. These efforts led to the invention of PNA, a nucleic acid mimic with remarkable binding properties and potential to be used in numerous therapeutic, diagnostic, and nanotechnology applications. The therapeutic potential of PNA, however, is hindered by its poor solubility, cellular uptake, and bioavailability, predominantly due to its uncharged backbone. Although various approaches have been taken to overcome these critical limitations and realize the full potential of PNA, more efficient and attractive solutions are still desired.

We hypothesized that negatively charged PNA analogues would electrostatically mimic DNA and RNA and thus be compatible with conventional nucleic acid delivery technologies. This dissertation will primarily focus on our studies to investigate the effects of negatively charged side chains on PNA. We investigated the duplex stability of charge-modified PNA with DNA and RNA (in Chapter 2), and the sequence recognition ability and duplex structures of modified PNA (in Chapter 3). Our results provide insight into the binding affinity and selectivity of modified PNA in antisense and antigene applications.

PNA also shows promise for use in synthetic biology applications, but the evolution of abiotic polymers such as PNA requires methods for sequence encoding and amplification. Nonenzymatic, templated polymerization allows the generation of

sequence-defined, genetically-encoded synthetic polymers with desired functional properties. Although significant work has been done related to DNA-templated PNA polymerization, a system that can execute polymerization from single-monomer building blocks with high fidelity is still needed. Chapter 4 of this dissertation will emphasize the Heemstra group's efforts toward developing a modified PNA monomer that could overcome the aforementioned limitation by taking advantage of dynamic covalent chemistry.

The Heemstra group is also involved in investigating DNA-based micelles, as they have the potential to be used as stimuli-responsive materials due to their ability to undergo programmable assembly and disassembly. Chapter 5 of this dissertation will highlight the design and synthesis of a potential micellar scaffold, which can undergo azide-alkyne cycloaddition with nucleic acids and polymers to generate multivalent amphiphilic monomers.

References

(1) Nielsen, P. E. Peptide Nucleic Acid. A Molecule with Two Identities. *Acc. Chem. Res.* **1999**, *32*, 624-630.

(2) Watson, J. D.; Crick, F. H. C. Molecular Structure of Nucleic Acids: A Structure for Deoxyribose Nucleic Acid. *Nature* **1953**, *171*, 737-738.

(3) Hoogsteen, K. The Crystal and Molecular Structure of a Hydrogen-Bonded Complex Between 1-Methylthymine and 9-Methyladenine. *Acta Cryst.* **1963**, *16*, 907-916.

(4) Crick, F. H. C. Codon—Anticodon Pairing: The Wobble Hypothesis. *J. Mol. Biol.* **1966**, *19*, 548-555.

(5) Pushpendra, S.; Pareek, A.; Bhandari, A.: Nucleic Acids as Therapeutics. In *From Nucleic Acids Sequences to Molecular Medicine, RNA Technologies*; Erdmann, V. A., Barciszewski, J., Eds.; Springer: Verlag Berlin Heidelberg 2012; 19-45.

(6) Stephenson, M. L.; Zamecnik, P. C. Inhibition of Rous sarcoma Viral RNA Translation by a Specific Oligodeoxyribonucleotide. *Proc. Natl. Acad. Sci.* **1978**, *75*, 285-288.

(7) Hélène, C. The Anti-gene Strategy: Control of Gene Expression by Triplex-Forming-Oligonucleotides. *Anti-cancer Drug Design* **1991**, *6*, 569-584.

(8) Jain, M. L.; Bruice, P. Y.; Szabó, I. E.; Bruice, T. C. Incorporation of Positively Charged Linkages into DNA and RNA Backbones: A Novel Strategy for Antigene and Antisense Agents. *Chem. Rev.* **2011**, *112*, 1284-1309.

(9) Bennett, C. F.; Swayze, E. E. RNA Targeting Therapeutics: Molecular Mechanisms of Antisense Oligonucleotides as a Therapeutic Platform. *Annu. Rev. Pharmacol. Toxicol.* **2010**, *50*, 259-293.

(10) Sharma, V. K.; Rungta, P.; Prasad, A. K. Nucleic Acid Therapeutics: Basic Concepts and Recent Developments. *RSC Adv.* **2014**, *4*, 16618-16631.

(11) Mulamba, G. B.; Hu, A.; Azad, R. F.; Anderson, K. P.; Coen, D. M. Human Cytomegalovirus Mutant with Sequence-Dependent Resistance to the Phosphorothioate Oligonucleotide Fomivirsen (ISIS 2922). *Antimicrob. Agents Chemother.* **1998**, *42*, 971-973.

(12) Kvaerno, L.; Wengel, J. Antisense Molecules and Furanose Conformations-is it Really that Simple? *Chem. Commun.* **2001**, 1419-1424.

(13) Froehler, B.; Ng, P.; Matteucci, M. Phosphoramidate Analogues of DNA: Synthesis and Thermal Stability of Heteroduplexes. *Nucleic Acids Res.* **1988**, *16*, 4831-4839.

(14) Pongracz, K.; Gryaznov, S. Oligonucleotide N3′→P5′ Thiophosphoramidates: Synthesis and Properties. *Tetrahedron Lett.* **1999**, *40*, 7661-7664.

(15) Gryaznov, S. M. Oligonucleotide N3′→P5′ Phosphoramidates and Thio-Phoshoramidates as Potential Therapeutic Agents. *Chem. Biodiver.* **2010**, *7*, 477-493.

(16) Merki, E.; Graham, M. J.; Mullick, A. E.; Miller, E. R.; Crooke, R. M.; Pitas, R. E.; Witztum, J. L.; Tsimikas, S. Antisense Oligonucleotide Directed to Human Apolipoprotein B-100 Reduces Lipoprotein(a) Levels and Oxidized Phospholipids on Human Apolipoprotein B-100 Particles in Lipoprotein(a) Transgenic Mice. *Circulation* **2008**, *118*, 743-753.

(17) Damha, M. J.; Wilds, C. J.; Noronha, A.; Brukner, I.; Borkow, G.; Arion, D.; Parniak, M. A. Hybrids of RNA and Arabinonucleic Acids (ANA and 2'F-ANA) are Substrates of Ribonuclease H. *J. Am. Chem. Soc.* **1998**, *120*, 12976-12977.

(18) Wang, J.; Herdewijn, P. Enantioselective Synthesis and Conformational Study of Cyclohexene Carbocyclic Nucleosides. *J. Org. Chem.* **1999**, *64*, 7820-7827.

(19) Obika, S.; Nanbu, D.; Hari, Y.; Morio, K.-i.; In, Y.; Ishida, T.; Imanishi, T. Synthesis of 2′-O,4′-C-Methyleneuridine and -cytidine. Novel Bicyclic Nucleosides Having a Fixed C3, -endo Sugar Puckering. *Tetrahedron Lett.* **1997**, *38*, 8735-8738.

(20) Koshkin, A. A.; Singh, S. K.; Nielsen, P.; Rajwanshi, V. K.; Kumar, R.; Meldgaard, M.; Olsen, C. E.; Wengel, J. LNA (Locked Nucleic Acids): Synthesis of the Adenine, Cytosine, Guanine, 5-Methylcytosine, Thymine and Uracil Bicyclonucleoside Monomers, Oligomerisation, and Unprecedented Nucleic Acid Recognition. *Tetrahedron* **1998**, *54*, 3607-3630.

(21) Astakhova, I. K.; Wengel, J. Scaffolding along Nucleic Acid Duplexes Using 2′-Amino-Locked Nucleic Acids. *Acc. Chem. Res.* **2014**, *47*, 1768-1777.

(22) Campbell, M. A.; Wengel, J. Locked vs. Unlocked Nucleic Acids (LNA vs. UNA): Contrasting Structures Work towards Common Therapeutic Goals. *Chem. Soc. Rev.* **2011**, *40*, 5680-5689.

(23) Meggers, E.; Zhang, L. Synthesis and Properties of the Simplified Nucleic Acid Glycol Nucleic Acid. *Acc. Chem. Res.* **2010**, *43*, 1092-1102.

(24) *Peptide Nucleic Acids, Morpholinos and Related Antisense Biomolecules*; Janson, C. G.; During, M. J., Eds.; Springer: US, 2006.

(25) Nielsen, P. E. Peptide Nucleic Acids (PNA) in Chemical Biology and Drug Discovery. *Chem. Biodivers.* **2010**, *7*, 786-804.

(26) Nielsen, P. E.; Egholm, M.; Berg, R. H.; Buchardt, O. Sequence-Selective Recognition of DNA by Strand Displacement with a Thymine-Substituted Polyamide. *Science* **1991**, *254*, 1497-1500.

(27) Egholm, M.; Buchardt, O.; Nielsen, P. E.; Berg, R. H. Peptide Nucleic Acids (PNA). Oligonucleotide Analogs with an Achiral Peptide Backbone. *J. Am. Chem. Soc.* **1992**, *114*, 1895-1897.

(28) Egholm, M.; Buchardt, O.; Christensen, L.; Behrens, C.; Freier, S. M.; Driver, D. A.; Berg, R. H.; Kim, S. K.; Norden, B.; Nielsen, P. E. PNA Hybridizes to Complementary Oligonucleotides Obeying the Watson–Crick Hydrogen-Bonding Rules. *Nature* **1993**, *365*, 566-568.

(29) Demidov, V. V.; Potaman, V. N.; Frank-Kamenetskil, M. D.; Egholm, M.; Buchard, O.; Sönnichsen, S. H.; Nielsen, P. E. Stability of Peptide Nucleic Acids in Human Serum and Cellular Extracts. *Biochem. Pharmacol.* **1994**, *48*, 1310-1313.

(30) *Peptide Nucleic Acids: Protocols and Applications*, 2nd ed.; Nielsen, P. E., Ed.; Horizon Bioscience: United Kingdom, 2004.

(31) Marchelli, R.; Corradini, R.; Manicardi, A.; Sforza, S.; Tedeschi, T.; Fabbri, E.; Borgatti, M.; Bianchi, N.; Gambari, R.: Gene Modulation by Peptide Nucleic Acids (PNAs) Targeting microRNAs (miRs). In *Targets in Gene Therapy*; You, Y., Ed.; InTech, 2011; pp 29-46.

(32) Ratilainen, T.; Holmén, A.; Tuite, E.; Nielsen, P. E.; Nordén, B. Thermodynamics of Sequence-Specific Binding of PNA to DNA†. *Biochemistry* **2000**, *39*, 7781-7791.

(33) Rapireddy, S.; He, G.; Roy, S.; Armitage, B. A.; Ly, D. H. Strand Invasion of Mixed-Sequence B-DNA by Acridine-Linked, γ-Peptide Nucleic Acid (γ-PNA). *J. Am. Chem. Soc.* **2007**, *129*, 15596-15600.

(34) Bahal, R.; Sahu, B.; Rapireddy, S.; Lee, C.-M.; Ly, D. H. Sequence-Unrestricted, Watson–Crick Recognition of Double Helical B-DNA by (R)-MiniPEG-γPNAs. *ChemBioChem* **2012**, *13*, 56-60.

(35) Nielsen, P. E. Peptide Nucleic Acid (PNA): A Model Structure for the Primordial Genetic Material? *Orig. Life Evol. Biosph.* **1993**, *23*, 323-327.

(36) Banack, S. A.; Metcalf, J. S.; Jiang, L.; Craighead, D.; Ilag, L. L.; Cox, P. A. Cyanobacteria Produce N-(*2*-Aminoethyl)Glycine, a Backbone for Peptide Nucleic Acids Which May Have Been the First Genetic Molecules for Life on Earth. *PLoS ONE* **2012**, *7*, e49043.

(37) Eriksson, M.; Nielsen, P. E. Solution Structure of a Peptide Nucleic Acid-DNA Duplex. *Nat. Struct. Mol. Biol.* **1996**, *3*, 410-413.

(38) Brown, S. C.; Thompson, S. A.; Veal, J. M.; Davis, D. G. NMR Solution Structure of a Peptide Nucleic Acid Complexed with RNA. *Science* **1994**, *265*, 777-780.

(39) Betts, L.; Josey, J. A.; Veal, J. M.; Jordan, S. R. A Nucleic Acid Triple Helix Formed by a Peptide Nucleic Acid-DNA Complex. *Science* **1995**, *270*, 1838-1841.

(40) Rasmussen, H.; Kastrup, J. S.; Nielsen, J. N.; Nielsen, J. M.; Nielsen, P. E. Crystal Structure of a Peptide Nucleic Acid (PNA) Duplex at 1.7 Å Resolution. *Nat. Struct. Mol. Biol.* **1997**, *4*, 98-101.

(41) Yeh, J. I.; Shivachev, B.; Rapireddy, S.; Crawford, M. J.; Gil, R. R.; Du, S.; Madrid, M.; Ly, D. H. Crystal Structure of Chiral γPNA with Complementary DNA Strand:

Insights into the Stability and Specificity of Recognition and Conformational Preorganization. *J. Am. Chem. Soc.* **2010**, *132*, 10717-10727.

(42) Menchise, V.; De Simone, G.; Tedeschi, T.; Corradini, R.; Sforza, S.; Marchelli, R.; Capasso, D.; Saviano, M.; Pedone, C. Insights into Peptide Nucleic Acid (PNA) Structural Features: The Crystal Structure of a d-Lysine-Based Chiral PNA–DNA Duplex. *Proc. Natl. Acad. Sci., U.S.A.* **2003**, *100*, 12021-12026.

(43) Lagriffoule, P.; Wittung, P.; Eriksson, M.; Jensen, K. K.; Nordén, B.; Buchardt, O.; Nielsen, P. E. Peptide Nucleic Acids with a Conformationally Constrained Chiral Cyclohexyl-Derived Backbone. *Chem. Eur. J.* **1997**, *3*, 912-919.

(44) Pokorski, J. K.; Witschi, M. A.; Purnell, B. L.; Appella, D. H. (*S*,*S*)-trans-Cyclopentane-Constrained Peptide Nucleic Acids. A General Backbone Modification that Improves Binding Affinity and Sequence Specificity. *J. Am. Chem. Soc.* **2004**, *126*, 15067-15073.

(45) Jordan, S.; Schwemler, C.; Kosch, W.; Kretschmer, A.; Stropp, U.; Schwenner, E.; Mielke, B. New Hetero-Oligomeric Peptide Nucleic Acids with Improved Binding Properties to Complementary DNA. *Bioorg. Med. Chem. Lett.* **1997**, *7*, 687-690.

(46) Kleiner, R. E.; Brudno, Y.; Birnbaum, M. E.; Liu, D. R. DNA-Templated Polymerization of Side-Chain-Functionalized Peptide Nucleic Acid Aldehydes. *J. Am. Chem. Soc.* **2008**, *130*, 4646-4659.

(47) Englund, E. A.; Appella, D. H. γ-Substituted Peptide Nucleic Acids Constructed from L-Lysine are a Versatile Scaffold for Multifunctional Display. *Angew. Chem., Int. Ed.* **2007**, *46*, 1414-1418.

(48) Sahu, B.; Chenna, V.; Lathrop, K. L.; Thomas, S. M.; Zon, G.; Livak, K. J.; Ly, D. H. Synthesis of Conformationally Preorganized and Cell-Permeable Guanidine-Based γ-Peptide Nucleic Acids (γGPNAs). *J. Org. Chem.* **2009**, *74*, 1509-1516.

(49) Sahu, B.; Sacui, I.; Rapireddy, S.; Zanotti, K. J.; Bahal, R.; Armitage, B. A.; Ly, D. H. Synthesis and Characterization of Conformationally Preorganized, (*R*)-Diethylene Glycol-Containing γ-Peptide Nucleic Acids with Superior Hybridization Properties and Water Solubility. *J. Org. Chem.* **2011**, *76*, 5614-5627.

(50) Mitra, R.; Ganesh, K. N. PNAs Grafted with (α/γ, *R*/*S*)-Aminomethylene Pendants: Regio and Stereo Specific Effects on DNA Binding and Improved Cell Uptake. *Chem. Commun.* **2011**, *47*, 1198-1200.

(51) Dragulescu-Andrasi, A.; Rapireddy, S.; Frezza, B. M.; Gayathri, C.; Gil, R. R.; Ly, D. H. A Simple γ-Backbone Modification Preorganizes Peptide Nucleic Acid into a Helical Structure. *J. Am. Chem. Soc.* **2006**, *128*, 10258-10267.

(52) Sugiyama, T.; Imamura, Y.; Demizu, Y.; Kurihara, M.; Takano, M.; Kittaka, A. β-PNA: Peptide Nucleic Acid (PNA) with a Chiral Center at the β-Position of the PNA Backbone. *Bioorg. Med. Chem. Lett.* **2011**, *21*, 7317-7320.

(53) Crawford, M. J.; Rapireddy, S.; Bahal, R.; Sacui, I.; Ly, D. H. Effect of Steric

Constraint at the γ-Backbone Position on the Conformations and Hybridization Properties of PNAs. *J. Nucleic Acids* **2011**, *2011*, 652702.

(54) Rajeev, K. G.; Maier, M. A.; Lesnik, E. A.; Manoharan, M. High-Affinity Peptide Nucleic Acid Oligomers Containing Tricyclic Cytosine Analogues†. *Org. Lett.* **2002**, *4*, 4395-4398.

(55) Li, M.; Zengeya, T.; Rozners, E. Short Peptide Nucleic Acids Bind Strongly to Homopurine Tract of Double Helical RNA at pH 5.5. *J. Am. Chem. Soc.* **2010**, *132*, 8676-8681.

(56) Rozners, E. Recent Advances in Chemical Modification of Peptide Nucleic Acids. *J. Nucleic Acids* **2012**, *2012*, 518162.

(57) Rathee, P.; Rathee, D.; Hooda, A.; Kumar, V.; Rathee, S. Peptide Nucleic Acids: An Overview. *The Pharma Innovation* **2012**, *1*, 25-42.

(58) Taylor, R. W.; Chinnery, P. F.; Turnbull, D. M.; Lightowlers, R. N. Selective Inhibition of Mutant Human Mitochondrial DNA Replication in Vitro by Peptide Nucleic Acids. *Nat. Genet.* **1997**, *15*, 212-215.

(59) Hamilton, S. E.; Simmons, C. G.; Kathiriya, I. S.; Corey, D. R. Cellular Delivery of Peptide Nucleic Acids and Inhibition of Human Telomerase. *Chem. Biol.* **1999**, *6*, 343-351.

(60) Cutrona, G.; Carpaneto, E. M.; Ulivi, M.; Roncella, S.; Landt, O.; Ferrarini, M.; Boffa, L. C. Effects in Live Cells of a c-Myc Antigene PNA Linked to a Nuclear Localization Signal. *Nat. Biotech.* **2000**, *18*, 300-303.

(61) Hanvey, J. C.; Peffer, N. J.; Bisi, J. E.; Thomson, S. A.; Cadilla, R.; Josey, J. A.; Ricca, D. J.; Hassman, C. F.; Bonham, M. A.; Au, K. G.; Carter, S. G.; Bruckenstein, D. A.; Boyd, A. L.; Noble, S. A.; Babiss, L. E. Antisense and Antigene Properties of Peptide Nucleic Acids. *Science* **1992**, *258*, 1481-1485.

(62) Stock, R. P.; Olvera, A.; Sanchez, R.; Saralegui, A.; Scarfi, S.; Sanchez-Lopez, R.; Ramos, M. A.; Boffa, L. C.; Benatti, U.; Alagon, A. Inhibition of Gene Expression in Entamoeba Histolytica with Antisense Peptide Nucleic Acid Oligomers. *Nat. Biotech.* **2001**, *19*, 231-234.

(63) Good, L.; Nielsen, P. E. Inhibition of Translation and Bacterial Growth by Peptide Nucleic Acid Targeted to Ribosomal RNA. *Proc. Natl. Acad. Sci.* **1998**, *95*, 2073-2076.

(64) Ali, M.; Neumann, R.; Ensinger, W. Sequence-Specific Recognition of DNA Oligomer Using Peptide Nucleic Acid (PNA)-Modified Synthetic Ion Channels: PNA/DNA Hybridization in Nanoconfined Environment. *ACS Nano* **2010**, *4*, 7267-7274.

(65) Wittung, P.; Kajanus, J.; Edwards, K.; Haaima, G.; Nielsen, P. E.; Nordén, B.; Malmström, B. G. Phospholipid Membrane Permeability of Peptide Nucleic Acid. *FEBS Lett.* **1995**, *375*, 27-29.

(66) AdvanDx: In *http://www.advandx.com/AdvanDX/media/Downloads/Assay%20Overviews/EC-PA-PNA-FISH-Overview.png*

(67) Shiraishi, T.; Nielsen, P. E. Enhanced Delivery of Cell-Penetrating Peptide-Peptide Nucleic Acid Conjugates by Endosomal Disruption. *Nat. Protoc.* **2006**, *1*, 633-636.

(68) Zhou, P.; Wang, M.; Du, L.; Fisher, G. W.; Waggoner, A.; Ly, D. H. Novel Binding and Efficient Cellular Uptake of Guanidine-Based Peptide Nucleic Acids (GPNA). *J. Am. Chem. Soc.* **2003**, *125*, 6878-6879.

(69) Nagahara, H.; Vocero-Akbani, A. M.; Snyder, E. L.; Ho, A.; Latham, D. G.; Lissy, N. A.; Becker-Hapak, M.; Ezhevsky, S. A.; Dowdy, S. F. Transduction of Full-Length TAT Fusion Proteins into Mammalian Cells: TAT-$p27^{Kip1}$ Induces Cell Migration. *Nat. Med.* **1998**, *4*, 1449-1452.

(70) Wender, P. A.; Mitchell, D. J.; Pattabiraman, K.; Pelkey, E. T.; Steinman, L.; Rothbard, J. B. The Design, Synthesis, and Evaluation of Molecules that Enable or Enhance Cellular Uptake: Peptoid Molecular Transporters. *Proc. Natl. Acad. Sci.* **2000**, *97*, 13003-13008.

(71) Mitra, R.; Ganesh, K. N. Aminomethylene Peptide Nucleic Acid (am-PNA): Synthesis, Regio-/Stereospecific DNA Binding, and Differential Cell Uptake of (α/γ,*R*/*S*)am-PNA Analogues. *J. Org. Chem.* **2012**, *77*, 5696-5704.

(72) Dragulescu-Andrasi, A.; Zhou, P.; He, G.; Ly, D. H. Cell-Permeable GPNA with Appropriate Backbone Stereochemistry and Spacing Binds Sequence-Specifically to RNA. *Chem. Commun.* **2005**, 244-246.

(73) Whitehead, K. A.; Langer, R.; Anderson, D. G. Knocking Down Barriers: Advances in siRNA Delivery. *Nat. Rev. Drug Discov.* **2009**, *8*, 129-138.

(74) Juliano, R.; Alam, M. R.; Dixit, V.; Kang, H. Mechanisms and Strategies for Effective Delivery of Antisense and siRNA Oligonucleotides. *Nucleic Acids Res.* **2008**, *36*, 4158-4171.

(75) Gambari, R. Peptide Nucleic Acids: a Review on Recent Patents and Technology Transfer. *Expert Opin. Ther. Patents* **2014**, *24*, 267-294.

(76) Uhlmann, E.; Will, D. W.; Breipohl, G.; Langner, D.; Ryte, A. Synthesis and Properties of PNA/DNA Chimeras. *Angew. Chem., Int. Ed.* **1996**, *35*, 2632-2635.

(77) Shiraishi, T.; Hamzavi, R.; Nielsen, P. E. Subnanomolar Antisense Activity of Phosphonate-Peptide Nucleic Acid (PNA) Conjugates Delivered by Cationic Lipids to HeLa Cells. *Nucleic Acids Res.* **2008**, *36*, 4424-4432.

(78) Peyman, A.; Uhlmann, E.; Wagner, K.; Augustin, S.; Weiser, C.; Will, D. W.; Breipohl, G. PHONA – PNA Co-Oligomers: Nucleic Acid Mimetics with Interesting Properties. *Angew. Chem., Int. Ed.* **1997**, *36*, 2809-2812.

(79) Efimov, V. A.; Choob, M. V.; Buryakova, A. A.; Kalinkina, A. L.; Chakhmakhcheva, O. G. Synthesis and Evaluation of Some Properties of Chimeric Oligomers

Containing PNA and Phosphono-PNA Residues. *Nucleic Acids Res.* **1998**, *26*, 566-575.

(80) Efimov, V. A.; Chakhmakhcheva, O. G.; Wickstrom, E. Synthesis and Application of Negatively Charged PNA Analogues. *Nucleos. Nucleot. Nucl.* **2005**, *24*, 1853-1874.

(81) Tang, X.; Maegawa, S.; Weinberg, E. S.; Dmochowski, I. J. Regulating Gene Expression in Zebrafish Embryos Using Light-Activated, Negatively Charged Peptide Nucleic Acids. *J. Am. Chem. Soc.* **2007**, *129*, 11000-11001.

(82) Urtishak, K. A.; Choob, M.; Tian, X.; Sternheim, N.; Talbot, W. S.; Wickstrom, E.; Farber, S. A. Targeted Gene Knockdown in Zebrafish Using Negatively Charged Peptide Nucleic Acid Mimics. *Dev. Dyn.* **2003**, *228*, 405-413.

(83) Dorn, S.; Aghaallaei, N.; Jung, G.; Bajoghli, B.; Werner, B.; Bock, H.; Lindhorst, T.; Czerny, T. Side Chain Modified Peptide Nucleic Acids (PNA) for Knock-down of six3 in Medaka Embryos. *BMC Biotechnol.* **2012**, *12*, 50.

(84) Haaima, G.; Lohse, A.; Buchardt, O.; Nielsen, P. E. Peptide Nucleic Acids (PNAs) Containing Thymine Monomers Derived from Chiral Amino Acids: Hybridization and Solubility Properties of D-Lysine PNA. *Angew. Chem., Int. Ed.* **1996**, *35*, 1939-1942.

(85) Sforza, S.; Haaima, G.; Marchelli, R.; Nielsen, P. E. Chiral Peptide Nucleic Acids (PNAs): Helix Handedness and DNA Recognition. *Eur. J. Org. Chem.* **1999**, *1999*, 197-204.

(86) Avitabile, C.; Moggio, L.; Malgieri, G.; Capasso, D.; Di Gaetano, S.; Saviano, M.; Pedone, C.; Romanelli, A. γ Sulphate PNA (PNA S): Highly Selective DNA Binding Molecule Showing Promising Antigene Activity. *PLoS ONE* **2012**, *7*, e35774.

CHAPTER 2

TAILORING PEPTIDE NUCLEIC ACIDS TO ELECTROSTATICALLY MIMIC DNA AND RNA[1]

Introduction

Peptide nucleic acid (PNA) is a nucleic acid mimic that shows tremendous potential for use in therapeutic and biosensing applications due to its high binding affinity and selectivity for DNA and RNA and its excellent biostability.[1,2] The therapeutic potential of PNA, however, is hindered by its poor solubility, cellular uptake, and bioavailability, predominantly due to its uncharged backbone. The Heemstra group hypothesizes that negatively charged PNA analogues would electrostatically mimic DNA and RNA, overcoming the abovementioned challenges by taking advantage of the multitude of charge-based delivery technologies currently being developed for DNA and RNA. However, the enhanced thermodynamic stability of PNA:DNA and PNA:RNA duplexes compared with DNA:DNA and DNA:RNA duplexes has been in part attributed to the lack of electrostatic repulsion between the uncharged PNA backbone and negatively charged DNA or RNA backbone.[3] This previous hypothesis has led to the belief that having a negative charge on PNA is detrimental to the duplex formation of PNA with native nucleic acids, and thus discouraged the development of negatively charged PNA analogues.

This hypothesis is further supported by the reduced binding affinities observed in

---

[1] Adapted under the terms of the Creative Commons Attribution License from De Costa, N. T. S.; Heemstra, J. M. Evaluating the Effect of Ionic Strength on Duplex Stability for PNA Having Negatively or Positively Charged Side Chains. *PLoS ONE* **2013**, *8*, e58670.

some of the previously reported negatively charged PNA analogues.[4-6] For example, negatively charged pPNA:DNA and pPNA:RNA duplexes were found to have T_m values significantly lower than those of PNA:DNA and PNA:RNA, and, in fact, even lower than those of the corresponding DNA:DNA and DNA:RNA duplexes. But alternating pPNA monomers with PNA monomers to give a pPNA-PNA hybrid resulted in duplex stabilities with DNA and RNA that approached those of PNA:DNA and PNA:RNA.[6] In addition, oligomers of alternating pPNA-HypNA monomers showed higher duplex stabilities with DNA and RNA than oligomers of pPNA-PNA, yet lower than PNA:DNA and PNA:RNA.[6] The results of these studies could be interpreted to conclude that increasing negative charge decreases PNA duplex stability via electrostatic repulsion. However, it is important to note that the backbone conformation of pPNA is likely to differ significantly from that of PNA and α- or γ-substituted PNA. Thus the decreased duplex stability of pPNA may result predominantly from structural rather than electrostatic effects.

Previous studies have also attempted to introduce charged side chains at the α- and γ-positions of the PNA backbone. For example, incorporation of negatively charged (D-Glu, L-Asp) or neutral (L-Leu, L-Ile) side chains at the α-position reduces binding affinity with DNA, whereas the incorporation of positively charged (D-Lys) side chains increases binding affinity with DNA and has negligible effects on binding affinity with RNA.[7-9] However, these studies were only carried out at a single salt concentration, and the binding affinity of negatively charged PNA with RNA was not studied. In the case of γ-substituted PNA, positively charged (L-Lys, L-Arg), or neutral side chains (L-Phe, L-Val) increase the binding affinity with DNA,[10-15] though this increase is primarily attributed to steric or hydrogen-bonding effects leading to conformational preorganization of the PNA backbone.[16,17] There is evidence that negatively charged side chains (L-Glu, sulfate) are also tolerated at the γ-position,[11,18] but their effect on binding affinity with DNA at varying ionic strength has not been thoroughly studied. Additionally, the binding proper-

ties of γ-substituted PNA with RNA have only been minimally investigated.[10]

Although electrostatic repulsion can obstruct duplex formation between negatively charged nucleic acids and negatively charged PNA, we anticipate that Debye screening of this electrostatic repulsion by the counter ions in the medium could overcome this repulsion.[19,20] However, there are no reported studies that systematically evaluate the effect of ionic strength on duplex stability for PNAs having a charged backbone. Our attempts to study negatively charged PNA analogues focused on installing Asp residues at the γ-position of PNA. While our manuscript was under review,[21] Romanelli and coworkers reported a negatively charged PNA analogue containing γ-sulfate side chains.[18] They observed that doubling the salt concentration increased the stability of PNA_2:DNA triplexes containing γ-sulfate PNA; yet, they did not thoroughly evaluate the effect of ionic strength on duplex stability of negatively charged γ-sulfate PNA.

In this chapter, we present the first detailed investigation of the effect of ionic strength on binding affinity for charged PNA. We show that charge screening of electrostatic repulsion by counterions in solution enables negatively charged side chains to be incorporated into the PNA backbone without reducing duplex stability with DNA and RNA.[21] While electrostatic interactions do play a role in PNA binding, this effect is manifested in differential salt dependence, such that at medium to high salt concentrations, negatively charged PNA actually binds more strongly to DNA and RNA than does positively charged PNA.

Results and Discussion

Monomer synthesis

The desired γ-substituted PNA monomers were synthesized from commercially available Fmoc-L-aspartic acid β-*tert*-butyl ester **2.1a**, Fmoc-L-Lys(Boc)-OH **2.1b**, and Fmoc-L-Ala-OH **2.1c** using previously reported procedures (Scheme 2.1).[11] First, Fmoc-

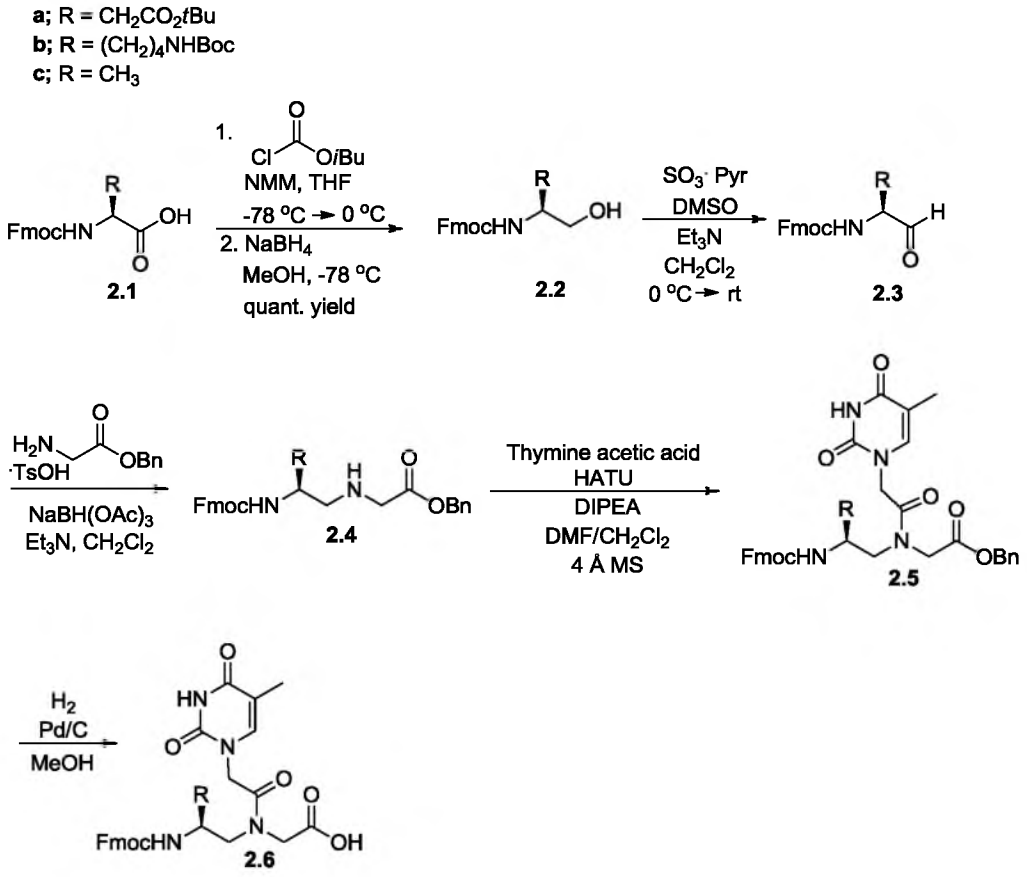

	Substrate (R =)	Yields 2.4	2.5	2.6
a	CH_2CO_2tBu	60	51	80
b	$(CH_2)_4NHBoc$	78	85	88
c	CH_3	66	40	63

Scheme 2.1. Synthesis of γ-substituted PNA monomers.

protected amino acid **2.1** was reduced to give the corresponding alcohol **2.2**[22] in quantitative yield, which was subsequently subjected to Parikh-Doering conditions[23] to yield aldehyde **2.3**.[24] Aldehyde **2.3** was immediately subjected to reductive amination with glycine benzyl ester 4-toluenesulfonate to afford the γ-substituted PNA backbone **2.4**. Subsequent coupling of **2.4** with thymine-1-acetic acid using HATU/DIPEA yielded amide **2.5**. Final removal of the benzyl ester via hydrogenation produced γ-substituted PNA monomer **2.6**.

Structure and sequence of modified PNA strands

To investigate the effect of ionic strength on duplex stability for charged PNA, negatively[25] and positively[11] charged PNA monomers and γ-methyl substituted PNA monomer[26] were synthesized using L-Asp, L-Lys and L-Ala residues, respectively to construct the ethylenediamine portion of the PNA backbone (Figure 2.1). We used the Nielsen decamer sequence H-GTAGATCACT-NH_2 [3] for the current study, as its hybridization to DNA and RNA has been thoroughly investigated. This sequence contains three equally-spaced thymine residues as convenient points for substitution with our charged monomers. We used solid-phase peptide synthesis[27] (SPPS) to generate our nonfunctionalized PNA (PNA **nf**), as well as PNA strands containing either one or three positively charged (PNA **1pos**/**3pos**), negatively charged (PNA **1neg**/**3neg**), or γ-methyl substituted (PNA **1Me**/**3Me**) PNA monomers (Table 2.1). With these sequences in hand, we investigated their thermal melting behavior with complementary DNA (DNA **1**) and RNA (RNA **1**) at varying salt concentrations.

The effect of ionic strength on duplex stability for DNA, RNA, and PNA

DNA:DNA and DNA:RNA duplexes are known to demonstrate positive salt dependence, in which increased ionic strength of the buffer solution leads to increased melting temperature (T_m) due to charge screening of the electrostatic repulsion between the negatively charged strands.[19] Thus, we were not surprised to see the T_m values of DNA **1**:DNA **2** and RNA **1**:DNA **2** increase with increasing concentrations of NaCl (Figure 2.2).

In contrast, PNA:DNA duplexes demonstrate negative salt dependence, in which increased ionic strength leads to a decrease in T_m.[3] The thermodynamic stability of PNA:DNA duplexes has been attributed in part to entropically favorable counterion release upon duplex formation.[28] Therefore, increasing the salt concentration destabilizes

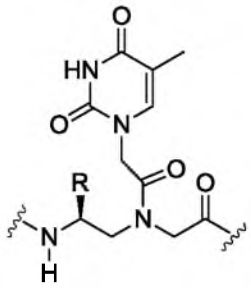

T : R = H
T_D: R = $CH_2CO_2^-$
T_K: R = $(CH_2)_4NH_3^+$
T_A: R = CH_3

Figure 2.1. Chemical structure of γ-substituted PNA monomers.

Table 2.1. PNA,* DNA, and RNA sequences.

Name	Sequence
PNA **nf**	H-GTAGATCACT-NH_2
PNA **1neg**	H-GTAGAT$_D$CACT-NH_2
PNA **3neg**	H-GT$_D$AGAT$_D$CACT$_D$-NH_2
PNA **1pos**	H-GTAGAT$_K$CACT-NH_2
PNA **3pos**	H-GT$_K$AGAT$_K$CACT$_K$-NH_2
PNA **1Me**	H-GTAGAT$_A$CACT-NH_2
PNA **3Me**	H-GT$_A$AGAT$_A$CACT$_A$-NH_2
DNA **1**	5'-AGTGATCTAC-3'
DNA **2**	5'-GTAGATCACT-3'
RNA **1**	5'-AGUGAUCUAC-3'

* PNAs are depicted like peptides by convention with the N-terminus at the left position and the C-terminus at the right.

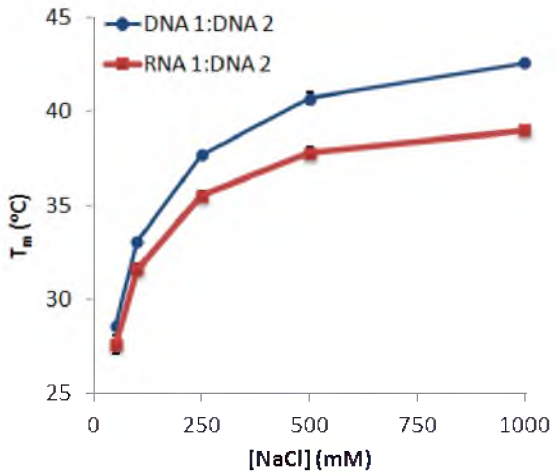

Figure 2.2. T_m vs [NaCl] for DNA **1**:DNA **2** and RNA **1**:DNA **2** duplexes. (Conditions: 3 μM DNA, 3 μM RNA, 10 mM sodium phosphate buffer with added NaCl, pH 7.2. Error bars represent standard deviation of three independent trials.)

the PNA:DNA duplex. However, the efflux of cations in PNA:DNA duplex formation is less than the influx of cations in DNA:DNA duplex formation, so the net salt effect is smaller for PNA:DNA relative to DNA:DNA. As anticipated, the T_m of PNA **nf**:DNA **1** shows a weak negative salt dependence (Figure 2.3, green line). In the case of PNA:RNA duplexes, ionic strength appears to have little effect on hybridization, as PNA **nf**:RNA **1** shows neutral salt dependence (Figure 2.4, green line). In previous work by Ly and colleagues, positively charged guanidinium-PNA (GPNA):DNA duplexes demonstrated negative salt dependence.[12] Conversely, Romanelli and coworkers have shown that in the case of PNA_2:DNA triplexes containing negatively charged PNA, doubling salt concentration increases stability.[18] Thus, we anticipated that our negatively charged PNA would demonstrate positive salt dependence in duplex formation with DNA and RNA.

Duplex stability of charged PNA with DNA at varying salt concentrations

The introduction of a single positive or negative-substituent was found to enhance PNA:DNA duplex stability, as PNA **1pos**:DNA **1** and PNA **1neg**:DNA **1** displayed higher T_m values than PNA **nf**:DNA **1** (Figure 2.3a). This increase in duplex stability can be attributed primarily to backbone preorganization induced by the γ-substituent, as an analogous PNA strand having a single γ-methyl substituent (PNA **1Me**) [29-31] demonstrated nearly identical T_m values to PNA **1pos** (Table 2.2). Similar to GPNA, PNA **1pos**:DNA **1** showed a negative salt dependence with increasing concentrations of NaCl. In contrast, PNA **1neg**:DNA **1** showed a neutral salt dependence, providing preliminary evidence that the presence of negative charge in PNA backbone can result in reversal of salt dependence for duplex formation.

Upon increasing the number of charged residues from one to three, a more pronounced effect on T_m was observed (Figure 2.3b). As anticipated, the duplex stabilities of PNA **3neg** and PNA **3pos** with DNA **1** were greater than that of PNA **nf** with DNA **1**,

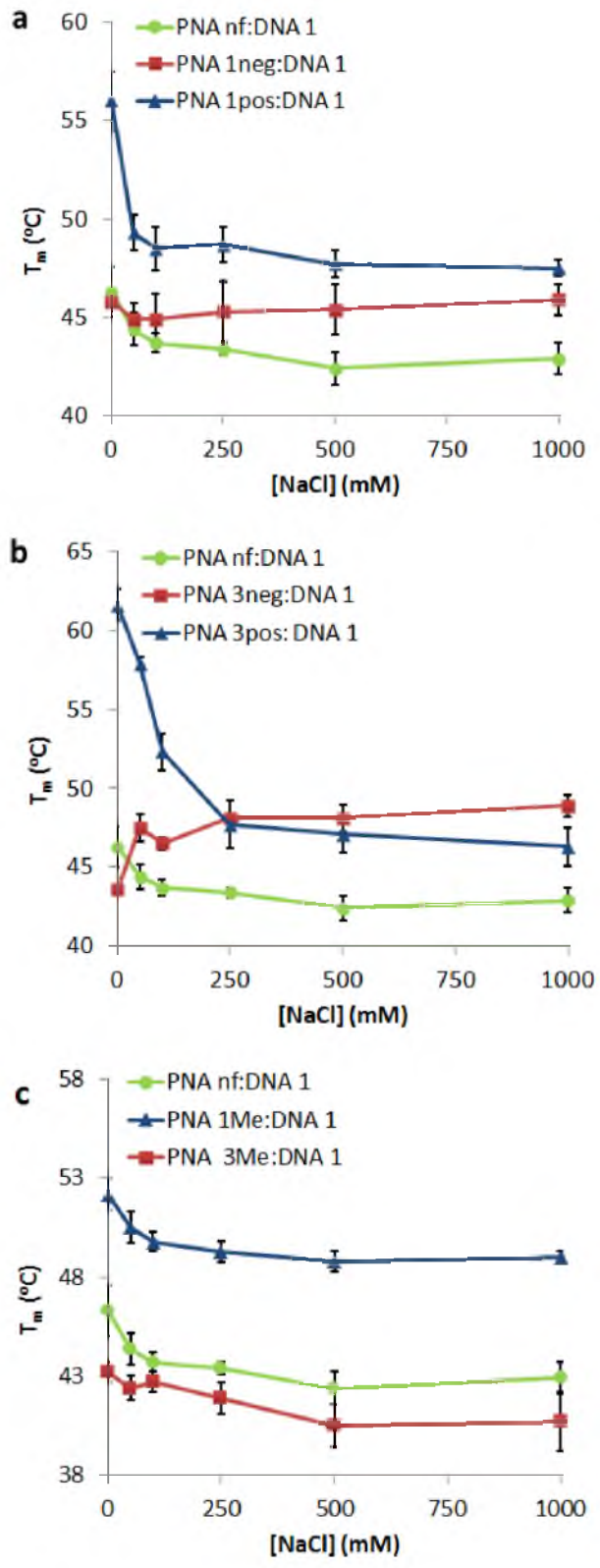

Figure 2.3. T_m vs [NaCl] for PNA:DNA **1** duplexes (a) PNA (**nf**/**1neg**/**1pos**): DNA **1**, (b) PNA (**nf**/**3neg**/**3pos**):DNA **1**, (c) PNA (**nf**/**1Me**/**3Me**):DNA **1**.

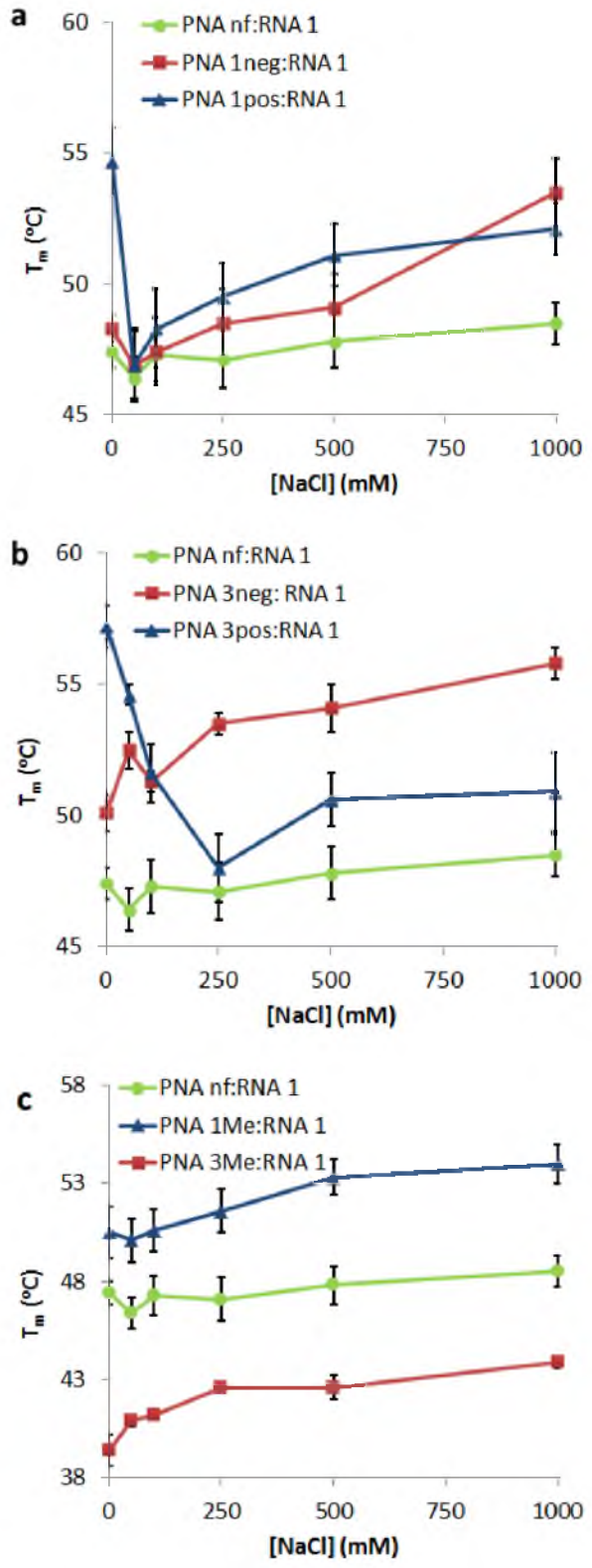

Figure 2.4. T_m vs [NaCl] for PNA:RNA **1** duplexes (a) PNA (**nf**/**1neg**/**1pos**): RNA **1**, (b) PNA (**nf**/**3neg**/**3pos**):RNA **1**, (c) PNA (**nf**/**1Me**/**3Me**):RNA **1**.

Table 2.2. T_m of PNA:DNA **1** duplexes at varying salt concentrations.*

[NaCl] =	0 M	50 mM	100 mM	250 mM	500 mM	1 M
PNA **nf**	46.3 ± 1.3	44.4 ± 0.8	43.7 ± 0.5	43.4 ± 0.3	42.4 ± 0.8	42.9 ± 0.8
PNA **1neg**	45.8 ± 0.5	44.9 ± 0.8	44.9 ± 1.3	45.3 ± 1.5	45.4 ± 1.3	45.9 ± 0.8
PNA **3neg**	43.6 ± 0.1	47.5 ± 0.9	46.5 ± 0.4	48.1 ± 0.3	48.1 ± 0.9	48.9 ± 0.7
PNA **1pos**	56.0 ± 1.5	49.3 ± 0.9	48.5 ± 1.1	48.7 ± 0.9	47.7 ± 0.7	47.5 ± 0.4
PNA **3pos**	61.6 ± 1.0	57.9 ± 0.4	52.3 ± 1.2	47.7 ± 1.5	47.1 ± 1.2	46.3 ± 1.2
PNA **1Me**	52.2 ± 0.8	50.5 ± 0.8	49.8 ± 0.5	49.3 ± 0.5	48.8 ± 0.5	49.0 ± 0.3
PNA **3Me**	43.2 ± 0.5	42.4 ± 0.6	42.7 ± 0.5	41.9 ± 0.8	40.5 ± 1.1	40.7 ± 1.5

*Conditions: 3 μM PNA, 3 μM DNA, 10 mM sodium phosphate buffer with added NaCl, pH 7.2. Errors represent standard deviation of three or four independent trials.

likely due to backbone preorganization by the γ-substituents. Similar to PNA **1pos**:DNA **1**, PNA **3pos**:DNA **1** showed a negative salt dependence with increasing NaCl concentration. However, as we anticipated, incorporation of three negative charges resulted in a positive salt dependence for PNA **3neg**:DNA **1**, as this duplex is presumably able to take advantage of charge screening when cations are present. In the presence of only 10 mM sodium (from the sodium phosphate buffer), T_m values follow the order of PNA **3pos**>PNA **nf**>PNA **3neg**, revealing the effect of unscreened electrostatic contributions. But, with added NaCl concentrations of 250 mM and above, PNA **3neg**:DNA **1** surprisingly becomes more stable than PNA **3pos**:DNA **1** (Figure 2.3b and Table 2.2).

We were also curious to investigate the duplex stability of γ-PNA having three neutral side chains (PNA **3Me**). Although PNA **1Me** demonstrated nearly identical T_m values to PNA **1pos**, PNA **3Me** showed T_m values even lower than those of PNA **nf** (Figure 2.3c and Table 2.2). These results are inconsistent with the well-known increase in T_m with an increasing number of γ-substituents. We believe that these inconsistent T_m

data are a result of the aggregation of PNA **3Me**.

Duplex stability of charged PNA with RNA at varying salt concentrations

We next investigated the binding of charged PNA strands with complementary RNA. As was the case for DNA, incorporation of one or three γ-substituted monomers in the PNA sequence increase the overall duplex stability with RNA (Figure 2.4 and Table 2.3). Both PNA **1neg**:RNA **1** and PNA **1pos**:RNA **1** showed an initial decrease in T_m going from 0 to 50 mM NaCl, followed by a gradual increase in T_m up to 1 M NaCl (Figure 2.4a). However, the T_m values of these two duplexes are the same within error at NaCl concentrations of 50 mM and above, indicating that the presence of a single charged residue has only minimal impact on PNA:RNA binding. Increasing the number of charged residues on PNA from one to three produced a more dramatic effect on RNA binding (Figure 2.4b).

Table 2.3. T_m of PNA:RNA **1** duplexes at varying salt concentrations.*

[NaCl] =	0 M	50 mM	100 mM	250 mM	500 mM	1 M
PNA **nf**	47.4 ± 0.6	46.4 ± 0.8	47.3 ± 1.0	47.1 ± 1.1	47.8 ± 1.0	48.5 ± 0.8
PNA **1neg**	48.3 ± 0.5	46.9 ± 1.3	47.4 ± 1.3	48.5 ± 1.3	49.1 ± 1.3	53.5 ± 1.3
PNA **3neg**	50.1 ± 0.7	52.5 ± 0.7	51.3 ± 0.4	53.5 ± 0.4	54.1 ± 0.9	55.8 ± 0.6
PNA **1pos**	54.7 ± 1.3	46.9 ± 1.4	48.3 ± 1.5	49.5 ± 1.3	51.1 ± 1.2	52.1 ± 1.0
PNA **3pos**	57.2 ± 0.8	54.6 ± 0.4	51.6 ± 1.1	48.0 ± 1.3	50.6 ± 1.0	50.9 ± 1.5
PNA **1Me**	50.5 ± 1.3	50.1 ± 1.1	50.6 ± 1.1	51.6 ± 1.1	53.3 ± 0.9	54.0 ± 1.0
PNA **3Me**	39.4 ± 0.8	40.9 ± 0.3	41.2 ± 0.1	42.6 ± 0.3	42.6 ± 0.6	43.9 ± 0.3

*Conditions: 3 μM PNA, 3 μM RNA, 10 mM sodium phosphate buffer with added NaCl, pH 7.2. Errors represent standard deviation of three or four independent trials.

Analogous to the above described binding results of triply charged PNA with DNA, PNA **3pos**:RNA **1** also displayed a negative salt dependence while PNA **3neg**:RNA **1** displayed a positive salt dependence. However, in the case of RNA, the threshold of negatively charged PNA to surpass positively charged PNA binding affinity was much lower at approximately 100 mM NaCl (Figure 2.4b and Table 2.3). As we observed with DNA, PNA **1Me** showed a higher duplex stability than PNA **nf** with RNA; but PNA **3Me** showed a lower duplex stability than PNA **nf** (Figure 2.4c and Table 2.3), which we again attribute to possible aggregation.

Duplex stability of charged PNA with DNA and RNA under physiological salt conditions

Given the increasing use of PNA for *in vivo* applications, we sought to investigate the duplex stability of our charged PNA with DNA and RNA in a buffer that mimics physiological salt conditions (0.49 mM $MgCl_2{\cdot}6H_2O$, 137 mM NaCl, 2.7 mM KCl, 1.5 mM KH_2PO_4, 8.1 mM Na_2HPO_4, pH 7.4)[32] (Table 2.4). Consistent with previous observations, negatively charged PNA binds slightly more weakly with DNA than does positively charged PNA. However, in the case of RNA binding, negatively charged PNA was again superior to positively charged PNA when three charged substituents were present on the PNA backbone. These results reinforce the observations outlined above and lead to the unexpected conclusion that adding negative charge to PNA may in fact increase binding affinity in RNA-targeted antisense therapeutics.

Thermodynamic data analysis

The thermodynamic parameters for the interactions of PNA with nucleic acids can be calculated by van't Hoff analysis of UV melting data and by calorimetric methods,

Table 2.4. T_m of PNA:DNA **1** and PNA:RNA **1** duplexes under simulated physiological buffer conditions.*

Complement	T_m with DNA **1** (°C)	T_m with RNA **1** (°C)
DNA **2**	37.2 ± 0.1	32.5 ± 0.8
PNA **nf**	43.2 ± 0.5	47.1 ± 1.1
PNA **1neg**	45.9 ± 0.8	48.1 ± 1.1
PNA **1pos**	46.9 ± 0.3	46.9 ± 0.8
PNA **1Me**	47.3 ± 1.3	48.1 ± 1.5
PNA **3neg**	46.1 ± 0.6	49.9 ± 1.5
PNA **3pos**	49.1 ± 1.0	46.5 ± 1.7
PNA **3Me**	40.0 ± 0.6	41.4 ± 0.6

*Conditions: 3 μM PNA, 3 μM DNA or RNA, 0.49 mM $MgCl_2{\cdot}6H_2O$, 137 mM NaCl, 2.7 mM KCl, 1.5 mM KH_2PO_4, 8.1 mM Na_2HPO_4, pH 7.4. Errors represent standard deviation of three independent trials.

including isothermal titration (ITC) and differential scanning calorimetry (DSC).[1] We performed van't Hoff analysis on the UV melting data to obtain the thermodynamic parameters for duplex formation of PNA **3neg** and PNA **3pos** with DNA and RNA in physiological buffer (Table 2.5).[33,34] As expected, the Gibbs free energy change (ΔG) follows a similar trend as the T_m values for the duplexes, with higher free energy gain observed for duplexes having higher values of T_m. In duplex formation with DNA, PNA **3neg** shows lower enthalpic driving force but also lower entropic cost, relative to PNA **3pos**. However, in the case of RNA duplex formation, the opposite is observed; PNA **3neg** shows higher enthalpic driving force but higher entropic cost, relative to PNA **3pos**.

The observed higher salt sensitivity of PNA:RNA duplexes can be attributed to the higher density of counterions associated with A-form structures than B-form structures. Thus, we hypothesize that the structural variation between PNA:DNA and PNA:RNA duplexes is responsible for the increased contribution of PNA backbone charge and NaCl concentration in PNA:RNA binding. This hypothesis is supported by

Table 2.5. Thermodynamic parameters for the formation of duplexes of PNA **3neg** and PNA **3pos** with DNA and RNA.*

Duplex	T_m (°C)	ΔG (kJ·mol^{-1})	ΔH (kJ·mol^{-1})	$T\Delta S$ (kJ·mol^{-1})
PNA **3neg**:DNA **1**	46.1 ± 0.6	-48.0 ± 0.3	-208.4 ± 1.0	-160.4 ± 1.0
PNA **3pos**:DNA **1**	49.1 ± 1.0	-49.8 ± 0.3	-213.2 ± 2.7	-163.4 ± 2.9
PNA **3neg**:RNA **1**	49.9 ± 1.5	-49.1 ± 0.8	-203.4 ± 3.6	-154.3 ± 2.9
PNA **3pos**:RNA **1**	46.5 ± 1.7	-47.9 ± 0.3	-191.5 ± 0.4	-143.6 ± 0.6

*Averages from van't Hoff analysis of three trials of UV melting data. Errors represent standard deviation of three independent trials.

the thermodynamic data in Table 2.5, where the PNA **3neg**:RNA duplex has greater enthalpic gain with greater entropic cost, relative to the PNA **3pos**:RNA duplex, as would be anticipated in the case of tight counterion binding to the PNA **3neg**:RNA duplex. We are intrigued by the fact that the charged PNA:RNA duplexes do not follow a logarithmic trend for T_m as a function of ionic strength, as is the case for DNA:DNA and DNA:RNA duplexes.[35]

It should be noted that the Asp and Lys residues used for this initial study have a slight variation in side chain length. However, given the fact that the PNA:DNA helix diameter is approximately 23 Å,[17] and previous studies have reported that the Lys side chains are not involved in non specific charge-charge interactions,[10] the two carbon difference in side chain length is anticipated to have little to no impact on duplex stability. Thus, we attribute the changes in duplex stability for negatively and positively charged PNA primarily to the differential electrostatic properties of these PNA strands.

Conclusion

Given the hypothesis that the lack of electrostatic repulsion plays a key role in PNA binding, it is surprising to discover that adding negatively charged side chains to PNA does not significantly decrease binding affinity with DNA and RNA at physiological ionic strength. Moreover, because positively charged PNA displays negative salt dependence and negatively charged PNA displays positive salt dependence, at medium to high salt concentrations, negatively charged PNA actually binds more strongly to DNA and RNA than does positively charged PNA. Presumably, preorganization of the PNA backbone via hydrogen bonding is primarily responsible for the enhanced duplex stability of PNA with DNA and RNA. This hypothesis has been previously reported in the literature,[36,37] and recent studies by Ganesh and coworkers[14] have demonstrated that additional backbone hydrogen bonding interactions can be used to further increase binding affinity or favor parallel versus antiparallel alignment of the nucleic acid strands. Future studies will utilize molecular dynamics simulations to provide greater insight into the effect of PNA charge on duplex structure.

In general, PNA:RNA duplexes are known to have higher thermal stabilities than PNA:DNA duplexes;[1,16] yet our data shows that positively charged PNA:DNA duplexes have a higher thermal stability than positively charged PNA:RNA duplexes.[21] This suggests that careful modification of PNA may be used to modulate the selectivity of binding to DNA and RNA.[38]

The recent popularity of antisense therapeutics such as siRNA has prompted the development of a multitude of technologies aimed at enhancing the circulation lifetime and cell permeability of nucleic acids *in vivo*.[39,40] However, nearly all of these technologies function on the basis of the negatively charged backbone found in native nucleic acids. Thus, the ability to impart negative charge to PNA without sacrificing binding affinity with DNA and RNA may enable the development of therapeutics that are able to take

advantage of the delivery technologies described above as well as the inherent benefits of PNA such as increased stability and enhanced binding affinity.[41] This process would open the door to previously unexplored nucleic acid-delivery vector combinations and may lead to the discovery of antisense therapeutics with enhanced *in vivo* efficacy. This concept is further supported by the recent work of Romanelli and coworkers, in which they observed the expression of antigene activity by γ-sulfate PNA delivered via cationic liposome, lipofectamine.[18]

Experimental Section

General techniques

Glassware for all reactions was oven dried or flame dried and cooled prior to use. All reactions were run under an atmosphere of nitrogen or argon unless otherwise stated. Tetrahydrofuran (THF) was distilled from sodium and benzophenone. Dichloromethane (CH_2Cl_2) and dimethylformamide (DMF) were passed through a solvent purification system (J. C. Meyer). Unless otherwise noted, all starting materials were obtained from commercial suppliers and were used without further purification. Thin layer chromatography was performed on Silica gel 60 F_{254} plates eluting with the solvent indicated, visualized by a 254/365 nm UV lamp, or stained with a solution of ninhydrin or potassium permanganate. Column chromatography was performed on Merck silica gel Kieselgel 60 (230-400 mesh, 40–63 μm particle size). Yields were calculated for material judged homogenous by thin layer chromatography and NMR. Compounds were named using CS ChemBioDraw Ultra 12.0. NMR spectra were acquired on a Varian Unity-300 or VXR 500 spectrometer. Chemical shifts for ^1H NMR spectra are reported in parts per million relative to the signal of residual $CHCl_3$ at 7.27 ppm or the center line of the residual acetone pentet at 2.05 ppm. Chemicals shifts for ^{13}C NMR spectra are reported in parts per million relative to the center line of the $CDCl_3$ triplet at 77.23 ppm or the center line of the

acetone septet at 29.9 ppm. The abbreviations s, d, dd, t, q, m, br, and rot stand for singlet, doublet, doublet of doublets, triplet, quartet, multiplet, broad, and rotamer respectively. IR spectra were obtained from Nicolet 380 FT-IR spectrometer. Optical rotations were obtained at ambient temperature on a Perkin Elmer Model 343 polarimeter (Na D line) using a microcell with a 1 decimeter path length, and the reported concentrations (c) are in g/100 ml. Mass spectra were recorded at the Mass Spectrometry facility in the Department of Chemistry of the University of Utah. DNA/RNA was purchased from the University of Utah DNA/Peptide Synthesis Core Facility. Milli-Q water was obtained from Millipore Simplicity UV water purification system.

Oligomer synthesis

PNA oligomers were synthesized on NovaSyn TGR R resin (0.2 mmol/g) according to published procedures using manual or semi-automated (Activo P-14 Peptide Synthesizer) solid-phase peptide synthesis.[27,42-45] The oligomers were cleaved from the resin using TFA:triisopropylsilane:H_2O (95:2.5:2.5) cocktail. The resulting mixtures were precipitated with ether, purified by RP-HPLC (Agilent ZORBAX 300SB-C18, 5 µM particle size, 9.4 x 250 mm) with a binary mixture of 0.1% TFA in water (eluent A) and 0.1% TFA in CH_3CN (eluent B). The linear gradient was 8-18% of eluent B for 26 min at 50 ºC at a flow rate of 4.0 mL/min. A small fraction of the purified compound was reinjected to RP-HPLC (Agilent ZORBAX 300SB-C18, 5 µM particle size, 4.6 x 250 mm) for analysis. The linear gradient was 8-18% of eluent B for 26 min at 50 ºC at a flow rate of 1.0 mL/min. PNA strands were characterized by MALDI-TOF mass spectrometry in reflectron positive mode using a Waters Micromass MALDI Micro MX. The concentrations of the PNA oligomers were determined from the OD at 260 nm recorded in a UV-VIS Spectrophotometer (SHIMADZU 1800), using the extinction coefficient 100,300 $M^{-1}cm^{-1}$ for the sequence GTAGATCACT.

UV melting studies

The thermal melting studies were performed by using the temperature dependence UV absorbance. All samples were prepared in buffer containing 10 mM sodium phosphate, pH 7.2, with added NaCl (0, 50, 100, 250, 500 1000 mM), except for the physiological buffer, which was 0.49 mM $MgCl_2{\cdot}6H_2O$, 137 mM NaCl, 2.7 mM KCl, 1.5 mM KH_2PO_4, 8.1 mM Na_2HPO_4, pH 7.4. The samples were incubated at 95 ^oC for 1 min, followed by gradual cooling to room temperature using a BioRad-MJ Mini Personal Thermal Cycler, before data collection. UV-Vis absorbance at 260 nm was recorded and corrected using the absorbance at 380 nm. The data were recorded at a rate of 1 ^oC/min, in 0.5 ^oC intervals, for both the heating (20-80 ^oC) and cooling (80-20 ^oC) runs (except PNA **3pos** from 20-90 ^oC and reverse). The T_m values were determined by taking the first derivative of the cooling profiles, using Origin 8.5.1 software. Final T_m is an average of three or four independent trials, and error bars represent the standard deviation.

Buffer preparation

Varying concentrations of NaCl were added to 10 mM phosphate buffer, pH 7.6, and initial pH measured. pH was adjusted to 7.2 using 6 M HCl or 5 M NaOH. The change of Na^+ concentration in the buffer due to NaOH is equal to or less than 0.4%.

Thermodynamic analysis

The UV melting data were analyzed to obtain van't Hoff transition enthalpies.[33,34] Baseline correction was applied to each plot of normalized absorbance vs temperature, providing plots of fraction melted (θ) vs temperature. The thermodynamic parameters were determined by plotting ln K_a vs 1/T (van't Hoff plot). Values of K_a, the affinity constant, at each temperature were determined using the following equation for bimolecular,

complementary oligonucleotides, where C_o is the initial strand concentration.

$$K_a = \frac{\theta}{\left[C_o \cdot (1-\theta)^2\right]}$$

For a two-state transition, if Δ*H* is independent of the temperature, then a plot of ln K_a vs 1/T is linear, giving -Δ*H*/R as the slope and Δ*S*/R as the y-intercept. Gibbs free energy (Δ*G*) was calculated using the following equation, where T = 298 K.

$$\Delta G = \Delta H - T\Delta S$$

Procedures and characterizations

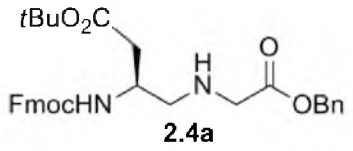

2.4a

(S)-tert-butyl3-((((9H-fluoren-9-yl)methoxy)carbonyl)amino)-4-((2-(benzyloxy)-2-oxoethyl)amino)butanoate 2.4a. To a solution of aldehyde **2.3a**[24] (1.61 mmol) in CH_2Cl_2 (20 mL), glycine benzyl ester 4-toluenesulfonate (0.652 g, 1.93 mmol) and Et_3N (0.67 mL, 4.8 mmol) were added at 0 ºC. After stirring for 30 min, sodium triacetoxy-borohydride (0.444 g, 2.09 mmol) was added and the reaction mixture was stirred at rt for 16 h. The reaction mixture was quenched with sat. $NaHCO_3$ (12 mL) and sat. Na_2CO_3 (4 mL). After stirring for 30 min, the mixture was extracted with CH_2Cl_2 (3 x 30 mL). The combined organic extracts were washed with brine, dried over Na_2SO_4, and concentrated. The crude material was purified by silica flash column chromatography (1:1 EtOAC:Hexane) to afford 0.526 g (60%, two steps from **2.2a**) of the secondary amine **2.4a** as a pale yellow oil (R_f = 0.4 in 1:1 EtOAC:Hexane); $[\alpha]_D^{25}$ = +0.4° (c 0.9, CH_2Cl_2); ^{1}H NMR (300 MHz, $CDCl_3$) δ 7.67 (d, *J* = 7.4 Hz, 2 H), 7.54-7.5 (m, 2 H), 7.33-7.17 (m, 9 H), 5.54 (br d, *J* = 8.4 Hz, 1 H), 5.08 (s, 2 H), 4.31 (d, *J* = 6.7 Hz, 2 H), 4.14 (t, *J* = 6.7 Hz, 1 H), 3.97 (br s, 1 H), 3.38 (d, *J* = 3.7 Hz, 2 H), 2.78-2.62 (m, 2 H), 2.51-2.38 (m, 2

H), 1.88 (br s, 1 H), 1.37 (s, 9 H); ^{13}C NMR (125 MHz, $CDCl_3$) 172.2, 170.9, 156.1, 143.8, 141.2, 135.5, 128.5, 128.32, 128.27, 127.6, 127, 125, 119.9, 81, 66.6, 64, 52, 50.5, 50.1, 47.2, 37.2, 28; IR (neat): 3330, 2975, 1724, 1521, 1450, 1251, 1158 cm^{-1}; HRMS (ESI) *m/z* for $C_{32}H_{36}N_2O_6$: 567.2477 (calcd $[M+Na]^+$ 567.2471).

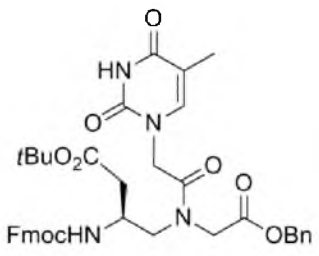

2.5a

(S)-tert-butyl3-((((9H-fluoren-9-yl)methoxy)carbonyl)amino)-4-(N-(2-(benzyloxy)-2-oxoethyl)-2-(5-methyl-2,4-dioxo-3,4-dihydropyrimidin-1(2H)-yl)acetamido)butanoate 2.5a. To a solution of thymine-1-acetic acid (0.059 g, 0.32 mmol), HATU (0.122 g, 0.320 mmol) and 4 Å MS in DMF (0.9 mL) at 0 °C, DIPEA (0.060 ml, 0.32 mmol) was added. After stirring at 0 °C for 15 min, a solution of secondary amine **2.4a** (0.146 g, 0.267 mmol) in CH_2Cl_2 (1.5 mL) was added and stirred at 0 °C for 10 min. After stirring at rt for 16 h, the reaction mixture was concentrated and washed with H_2O. The aqueous layer was extracted with EtOAc (3x). The combined organic extracts were washed with sat. NH_4Cl, sat. $NaHCO_3$, and brine, dried over Na_2SO_4, and concentrated. The crude mixture was purified by silica flash column chromatography (a gradient of EtOAC:Hexane from 3:7 to 8:2) to afford 0.037 g (20%) starting secondary amine **2.4a** and 0.097 g (51%) of amide **2.5a** as a pale yellow oil (R_f = 0.5 in 8:2 EtOAC:Hexane); $[\alpha]_D^{25}$ = +5.5° (c 0.2, CH_2Cl_2); ^{1}H NMR (500 MHz, $CDCl_3$) δ 9.7 (s, 0.6 H, rot 1), 9.66 (s, 0.4 H, rot 2), 7.62 (d, *J* = 7.7 Hz, 2 H), 7.49-7.46 (m, 2 H), 7.31-7.24 (m, 5 H), 7.23-7.15 (m, 4 H), 6.83 (s, 0.6 H, rot 1), 6.73 (s, 0.4 H, rot 2), 6.27 (d, *J* = 8.4 Hz, 0.5 H, rot 1), 5.81 (d, *J* = 8.4 Hz, 0.4 H, rot 2), 5.1 (s, 0.8 H, rot 1), 5.0 (s, 1.2 H, rot 2), 4.56 (s, 1 H, rot

1), 4.34-4.22 (m, 3 H), 4.2-4.0 (m, 4 H), 3.6-3.4 (m, 2 H), 2.56-2.49 (m, 1.2 H, rot 1), 2.44-2.34 (m, 0.8 H, rot 2), 1.73 (s, 1.7 H, rot 1), 1.72 (s, 1.3 H, rot 2), 1.34 (s, 5 H, rot 1), 1.32(s, 4 H, rot 2); ^{13}C NMR$_{\text{major rotamer}}$ (125 MHz, $CDCl_3$) 170.7, 169.1, 168.5, 168, 156.4, 151.5, 144, 143.8, 141.4, 135.2, 128.9, 128.7, 128.3, 127.8, 127.2, 125.2, 120.1, 110.7, 82, 67.3, 66.8, 51, 49.2, 47.9, 47.4, 47.2, 37.4, 28.1, 12.4; IR (neat): 3335, 2924, 1720, 1522, 1450, 1248, 1155 cm^{-1}; HRMS (ESI) *m/z* for $C_{39}H_{42}N_4O_9$: 733.2841 (calcd $[M+Na]^+$ 733.2849).

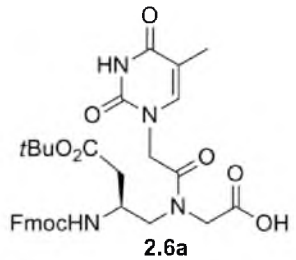

2.6a

(S)-2-(N-(2-((((9H-fluoren-9-yl)methoxy)carbonyl)amino)-4-(tert-butoxy)-4-oxobutyl)-2-(5-methyl-2,4-dioxo-3,4-dihydropyrimidin-1(2H)-yl)acetamido)acetic acid 2.6a. To a solution of amide **2.5a** (0.098 g, 0.14 mmol) in MeOH (5 mL) was added Pd/C (0.010 g) under N_2. The flask was evacuated, then flushed with H_2 gas. The reaction mixture was placed under H_2 (balloon pressure). After stirring for 16 h, the reaction mixture was filtered through a pad of Celite® and evaporated under reduced pressure to give 0.068 g (80%) of the modified peptide nucleic acid monomer **2.6a** as a white solid (R_f = 0.1 in 9:1 CH_2Cl_2:MeOH); mp = 88-90 °C; $[\alpha]_D^{25}$ = +2.4° (c 0.5, CH_3OH); ^{1}H NMR (500 MHz, acetone-d6) δ 10.67 (br s, 1 H), 7.82 (d, *J* = 6.8 Hz, 2 H), 7.66 (d, *J* = 4.9 Hz, 2 H), 7.38-7.23 (m, 5 H), 6.95 (br s, 0.5 H, rot 1), 6.7 (br s, 0.5 H, rot 2), 4.92-4.76 (br m, 1 H), 4.59 (br s, 1.6 H, rot 1), 4.43 (br s, 0.4 H, rot 2), 4.38-4.32 (partially obscured br m, 1.4 H, rot 1,2), 4.28 (partially obscured br s, 1.6 H, rot 1), 4.24-4.1 (partially obscured br m, 2 H), 3.91 (dd, *J* = 6.8 Hz, 0.5 H, rot 1), 3.64-3.54 (partially obscured m, 1 H, rot 1,2),

3.39 (dd, *J* = 6.8 Hz, 0.5 H, rot 2), 2.6-2.48 (m, 2 H), 1.74 (br s, 3 H), 1.42 (s, 4 H, rot 1), 1.39(s, 5 H, rot 2); ^{13}C $NMR_{major\ rotamer}$ (125 MHz, acetone-d6) 171, 169.4, 168.8, 165.5, 157.1, 152.5, 144.8, 143.1, 141.9, 128.5, 127.8, 124.9, 120.8, 110.3, 81.2, 67.4, 52 (br), 49.2 (br), 48.4, 47.9, 47.8, 43, 28.2, 12.3; IR (neat): 2978, 1662, 1477, 1230, 1155 cm^{-1}; HRMS (ESI) *m/z* for $C_{32}H_{36}N_4O_9$: 643.2396 (calcd $[M+Na]^+$ 643.2380).

References

(1) *Peptide Nucleic Acids: Protocols and Applications*, 2nd ed.; Nielsen, P. E., Ed.; Horizon Bioscience: United Kingdom, 2004.

(2) Nielsen, P. E.; Egholm, M.; Berg, R. H.; Buchardt, O. Sequence-Selective Recognition of DNA by Strand Displacement with a Thymine-Substituted Polyamide. *Science* **1991**, *254*, 1497-1500.

(3) Egholm, M.; Buchardt, O.; Christensen, L.; Behrens, C.; Freier, S. M.; Driver, D. A.; Berg, R. H.; Kim, S. K.; Norden, B.; Nielsen, P. E. PNA Hybridizes to Complementary Oligonucleotides Obeying the Watson–Crick Hydrogen-Bonding Rules. *Nature* **1993**, *365*, 566-568.

(4) Peyman, A.; Uhlmann, E.; Wagner, K.; Augustin, S.; Weiser, C.; Will, D. W.; Breipohl, G. PHONA – PNA Co-Oligomers: Nucleic Acid Mimetics with Interesting Properties. *Angew. Chem., Int. Ed.* **1997**, *36*, 2809-2812.

(5) Efimov, V. A.; Choob, M. V.; Buryakova, A. A.; Kalinkina, A. L.; Chakhmakhcheva, O. G. Synthesis and Evaluation of Some Properties of Chimeric Oligomers Containing PNA and Phosphono-PNA Residues. *Nucleic Acids Res.* **1998**, *26*, 566-575.

(6) Efimov, V. A.; Chakhmakhcheva, O. G.; Wickstrom, E. Synthesis and Application of Negatively Charged PNA Analogues. *Nucleosides, Nucleotides Nucleic Acids* **2005**, *24*, 1853-1874.

(7) Haaima, G.; Lohse, A.; Buchardt, O.; Nielsen, P. E. Peptide Nucleic Acids (PNAs) Containing Thymine Monomers Derived from Chiral Amino Acids: Hybridization and Solubility Properties of D-Lysine PNA. *Angew. Chem., Int. Ed.* **1996**, *35*, 1939-1942.

(8) Sforza, S.; Haaima, G.; Marchelli, R.; Nielsen, P. E. Chiral Peptide Nucleic Acids (PNAs): Helix Handedness and DNA Recognition. *Eur. J. Org. Chem.* **1999**, *1999*, 197-204.

(9) Zhou, P.; Wang, M.; Du, L.; Fisher, G. W.; Waggoner, A.; Ly, D. H. Novel Binding and Efficient Cellular Uptake of Guanidine-Based Peptide Nucleic Acids (GPNA). *J. Am. Chem. Soc.* **2003**, *125*, 6878-6879.

(10) Englund, E. A.; Appella, D. H. γ-Substituted Peptide Nucleic Acids Constructed from L-Lysine are a Versatile Scaffold for Multifunctional Display. *Angew. Chem., Int. Ed.* **2007**, *46*, 1414-1418.

(11) Kleiner, R. E.; Brudno, Y.; Birnbaum, M. E.; Liu, D. R. DNA-Templated Polymerization of Side-Chain-Functionalized Peptide Nucleic Acid Aldehydes. *J. Am. Chem. Soc.* **2008**, *130*, 4646-4659.

(12) Sahu, B.; Chenna, V.; Lathrop, K. L.; Thomas, S. M.; Zon, G.; Livak, K. J.; Ly, D. H. Synthesis of Conformationally Preorganized and Cell-Permeable Guanidine-Based γ-Peptide Nucleic Acids (γGPNAs). *J. Org. Chem.* **2009**, *74*, 1509-1516.

(13) Sahu, B.; Sacui, I.; Rapireddy, S.; Zanotti, K. J.; Bahal, R.; Armitage, B. A.; Ly, D. H. Synthesis and Characterization of Conformationally Preorganized, (*R*)-Diethylene Glycol-Containing γ-Peptide Nucleic Acids with Superior Hybridization Properties and Water Solubility. *J. Org. Chem.* **2011**, *76*, 5614-5627.

(14) Mitra, R.; Ganesh, K. N. PNAs Grafted with (α/γ, *R*/*S*)-Aminomethylene Pendants: Regio and Stereo Specific Effects on DNA Binding and Improved Cell Uptake. *Chem. Commun.* **2011**, *47*, 1198-1200.

(15) Crawford, M. J.; Rapireddy, S.; Bahal, R.; Sacui, I.; Ly, D. H. Effect of Steric Constraint at the γ-Backbone Position on the Conformations and Hybridization Properties of PNAs. *J. Nucleic Acids* **2011**, *2011*, 10.

(16) Dragulescu-Andrasi, A.; Rapireddy, S.; Frezza, B. M.; Gayathri, C.; Gil, R. R.; Ly, D. H. A Simple γ-Backbone Modification Preorganizes Peptide Nucleic Acid into a Helical Structure. *J. Am. Chem. Soc.* **2006**, *128*, 10258-10267.

(17) Yeh, J. I.; Shivachev, B.; Rapireddy, S.; Crawford, M. J.; Gil, R. R.; Du, S.; Madrid, M.; Ly, D. H. Crystal Structure of Chiral γPNA with Complementary DNA Strand: Insights into the Stability and Specificity of Recognition and Conformational Preorganization. *J. Am. Chem. Soc.* **2010**, *132*, 10717-10727.

(18) Avitabile, C.; Moggio, L.; Malgieri, G.; Capasso, D.; Di Gaetano, S.; Saviano, M.; Pedone, C.; Romanelli, A. γ Sulphate PNA (PNA S): Highly Selective DNA Binding Molecule Showing Promising Antigene Activity. *PLoS ONE* **2012**, *7*, e35774.

(19) Schildkraut, C.; Lifson, S. Dependence of the Melting Temperature of DNA on Salt Concentration. *Biopolymers* **1965**, *3*, 195-208.

(20) Gong, H.; Freed, K. F. Langevin-Debye Model for Nonlinear Electrostatic Screening of Solvated Ions. *Phys. Rev. Lett.* **2009**, *102*, 057603.

(21) De Costa, N. T. S.; Heemstra, J. M. Evaluating the Effect of Ionic Strength on Duplex Stability for PNA Having Negatively or Positively Charged Side Chains. *PLoS ONE* **2013**, *8*, e58670.

(22) Grimm, E. L.; Roy, B.; Aspiotis, R.; Bayly, C. I.; Nicholson, D. W.; Rasper, D. M.; Renaud, J.; Roy, S.; Tam, J.; Tawa, P.; Vaillancourt, J. P.; Xanthoudakis, S.; Zamboni, R. J. Solid Phase Synthesis of Selective Caspase-3 Peptide Inhibitors. *Bioorg. Med. Chem.* **2004**, *12*, 845-851.

(23) Parikh, J. R.; Doering, W. v. E. Sulfur Trioxide in the Oxidation of Alcohols by Dimethyl Sulfoxide. *J. Am. Chem. Soc.* **1967**, *89*, 5505-5507.

(24) Boxer, M. B.; Quinn, A. M.; Shen, M.; Jadhav, A.; Leister, W.; Simeonov, A.; Auld, D. S.; Thomas, C. J. A Highly Potent and Selective Caspase 1 Inhibitor that Utilizes a Key 3-Cyanopropanoic Acid Moiety. *ChemMedChem* **2010**, *5*, 730-738.

(25) Boyarskaya, N. P.; Kirillova, Y. G.; Stotland, E. A.; Prokhorov, D. I.; Zvonkova, E. N.; Shvets, V. I. Synthesis of Two New Thymine-Containing Negatively Charged PNA Monomers. *Dokl. Chem.* **2006**, *408*, 57-60.

(26) Wu, Y.; Xu, J.-C. Synthesis of Chiral Peptide Nucleic Acids Using Fmoc Chemistry. *Tetrahedron* **2001**, *57*, 8107-8113.

(27) Braasch, D. A.; Nulf, C. J.; Corey, D. R. Synthesis and Purification of Peptide Nucleic Acids. *Curr. Protoc. Nucleic Acid Chem.* **2002**, 4.11.11-14.11.18.

(28) Tomac, S.; Sarkar, M.; Ratilainen, T.; Wittung, P.; Nielsen, P. E.; Nordén, B.; Gräslund, A. Ionic Effects on the Stability and Conformation of Peptide Nucleic Acid Complexes. *J. Am. Chem. Soc.* **1996**, *118*, 5544-5552.

(29) Rapireddy, S.; He, G.; Roy, S.; Armitage, B. A.; Ly, D. H. Strand Invasion of Mixed-Sequence B-DNA by Acridine-Linked, γ-Peptide Nucleic Acid (γ-PNA). *J. Am. Chem. Soc.* **2007**, *129*, 15596-15600.

(30) He, G.; Rapireddy, S.; Bahal, R.; Sahu, B.; Ly, D. H. Strand Invasion of Extended, Mixed-Sequence B-DNA by γPNAs. *J. Am. Chem. Soc.* **2009**, *131*, 12088-12090.

(31) Rapireddy, S.; Bahal, R.; Ly, D. H. Strand Invasion of Mixed-Sequence, Double-Helical B-DNA by γ-Peptide Nucleic Acids Containing G-Clamp Nucleobases under Physiological Conditions. *Biochemistry* **2011**, *50*, 3913-3918.

(32) Dulbecco, R.; Vogt, M. Plaque Formation and Isolation of Pure Lines with Poliomyelitis Viruses. *J. Exp. Med.* **1954**, *99*, 167-182.

(33) Mergny, J.-L.; Lacroix, L. Analysis of Thermal Melting Curves. *Oligonucleotides* **2003**, *13*, 515-537.

(34) Marky, L. A.; Breslauer, K. J. Calculating Thermodynamic Data for Transitions of any Molecularity from Equilibrium Melting Curves. *Biopolymers* **1987**, *26*, 1601-1620.

(35) Manning, G. S. On the Application of Polyelectrolyte "Limiting Laws" to the Helix-Coil Transition of DNA. I. Excess Univalent Cations. *Biopolymers* **1972**, *11*, 937-949.

(36) Hyrup, B.; Egholm, M.; Buchardt, O.; Nielsen, P. E. A Flexible and Positively Charged PNA Analogue with an Ethylene-Linker to the Nucleobase: Synthesis and Hybridization Properties. *Bioorg. Med. Chem. Lett.* **1996**, *6*, 1083-1088.

(37) Topham, C. M.; Smith, J. C. Orientation Preferences of Backbone Secondary Amide Functional Groups in Peptide Nucleic Acid Complexes: Quantum Chemical Calculations Reveal an Intrinsic Preference of Cationic D-Amino Acid-Based Chiral PNA Analogues for the P-form. *Biophys. J.* **2007**, *92*, 769-786.

(38) Gourishankar, A.; Ganesh, K. N. (α,α-dimethyl)glycyl (*dmg*) PNAs: Achiral PNA Analogs that Form Stronger Hybrids with cDNA Relative to Isosequential RNA. *Artificial DNA: PNA & XNA* **2012**, *3*, 5-13.

(39) Whitehead, K. A.; Langer, R.; Anderson, D. G. Knocking Down Barriers: Advances in siRNA Delivery. *Nat. Rev. Drug Discov.* **2009**, *8*, 129-138.

(40) Juliano, R.; Alam, M. R.; Dixit, V.; Kang, H. Mechanisms and Strategies for Effective Delivery of Antisense and siRNA Oligonucleotides. *Nucleic Acids Res.* **2008**, *36*, 4158-4171.

(41) Shiraishi, T.; Hamzavi, R.; Nielsen, P. E. Subnanomolar Antisense Activity of Phosphonate-Peptide Nucleic Acid (PNA) Conjugates Delivered by Cationic Lipids to HeLa cells. *Nucleic Acids Res.* **2008**, *36*, 4424-4432.

(42) Merrifield, R. B. Solid Phase Peptide Synthesis. I. The Synthesis of a Tetrapeptide. *J. Am. Chem. Soc.* **1963**, *85*, 2149-2154.

(43) Thomson, S. A.; Josey, J. A.; Cadilla, R.; Gaul, M. D.; Fred Hassman, C.; Luzzio, M. J.; Pipe, A. J.; Reed, K. L.; Ricca, D. J.; Wiethe, R. W.; Noble, S. A. Fmoc Mediated Synthesis of Peptide Nucleic Acids. *Tetrahedron* **1995**, *51*, 6179-6194.

(44) Coin, I.; Beyermann, M.; Bienert, M. Solid-Phase Peptide Synthesis: from Standard Procedures to the Synthesis of Difficult Sequences. *Nat. Protoc.* **2007**, *2*, 3247-3256.

(45) Joshi, R.; Jha, D.; Su, W.; Engelmann, J. Facile Synthesis of Peptide Nucleic Acids and Peptide Nucleic Acid-Peptide Conjugates on an Automated Peptide Synthesizer. *J. Pept. Sci.* **2011**, *17*, 8-13.

CHAPTER 3

DIFFERENTIAL DNA AND RNA SEQUENCE DISCRIMINATION BY PNA HAVING CHARGED SIDE CHAINS[1]

Introduction

Peptide nucleic acid (PNA)[1] is a nucleic acid mimic that shows excellent potential for use in therapeutic and biosensing applications, due to its high binding affinity and selectivity for DNA and RNA.[2-4] PNA also benefits from excellent biostability, as the native nucleic acid sugar-phosphate backbone is replaced by an *N*-(2-aminoethyl)glycine unit.[5] A number of modifications have been made to the PNA backbone to enhance binding affinity, cellular uptake, and solubility.[6,7] Addition of side chains at the γ-position of the PNA backbone has proven to be particularly successful, as this modification increases binding affinity by preorganizing the backbone,[8] and enables a diverse range of chemical functionalities to be incorporated via simple amino acid building blocks.[9,10]

The Heemstra group is currently investigating PNAs having negatively charged γ-substituents, as these would electrostatically mimic DNA and RNA, and thus likely be compatible with conventional nucleic acid delivery technologies. In Chapter 2, we explored the effect of ionic strength on binding affinity for PNA having either negatively charged aspartic acid side chains or positively charged lysine side chains.[11] We observed that as ionic strength is increased, negatively charged PNA increases in

---

[1] Reprinted from *Bioorg. Med. Chem. Lett.*, 24, De Costa, N. T. S., Heemstra, J. M., Differential DNA and RNA Sequence Discrimination by PNA Having Charged Side Chains, 2360-2363, Copyright (2014), with permission from Elsevier.

affinity for DNA and RNA, whereas positively charged PNA decreases in affinity for DNA and RNA. Interestingly, the point at which these trends intersect hovers near physiological salt concentration. And, in simulated physiological buffer, negatively charged PNA shows slightly higher affinity for RNA whereas positively charged PNA shows slightly higher affinity for DNA.

Intrigued by the effect of side chain structure and electrostatics on binding affinity, we were also curious to explore the mismatch and orientation selectivity of these γ-substituted PNAs. In this chapter, we report that side chain structure also plays a surprising role in PNA binding selectivity. We find that introduction of γ-substituents results in similar or slightly decreased selectivity compared to unmodified PNA. However, for γ-substituted PNAs, positively charged side chains provide higher selectivity in DNA binding and negatively charged side chains provide higher selectivity in RNA binding.[12]

Results and Discussion

Structure and sequence of modified PNA strands

To investigate the role of side chain structure and electrostatics on sequence selectivity, we utilized our previous γ-functionalized sequences, PNA **3neg** and PNA **3pos** (Figure 3.1).[11,12] These sequences have three aspartic acid or lysine side chains, respectively, distributed across the well-studied Nielsen decamer sequence (Table 3.1).[4] The thermal melting stability of PNA **3neg,** PNA **3pos**, and unmodified PNA **nf** with complementary, single base mismatched, and parallel DNA and RNA sequences under simulated physiological salt conditions were measured. The complementary, antiparallel DNA **1** and RNA **1** sequences contain X=A, whereas the mismatched sequences contain X=G, C, or T/U. The mismatch was introduced in the middle of the sequence,[13]

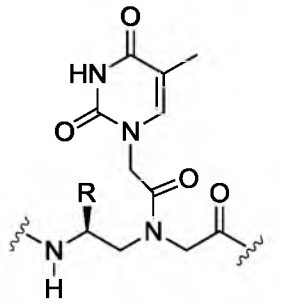

T : R = H
T_D: R = $CH_2CO_2^-$
T_K: R = $(CH_2)_4NH_3^+$

Figure 3.1. Chemical structure of γ-substituted PNA monomers.

Table 3.1. PNA, DNA, and RNA sequences.

Name	Sequence
PNA **nf**	H-GTAGATCACT-NH_2
PNA **3neg**	H-GT_DAGAT_DCACT_D-NH_2
PNA **3pos**	H-GT_KAGAT_KCACT_K-NH_2
DNA **1** (X = A,G,C,T)	5'-AGTGXTCTAC-3'
DNA **2**	5'-CATCTAGTGA-3'
DNA **3** (Y = T,C)	5'-AGTGAYCTAC-3'
RNA **1** (X = A,G,C,U)	5'-AGUGXUCUAC-3'
RNA **2**	5'-CAUCUAGUGA-3'
RNA **3** (Y = U,C)	5'-AGUGAYCUAC-3'

and was positioned opposite a γ-functionalized PNA monomer, as this was anticipated to maximize the impact of side chain structure on duplex stability. Sequences DNA **2** and RNA **2** are fully complementary to the PNA strands, but form duplexes in the less stable parallel orientation. The mismatch and orientation selectivity of γ-PNA having three neutral side chains (PNA **3Me**) were not examined; as discussed in Chapter 2, due to the unreliable data, which likely resulted from the aggregation of the sample.

The effect of side chain structure on mismatch and antiparallel versus parallel discrimination

We first investigated the effect of side chain structure on mismatch and antiparallel versus parallel discrimination in PNA:DNA duplexes. As shown in Figure 3.2a and Table 3.2a, PNA **nf** and PNA **3pos** showed similar levels of duplex destabilization after the introduction of a single base mismatch or reversal of strand orientation. However, the selectivity of PNA **3neg** is significantly lower, as evidenced by the smaller net ΔT_m values. In the case of PNA:RNA duplexes, we found that the effects of side chain electrostatics were reversed, as PNA **nf** and PNA **3neg** show similar levels of duplex destabilization upon introduction of a single base mismatch or reversal of strand orientation, and as the selectivity of PNA **3pos** is significantly lower (Figure 3.2b, Table 3.2b). In previous work by Ly and coworkers, positively charged guanidinium PNAs (GPNAs) have also exhibited a similar trend in binding by having a greater destabilization for most of the mismatched DNA over RNA sequences.[14]

Previous studies have been performed to understand the unmodified PNA:DNA sequence selectivity, in terms of best and worst mismatched base pairs, but data are quite contradictory at times since the impact created by mismatches varies with the contexts.[13] We were also curious to see whether the variation in the mismatched base from X=G, C, or T/U showed any significant trend. In comparing the identity of the mismatched base and the ΔT_m, we expected that X=G would result in a smaller duplex destabilization than X=C or X=T/U, as the T:G mismatch can still form a wobble base pair.[13,15,16] The data in Figure 3.2 show that this is the case for the PNA:RNA duplexes, but the PNA:DNA duplexes show a relative insensitivity to the identity of the mismatched base. Previous studies have observed quite inconsistent results for T:T mismatch, with T:T mismatch being either the most stable or the most unstable in considering the

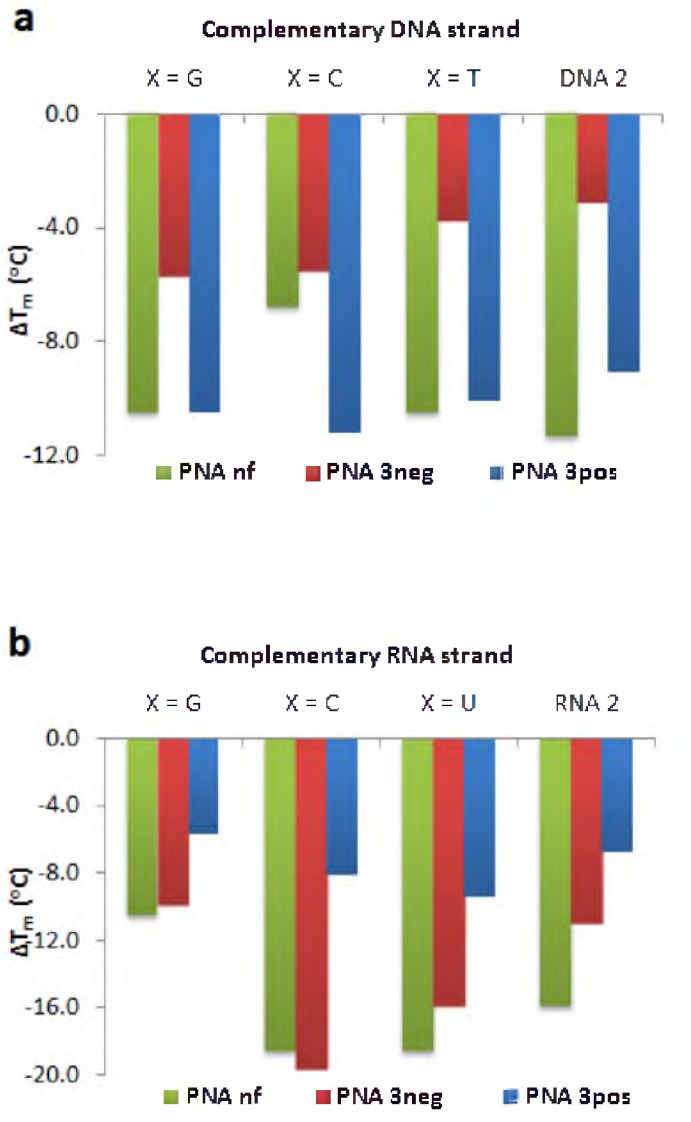

Figure 3.2. Comparative ΔT_m values of duplexes of PNA (**nf**/**3neg**/**3pos**) with mismatched and parallel sequences of (a) DNA and (b) RNA.

Table 3.2. T_m (°C) of (a) PNA:DNA and (b) PNA:RNA duplexes under simulated physiological buffer conditions.*

(a)	DNA 1 (X = A)	DNA 1 (X = G)	DNA 1 (X = C)	DNA 1 (X = T)	DNA 2
PNA **nf**	43.0 ± 0.7	32.5 ± 0.1	36.2 ± 0.3	32.5 ± 0.7	31.7 ± 1.5
PNA **3neg**	46.3 ± 0.7	40.6 ± 0.3	40.8 ± 1.0	42.6 ± 1.4	43.2 ± 0.8
PNA **3pos**	49.1 ± 1.0[a]	38.6 ± 1.3	37.9 ± 0.4	39.0 ± 0.7	40.0 ± 1.3

(b)	RNA 1 (X = A)	RNA 1 (X = G)	RNA 1 (X = C)	RNA 1 (X = U)	RNA 2
PNA **nf**	47.1 ± 1.1[a]	36.6 ± 0.4	28.5 ± 0.7	28.5 ± 0.7	31.2 ± 1.2
PNA **3neg**	49.9 ± 1.5[a]	40.0 ± 1.3	30.3 ± 1.0	34.0 ± 0.8	39.0 ± 1.1
PNA **3pos**	46.5 ± 1.7[a]	40.8 ± 1.3	38.4 ± 0.7	37.1 ± 1.2	39.7 ± 0.7

*Conditions: 3 μM PNA, 3 μM DNA or RNA, 0.49 mM $MgCl_2 \cdot 6H_2O$, 137 mM NaCl, 2.7 mM KCl, 1.5 mM KH_2PO_4, 8.1 mM Na_2HPO_4, pH 7.4. Errors represent standard deviation of three independent trials. [a]From Chapter 2.

stacking (size).[13] We observed T:T mismatch to be the most unstable in all three PNA:RNA duplexes, but only for some PNA:DNA duplexes.

Previous studies conducted on PNAs having neutral or positively charged γ-substituents have shown that modified PNAs have similar or improved selectivity relative to unmodified PNA.[8-10,14,16-19] The data presented here deviate from this trend, as in most cases PNA **nf** shows equal or higher binding selectivity relative to the γ-substituted PNAs. One potential source of this difference is the number of γ-substituents present in our PNA sequences. However, in the previous reports, substitution densities ranging from 1 to 10 substituents over a 10-mer sequence were investigated. Thus, it is unlikely that our choice of sequences having 3 substituents is the source of the observed deviation. Since previous studies investigated PNA strands having a structurally-diverse range of side chains,[8-10,14,16-19] our specific choices of aspartic acid and lysine are likely not the source of the observed deviation. Rather, in nearly all of the previous studies, duplex stability was measured at ionic strengths that were significantly weaker than the physiological salt conditions used in the current study. In fact, the studies which used

the lowest ionic strength resulted in the greatest observed selectivity for γ-substituted PNA relative to unmodified PNA.[16,18,19]

We and others have previously observed that ionic strength plays a significant role in PNA:DNA and PNA:RNA duplex stability,[11,20] and for unmodified PNA, the highest stability is observed at the lowest ionic strength due to the polyelectrolyte behaviour of PNA duplexes. The stability of a mismatched PNA:DNA duplex is nearly the same at low and high ionic strengths. However, the presence of mismatches prevent the duplex stabilization at low ionic strength, thus sequence selectivity with DNA has been shown to be highest at low ionic strength.[21,22] Hence, we hypothesize that the relatively higher ionic strength of the simulated physiological buffer is primarily responsible for the difference between our results and those reported in previous studies.

Thermodynamic data analysis

Thermodynamic parameters for duplex formation of PNA **3neg** and PNA **3pos** with DNA and RNA were derived using van't Hoff analysis of the UV thermal melting data (Tables 3.3-3.6).[23] As expected, the calculated ΔG values mirror the measured T_m values for each duplex, with reduced Gibbs free energy gain in duplexes having lower values of T_m. In general, duplex formation with mismatched or parallel sequences experienced a lower enthalpic driving force; but this was partially compensated for by a reduced entropic cost, except for the PNA **3pos**:RNA duplexes with X=G and RNA **2**. This result is logical, as the introduction of mismatches reduces the enthalpy gained from Watson-Crick base-pairing interactions, and the conformational freedom gained from loss of these interactions would be expected to be entropically favorable.[13] This enthalpy-entropy compensation could result from combined effects of interruption of

Table 3.3. Thermodynamic parameters for the formation of duplexes of PNA **3neg** with DNA.*

Duplex	T_m (°C)	ΔG (kJ•mol^{-1})	ΔH (kJ•mol^{-1})	TΔS (kJ•mol^{-1})
DNA **1** (X = A)	46.3 ± 0.7	-48.0 ± 0.1	-200.2 ± 6.2	-152.2 ± 6.2
DNA **1** (X = G)	40.6 ± 0.3 (-5.7)	-45.6 ± 0.1 (2.4)	-151.4 ± 5.3 (48.8)	-105.7 ± 5.1 (46.5)
DNA **1** (X = C)	40.8 ± 1.0 (-5.5)	-46.2 ± 0.5 (1.8)	-167.7 ± 15.7 (32.5)	-121.5 ± 15.2 (30.7)
DNA **1** (X = T)	42.6 ± 1.4 (-3.7)	-45.9 ± 0.3 (2.1)	-175.1 ± 9.4 (25.1)	-129.2 ± 9.3 (23.0)
DNA **2**	43.2 ± 0.8 (-3.1)	-46.4 ± 0.2 (1.6)	-172.7 ± 12.6 (27.5)	-126.3 ± 12.4 (25.9)

Table 3.4. Thermodynamic parameters for the formation of duplexes of PNA **3pos** with DNA.*

Duplex	T_m (°C)	ΔG (kJ•mol^{-1})	ΔH (kJ•mol^{-1})	TΔS (kJ•mol^{-1})
DNA **1** (X = A)	49.1 ± 1.0[11]	-50.2 ± 0.4	-217.0 ± 2.1	-166.8 ± 2.2
DNA **1** (X = G)	38.6 ± 1.3 (-10.5)	-44.9 ± 0.4 (5.3)	-162.9 ± 5.5 (54.1)	-118.0 ± 5.2 (48.8)
DNA **1** (X = C)	37.9 ± 0.4 (-11.2)	-44.8 ± 0.2 (5.4)	-183.3 ± 14.1 (33.7)	-138.5 ± 14.1 (28.3)
DNA **1** (X = T)	39.0 ± 0.7 (-10.1)	-45.2 ± 0.3 (5.0)	-177.2 ± 7.1 (39.8)	-132.0 ± 6.9 (34.8)
DNA **2**	40.0 ± 1.3 (-9.1)	-45.7 ± 0.4 (4.5)	-188.5 ± 4.4 (28.5)	-142.8 ± 4.4 (24.0)

Table 3.5. Thermodynamic parameters for the formation of duplexes of PNA **3neg** with RNA.*

Duplex	T_m (°C)	ΔG (kJ•mol^{-1})	ΔH (kJ•mol^{-1})	TΔS (kJ•mol^{-1})
RNA **1** (X = A)	49.9 ± 1.5[11]	-49.7 ± 0.9	-211.3 ± 5.1	-161.6 ± 4.3
RNA **1** (X = G)	40.0 ± 1.3 (-9.9)	-45.8 ± 0.1 (3.9)	-197.9 ± 13.3 (13.4)	-152.2 ± 13.4 (9.4)
RNA **1** (X = C)	30.3 ± 1.0 (-19.6)	-41.2 ± 0.1[a] (8.5)	-125.5 ± 1.2[a] (85.8)	-84.4 ± 1.3[a] (77.2)
RNA **1** (X = U)	34.0 ± 0.8 (-15.9)	-42.0 ± 0.4[b] (7.7)	-128.6 ± 6.9[b] (82.7)	-86.6 ± 6.5[b] (75.0)
RNA **2**	39.0 ± 1.1 (-10.9)	-45.1 ± 0.5 (4.6)	-147.3 ± 9.7 (64.0)	-102.2 ± 9.3 (59.4)

Data were calculated over a temperature range of [a]7-85 °C and [b]15-85 °C.

Table 3.6. Thermodynamic parameters for the formation of duplexes of PNA **3pos** with RNA.*

Duplex	T_m (°C)	ΔG (kJ•mol^{-1})	ΔH (kJ•mol^{-1})	TΔS (kJ•mol^{-1})
RNA **1** (X = A)	46.5 ± 1.7[11]	-47.6 ± 0.8	-186.2 ± 6.0	-138.5 ± 5.3
RNA **1** (X = G)	40.8 ± 1.3 (-5.7)	-46.2 ± 0.5 (1.4)	-203.2 ± 0.8 (-17.0)	-157.0 ± 0.3 (-18.5)
RNA **1** (X = C)	38.4 ± 0.7 (-8.1)	-44.8 ± 0.2 (2.8)	-167.4 ± 1.9 (18.8)	-122.6 ± 2.1 (15.9)
RNA **1** (X = U)	37.1 ± 1.2 (-9.4)	-45.9 ± 0.5 (1.7)	-158.3 ± 5.2 (27.9)	-112.4 ± 5.7 (26.1)
RNA **2**	39.7 ± 0.7 (-6.8)	-45.5 ± 0.4 (2.1)	-187.6 ± 4.4 (-1.4)	-142.1 ± 4.1 (-3.6)

*Averages from van't Hoff analysis of UV melting data. Errors represent standard deviation of three or four independent trials. Red colored values in parenthesis represent the difference with respect to the matched, antiparallel sequence.

base pair formation and stacking, as well as rearrangement of solvent molecules and ions.

The effect of varying the position of the mismatch site relative to the side chains on mismatch discrimination

In an effort to study the generality of the observed trends, we shifted the mismatched base by one position, so that it was still in the middle of the duplex but opposite an unmodified PNA monomer. We chose to investigate the A:C mismatch at this position, as this was the most suitable mismatched pair for direct comparison to the data in Table 3.2. The complementary, antiparallel DNA **3** and RNA **3** sequences contain Y=T/U, whereas the mismatched sequences contain Y=C. We found that again PNA **3pos** showed higher selectivity for DNA and PNA **3neg** showed higher selectivity for RNA (Table 3.7).

Table 3.7. T_m data (°C) of PNA:DNA **3**/RNA **3** duplexes under simulated physiological salt conditions.*

	T_m with DNA (°C)		T_m with RNA (°C)	
	DNA **3** (Y = T)	DNA **3** (Y = C)	RNA **3** (Y = U)	RNA **3** (Y = C)
PNA **nf**	43.0 ± 0.7	32.7 ± 1.0 (-10.3)	47.1 ± 1.1[a]	30.1 ± 1.0 (-17.0)
PNA **3neg**	46.3 ± 0.7	44.3 ± 0.7 (-2.0)	49.9 ± 1.5[a]	37.9 ± 0.4 (-12.0)
PNA **3pos**	49.1 ± 1.0[a]	38.1 ± 1.4 (-11.0)	46.5 ± 1.7[a]	36.0 ± 0.4 (-10.5)

*Conditions: 3 μM PNA, 3 μM DNA or RNA, 0.49 mM $MgCl_2 \cdot 6H_2O$, 137 mM NaCl, 2.7 mM KCl, 1.5 mM KH_2PO_4, 8.1 mM Na_2HPO_4, pH 7.4. Errors represent standard deviation of three independent trials. [a]From Chapter 2.

Structural analysis by circular dichroism (CD) spectroscopy

We initially hypothesized that the difference in selectivity between PNA **3neg** and PNA **3pos** may be due to differences in duplex structure caused by the charged side chains. Using CD spectroscopy, we first analysed each of the PNA strands alone in simulated physiological buffer conditions (Figure 3.3). As expected, achiral PNA **nf** shows no CD signal; but γ-modified PNAs **3neg** and **3pos** show maxima at 220 and 260 nm and minima at 210 and 240 nm respectively, indicative of preorganization into a right-handed helix.[8,9,24] All three PNA:DNA duplexes show similar CD spectra, with peak shapes and wavelengths (maxima at ~275 nm and minima at ~240 nm) characteristic of a B-form helix; and all three PNA:RNA duplexes show similar CD spectra, with peak shapes and wavelengths (maxima at ~260 nm and minima at ~210 nm) characteristic of an A-form helix (Figure 3.4 and 3.5).[4] This result was unexpected, given the dramatically different mismatch selectivity of PNAs **3neg** and **3pos**. However, we hypothesize that the charged side chains may still give rise to local structural perturbations, which could impact selectivity without significantly altering the overall CD spectrum. We are currently pursuing computational studies in an attempt to gain more detailed insight into the impact of the charged side chains on PNA:DNA and PNA:RNA duplex structure.

Conclusion

The results discussed here is the first to directly compare sequence selectivity for γ-modified PNAs having positively or negatively charged side chains. For these γ-modified PNA strands, PNA **3pos** shows superior binding selectivity with DNA; and PNA **3neg** shows superior binding selectivity with RNA. CD studies reveal that the side chains do not significantly alter the overall structure of the PNA:DNA or PNA:RNA

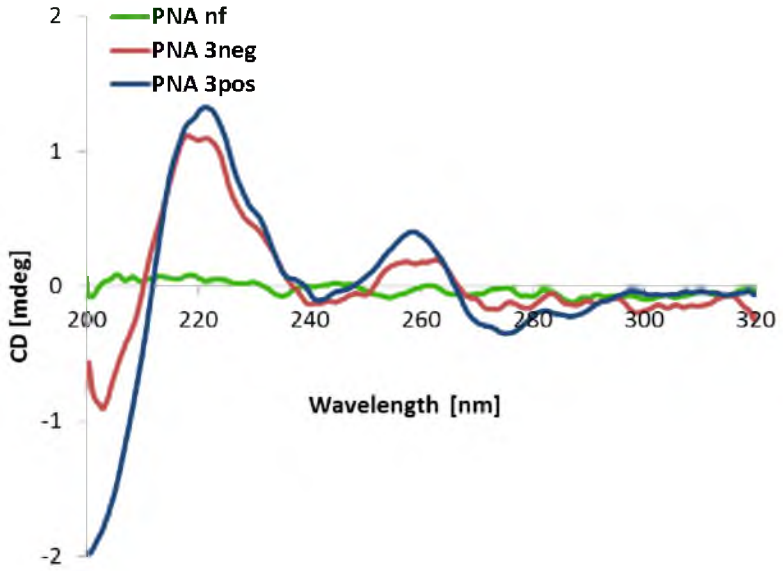

Figure 3.3. CD spectra of PNA (**nf**/**3neg**/**3pos**) under simulated physiological buffer conditions.
(Conditions: 10 μM PNA, 0.49 mM $MgCl_2 \cdot 6H_2O$, 137 mM NaCl, 2.7 mM KCl, 1.5 mM KH_2PO_4, 8.1 mM Na_2HPO_4, pH 7.4, 20 °C).

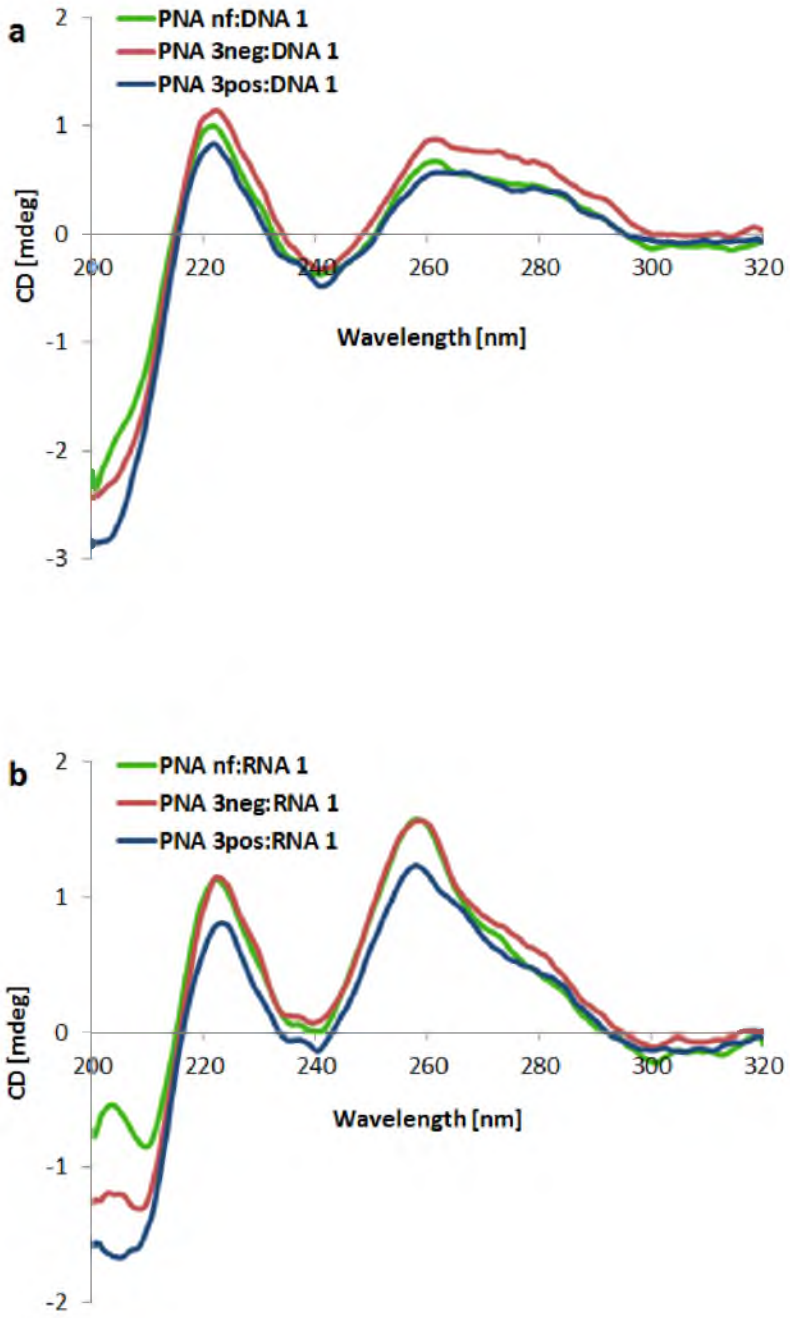

Figure 3.4. CD spectra of PNA (**nf**/**3neg**/**3pos**) with complementary (a) DNA **1** and (b) RNA **1** under simulated physiological buffer conditions. (Conditions: 5 μM PNA, 5 μM DNA or RNA, 0.49 mM $MgCl_2{\cdot}6H_2O$, 137 mM NaCl, 2.7 mM KCl, 1.5 mM KH_2PO_4, 8.1 mM Na_2HPO_4, pH 7.4, 20 °C).

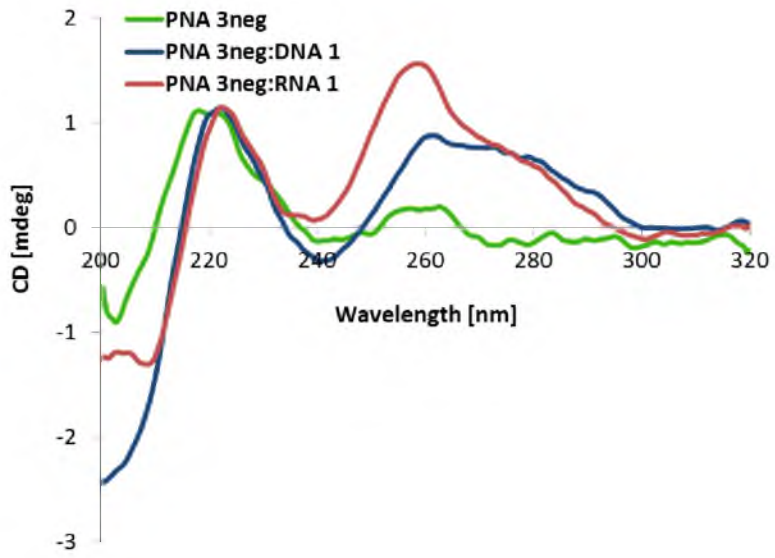

Figure 3.5. Representative CD spectra overlap to demonstrate the structural variations of single stranded γ-PNA and γ-PNA in duplex formation with DNA and RNA.

duplexes. However, they may still provide sufficient local perturbation to account for the observed differences in selectivity. It should be noted that the aspartic acid and lysine monomers used in this initial study have slightly different side chain lengths. In lysine monomer, the charged atom is two carbons away from the PNA backbone compared to aspartic acid monomer. This may have a minor impact on counterion binding and backbone hydration, but data from our previous study support the hypothesis that the net charge of the backbone is the prevailing factor in determining duplex stability.[11]

γ-PNAs structural stability is influenced by the tri-centered backbone-water-nucleobase interactions. Specifically, the availability of numerous donor and acceptor sites in the backbone may further impact the solvent interactions.[25] We hypothesize that the functionality in the incorporated γ-side chains together with the variations in structure of native nucleic acids could influence the solvation network, H-bonding, and cation-binding interactions; hence resulting in differential binding properties and sequence recognition of side chain functionalized PNAs.

Thus, in the development of γ-substituted PNA strands for specific biological targets, it may be important to investigate the selectivity of each individual sequence. Additionally, our results highlight the potential importance of investigating PNA binding affinity and selectivity under physiological conditions when biological applications are anticipated. Together, this research provides insight into the surprising impact of side chain structure on binding selectivity for γ-substituted PNA, and suggests that the ideal side chains for PNA:DNA duplex formation may be different from those that are ideal for PNA:RNA duplex formation. We anticipate that PNA together with its enhanced sequence specificity and differential binding ability would play a revolutionary role in the detection of single point mutations.

This work highlights that the variation of functional group in the γ-position allows differential binding tendency toward nucleic acids. Future studies in spectroscopic, crystallographic, and computational fields are required to fully understand our findings. Future investigations are also needed to explore the effect of side chain length on duplex stability and mismatch discrimination. While we do observe that side chain structure and electrostatics are the prevailing factors in determining selectivity, the positioning of the side chains relative to the mismatch site may also have a subtle impact. Also, further work is needed to understand the effect of numerous side chains, sequences, and sequence lengths on mismatch discrimination of γ-substituted PNAs.

Experimental Section

General techniques

DNA/RNA was purchased from the University of Utah DNA/Peptide Synthesis Core Facility. Mass spectra were recorded at the Mass Spectrometry facility in the Department of Chemistry of the University of Utah. Milli-Q water was obtained from

Millipore Simplicity UV water purification system.

UV melting studies

All samples were prepared in buffer containing 0.49 mM $MgCl_2 \cdot 6H_2O$, 137 mM NaCl, 2.7 mM KCl, 1.5 mM KH_2PO_4, 8.1 mM Na_2HPO_4, pH 7.4.[26] The samples were incubated at 95 °C for 1 min, followed by cooling to room temperature at a rate of 0.1 °C/sec using a BioRad-MJ Mini Personal Thermal Cycler, before data collection. UV-Vis absorbance at 260 nm was recorded and corrected using the absorbance at 380 nm (UV cell path length = 1 cm). The data were recorded at a rate of 1 °C/min, in 0.5 °C intervals, for both the heating and cooling runs. The T_m values were determined by taking the first derivative of the cooling profiles (85-20 °C), using Origin 8.5.1 software. Final T_m is an average of three or four independent trials, and error bars represent the standard deviation.

Thermodynamic analysis

The UV melting data were analyzed to obtain van't Hoff transition enthalpies.[23,27] Baseline correction was applied to each plot of normalized absorbance versus temperature (over 20-85 °C range), providing plots of fraction melted (θ) versus temperature. The thermodynamic parameters were determined by plotting ln K_a vs 1/T (van't Hoff plot). Values of K_a, the affinity constant, at each temperature were determined using the following equation for bimolecular, non-self-complementary oligonucleotides, where C_o is the initial strand concentration.

$$K_a = \frac{\theta}{\left[C_o \cdot (1-\theta)^2\right]}$$

In order to have a precise K_a, θ values lying in the range of $0.15<\theta<0.85$ are

taken for the van't Hoff plot. For a two-state transition, if ΔH is independent of the temperature, then a plot of ln K_a vs 1/T is linear, giving -ΔH/R as the slope and ΔS/R as the y-intercept. Gibbs free energy (ΔG) was calculated using the following equation, where T = 298.15 K.

$$\Delta G = \Delta H - T\Delta S$$

Circular dichroism (CD) analysis

CD spectra were recorded on JASCO J815 CD spectrometer. All samples were prepared in a buffer containing 0.49 mM $MgCl_2 6H_2O$, 137 mM NaCl, 2.7 mM KCl, 1.5 mM KH_2PO_4, 8.1 mM Na_2HPO_4, pH 7.4.[26] The samples of PNA:DNA/RNA duplexes were incubated at 95 ^oC for 1 min, followed by cooling to room temperature at a rate of 0.1 ^oC/sec using a BioRad-MJ Mini Personal Thermal Cycler, before data collection. All CD spectra were recorded at 20 °C in the range 200−320 nm (cell path length = 1.00 mm). Final spectra are an average of 10 scans, which were scanned at a speed of 100 nm/min. Buffer data was subtracted from the sample data, which was then smoothed via 40 point Adjacent Averaging algorithm using Origin 8.5.1 software.

References

(1) Nielsen, P. E.; Egholm, M.; Berg, R. H.; Buchardt, O. Sequence-Selective Recognition of DNA by Strand Displacement with a Thymine-Substituted Polyamide. *Science* **1991**, *254*, 1497-1500.

(2) *Peptide Nucleic Acids: Protocols and Applications*, 2nd ed.; Nielsen, P. E., Ed.; Horizon Bioscience: United Kingdom, 2004.

(3) *Peptide Nucleic Acids, Morpholinos and Related Antisense Biomolecules*; Janson, C. G.; During, M. J., Eds.; Springer: US, 2006.

(4) Egholm, M.; Buchardt, O.; Christensen, L.; Behrens, C.; Freier, S. M.; Driver, D. A.; Berg, R. H.; Kim, S. K.; Norden, B.; Nielsen, P. E. PNA Hybridizes to Complementary Oligonucleotides Obeying the Watson–Crick Hydrogen-Bonding Rules. *Nature* **1993**, *365*, 566-568.

(5) Demidov, V. V.; Potaman, V. N.; Frank-Kamenetskil, M. D.; Egholm, M.; Buchard, O.; Sönnichsen, S. H.; Nielsen, P. E. Stability of Peptide Nucleic Acids in Human Serum and Cellular Extracts. *Biochem. Pharmacol.* **1994**, *48*, 1310-1313.

(6) Rozners, E. Recent Advances in Chemical Modification of Peptide Nucleic Acids. *J. Nucleic Acids* **2012**, *2012*, 518162.

(7) Sugiyama, T.; Kittaka, A. Chiral Peptide Nucleic Acids with a Substituent in the N-(2-Aminoethy)glycine Backbone. *Molecules* **2012**, *18*, 287-310.

(8) Dragulescu-Andrasi, A.; Rapireddy, S.; Frezza, B. M.; Gayathri, C.; Gil, R. R.; Ly, D. H. A Simple γ-Backbone Modification Preorganizes Peptide Nucleic Acid into a Helical Structure. *J. Am. Chem. Soc.* **2006**, *128*, 10258-10267.

(9) Englund, E. A.; Appella, D. H. γ-Substituted Peptide Nucleic Acids Constructed from L-Lysine are a Versatile Scaffold for Multifunctional Display. *Angew. Chem., Int. Ed.* **2007**, *46*, 1414-1418.

(10) Crawford, M. J.; Rapireddy, S.; Bahal, R.; Sacui, I.; Ly, D. H. Effect of Steric Constraint at the γ-Backbone Position on the Conformations and Hybridization Properties of PNAs. *J. Nucleic Acids* **2011**, *2011*, 652702.

(11) De Costa, N. T. S.; Heemstra, J. M. Evaluating the Effect of Ionic Strength on Duplex Stability for PNA Having Negatively or Positively Charged Side Chains. *PLoS ONE* **2013**, *8*, e58670.

(12) De Costa, N. T. S.; Heemstra, J. M. Differential DNA and RNA Sequence Discrimination by PNA Having Charged Side Chains. *Bioorg. Med. Chem. Lett.* **2014**, *24*, 2360-2363.

(13) Ratilainen, T.; Holmén, A.; Tuite, E.; Nielsen, P. E.; Nordén, B. Thermodynamics of Sequence-Specific Binding of PNA to DNA†. *Biochemistry* **2000**, *39*, 7781-7791.

(14) Sahu, B.; Chenna, V.; Lathrop, K. L.; Thomas, S. M.; Zon, G.; Livak, K. J.; Ly, D.

H. Synthesis of Conformationally Preorganized and Cell-Permeable Guanidine-Based γ-Peptide Nucleic Acids (γGPNAs). *J. Org. Chem.* **2009**, *74*, 1509-1516.

(15) Allawi, H. T.; SantaLucia, J. Jr. Thermodynamics and NMR of Internal G·T Mismatches in DNA. *Biochemistry* **1997**, *36*, 10581-10594.

(16) Sahu, B.; Sacui, I.; Rapireddy, S.; Zanotti, K. J.; Bahal, R.; Armitage, B. A.; Ly, D. H. Synthesis and Characterization of Conformationally Preorganized, (*R*)-Diethylene Glycol-Containing γ-Peptide Nucleic Acids with Superior Hybridization Properties and Water Solubility. *J. Org. Chem.* **2011**, *76*, 5614-5627.

(17) Englund, E. A.; Appella, D. H. Synthesis of γ-Substituted Peptide Nucleic Acids: A New Place to Attach Fluorophores without Affecting DNA Binding. *Org. Lett.* **2005**, *7*, 3465-3467.

(18) Mitra, R.; Ganesh, K. N. PNAs Grafted with (α/ γ, *R*/*S*)-Aminomethylene Pendants: Regio and Stereo Specific Effects on DNA Binding and Improved Cell Uptake. *Chem. Commun.* **2011**, *47*, 1198-1200.

(19) Mitra, R.; Ganesh, K. N. Aminomethylene Peptide Nucleic Acid (am-PNA): Synthesis, Regio-/Stereospecific DNA Binding, and Differential Cell Uptake of (α/ γ, *R*/*S*)am-PNA Analogues. *J. Org. Chem.* **2012**, *77*, 5696-5704.

(20) Tomac, S.; Sarkar, M.; Ratilainen, T.; Wittung, P.; Nielsen, P. E.; Nordén, B.; Gräslund, A. Ionic Effects on the Stability and Conformation of Peptide Nucleic Acid Complexes. *J. Am. Chem. Soc.* **1996**, *118*, 5544-5552.

(21) Park, H.; Germini, A.; Sforza, S.; Corradini, R.; Marchelli, R.; Knoll, W. Effect of Ionic Strength on PNA-DNA Hybridization on Surfaces and in Solution. *Biointerphases* **2007**, *2*, 80-88.

(22) Ghosh, S.; Mishra, S.; Banerjee, T.; Mukhopadhyay, R. Facilitating Mismatch Discrimination by Surface-Affixed PNA Probes via Ionic Regulation. *Langmuir* **2013**, *29*, 3370-3379.

(23) Marky, L. A.; Breslauer, K. J. Calculating Thermodynamic Data for Transitions of any Molecularity from Equilibrium Melting Curves. *Biopolymers* **1987**, *26*, 1601-1620.

(24) *Circular Dichroism: Principles and Applications*, 2nd ed.; Berova, N.; Nakanishi, K.; Woody, R. W., Eds.; Wiley-VCH: New York, 2000.

(25) Yeh, J. I.; Shivachev, B.; Rapireddy, S.; Crawford, M. J.; Gil, R. R.; Du, S.; Madrid, M.; Ly, D. H. Crystal Structure of Chiral γPNA with Complementary DNA Strand: Insights into the Stability and Specificity of Recognition and Conformational Preorganization. *J. Am. Chem. Soc.* **2010**, *132*, 10717-10727.

(26) Dulbecco, R.; Vogt, M. Plaque Formation and Isolation of Pure Lines with Poliomyelitis Viruses. *J. Exp. Med.* **1954**, *99*, 167-182.

(27) Mergny, J.-L.; Lacroix, L. Analysis of Thermal Melting Curves. *Oligonucleotides* **2003**, *13*, 515-537.

CHAPTER 4

TOWARD DNA-TEMPLATED PNA POLYMERIZATION USING DYNAMIC COVALENT CHEMISTRY

Introduction

Nucleic acid-templated polymerization translates genetic information into functional macromolecules and allows the evolution of biopolymers.[1] The molecular recognition capability of oligonucleotides can be used to direct the programmable assembly of reactive partners to engage in chemical reactions.[2] Groundbreaking work by the Gilham[3] and Orgel[4] groups revealed that oligonucleotide templates can drive the ligation of complementary strands having activated phosphodiesters. This pioneering work, together with the curiosity to unveil the mysteries of prebiotic chemistry, has driven the exploration of various template-driven chemical reactions. Significant progress has been achieved with translating information from oligonucleotide sequences into functional materials and novel architectures (conductive polymers, nanopatterns), fluorescent or bioactive molecules, and synthetic polymers.[2,5]

In template-driven reactions, the spontaneous reaction between unbound reactants is inhibited in the absence of the template. In the presence of the template, the effective concentrations of the reactive partners are increased upon binding, thereby increasing the rate of the reaction.[2] Numerous chemical functionalities and reactions have been investigated in template driven systems. Nucleic acid-templated reactions can be divided into three types, (1) templated inter-strand crosslinking, (2) templated strand ligation, and (3) templated transformation without ligation (Figure 4.1).[2]

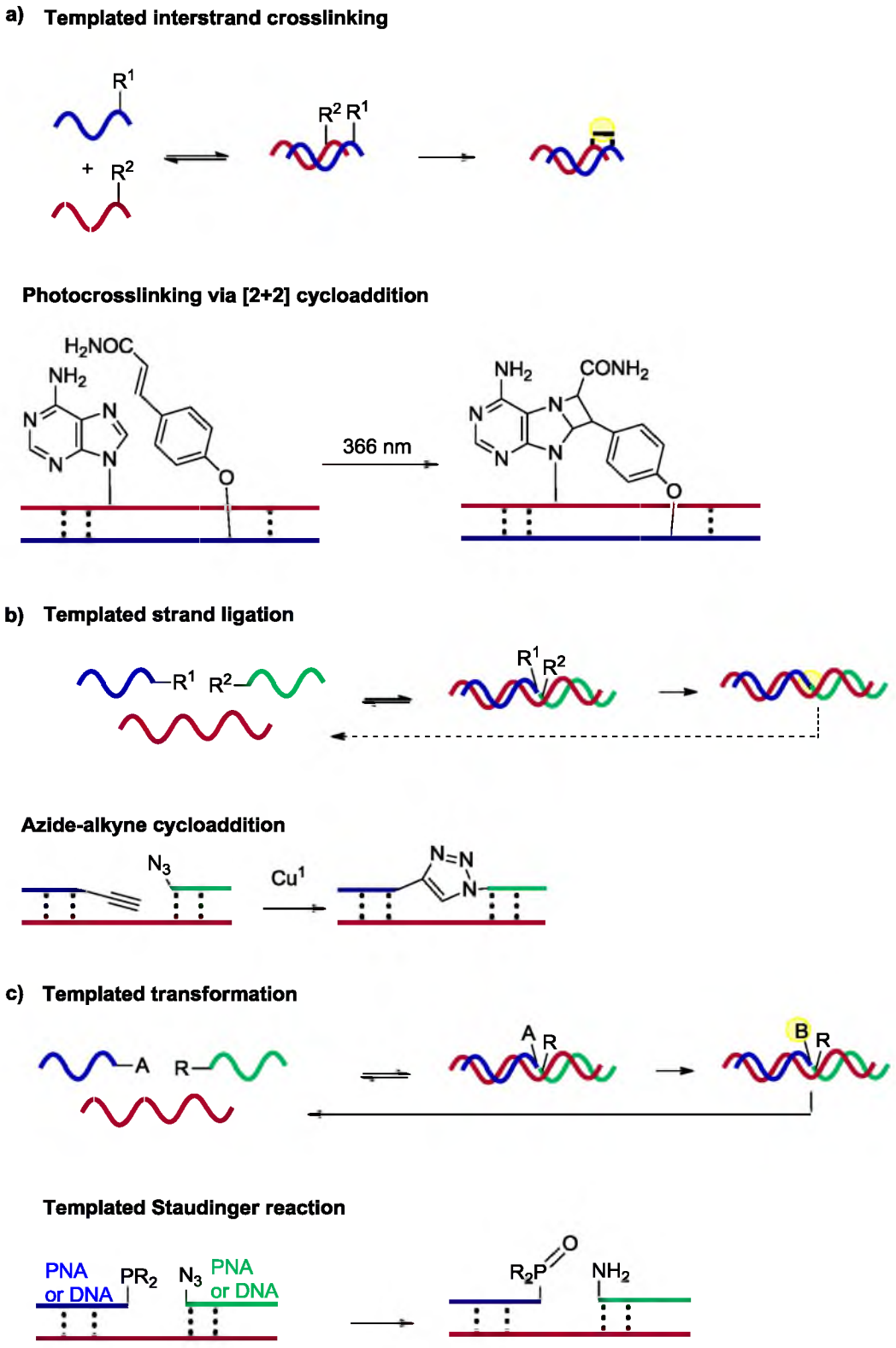

Figure 4.1. Three types of nucleic acid-templated reactions with representative examples [adapted with permission from (Gorska, K.; Winssinger, N. *Angew. Chem. Int. Ed.* **2013**, *52*, 6820-6843), copyright © (2013) WILEY-VCH Verlag GmbH & Co. KGaA, Weinheim].

"Inter-strand crosslinking" approaches have been used for the selective capturing of complementary strands, followed by light or oxidant-induced crosslinking (Figure 4.1a). These are utilized in applications such as single-nucleotide polymorphism (SNP) detection.[6] The second approach, "templated ligation" was the first nucleic acid-templated reaction to become popular because of its relevance to the origin of life as templated ligations are required for the enzyme free amplification of genetic material. Thus, numerous efficient, orthogonal, and biocompatible templated ligations have been studied based on reactions such as photoligation, azide–alkyne cycloaddition,[7,8] nucleophilic substitution, and condensation (Figure 4.1b).[2] These ligation chemistries have been used in applications including SNP detection, generation of fluorogenic probes,[9] and construction of sophisticated nanostructures such as catenanes,[10] dendrimers, G-quaduplexes, and conducting polymers.[2] The third type of templated reaction, "templated transformations", are required for the synthesis of functional molecules (proteins) using the information encoded in the nucleic acid sequences (Figure 4.1c). Various templated transformation reactions, such as templated hydrolysis, acyl transfer, azide reduction,[11,12] and Wittig reaction, have been investigated (Figure 4.2a).[2] Interestingly, the Liu group performed one-pot, six-step, DNA-templated synthesis utilizing this method (Figure 4.2b).[13]

In fact, one of the ultimate goals of the aforementioned nucleic acid-templated reactions is to find a suitable method to translate information encoded in a DNA sequence into an evolvable synthetic polymer. In particular, the ability of biopolymers to translate from DNA and RNA, and then mutate and evolve allows them to expand their potential, performing functions essential for life. As discussed previously, the use of natural polymers in numerous applications is limited due to their stability, bioavailability, and immunogenicity. Artificial polymers can be tailored to overcome the above limitations. However, *in vitro* selection methods such as phage display[14] and SELEX[15]

a)

b)

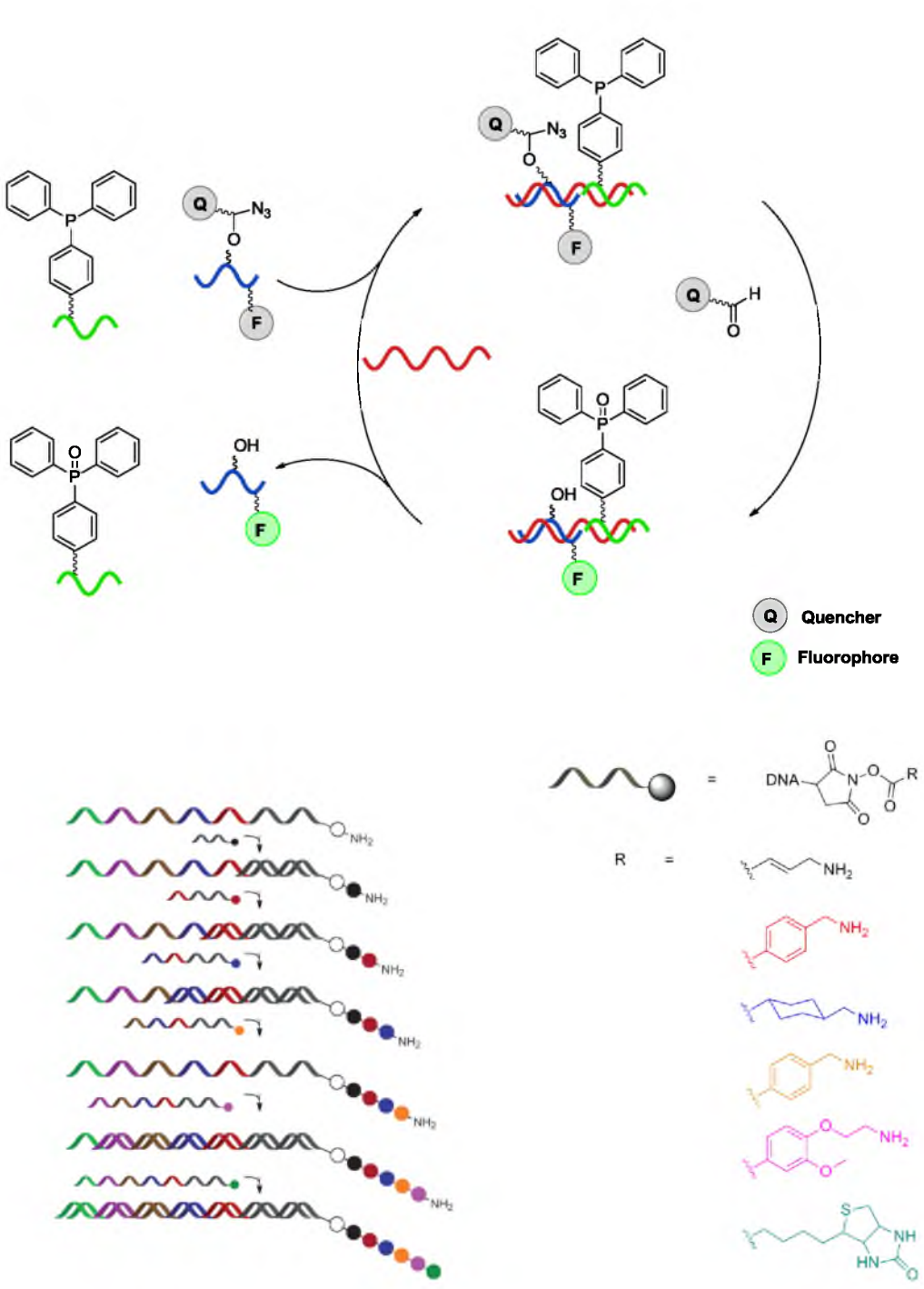

Figure 4.2. Selected applications of nucleic acid-templated reactions (a) fluorogenic probes,* (b) six-step DNA-templated synthesis.** [*Adapted with permission from (Franzini, R. M.; Kool, E. T. *J. Am. Chem. Soc.* 2009, *131*, 16021-16023), copyright © (2009) American Chemical Society. **Reprinted with permission from (Gorska, K.; Winssinger, N. *Angew. Chem. Int. Ed.* **2013**, *52*, 6820-6843), copyright © (2013) WILEY-VCH Verlag GmbH & Co. KGaA, Weinheim].

are limited to biopolymers. Therefore, the evolution of abiotic polymers, including PNA,[16] requires methods for sequence encoding and amplification. Towards this endeavor, polymerase catalyzed templated synthesis of nucleic acids with modified bases and backbone-modified nucleic acid analogues, such as oligonucleotides of phosphorothioates, phosphoramidates, 2'-modified ribose, TNA (threose nucleic acid),[17] HNA, GNA, and LNA have been investigated.[1] In addition, protein synthesis by ribosomal machinery has been mimicked to generate artificial peptides and polyesters.[18,19] However, the structural and functional diversity of nonnatural polymers derived from biosynthetic pathways is limited by the need for compatibility with polymerases or the ribosome.[1]

Nonenzymatic, templated polymerization allows for the generation of sequence-defined, genetically-encoded synthetic polymers having desired functional properties. Nonenzymatic ligation of hexitol and altritol nucleic acids has been investigated, but the polymerization was limited to only tetramers.[1] Also, PNA-templated RNA polymerization has been examined, but suffers from regioselectivity issues in polymerization. Lynn and coworkers expanded the substrate scope of nonenzymatic ligations by introducing amine-DNA and amido-DNA, in which reductive amination was used as an alternative strategy for polymerizations that do not contain phoshodiester linkages.[1,20]

Recently, the Liu group has put forth strategies to overcome the limitations of nonenzymatic, templated polymerization by taking advantage of PNA in DNA-templated polymerizations.[1,21-23] The favorable stability and affinity of PNA together with speculation of its prebiotic relevance has made PNA an attractive tool for templated polymerizations.[24] Early studies of DNA-templated PNA polymerization used amine acylation as the coupling reaction.[25] Based on the pioneering work by the Lynn group, the Liu group demonstrated the condensation of PNA oligomers under reductive amination conditions.[21] Reductive amination conditions are advantageous over acylation

conditions, as the initial imine intermediate forms reversibly, thus driving the assembly of the oligomers of fully complementary sequence.

The Liu group tested the templated ligation of PNA fragments containing one or multiple side chains at various positions to generate a 40-mer PNA, having 24 side-chain modifications.[22] This innovation opens up potential applications of nonenzymatic translation of nucleic acid sequences to multifunctional synthetic polymers. They further ensured the success of this method by presenting both the transcription of DNA templates to synthetic PNA polymers, as well as a method for selection, amplification, and retranscription of these PNA sequences.[26] Although significant work has been done related to DNA-templated PNA polymerization, all of the previous systems utilized polymerization between small blocks of oligomers, rather than single monomers.

As an alternative to templated polymerization via backbone ligation, the groups of Liu[23] and Ghadiri[27] concurrently reported a base-filling approach, in which nucleobases were added to a preformed abasic PNA backbone (Figure 4.3). In the method reported by the Liu group, four nucleobase aldehydes or acids were incubated into PNA duplexes having an abasic site, and subsequently subjected to reductive amination conditions or carboxylic acid activation conditions.[23] They were able to successfully isolate the complementary base-filled PNA duplex with high yield and selectivity under reductive amination conditions. The method reported by Ghadiri group utilized a trans-thioesterification between cysteine residues in an abasic peptide backbone and nucleobase thioesters.[27]

Dynamic covalent chemistry is defined as chemical ligation reactions that are carried out reversibly under equilibrium control.[28] This reversible nature of the reactions allows error checking and proofreading, thus yielding the more thermodynamically stable final product. Although numerous dynamic covalent chemical reactions have been investigated in supramolecular assembly systems, our interest was drawn towards the

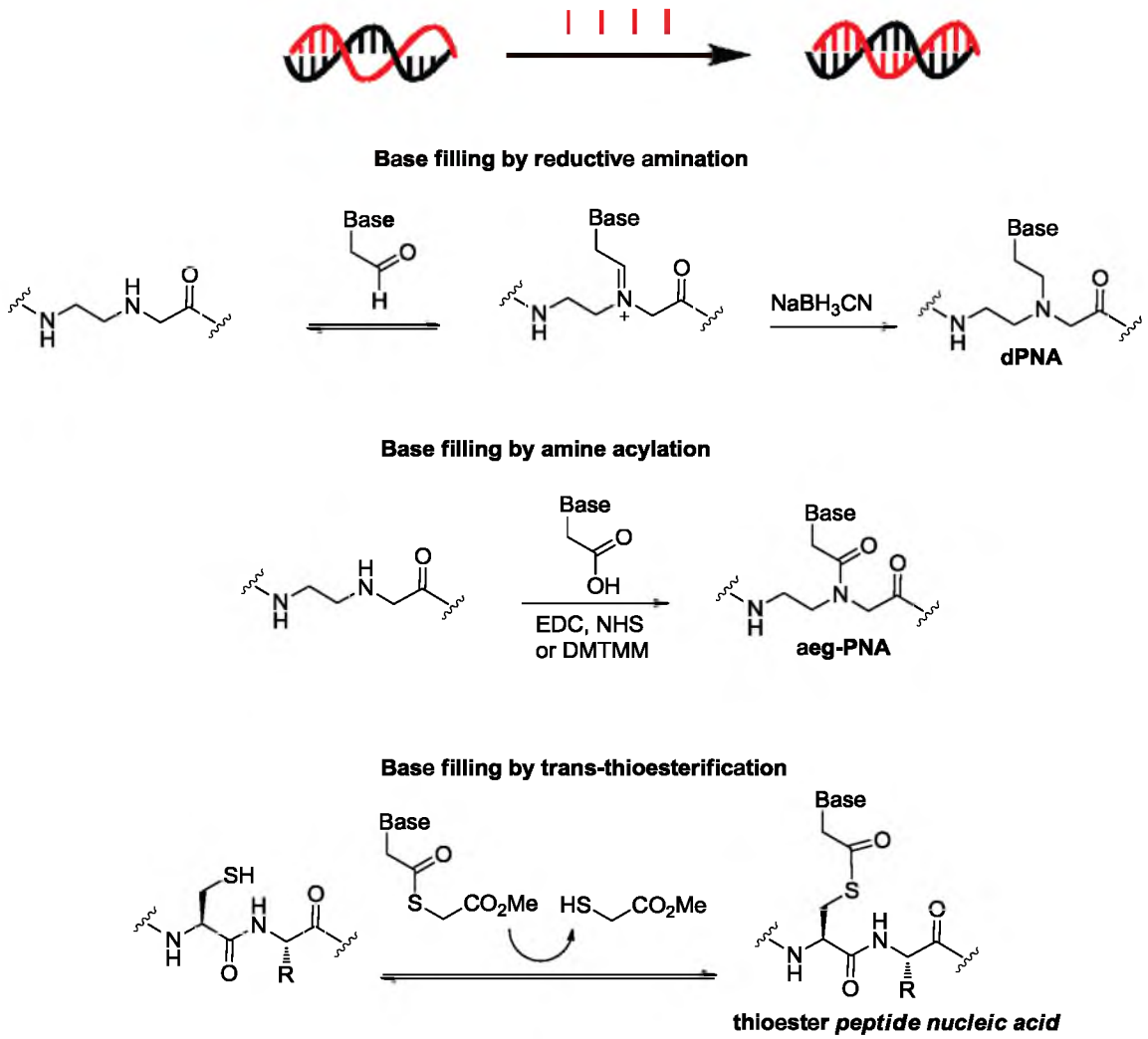

Figure 4.3. Templated polymerization via base filling [adapted from (*ACS AuthorChoice* article: Heemstra, J. M.; Liu, D. R. *J. Am. Chem. Soc.* **2009**, *131*, 11347-11349) and (Ura, Y.; Beierle, J. M.; Leman, L. J.; Orgel, L. E.; Ghadiri, M. R. *Science* **2009**, *325*, 73-77, with permission from AAAS)].

thiolactone exchange zip-reaction,[29] as thioesters are ubiquitous in nature and also postulated as precursors to life.[30]

Previous work by the Seitz group utilized native chemical ligation (NCL) for the coupling of PNA fragments.[31,32] They achieved higher yield and turnover rates when using PNA fragments containing isocysteine at the N-terminus and glycine thioesters at the C-terminus (Figure 4.4).[2,32] In addition, templated acyl transfer reactions have used

Figure 4.4. Templated native chemical ligation of PNA [adapted with permission from (Gorska, K.; Winssinger, N. *Angew. Chem. Int. Ed.* **2013**, *52*, 6820-6843), copyright © (2013) WILEY-VCH Verlag GmbH & Co. KGaA, Weinheim].

the NCL strategy to achieve rapid, robust reactions with high turnover rates.[32] In some instances, nontemplated hydrolysis of the thioester led to background signal, but careful optimization of conditions allowed for these limitations to be overcome.[32] Additionally, as we mentioned above, the Ghadiri group used a trans-thioesterification between cysteine residues in an abasic peptide backbone and nucleobase thioesters in their base-filling method.[27]

In an attempt to achieve single-nucleotide templated polymerization, we designed the PNA monomer **4.1** that can take advantage of the reversible thiol-thiolactone ring opening reaction (Figure 4.5). We anticipate that the dynamic nature of the ligation chemistry will allow the editing of misincorporated nucleotides, analogous to the exonuclease activity of polymerases. Our current research on this project mainly involves the synthesis of modified PNA monomer **4.1**. Outlined here in the fourth chapter of this dissertation are studies directed toward the synthesis of the modified PNA monomer. Upon synthesis of the monomer, the ability of base pairing and base stacking to drive the templated polymerization will be investigated.

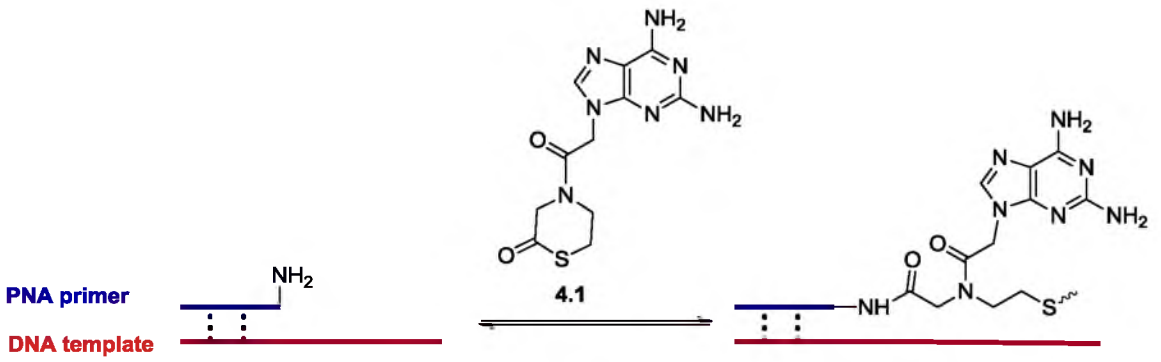

Figure 4.5. Proposed DNA-templated PNA polymerization via thiol-thiolactone ring opening method.

Results and Discussion

Retrosynthesis

We initially planned on synthesizing the modified PNA monomer via two different approaches, a convergent route and linear route. In the convergent route, it was envisioned that the desired cyclic monomer **4.1** would arise from amide bond formation between diaminopurine acetic acid **4.2** and thiomorpholinone **4.3** (Scheme 4.1). Thiomorpholinone **4.3** would be obtained from disulfide bond cleavage of dimer **4.4** followed by thioesterification. Alkylation of the amines of cystamine dihydrochloride **4.5** with bromoacetyl ester would give **4.4**.

In the linear route, it was envisioned that the cyclic monomer **4.1** would arise from thioesterification of modified PNA backbone **4.6**, which would be obtained from disulfide bond cleavage of dimer **4.7** (Scheme 4.2). The alkylation of cystamine dihydrochloride **4.5** with bromoacetyl ester, followed by amide bond formation with diaminopurine acetic acid **4.2**, would give dimer **4.7**.

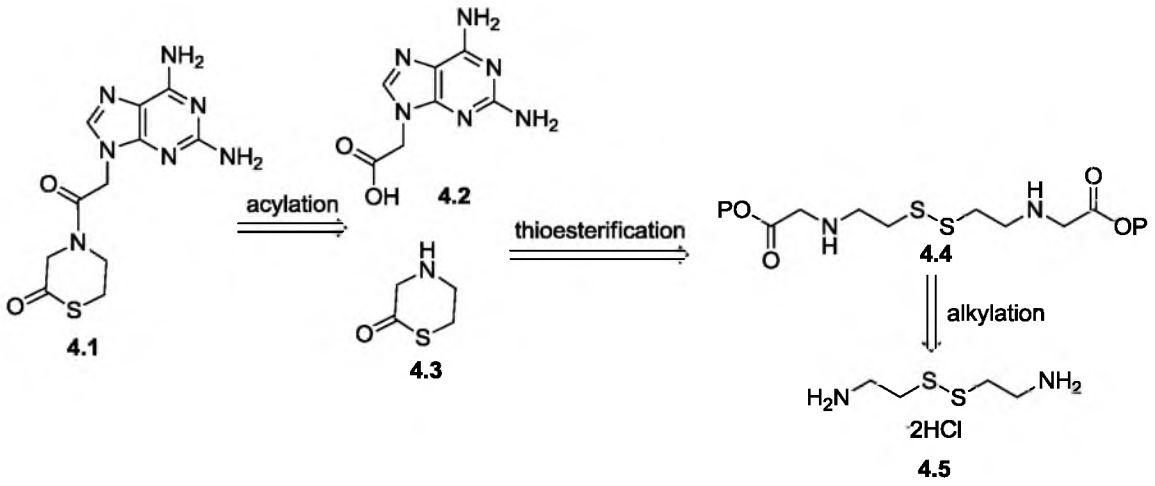

Scheme 4.1. Retrosynthetic analysis of convergent route.

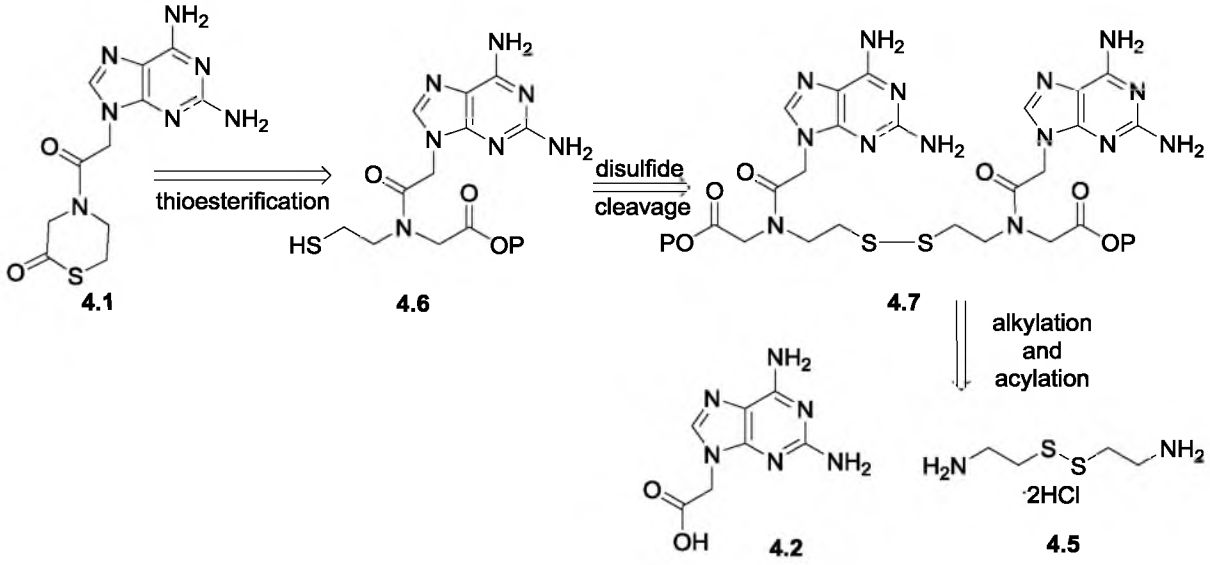

Scheme 4.2. Retrosynthetic analysis of linear route.

Studies toward the synthesis of cyclic PNA monomer via convergent route

First, alkylation of diaminopurine **4.8** with bromoacetic acid ethyl ester afforded alkylated diaminopurine **4.9**, and subsequent ester hydrolysis provided diaminopurine acetic acid **4.2** (Scheme 4.3).[33] Although we attempted direct coupling of diaminopurine with bromoacetic acid to obtain diaminopurine acetic acid **4.2**, we isolated unidentified byproducts along with the product. Therefore, we decided to follow the previous route, which provided the clean product.

We decided to use the commercially available disulfide-containing dimer cystamine, in which the thiol is inherently protected. First, cystamine dihydrochloride **4.5** was alkylated with bromoacetic acid benzyl ester to give the dibenzyl ester compound **4.10** (Scheme 4.4). Deprotection of the benzyl esters to give diacid **4.11** was sluggish under hydrogenation conditions. This was possibly due to poisoning of the palladium catalyst by sulfur in the substrate. Although deprotection under HCOOH acid and Pd/C seemed promising, it required nearly equivalent amounts of Pd/C for an efficient reaction.[34] Thus, we decided to use a *t*-butyl ester instead of a benzyl ester for alkylation of cystamine **4.5**.

Cystamine **4.5** was alkylated with bromoacetic acid *t*-butyl ester to give the di-*t*-butyl ester compound **4.12** in 46% yield (Scheme 4.5). Then, disulfide bond cleavage of dimer **4.12**[35] using TCEP[36] gave monomer **4.13**,[37] and removal of the *t*-butyl ester with TFA provided mercaptoethyl glycine **4.14**[38] in quantitative yield. With **4.14** in hand, next we investigated the formation of thiomorpholinone **4.3** under peptide coupling and dehydration conditions. However, we were not able to successfully isolate the product. This was possibly due to the free amine interfering with the reactive thioester bond.

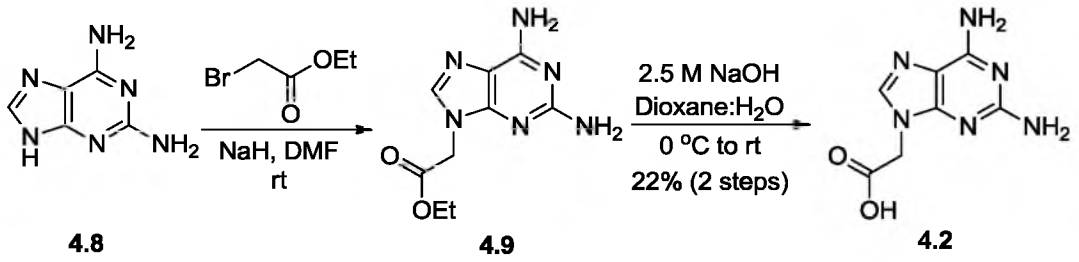

Scheme 4.3. Synthesis of diaminopurine acetic acid **4.2**.

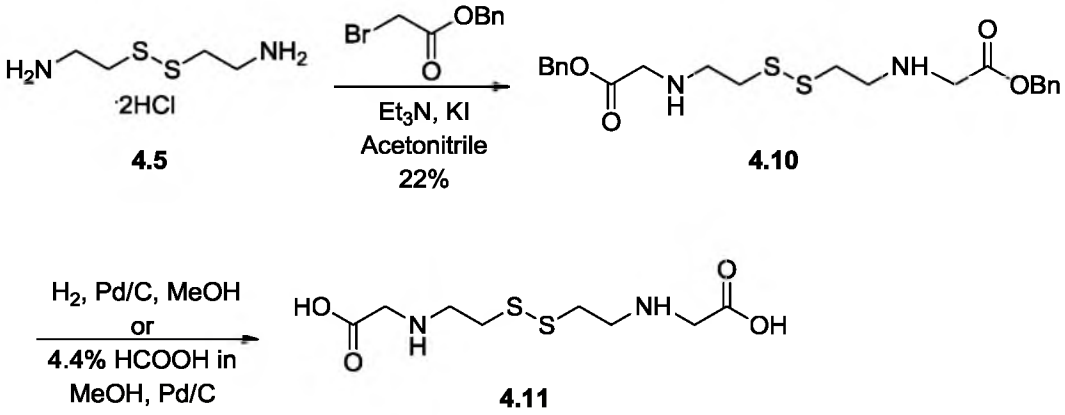

Scheme 4.4. Synthetic attempts for alkylated cystamine dihydrochloride **4.11**.

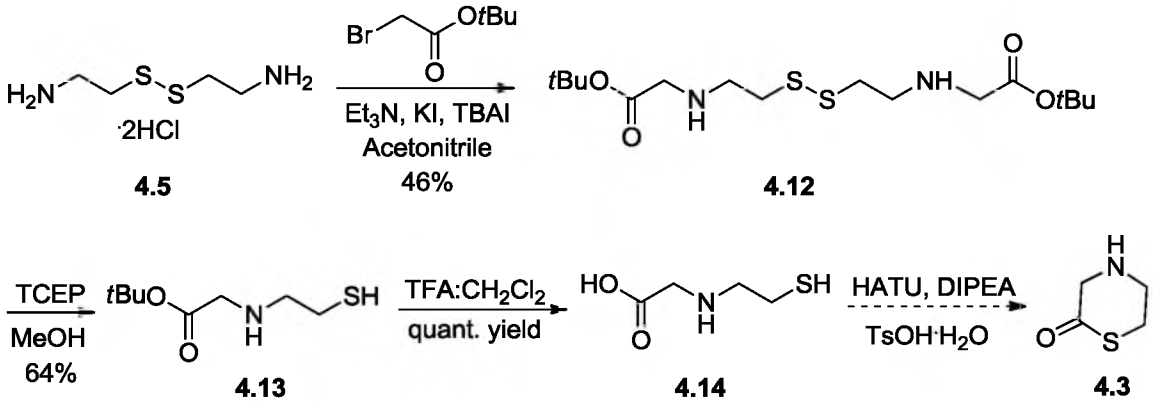

Scheme 4.5. Synthetic attempts for cyclic PNA monomer **4.3**.

Next, we decided to protect the free amine to avoid the aforementioned problems. Deciding on the best protecting group that would require mild deprotection conditions became demanding. Solid phase peptide synthesis (SPPS)[39,40] using Fmoc[40] protecting groups is known to be more attractive than SPPS using Boc protecting groups due to the milder basic deprotection of Fmoc in comparison to the harsh acidic conditions required for Boc. However, the use of popular SPPS Fmoc removal base, piperidine, becomes problematic when thioester functional groups are present in the substrates. Previous work has reported the use of DBU as a safe alternative to piperidine in the presence of the thioester functionality.[41,42] Hence, we chose Fmoc as the choice of protecting group for our substrate **4.12**.[35]

Accordingly, Fmoc protection of the amino groups of **4.12**[35] provided the di-Fmoc protected compound **4.15**, and subsequent disulfide bond cleavage gave the cyclization precursor **4.16**[43] (Scheme 4.6). The known thiol compound **4.16** was then subjected to dehydration conditions under Dean-Stark apparatus to provide Fmoc-protected thiomorpholinone product **4.17**.[44] However, isolation of thiomorpholinone **4.3** after removal of the Fmoc group was not successful under numerous conditions. This could possibly be due to the instability of the thioester group and the reactivity of the secondary amine group. Consequently, we decided not to isolate the free amine compound **4.3**, and instead attempt a one-pot procedure for Fmoc removal from **4.17** and subsequent amide bond formation with diaminopurine acetic acid **4.2** to give the desired cyclic PNA monomer **4.1** (Scheme 4.7). Accordingly, we investigated an addition of Fmoc protected thiomorpholinone **4.17** to the activated acid of **4.2**, with a base in the medium. However, we were not able to isolate the product **4.1**, nor completely recover the starting thiomorpholinone **4.17**.

Although our attempts to optimize the conditions of the aforementioned one-pot synthesis are currently underway, we propose an alternative route for future attempts by

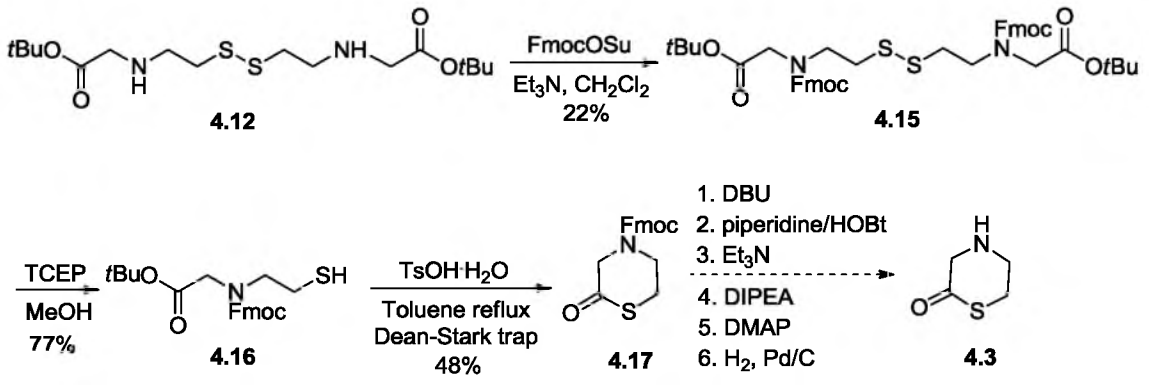

Scheme 4.6. Synthetic attempts for cyclic PNA monomer **4.3** via Fmoc-protected route.

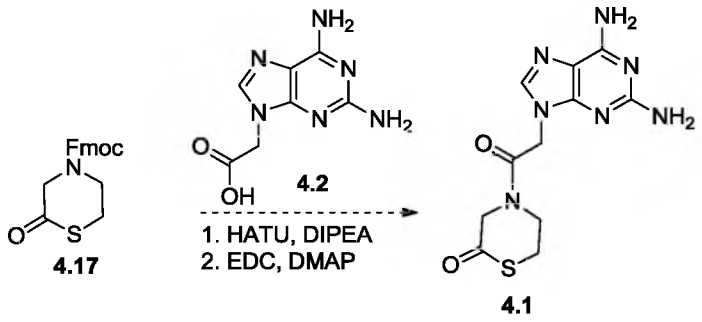

Scheme 4.7. Synthetic attempts for cyclic PNA monomer **4.1**.

modifying our choice of protecting groups. We anticipate that alkylation of cystamine **4.5** with bromoacetic acid ethyl ester, followed by protection of the diamines with a Boc protecting group will provide **4.18** (Scheme 4.8). Then, we envision that sequential disulfide cleavage, ester hydrolysis, and thiolactonization[45] will afford **4.19**. We predict that acidic deprotection of the Boc group will not hydrolyse the thioester, thus enabling isolation of thiomorpholinone **4.3** as a TFA salt. Finally, amide bond formation with Boc-protected diaminopurine acetic acid **4.20**, followed by Boc removal, would provide the desired cyclic PNA monomer **4.1** as a TFA salt.

Meanwhile, we also attempted the linear route that we initially proposed. Although the amide bond formation between diaminopurine acetic acid **4.2** and benzyl

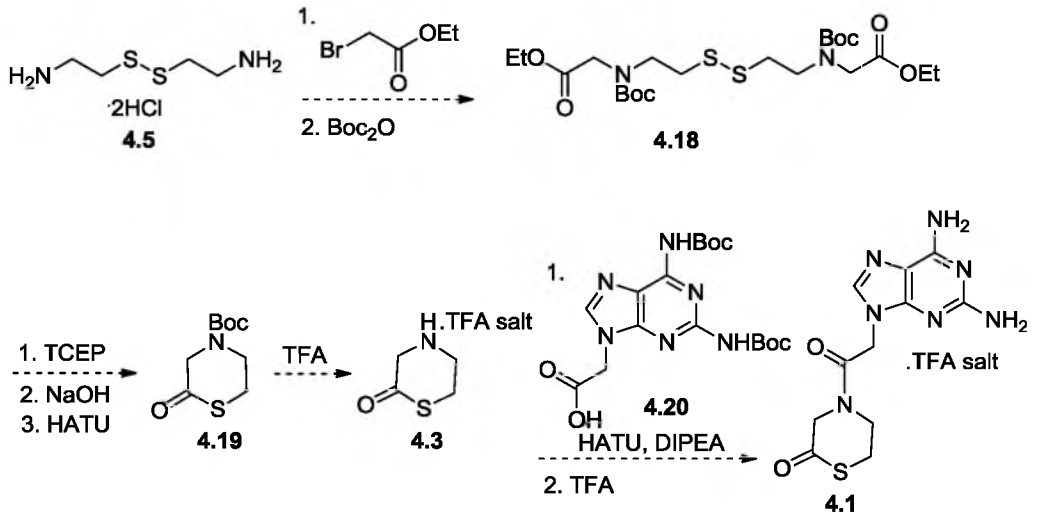

Scheme 4.8. Proposed convergent synthetic route for cyclic PNA monomer **4.1**.

ester protected dimer **4.10** seemed promising, *t*-butyl ester protected dimer **4.12** yielded decomposed material (Scheme 4.9), and we did not further investigate this route. Nevertheless, in future attempts, we recommend the use of Boc protected diaminopurine acetic acid **4.20** for coupling to minimize side reactions.

Conclusion

The research presented here shows our initial efforts towards synthesizing the desired PNA monomer **4.1**. Some of the difficulties associated with successful isolation of the desired PNA monomer can be attributed to the labile thioester moiety being sensitive to aqueous, basic, and nucleophilic conditions. This indeed challenges the use of this monomer in future experiments, which would be mainly conducted under aqueous conditions. However, previous successful examples of the use of thioesterification and thioester functional groups in experimental settings similar to physiological conditions suggest the viability of our monomer in similar settings.

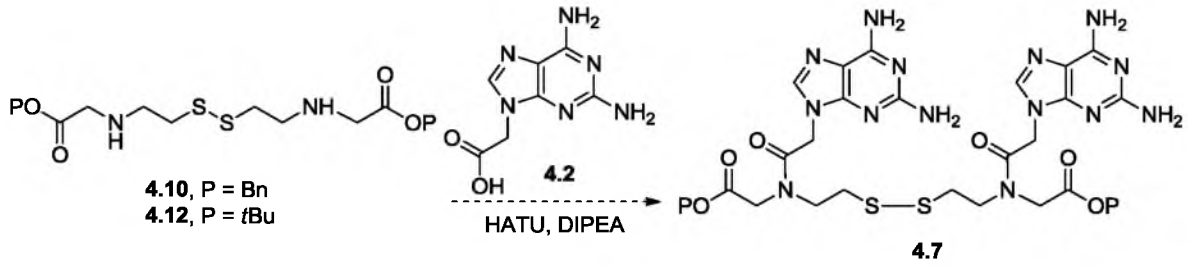

Scheme 4.9. Synthetic attempts via proposed linear route.

Upon synthesis of the monomer, the ability of base pairing and base stacking to drive the templated polymerization will be investigated. If successful, our efforts will lead to a templated PNA polymerization system that can execute polymerization from single-monomer building blocks with high fidelity.

Experimental Section

General techniques

Glassware for all reactions was oven dried or flame dried and cooled prior to use. All reactions were run under an atmosphere of nitrogen or argon unless otherwise stated. Dichloromethane (CH_2Cl_2) and dimethylformamide (DMF) were passed through a solvent purification system (J. C. Meyer). Unless otherwise noted, all starting materials were obtained from commercial suppliers and were used without further purification. Thin layer chromatography was performed on Silica gel 60 F_{254} plates eluting with the solvent indicated, visualized by a 254/365 nm UV lamp, or stained with a solution of ninhydrin, p-anisaldehyde, or potassium permanganate. Column chromatography was performed on Merck silica gel Kieselgel 60 (230-400 mesh, 40–63 μm particle size) or aluminium oxide (activated, neutral, Brockmann 1, ~150 mesh, 58 Å pore size). Yields were calculated for material judged homogenous by thin layer chromatography and NMR. Compounds were named using CS ChemBioDraw Ultra 12.0. NMR spectra were

acquired on a Varian Unity-300 or VXR 500 spectrometer. Chemical shifts for ^{1}H NMR spectra are reported in parts per million relative to the signal of residual $CHCl_3$ at 7.27 ppm or the center line of the residual DMSO pentet at 2.50 ppm. Chemicals shifts for ^{13}C NMR spectra are reported in parts per million relative to the center line of the $CDCl_3$ triplet at 77.23 ppm or the center line of the DMSO septet at 39.51 ppm. The abbreviations s, d, t, m, br, and rot stand for singlet, doublet, triplet, multiplet, broad, and rotamer, respectively. IR spectra were obtained from Nicolet 380 FT-IR spectrometer. Mass spectra were recorded at the Mass Spectrometry facility in the Department of Chemistry of the University of Utah.

Procedures and characterizations

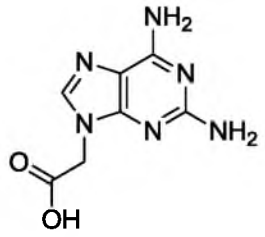

4.2

2-(2,6-Diamino-9H-purin-9-yl)acetic acid 4.2. To a suspension of 2,6-diaminopurine **4.8** (2.00 g, 13.3 mmol) in dry DMF (25 mL) was added portionwise NaH (0.586 g, 60% in oil, 14.7 mmol) under an atmosphere of N_2. After stirring for 40 min, ethyl bromoacetate (1.92 mL, 17.3 mmol) was added and the reaction mixture was stirred at rt for 20 h. The reaction mixture was then filtered over a pad of Celite® and the clear orange solution was reduced in volume. The mixture was dissolved in EtOAc and washed with sat. NH_4Cl. The organic layer was separated and the aqueous layer was extracted with EtOAc (3x). The combined organic extracts were washed with brine, dried over Na_2SO_4, and concentrated to afford alkylated diaminopurine **4.9**,[33] which was used

forward without further purification.

To the above crude product **4.9**[33] (13.3 mmol) in dioxane:H_2O (1:1, 40 mL) was added 2.5 M NaOH (30 mL) for 5 min at 0 ºC. After stirring for 15 min, ice bath was removed, and stirred at rt for 1 h. Then the mixture was washed with EtOAc and the aqueous layer was acidified to ~pH 3 with HCl. The solid product was filtered, washed with water, and dried over Drierite™ under vacuum to yield diaminopurine acetic acid **4.2** (0.60 g, 22%) as a pale orange solid (R_f = 0.1 in 9:1 CH_2Cl_2:MeOH); ^{1}H NMR (500 MHz, DMSO) δ 7.66 (s, 1 H), 6.65 (br s, 2 H), 5.79 (br s, 2 H), 4.69 (s, 2 H); IR (neat): 3416, 1662, 1003, 823, 761 cm^{-1}; HRMS (ESI) *m/z* for $C_7H_8N_6O_2$: 209.0791 (calcd $[M+H]^+$ 209.0787).

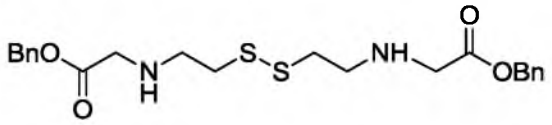

4.10

Dibenzyl-2,2'-((disulfanediylbis(ethane-2,1-diyl))bis(azanediyl))diacetate

4.10. To a suspension of cystamine dihydrochloride **4.5** (6.00 g, 26.6 mmol) and KI (0.221 g, 1.33 mmol) in acetonitrile (100 mL), Et_3N (16.3 mL, 117 mmol) was added for 5 min at rt under an atmosphere of N_2. Then benzyl bromoacetate (8.4 mL, 53 mmol) was added for 5 min. After stirring for 20 h, the reaction mixture was concentrated, dissolved in EtOAc, and washed with sat. NH_4Cl. The organic layer was separated and the aqueous layer was extracted with EtOAc (3x). The combined organic extracts were washed with brine, dried over Na_2SO_4, and concentrated to a brown oil. The crude mixture was purified by alumina (activated, neutral) flash column chromatography (9:1 CH_2Cl_2:MeOH) to yield dibenzyl ester **4.10** (2.63 g, 22%) as a yellowish brown oil (R_f = 0.6 in 9:1 CH_2Cl_2:MeOH); ^{1}H NMR (500 MHz, $CDCl_3$) δ 7.37 (m, 10 H), 5.18 (s, 4 H), 3.50 (s, 4 H), 2.96 (t, *J* = 6.2 Hz, 4 H), 2.83 (t, *J* = 6.4 Hz, 4 H), 1.98 (br s, 2 H); ^{13}C

NMR (125 MHz, $CDCl_3$) 171.7, 135.4, 128.2, 128, 127.97, 66.1, 50.2, 47.5, 38.7; IR (neat): 3032, 2914, 1733, 1455, 1140, 978, 737 cm^{-1}; LRMS (ESI) *m/z* for $C_{22}H_{28}N_2O_4S_2$: 449.1 (calcd $[M+H]^+$ 449.16), 471.1 (calcd $[M+Na]^+$ 471.14).

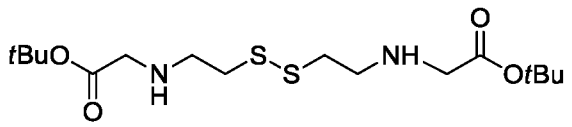

4.12

Di-*tert*-butyl-2,2'-((disulfanediylbis(ethane-2,1-diyl))bis(azanediyl))diacetate

4.12. To a suspension of cystamine dihydrochloride **4.5** (5.00 g, 22.2 mmol) and KI (0.737 g, 4.44 mmol) in acetonitrile (150 mL), Et_3N (13.0 mL, 93.2 mmol) was added for 10 min at rt under an atmosphere of N_2. After stirring for 5 min, *t*-butyl bromoacetate (6.9 mL, 47 mmol) was added for 10 min. After stirring for 40 h, the reaction mixture was refluxed for 3 h, cooled to rt, and TBAI (0.01 eq.) was added. The mixture was refluxed for another 3 h and stirred at rt for 20 h. Then the reaction mixture was filtered to remove a white precipitate and filtrate was concentrated. The concentrate was dissolved in EtOAc, washed with sat. NH_4Cl and brine, dried over Na_2SO_4, and concentrated to a brown oil. The crude mixture was purified by alumina (neutral, activated) flash column chromatography (a gradient of 8:2 EtOAC:Hexane to 9:1 CH_2Cl_2:MeOH) to yield di-*t*-butyl ester **4.12** (3.88 g, 46%) as a yellowish brown oil (R_f = 0.8 in 9:1 CH_2Cl_2:MeOH); ^1H NMR (500 MHz, $CDCl_3$) δ 3.2 (s, 4 H), 2.81 (t, *J* = 6.1 Hz, 4 H), 2.70 (t, *J* = 6.3 Hz, 4 H), 2.12 (br s, 2 H), 1.34 (s, 18 H); ^{13}C NMR (75 MHz, $CDCl_3$) 171.2, 81.1, 51.3, 47.7, 38.8, 28.0 IR (neat): 2977, 1731, 1456, 1367, 1228, 1154 cm^{-1}; HRMS (ESI) *m/z* for $C_{16}H_{32}N_2O_4S_2$: 403.1709 (calcd $[M+Na]^+$ 403.1701).

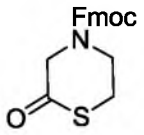

4.17

(9H-fluoren-9-yl)methyl2-oxothiomorpholine-4-carboxylate 4.17. To a solution of di-*t*-butyl ester **4.12** (2.10 g, 5.53 mmol) in CH_2Cl_2 (55 mL), FmocOSu (3.768 g, 11.17 mmol) was added at 0 °C under an atmosphere of N_2. After stirring for 5 min, Et_3N (1.6 mL, 11.2 mmol) was added for 5 min and stirred at 0 °C for 0.5 h. Then the reaction mixture was warmed to rt and stirred for 16 h. The mixture was concentrated and purified by silica flash column chromatography (a gradient of EtOAC:Hexane from 2:8 to 8:2) to yield the di-Fmoc compound **4.15** (1.01 g, 22%) as a yellowish oil (R_f = 0.3 in 1:1 EtOAC:Hexane), which was subjected to next step without further characterization.

To the above product **4.15** (0.423 g, 0.513 mmol) in MeOH (10 mL), TCEP (0.147 g, 0.513 mmol) was added at 0 °C under an atmosphere of N_2. After stirring for 5 min, ice bath was removed and stirred at rt for 25 min. The mixture was concentrated, triturated with Et_2O, and concentrated. Then the resulting white precipitate was dissolved in Et_2O. Et_2O layer was separated and concentrated to yield the known thiol **4.16** (crude 0.32 g, 77%),[43] as a yellow oil, which was subjected to next step without further purification.

To the above crude thiol **4.16**[43] (0.44 mmol) in toluene (5 mL), $TsOH{\cdot}H_2O$ (0.083 g, 0.44 mmol) was added (prior to the addition, $TsOH{\cdot}H_2O$ was dissolved in benzene and concentrated). The mixture was refluxed under Dean-Stark apparatus for 16 h (the reaction set up was covered with Al foil during the reaction). The reaction mixture was purified by silica flash column chromatography (1:1 EtOAC:Hexane) to afford thiomorpholinone **4.17** (0.071 g, 48%) as a pale yellow oil (R_f = 0.6 in 1:1 EtOAC:Hexane); ^{1}H NMR (500 MHz, $CDCl_3$) 7.75 (d, *J* = 6.7 Hz, 2 H), 7.53 (s, 2 H), 7.39

(t, *J* = 7.4 Hz, 2 H), 7.31 (t, *J* = 7.4 Hz, 2 H), 4.56-4.48 (m, 2 H), 4.27-4.2 (m, 3 H), 3.82 (br s, 1 H, rot 1), 3.61 (br s, 1 H, rot 2), 3.21 (br s, 1 H, rot 1), 2.98 (br s, 1 H, rot 2); ^{13}C $NMR_{major\ rotamer}$ (125 MHz, $CDCl_3$) 195.6, 154.8, 143.7, 141.5, 128.1, 127.3, 125, 120.3, 68.2, 55.5, 47.4, 42.7, 28.7; IR (neat): 2921, 1699, 1451, 1227, 1117, 739 cm^{-1}; HRMS (ESI) *m/z* for $C_{19}H_{17}NO_3S$: 362.0835 (calcd $[M+Na]^+$ 362.0827).

References

(1) Brudno, Y.; Liu, D. R. Recent Progress Toward the Templated Synthesis and Directed Evolution of Sequence-Defined Synthetic Polymers. *Chem. Biol.* **2009**, *16*, 265-276.

(2) Gorska, K.; Winssinger, N. Reactions Templated by Nucleic Acids: More Ways to Translate Oligonucleotide-Based Instructions into Emerging Function. *Angew. Chem. Int. Ed.* **2013**, *52*, 6820-6843.

(3) Naylor, R.; Gilham, P. T. Studies on Some Interactions and Reactions of Oligonucleotides in Aqueous Solution*. *Biochemistry* **1966**, *5*, 2722-2728.

(4) Orgel, L. E. Unnatural Selection in Chemical Systems. *Acc. Chem. Res.* **1995**, *28*, 109-118.

(5) Kleiner, R. E.; Dumelin, C. E.; Liu, D. R. Small-Molecule Discovery from DNA-Encoded Chemical Libraries. *Chem. Soc. Rev.* **2011**, *40*, 5707-5717.

(6) Ami, T.; Ito, K.; Yoshimura, Y.; Fujimoto, K. Sequence Specific Interstrand Photocrosslinking for Effective SNP Typing. *Org. Biomol. Chem.* **2007**, *5*, 2583-2586.

(7) Chouikhi, D.; Barluenga, S.; Winssinger, N. Clickable Peptide Nucleic Acids (cPNA) with Tunable Affinity. *Chem. Commun.* **2010**, *46*, 5476-5478.

(8) El-Sagheer, A. H.; Brown, T. Click chemistry with DNA. *Chem. Soc. Rev.* **2010**, *39*, 1388-1405.

(9) Jentzsch, E.; Mokhir, A. A Fluorogenic, Nucleic Acid Directed "Click" Reaction. *Inorg. Chem.* **2009**, *48*, 9593-9595.

(10) Kumar, R.; El-Sagheer, A.; Tumpane, J.; Lincoln, P.; Wilhelmsson, L. M.; Brown, T. Template-Directed Oligonucleotide Strand Ligation, Covalent Intramolecular DNA Circularization and Catenation Using Click Chemistry. *J. Am. Chem. Soc.* **2007**, *129*, 6859-6864.

(11) Franzini, R. M.; Kool, E. T. Efficient Nucleic Acid Detection by Templated Reductive Quencher Release. *J. Am. Chem. Soc.* **2009**, *131*, 16021-16023.

(12) Pianowski, Z. L.; Winssinger, N. Fluorescence-Based Detection of Single Nucleotide Permutation in DNA via Catalytically Templated Reaction. *Chem. Commun.* **2007**, 3820-3822.

(13) He, Y.; Liu, D. R. A Sequential Strand-Displacement Strategy Enables Efficient Six-Step DNA-Templated Synthesis. *J. Am. Chem. Soc.* **2011**, *133*, 9972-9975.

(14) Smith, G. P. Filamentous Fusion Phage:Novel Expression Vectors that Display Cloned Antigens on the Virion Surface. *Science* **1985**, *228*, 1315-1317.

(15) Tuerk, C.; Gold, L. Systematic Evolution of Ligands by Exponential Enrichment: RNA Ligands to Bacteriophage T4 DNA Polymerase. *Science* **1990**, *249*, 505-510.

(16) Nielsen, P. E.; Egholm, M.; Berg, R. H.; Buchardt, O. Sequence-Selective Recognition of DNA by Strand Displacement with a Thymine-Substituted Polyamide. *Science* **1991**, *254*, 1497-1500.

(17) Yu, H.; Zhang, S.; Dunn, M. R.; Chaput, J. C. An Efficient and Faithful in Vitro Replication System for Threose Nucleic Acid. *J. Am. Chem. Soc.* **2013**, *135*, 3583-3591.

(18) Ohta, A.; Yamagishi, Y.; Suga, H. Synthesis of Biopolymers Using Genetic Code Reprogramming. *Curr. Opin. Chem. Biol.* **2008**, *12*, 159-167.

(19) Xie, J.; Schultz, P. G. A Chemical Toolkit for Proteins-an Expanded Genetic Code. *Nat. Rev. Mol. Cell Biol.* **2006**, *7*, 775-782.

(20) Goodwin, J. T.; Lynn, D. G. Template-Directed Synthesis: Use of a Reversible Reaction. *J. Am. Chem. Soc.* **1992**, *114*, 9197-9198.

(21) Rosenbaum, D. M.; Liu, D. R. Efficient and Sequence-Specific DNA-Templated Polymerization of Peptide Nucleic Acid Aldehydes. *J. Am. Chem. Soc.* **2003**, *125*, 13924-13925.

(22) Kleiner, R. E.; Brudno, Y.; Birnbaum, M. E.; Liu, D. R. DNA-Templated Polymerization of Side-Chain-Functionalized Peptide Nucleic Acid Aldehydes. *J. Am. Chem. Soc.* **2008**, *130*, 4646-4659.

(23) Heemstra, J. M.; Liu, D. R. Templated Synthesis of Peptide Nucleic Acids via Sequence-Selective Base-Filling Reactions. *J. Am. Chem. Soc.* **2009**, *131*, 11347-11349.

(24) Nielsen, P. E. Peptide Nucleic Acid (PNA): A Model Structure for the Primordial Genetic Material? *Orig. Life Evol. Biosph.* **1993**, *23*, 323-327.

(25) Bohler, C.; Nielsen, P. E.; Orgel, L. E. Template Switching between PNA and RNA Oligonucleotides. *Nature* **1995**, *376*, 578-581.

(26) Brudno, Y.; Birnbaum, M. E.; Kleiner, R. E.; Liu, D. R. An in Vitro Translation, Selection and Amplification System for Peptide Nucleic Acids. *Nat. Chem. Biol.* **2010**, *6*, 148-155.

(27) Ura, Y.; Beierle, J. M.; Leman, L. J.; Orgel, L. E.; Ghadiri, M. R. Self-Assembling Sequence-Adaptive Peptide Nucleic Acids. *Science* **2009**, *325*, 73-77.

(28) Rowan, S. J.; Cantrill, S. J.; Cousins, G. R. L.; Sanders, J. K. M.; Stoddart, J. F. Dynamic Covalent Chemistry. *Angew. Chem. Int. Ed.* **2002**, *41*, 898-952.

(29) Tam, J. P.; Lu, Y.-A.; Yu, Q. Thia Zip Reaction for Synthesis of Large Cyclic Peptides: Mechanisms and Applications. *J. Am. Chem. Soc.* **1999**, *121*, 4316-4324.

(30) de Duve, C. The Beginnings of Life on Earth. *Am. Sci.* **1995**, *83*, 428–437.

(31) Mattes, A.; Seitz, O. Sequence Fidelity of a Template-Directed PNA-Ligation Reaction. *Chem. Commun.* **2001**, 2050-2051.

(32) Vázquez, O.; Seitz, O. Templated Native Chemical Ligation: Peptide Chemistry beyond Protein Synthesis. *J. Pept. Sci.* **2014**, *20*, 78-86.

(33) Haaima, G.; Hansen, H. F.; Christensen, L.; Dahl, O.; Nielsen, P. E. Increased DNA Binding and Sequence Discrimination of PNA Oligomers Containing 2,6-Diaminopurine. *Nucleic Acids Res.* **1997**, *25*, 4639-4643.

(34) ElAmin, B.; Anantharamaiah, G. M.; Royer, G. P.; Means, G. E. Removal of Benzyl-Type Protecting Groups from Peptides by Catalytic Transfer Hydrogenation with Formic Acid. *J. Org. Chem.* **1979**, *44*, 3442-3444.

(35) Byk, G.; Duchesne, M.; Parker, F.; Lelievre, Y.; Guitton, J. D.; Clerc, F. F.; Becquart, J.; Tocque, B.; Scherman, D. Local Constrained Shifty Pseudopeptides Inhibitors of Rasfarnesyl Transferase. *Bioorg. Med. Chem. Lett.* **1995**, *5*, 2677-2682.

(36) Burns, J. A.; Butler, J. C.; Moran, J.; Whitesides, G. M. Selective Reduction of Disulfides by Tris(2-carboxyethyl)phosphine. *J. Org. Chem.* **1991**, *56*, 2648-2650.

(37) Harwig, C. W.; Hoffman, T. Z.; Wentworth, A. D.; Janda, K. D. A One-Pot Multistep Approach to α-Azido-phosphonate and Phosphonothioate Diesters: Key Intermediates in the Synthesis of Haptens for the Generation of Antibody Ligases. *Bioorg. Med. Chem. Lett.* **2000**, *10*, 915-918.

(38) Mercey, G.; Lohier, J.-F.; Gaumont, A.-C.; Levillain, J.; Gulea, M. Versatile Synthesis of Secondary 2-Amino Thiols and/or Their Disulfides via Thiazolinium Salts. *Eur. J. Org. Chem.* **2009**, *2009*, 4357-4364.

(39) Merrifield, R. B. Solid Phase Peptide Synthesis. I. The Synthesis of a Tetrapeptide. *J. Am. Chem. Soc.* **1963**, *85*, 2149-2154.

(40) Carpino, L. A.; Han, G. Y. 9-Fluorenylmethoxycarbonyl Amino-Protecting Group. *J. Org. Chem.* **1972**, *37*, 3404-3409.

(41) Katritzky, A. R.; Abo-Dya, N. E.; Tala, S. R.; Abdel-Samii, Z. K. The Chemical Ligation of Selectively *S*-Acylated Cysteine Peptides to Form Native Peptides via 5-, 11- and 14-Membered Cyclic Transition States. *Org. Biomol. Chem.* **2010**, *8*, 2316-2319.

(42) Bu, X.; Xie, G.; Law, C. W.; Guo, Z. An Improved Deblocking Agent for Direct Fmoc Solid-Phase Synthesis of Peptide Thioesters. *Tet. Lett.* **2002**, *43*, 2419-2422.

(43) Görmer, K.; Bürger, M.; Kruijtzer, J. A. W.; Vetter, I.; Vartak, N.; Brunsveld, L.; Bastiaens, P. I. H.; Liskamp, R. M. J.; Triola, G.; Waldmann, H. Chemical-Biological Exploration of the Limits of the Ras De- and Repalmitoylating Machinery. *ChemBioChem* **2012**, *13*, 1017-1023.

(44) Stoermer, D.; Vitharana, D.; Hin, N.; Delahanty, G.; Duvall, B.; Ferraris, D. V.; Grella, B. S.; Hoover, R.; Rojas, C.; Shanholtz, M. K.; Smith, K. P.; Stathis, M.; Wu, Y.; Wozniak, K. M.; Slusher, B. S.; Tsukamoto, T. Design, Synthesis, and Pharmacological Evaluation of Glutamate Carboxypeptidase II (GCPII) Inhibitors Based on Thioalkylbenzoic Acid Scaffolds. *J. Med. Chem.* **2012**, *55*, 5922-5932.

(45) Majer, P.; Hin, B.; Stoermer, D.; Adams, J.; Xu, W.; Duvall, B. R.; Delahanty, G.; Liu, Q.; Stathis, M. J.; Wozniak, K. M.; Slusher, B. S.; Tsukamoto, T. Structural Optimization of Thiol-Based Inhibitors of Glutamate Carboxypeptidase II by Modification of the P1‘ Side Chain. *J. Med. Chem.* **2006**, *49*, 2876-2885.

CHAPTER 5

A MULTIVALENT SCAFFOLD FOR USE IN THE SYNTHESIS OF DNA-POLYMER CONJUGATES

Introduction

The molecular recognition properties of biomacromolecules can be tailored to develop programmable materials for biosensing and controlled drug release. In particular, targeted drug delivery and release in a stimuli-responsive manner has significant potential for use in therapeutics, but substantial challenges remain, including low efficacy, occurrence of side effects, and uncontrolled release.[1,2] Numerous drug delivery systems, including micelles, have been investigated to overcome the aforementioned challenges.[3] Micelles are formed by the self-assembly of amphiphilic monomers into well-defined, three-dimensional nanostructures having a hydrophobic core and a hydrophilic surface in aqueous environments. Thus, small, hydrophobic molecules can be entrapped in the core region of the micelles.

Due to the dynamic nature of micelles, guest molecules are in equilibrium with the surrounding solution and can diffuse out. In addition, micelles can be dissociated by high temperatures, low monomer concentrations, and changes in surrounding solvent conditions, thus leading to an uncontrolled release of entrapped molecules.[4] Consequently, numerous methods have been explored to covalently crosslink the micellar monomers, such as radical polymerization and disulfide bond formation,[4] and the stability and rate of guest molecule release from crosslinked micelles are directly proportional to crosslink density.[5]

Micellar structures that can dissociate in a stimuli-responsive manner using pH, light, temperature, and redox potential have been reported.[6] Additionally, amphiphilic micelles containing DNA[7] as the hydrophilic component have been used in various applications such as nucleic acid detection[8] and drug delivery.[9,10] For example, anticancer micelles have been designed for targeting folate receptors, which are highly expressed in many types of cancers, including ovarian, lung, breast, and bladder.[11] DNA strands of these micellar monomers were conjugated to folic acid, which can recognize the folate receptors of cancer cells.[10] In addition, doxorubicin was incorporated in the hydrophobic core of micelles. The selective uptake of these doxorubicin-loaded micelles resulted in the death of cancer cells, without affecting the normal cells. However, the assembly, disassembly, and guest release of micelles, triggered by the response of DNA to a specific chemical or biological signal, has yet to be explored.

The Heemstra group has proposed the design of programmable DNA-based micelles to control the release of guest molecules using the molecular recognition properties of DNA. In contrast to covalent crosslinking,[4] we hypothesized that the inherent Watson-Crick base pairing[12] between complementary DNA strands could provide noncovalent crosslinks that can stabilize the micellar structure, preventing the escape of guest molecules. In addition, these DNA-crosslinked micelles (DCMs) will be designed to respond to stimuli such as nucleic acids, small molecules, or enzymes that can disrupt the DNA crosslinks. Consequently, specific chemical or biological signals will be converted into the physical outputs of micelle dissociation and guest release (Figure 5.1).

We envisioned that DCMs would perform a multitude of applications, ranging from biosensors to drug carriers, depending on the nature of the guest molecules and DNA sequences. For instance, DCMs would act as a user-friendly biosensor, giving a visual output when the guest molecule is a solvatochromic dye that is sensitive to

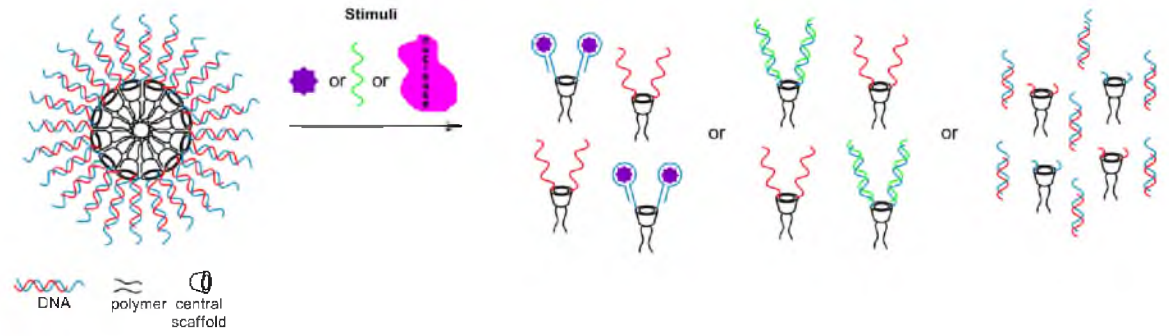

Figure 5.1. Stimuli-responsive dissociation of DNA-crosslinked micelles (Stimuli: small molecule, nucleic acid, or restriction endonuclease).

solvent polarity. If the DCMs are prepared by incorporating a therapeutic agent, they would act as a selective drug delivery vehicle capable of releasing the payload upon exposure to a specific toxin or pathogen. Quick, stimuli-responsive drug release is essential in many situations, such as war zones or areas hit with an epidemic crisis. For instance, the survival rate of army personnel and civilians exposed to chemical or biological warfare agents can be enhanced by pretreatment with micelles containing drugs known to counteract these harmful agents. Thus, the chemical or biological stimuli from warfare agents will disrupt the micelle, facilitating immediate drug release.

Aptamers are nucleic acid sequences that selectively bind to small molecules or proteins and can be generated for a wide range of targets using the SELEX process.[13-15] We envision that functionalizing the micellar monomers with known aptamers will facilitate the disassembly of the micelles upon exposure to the desired target (small molecule or nucleic acid), releasing the guest molecules. Similarly, when DCMs have complementary sequences of the EcoRI target sequence, crosslinks can be cleaved in the presence of restriction endonuclease enzymes.

To develop our DCMs, we intended to synthesize amphiphilic monomers comprised of DNA strands (including known aptamers) and hydrophobic polymers (including PNIPAAm) joined through a central multivalent scaffold. The DNA strands

within each monomer would be identical to one another in sequence and orientation. We would also synthesize a second monomer having DNA sequences complementary to the first. In addition, in order to have the desired crosslinking throughout the micelle, each monomer should have at least three (ideally four) DNA strands. A monomer having only two DNA strands (A_2) can only form an isolated dimer with a complementary monomer (B_2), preventing further crosslinks (Figure 5.2). However, when four DNA strands are present on one monomer, though two DNA strands of monomer (A_4) pair with two DNA strands of a complementary monomer (B_4), and steric effects would avoid further dimerization. Sequential base pairing between complementary DNA sequences on different monomers would then form noncovalent crosslinks to facilitate the assembly of the micellar structure and the entrapment of small guest molecules.

Our desired central scaffold would contain azide and alkyne moieties installed in the same synthetic unit, enabling it to undergo azide-alkyne cycloaddition with nucleic acids and polymers in a modular fashion to generate multivalent amphiphilic monomers (Figure 5.3).[16] This modular assembly would facilitate the optimization of multivalent scaffold by enabling variation in the extent of crosslinking, and hydrophobicity of the polymer. Originally, we decided to use calix[4]arene as the central unit of multivalent scaffold, as it is an attractive macrocyclic receptor in supramolecular chemistry, having a rigid, bowl-shaped structure that can be easily functionalized.[17] It can hold four spatially segregated DNA strands, and also, calixarene-DNA conjugates are known to form micellar structures.[18] Outlined here in this chapter are studies directed toward the design and synthesis of a potential micellar scaffold.

Results and Discussion

Our original design was to synthesize calixarene-based multivalent scaffold **5.1** (Scheme 5.1). The upper rim of calixarene **5.2** was converted to azidomethyl calixarene

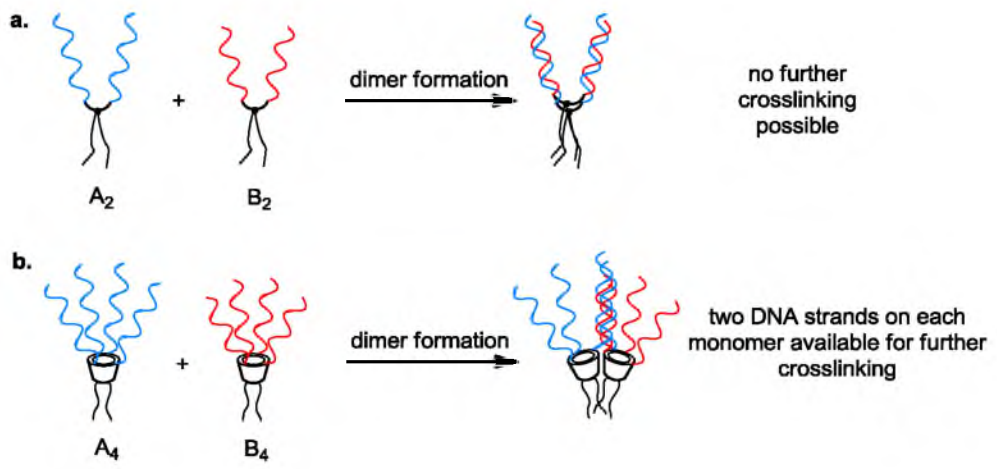

Figure 5.2. Monomers having two or four DNA strands (a) monomers having two DNA strands may form isolated dimers, (b) monomers having four DNA strands dimerize but retain the capacity to further crosslink.

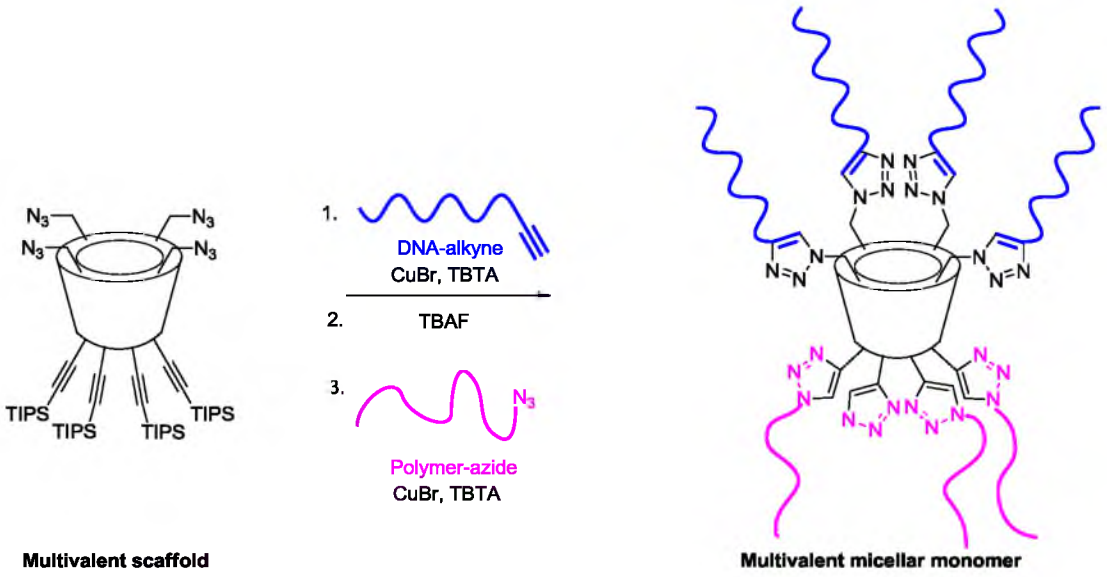

Figure 5.3. Modular assembly of multivalent micellar monomer.

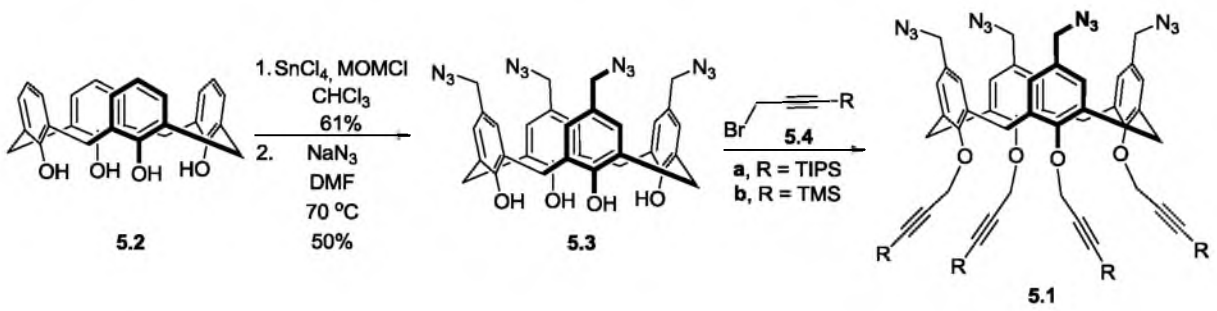

Scheme 5.1. Synthetic attempts for calixarene-based multivalent scaffold **5.1**.

5.3 in a two-step procedure.[19] Then, we investigated phenolic alkylation with TIPS-protected propargyl bromide **5.4a** in the lower rim of calixarene.[20] As it was not successful, alkylation with less sterically hindered TMS-protected propargyl bromide **5.4b** was attempted. After several synthetic attempts using numerous methods, however, we could not optimize suitable reaction conditions for installing the alkynes in the presence of the azides, or vice versa.

Therefore, we redesigned the multivalent scaffold; the desired multivalent scaffold is required to have at least three azide functionalities for the attachment of DNA and preferably two or more protected alkyne functionalities for the attachment of polymer chains. Our second generation designs were **5.5** with two alkynes and three azides, and **5.6** with two alkynes and four azides (Figure 5.4). In this chapter, we will only discuss the synthesis of **5.5**, as we were not able to complete the synthesis of **5.6** during the time frame of the project.

Retrosynthesis of multivalent scaffold 5.5

We envisioned that the desired multivalent scaffold **5.5** would arise from a convergent route via the phenolic etherification between gallic acid amide compound **5.7** and azido iodopropane **5.8** (Scheme 5.2). The amide bond formation between gallic acid **5.9** and amine **5.10** would yield amide **5.7**.

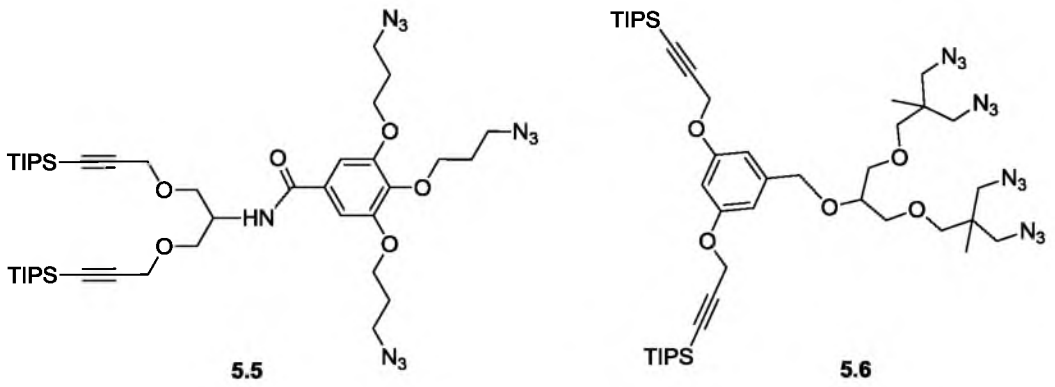

Figure 5.4. Second generation multivalent scaffold designs.

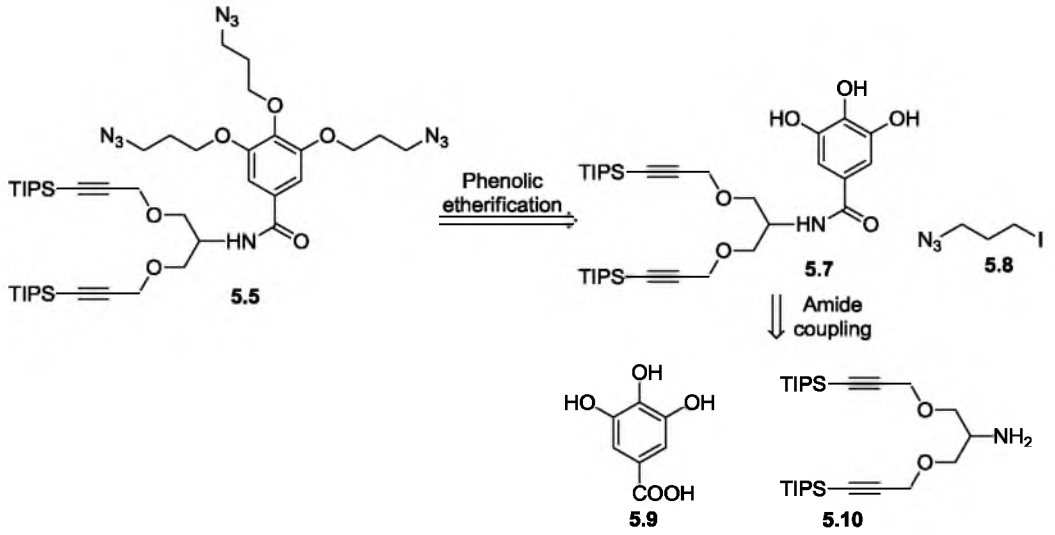

Scheme 5.2. Retrosynthetic analysis of multivalent scaffold **5.5**.

Synthesis of multivalent scaffold 5.5

In order to synthesize the TIPS-protected subunit **5.10**, commercially available 2-aminoglycerol **5.11** was reacted with Boc_2O to give Boc-protected amine **5.12** (Scheme 5.3).[21] Although the direct coupling of **5.12** with TIPS-protected propargyl bromide[20] and KOH was attempted, basic reaction conditions led to the removal of the TIPS group, yielding dipropargylic ether compound **5.13** in 40% yield. Instead, treatment of amine **5.12** with propargyl bromide and KOH afforded the dipropargylic ether compound **5.13**.

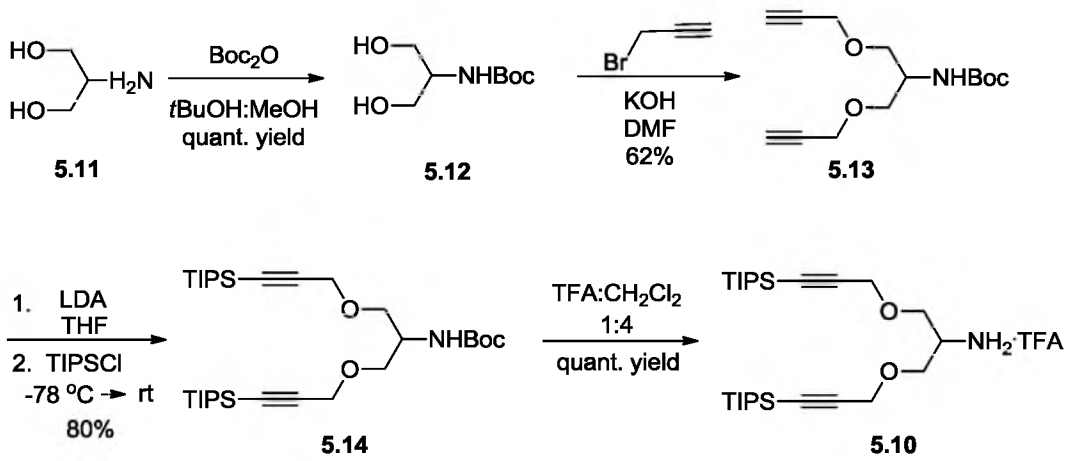

Scheme 5.3. Synthesis of amine coupling precursor **5.10**.

Subsequent deprotonation of the alkyne of **5.13** and treatment with TIPSCl provided the TIPS-protected dipropargylic ether compound **5.14**. Finally, removal of the Boc-protecting group of **5.14** with TFA afforded the TIPS-protected bis-alkyne portion of scaffold **5.10**.

Next, we investigated coupling of amine **5.10** with the central subunit in the scaffold, gallic acid **5.9**. Previous work has reported amide bond formation with gallic acid while having the phenolic groups unprotected.[22] Therefore, different amide bond formation conditions were screened with unprotected gallic acid **5.9** and amine precursor **5.10** to obtain gallic acid amide **5.7** (Scheme 5.4). However, we were not successful in isolating the desired product under these conditions due to polymerization, as indicated by mass values from MALDI-MS. Next, coupling conditions **a**, **b**, and **c** were investigated with gallic acid trimethyl ether **5.15** to obtain amide **5.16**. We found that both **b** and **c** conditions gave the desired amide product (Scheme 5.5). However, the attempt to remove methyl ethers of **5.16** with BBr_3 was unsuccessful.

Consequently, we decided to investigate amide coupling condition with acetyl-protected gallic acid **5.17** (Scheme 5.6).[23] Acetyl protection of phenol **5.9** gave tri-acetyl

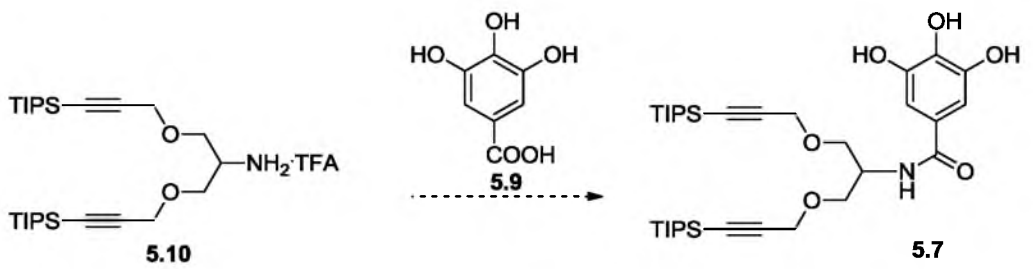

	Conditions
a)	EDCI, HOBt, DIPEA, DMF, CH_2Cl_2
b)	HATU, DIPEA, DMF, CH_2Cl_2
c)	PyBOP, HOBt, DIPEA, DMF, CH_2Cl_2
d)	TOTU, Et_3N, THF, DMAP
e)	IBCF, NMM, THF, DMAP

Scheme 5.4. Synthetic attempts for gallic acid amide compound **5.7** from gallic acid.

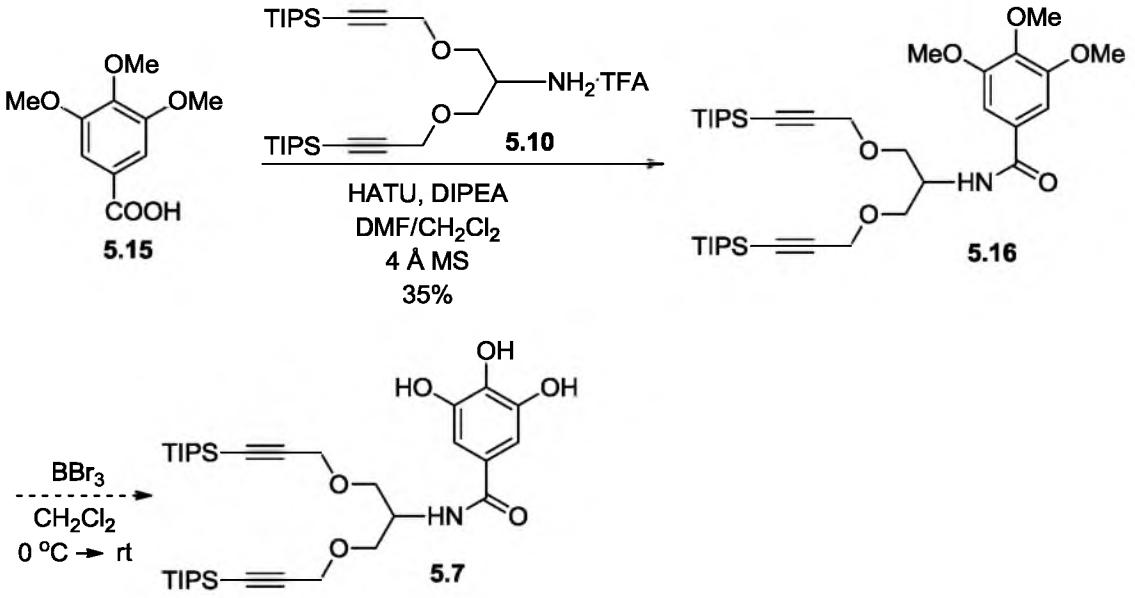

Scheme 5.5. Synthetic attempts for gallic acid amide **5.7** from methylated gallic acid.

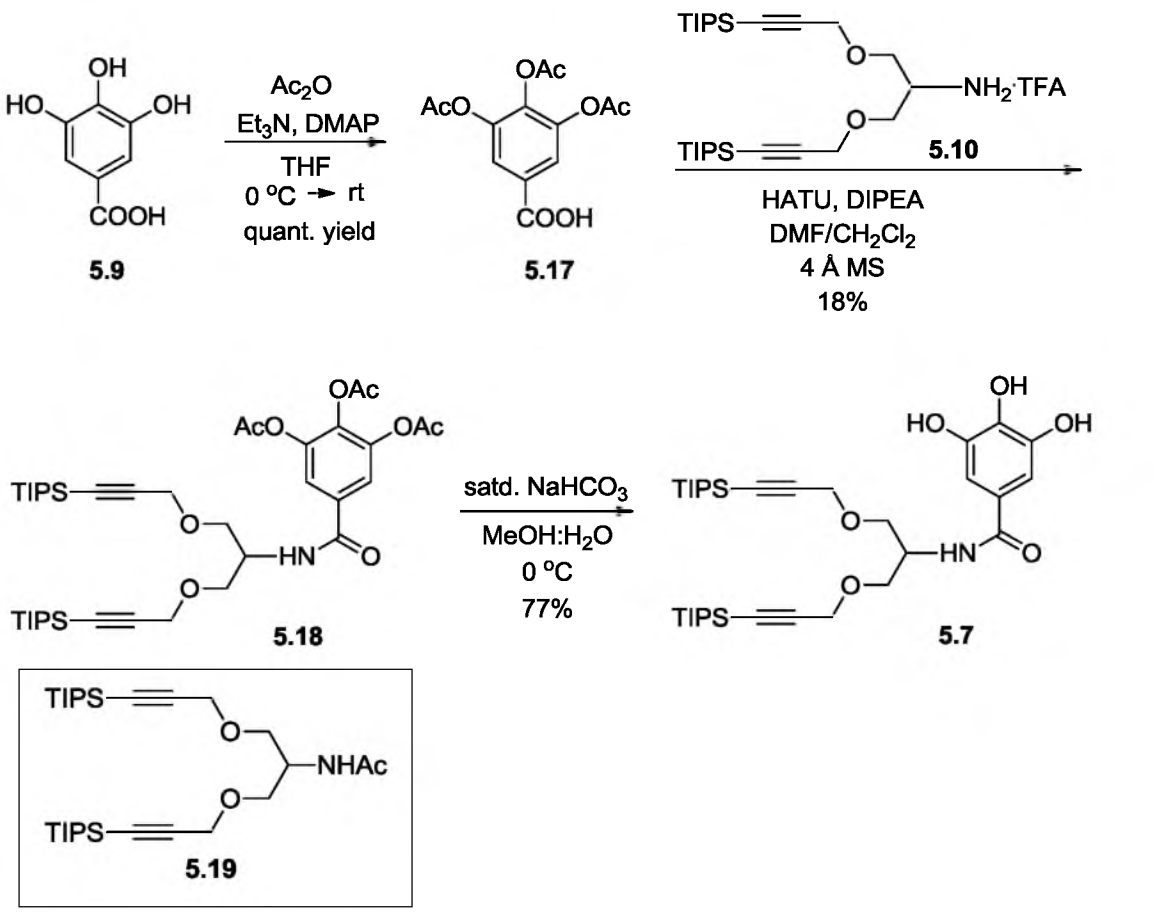

Scheme 5.6. Synthesis of gallic acid amide **5.7**.

protected gallic acid **5.17**. Next, coupling of **5.17** with amine **5.10** using HATU/DIPEA conditions yielded gallic acid amide compound **5.18**. In addition, acetyl-protected amine **5.19** was isolated as a byproduct. Different ester hydrolysis conditions were then investigated to remove acetyl esters of **5.18**, and finally, basic hydrolysis with $NaHCO_3$ yielded the phenol coupling precursor **5.7**.[24] Concurrently, 1-azido-3-iodopropane **5.8** was synthesized as previously reported.[25,26] Lastly, etherification of phenols of **5.7** by treating with azido-iodopropane **5.8** and K_2CO_3 formed the desired multivalent scaffold **5.5** (Scheme 5.7).

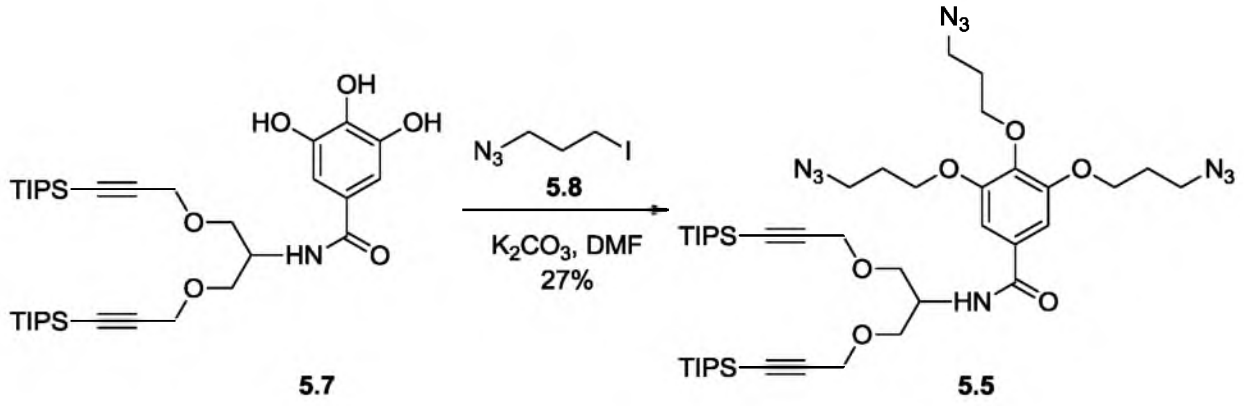

Scheme 5.7. Synthesis of multivalent scaffold **5.5**.

Conclusion

DNA-based micelles have potential to serve as stimuli-responsive materials due to their ability to undergo programmable assembly and disassembly. In order to develop our desired DCMs, we anticipated synthesizing amphiphilic monomers containing DNA strands and hydrophobic polymers joined through a central, multivalent scaffold. We were not able to successfully synthesize the calixarene-based scaffold **5.1** during the time frame of the project, but we were able to synthesize second generation multivalent scaffold **5.5** via a convergent route. However, attempts to find conditions to couple three DNA strands to obtain the amphiphilic monomer were not successful, likely due to unfavorable steric effects.[27] Studies to generate DNA-based micelles using new scaffolds are currently underway.

Experimental Section

General techniques

Glassware for all reactions was oven dried or flame dried and cooled prior to use. All reactions were run under an atmosphere of nitrogen or argon unless otherwise

stated. Tetrahydrofuran (THF) was distilled from sodium and benzophenone. Dichloromethane (CH_2Cl_2) and dimethylformamide (DMF) were passed through a solvent purification system (J. C. Meyer). Unless otherwise noted, all starting materials were obtained from commercial suppliers and were used without further purification. Thin layer chromatography was performed on Silica gel 60 F_{254} plates eluting with the solvent indicated, visualized by a 254/365 nm UV lamp, or stained with a solution of ninhydrin, p-anisaldehyde, or potassium permanganate. Column chromatography was performed on Merck silica gel Kieselgel 60 (230-400 mesh, 40–63 μm particle size). Yields were calculated for material judged homogenous by thin layer chromatography and NMR. Compounds were named using CS ChemBioDraw Ultra 12.0. NMR spectra were acquired on a Varian Unity-300, Inova 400, or VXR 500 spectrometer. Chemical shifts for ^1H NMR spectra are reported in parts per million relative to the signal of residual $CHCl_3$ at 7.27 ppm. Chemicals shifts for ^{13}C NMR spectra are reported in parts per million relative to the center line of the $CDCl_3$ triplet at 77.23 ppm. The abbreviations s, d, dd, t, p, m, and br stand for singlet, doublet, doublet of doublets, triplet, pentet, multiplet, and broad, respectively. IR spectra were obtained from Nicolet 380 FT-IR spectrometer. Mass spectra were recorded at the Mass Spectrometry facility in the Department of Chemistry of the University of Utah.

Procedures and characterizations

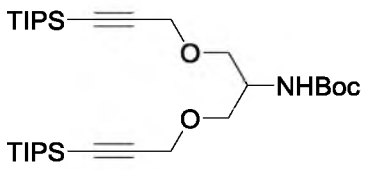

5.14

(tert-Butyl(3,3,15,15-tetraisopropyl-2,16-dimethyl-7,11-dioxa-3,15-disilaheptadeca-4,13-diyn-9-yl)carbamate 5.14. To a solution of Boc-protected 2-aminoglycerol

5.12[21] (2.000 g, 10.46 mmol) in DMF (40 mL), propargyl bromide (80 wt.% in toluene, 2.80 mL, 31.4 mmol) were added at 0 ºC under a nitrogen atmosphere. Then portions of finely ground KOH (2.349 g, 41.86 mmol) were added over a period of 15 min. The reaction mixture was then heated to 35 °C and stirred for 24 h. To the resulting brown mixture, ethyl acetate (10 mL) was added, poured into a separatory funnel containing ethyl acetate, and washed with water (3x30 mL). The organic layer was washed with brine, dried over Na_2SO_4, and concentrated. The crude material was purified by silica flash column chromatography (a gradient of EtOAC:Hexane from 1:9 to 3:7) to yield propargyl coupled amine **5.13** (1.73 g, 62%) as a brown oil (R_f = 0.8 in 3:7 EtOAC:Hexane). The amine was subjected to the alkyne TIPS protection without further characterization.

To the above product **5.13** (1.73 g, 6.48 mmol) in THF (70 mL), LDA (1.8 M in THF, 12.6 mL, 22.7 mmol) was added at -78 ºC under a nitrogen atmosphere. After stirring for 30 min, TIPSCl (3.16 mL, 14.9 mmol) was added and stirred at -78 °C for 10 min. Then the reaction mixture was warmed to rt and stirred for 2 h. The reaction mixture was concentrated and dissolved in CH_2Cl_2. The resulting mixture was washed with 2 N HCl and brine, dried over Na_2SO_4, and concentrated. The crude material was purified by silica flash column chromatography (a gradient of EtOAC:Hexane from 5:95 to 3:7) to afford TIPS-protected alkyne **5.14** (3.0 g, 80%) as a pale yellow oil (R_f = 0.8 in 3:7 EtOAC:Hexane); ^{1}H NMR (500 MHz, $CDCl_3$) δ 4.93 (d, *J* = 7.7 Hz, 1 H), 4.37-4.27 (m, 1 H), 4.19 (dd, *J* = 16.2, 4.7 Hz, 4 H), 3.63-3.62 (m, 4 H), 1.44 (s, 9 H), 1.07 (s, 42 H); ^{13}C NMR (125 MHz, $CDCl_3$) 155.5, 103.3, 87.8, 79.3, 68.3, 59.2, 49.5, 28.4, 18.7, 11.3; IR (neat): 2943, 2865, 1721, 1500, 1464, 1366, 1252, 1100, 998, 883 cm^{-1}; HRMS (ESI) *m/z* for $C_{32}H_{61}NO_4Si_2$: 602.4048 (calcd $[M+Na]^+$ 602.4037).

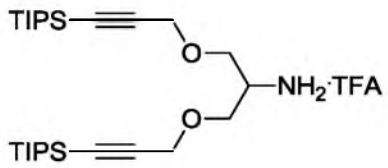

5.10

The TFA salt of 3,3,15,15-tetraisopropyl-2,16-dimethyl-7,11-dioxa-3,15-disilaheptadeca-4,13-diyn-9-amine 5.10. To a solution of the alkyne-TIPS-protected amine product **5.14** (2.42 g, 4.18 mmol) in CH_2Cl_2 (40 mL), TFA (5 mL) was added dropwise at 0 ºC under an atmosphere of N_2. After the addition, reaction mixture was stirred at 0 ºC for 15 min. Then the reaction mixture was slowly warmed to rt, stirred for another 2 h, and concentrated. The trituration of the crude reaction mixture with Et_2O yielded **5.10**, which was used forward without further purification.

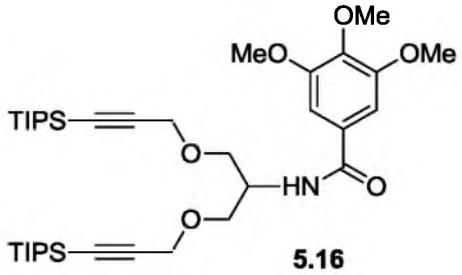

5.16

3,4,5-Trimethoxy-N-(3,3,15,15-tetraisopropyl-2,16-dimethyl-7,11-dioxa-3,15-disilaheptadeca-4,13-diyn-9-yl)benzamide 5.16. To a solution of gallic acid trimethyl ether **5.15** (0.623 g, 2.94 mmol), HATU (1.21 g, 3.18 mmol), and 4 Å MS in DMF (12 mL), DIPEA (3.84 mL, 22.0 mmol) was added at 0 °C under a nitrogen atmosphere. After stirring at 0 °C for 10 min, a solution of amine **5.10** (1.173 g, 2.447 mmol) in CH_2Cl_2 (15 mL) was added and stirred at 0 °C for 10 min. After stirring at rt for 16 h, the reaction mixture was concentrated and dissolved in EtOAc. The resulting mixture was washed with H_2O, sat. NH_4Cl, sat. $NaHCO_3$, and brine. The organic layer was dried over Na_2SO_4, and concentrated. The crude mixture was purified by silica flash column

chromatography (3:7 EtOAC:Hexane) to yield gallic acid amide **5.16** (0.59 g, 35%) as a yellow oil (R_f = 0.5 in 3:7 EtOAC:Hexane); ^{1}H NMR (300 MHz, $CDCl_3$) δ 7.01 (s, 2 H), 6.58 (d, *J* = 8.4 Hz, 1 H), 4.54-4.51 (m, 1 H), 4.24 (dd, *J* = 16.1, 5.4 Hz, 4 H), 3.89 (s, 9 H), 3.77 (d, *J* = 5 Hz, 4 H), 1.06 (s, 42 H); ^{13}C NMR (75 MHz, $CDCl_3$) 166.7, 153.1, 141, 130, 104.6, 103, 87.9, 68.1, 60.8, 59.1, 56.3, 48.7, 18.5, 11.1; IR (neat): 2941, 2865, 2171, 1584, 1463, 1352, 1232, 1127, 997, 882, 678 cm^{-1}; HRMS (ESI) *m/z* for $C_{37}H_{63}NO_6Si_2$: 696.4104 (calcd $[M+Na]^+$ 696.4092).

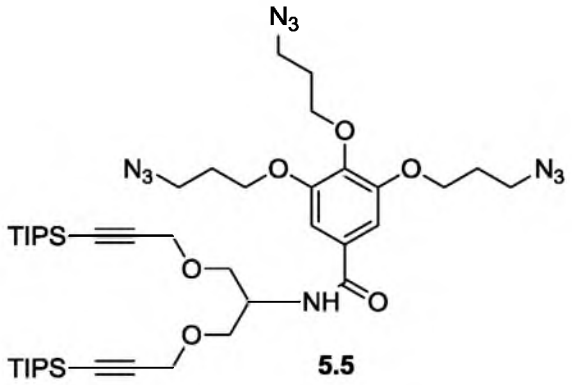

5.5

3,4,5-Tris(3-azidopropoxy)-N-(3,3,15,15-tetraisopropyl-2,16-dimethyl-7,11-dioxa-3,15-disilaheptadeca-4,13-diyn-9-yl)benzamide 5.5. To a solution of tri-acetyl protected gallic acid **5.17**[23] (0.84 g, 2.8 mmol), HATU (1.168 g, 3.073 mmol), and 4 Å MS in DMF (5 mL), DIPEA (3.7 mL, 21 mmol) was added at 0 °C under a nitrogen atmosphere. After stirring at 0 °C for 10 min, a solution of amine **5.10** (1.133 g, 2.364 mmol) in CH_2Cl_2 (14 mL) was added and stirred at 0 °C for 10 min. After stirring at rt for 16 h, the reaction mixture was concentrated and dissolved in EtOAc. The resulting mixture was washed with H_2O, sat. NH_4Cl, and brine. The organic layer was dried over Na_2SO_4 and concentrated. The crude mixture was purified by silica flash column chromatography (3:7 EtOAC:Hexane) to yield tri-acetyl gallic amide **5.18** (0.33 g, 18%) as a yellow oil (R_f = 0.4 in 3:7 EtOAC:Hexane). The amide was subjected to the next

step without further characterization.

To the above tri-acetyl protected gallic amide **5.18** (0.187 g, 0.247 mmol) in MeOH:H_2O (5:1, 12 mL), sat. $NaHCO_3$ (8 mL) was added for 20 min at 0 ºC. After stirring for 1 h, ice bath was removed, and stirred at rt for 7 h. As some starting material was still remaining, the reaction mixture was cooled to 0 ºC and sat. $NaHCO_3$ (5 mL) added for 10 min. After stirring for 10 min, ice bath was removed, and stirred at rt. Then, the reaction mixture was concentrated and dissolved in EtOAc and H_2O. The aqueous layer was washed with EtOAc and acidified to ~pH 3 with HCl. The aqueous layer was extracted with EtOAc. The organic layer was washed with brine, dried over Na_2SO_4, and concentrated to afford gallic amide **5.7** (crude 0.12 g, 77%), which was used forward without further purification.

To the above gallic amide **5.7** (0.1 g, 0.16 mmol) in DMF (0.5 mL), K_2CO_3 (0.098 g, 0.71 mmol) was slowly added at 0 °C under a nitrogen atmosphere. After stirring at 0 °C for 10 min, a solution of 1-azido-3-iodopropane **5.8**[25,26] (1.12 g, 0.583 mmol) in DMF (1 mL) was added and stirred at 0 °C for 1 h (Caution! azide containing reaction). After stirring at rt for 16 h, the reaction mixture was warmed to ~50 °C and stirred for another 16 h. The reaction mixture was filtered, diluted with EtOAc, and washed with ~0.5 N HCl. The aqueous layer was extracted with EtOAc. Then, combined organic layers were washed with brine, dried over Na_2SO_4, and concentrated to an oil. The crude mixture was purified by silica flash column chromatography (3:7 EtOAC:Hexane) to afford the multivalent scaffold **5.5** (0.038 g, 27%) as a pale yellow oil (R_f = 0.3 in 2:8 EtOAC:Hexane); ^{1}H NMR (500 MHz, $CDCl_3$) δ 7.00 (s, 2 H), 6.40 (d, *J* = 8.7 Hz, 1 H), 4.52-4.50 (m, 1 H), 4.24 (dd, *J* = 16.1, 9.4 Hz, 4 H), 4.13 (t, *J* = 6.5 Hz, 4 H), 4.07 (t, *J* = 5.8 Hz, 2 H), 3.75 (d, *J* = 4.7 Hz, 4 H), 3.60 (t, *J* = 6.6 Hz, 2 H), 3.55 (t, *J* = 7.6 Hz, 4 H), 2.10 (p, *J* = 7.4 Hz, 4 H), 2.00 (p, *J* = 7.4 Hz, 2 H), 1.06 (s, 42 H); ^{13}C NMR (100 MHz, $CDCl_3$) 166.7, 152.7, 140.7, 130.5, 106.4, 103.1, 88.3, 70.2, 68.3, 66.2,

59.4, 53.6, 48.4, 29.9, 29.1, 18.8, 11.3; IR (neat): 2943, 2866, 2096, 1582, 1464, 1354, 1234, 1099, 997, 884 cm^{-1}; HRMS (ESI) *m/z* for $C_{43}H_{72}N_{10}O_6Si_2$: 903.5078 (calcd $[M+Na]^+$ 903.5073).

References

(1) Mura, S.; Nicolas, J.; Couvreur, P. Stimuli-Responsive Nanocarriers for Drug Delivery. *Nat. Mater.* **2013**, *12*, 991-1003.

(2) Hoffman, A. S. Stimuli-Responsive Polymers: Biomedical Applications and Challenges for Clinical Translation. *Advanced Drug Deliver. Rev.* **2013**, *65*, 10-16.

(3) Kim, S.; Shi, Y.; Kim, J. Y.; Park, K.; Cheng, J.-X. Overcoming the Barriers in Micellar Drug Delivery: Loading Efficiency, in vivo Stability, and Micelle–Cell Interaction. *Expert Opin. Drug Del.* **2010**, *7*, 49-62.

(4) O'Reilly, R. K.; Hawker, C. J.; Wooley, K. L. Cross-Linked Block Copolymer Micelles: Functional Nanostructures of Great Potential and Versatility. *Chem. Soc. Rev.* **2006**, *35*, 1068-1083.

(5) Jiwpanich, S.; Ryu, J.-H.; Bickerton, S.; Thayumanavan, S. Noncovalent Encapsulation Stabilities in Supramolecular Nanoassemblies. *J. Am. Chem. Soc.* **2010**, *132*, 10683-10685.

(6) Klaikherd, A.; Nagamani, C.; Thayumanavan, S. Multi-Stimuli Sensitive Amphiphilic Block Copolymer Assemblies. *J. Am. Chem. Soc.* **2009**, *131*, 4830-4838.

(7) Alemdaroglu, F. E.; Herrmann, A. DNA Meets Synthetic Polymers-Highly Versatile Hybrid Materials. *Org. Biomol. Chem.* **2007**, *5*, 1311-1320.

(8) Li, Z.; Zhang, Y.; Fullhart, P.; Mirkin, C. A. Reversible and Chemically Programmable Micelle Assembly with DNA Block-Copolymer Amphiphiles. *Nano Lett.* **2004**, *4*, 1055-1058.

(9) Kwak, M.; Herrmann, A. Nucleic Acid Amphiphiles: Synthesis and Self-Assembled Nanostructures. *Chem. Soc. Rev.* **2011**, *40*, 5745-5755.

(10) Kwak, M.; Herrmann, A. Nucleic Acid/Organic Polymer Hybrid Materials: Synthesis, Superstructures, and Applications. *Angew. Chem. Int. Ed.* **2010**, *49*, 8574-8587.

(11) Parker, N.; Turk, M. J.; Westrick, E.; Lewis, J. D.; Low, P. S.; Leamon, C. P. Folate Receptor Expression in Carcinomas and Normal Tissues Determined by a Quantitative Radioligand Binding Assay. *Anal. Biochem.* **2005**, *338*, 284-293.

(12) Watson, J. D.; Crick, F. H. C. Molecular Structure of Nucleic Acids: A Structure for Deoxyribose Nucleic Acid. *Nature* **1953**, *171*, 737-738.

(13) Tuerk, C.; Gold, L. Systematic Evolution of Ligands by Exponential Enrichment: RNA Ligands to Bacteriophage T4 DNA Polymerase. *Science* **1990**, *249*, 505-510.

(14) Ellington, A. D.; Szostak, J. W. In vitro Selection of RNA Molecules that Bind Specific Ligands. *Nature* **1990**, *346*, 818-822.

(15) Cho, E. J.; Lee, J.-W.; Ellington, A. D. Applications of Aptamers as Sensors. *Annual Rev. Anal. Chem.* **2009**, *2*, 241-264.

(16) Huisgen, R. Centenary Lecture - 1,3-Dipolar Cycloadditions. *P. Chem. Soc.* **1961**, 357-396.

(17) Gutsche, C. D.; Nam, K. C. Calixarenes. 22. Synthesis, Properties, and Metal Complexation of Aminocalixarenes. *J. Am. Chem. Soc.* **1988**, *110*, 6153-6162.

(18) Consoli, G. M. L.; Granata, G.; Lo Nigro, R.; Malandrino, G.; Geraci, C. Spontaneous Self-Assembly of Water-Soluble Nucleotide−Calixarene Conjugates in Small Micelles Coalescing to Microspheres. *Langmuir* **2008**, *24*, 6194-6200.

(19) Zhao, M.; Zhang, X.-Y.; Ma, J.-P.; Huang, R.-Q.; Guo, D.-S. Self-Inclusion Structure of 5,11,17,23-Tetrakis(azidomethyl)-25,26,27,28-tetrahydroxycalix[4]arene, and 5,11,17,23-Tetra-tert-butyl-25,27-bis(chloroacetoxy)-26,28-bis(2-pyridylmethoxy)calix[4]arene. *Acta Crystallogr. C* **2009**, *65*, o186-o190.

(20) Hoogboom, J.; Swager, T. M. Increased Alignment of Electronic Polymers in Liquid Crystals via Hydrogen Bonding Extension. *J. Am. Chem. Soc.* **2006**, *128*, 15058-15059.

(21) Choi, J. Y.; Borch, R. F. Highly Efficient Synthesis of Enantiomerically Enriched 2-Hydroxymethylaziridines by Enzymatic Desymmetrization. *Org. Lett.* **2007**, *9*, 215-218.

(22) Altman, M. D.; Ali, A.; Kumar Reddy, G. S. K.; Nalam, M. N. L.; Anjum, S. G.; Cao, H.; Chellappan, S.; Kairys, V.; Fernandes, M. X.; Gilson, M. K.; Schiffer, C. A.; Rana, T. M.; Tidor, B. HIV-1 Protease Inhibitors from Inverse Design in the Substrate Envelope Exhibit Subnanomolar Binding to Drug-Resistant Variants. *J. Am. Chem. Soc.* **2008**, *130*, 6099-6113.

(23) Elsinghorst, P. W.; Cieslik, J. S.; Mohr, K.; Tränkle, C.; Gütschow, M. First Gallamine−Tacrine Hybrid: Design and Characterization at Cholinesterases and the M2 Muscarinic Receptor. *J. Med. Chem.* **2007**, *50*, 5685-5695.

(24) Buechi, G.; Weinreb, S. M. Total Syntheses of Aflatoxins M1 and G1 and an Improved Synthesis of Aflatoxin B1. *J. Am. Chem. Soc.* **1971**, *93*, 746-752.

(25) Hong, V.; Presolski, S. I.; Ma, C.; Finn, M. G. Analysis and Optimization of Copper-Catalyzed Azide–Alkyne Cycloaddition for Bioconjugation. *Angew. Chem., Int. Ed.* **2009**, *48*, 9879-9883.

(26) Conrad, P. C.; Kwiatkowski, P. L.; Fuchs, P. L. Rapid Access to a Series of Highly Functionalized α, β-Unsaturated Cyclopentenones. A Caveat on Aminospirocyclization. *J. Org. Chem.* **1987**, *52*, 586-591.

(27) Peterson, A. M.; Heemstra, J. M.: Unpublished results.

CHAPTER 6

CONCLUSION AND FUTURE DIRECTIONS

Peptide nucleic acid (PNA)[1] shows tremendous potential to be used in numerous therapeutic, biosensing, and nanotechnology applications due to its excellent biostability, strong binding affinity, and high selectivity toward nucleic acids.[2-4] However, PNA faces challenges for *in vivo* applications such as poor solubility, cellular uptake, and bioavailability, predominantly due to its uncharged backbone. The Heemstra group hypothesized that negatively charged PNA analogues would overcome the abovementioned limitations by taking advantage of the delivery methods available for DNA and RNA. However, it has been hypothesized that the high binding affinity of PNA to DNA and RNA is due to the lack of electrostatic repulsion in duplex formation between charge neutral PNA and negatively charged nucleic acids.[4] According to this hypothesis, incorporation of negative charge to PNA backbone would be detrimental in duplex formation with DNA and RNA, yet, there were not any studies in literature that investigated this hypothesis. Thus, the major objectives of this dissertation were to investigate whether there is a role of electrostatics in PNA:DNA and PNA:RNA duplex formation and whether negatively charged groups could be incorporated into the PNA backbone without affecting its binding affinity and selectivity with DNA and RNA.

Towards these goals, we explored the effect of ionic strength on binding affinity for γ-modified PNAs having either negatively charged aspartic acid side chains or positively charged lysine side chains.[5] We observed that electrostatic effects do play a role in binding of PNA to DNA and RNA, as negatively charged PNA shows lowest

duplex stability at low ionic strength. However, with the increase of ionic strength, charge screening of electrostatic repulsion by counterions in solution enables negatively charged side chains to be incorporated into the PNA backbone without reducing duplex stability with DNA and RNA. Presumably, preorganization of the PNA backbone via hydrogen bonding is primarily responsible for the enhanced duplex stability of PNA with DNA and RNA.[6,7] We observed that at medium to high salt concentrations, negatively charged PNA actually binds more strongly to DNA and RNA than does positively charged PNA. Interestingly, in a simulated physiological buffer, negatively charged PNA shows higher affinity for RNA whereas positively charged PNA shows higher affinity for DNA.

Intrigued by the effect of side chain structure and electrostatics on binding affinity, we were also curious to explore the mismatch and orientation selectivity of these γ-substituted PNAs.[8] We found that introduction of γ-substituents results in similar or slightly decreased selectivity compared to unmodified PNA. However, for γ-substituted PNAs, positively charged side chains provide higher selectivity in DNA binding and negatively charged side chains provide higher selectivity in RNA binding. Although we obtained CD spectra to understand these differential binding properties, these studies revealed that the side chains do not significantly alter the overall structure of the PNA:DNA or PNA:RNA duplexes. However, we hypothesize that side chains may still provide sufficient local perturbation to account for the observed differences in affinity and selectivity.

Appella and coworkers have previously reported a γ-Lys PNA:DNA duplex model in which side chains with *S* stereochemistry orient along the periphery of the duplex, whereas side chains with *R* stereochemistry point towards the interior of the duplex (Figure 6.1).[9] Similarly, the Ly group observed that methyl group of L-Ala γ-PNA point towards the solvent (Figure 6.2).[10] Thus, γ-substituents are less likely to introduce steric effects on base pairing and base stacking interactions of a duplex.[11] In addition, the

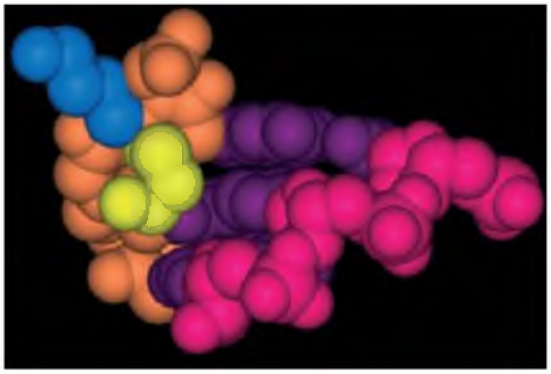

Figure 6.1. γ-Lys PNA:DNA duplex model [Side chain derived from l-(*S*)-lysine projects away from the duplex (blue) and side chain from d-(*R*)-lysine projects into the minor groove (yellow). Purple=base pairs, orange=PNA backbone, and fuscia=DNA backbone]. Reproduced with permission from (Englund, E. A.; Appella, D. H. *Angew. Chem., Int. Ed.* **2007**, *46*, 1414-1418), copyright © (2007) WILEY-VCH Verlag GmbH & Co. KGaA, Weinheim.

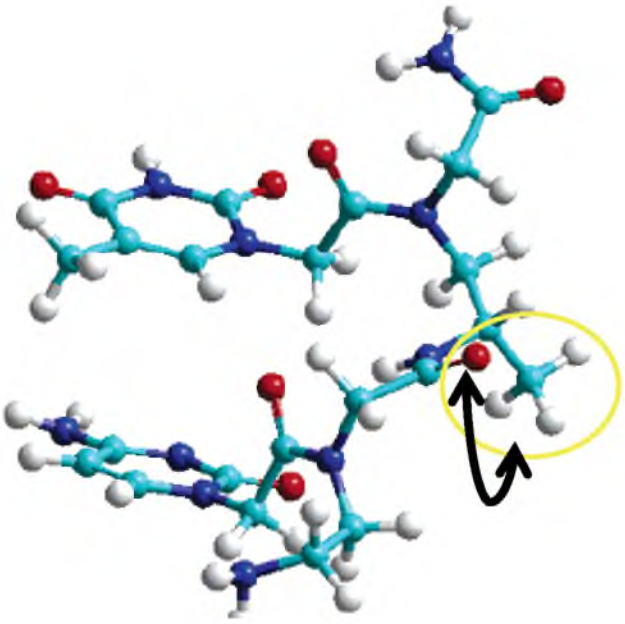

Figure 6.2. Solution structure of L-Ala γ-PNA determined from NMR (arrow points toward the backbone carbonyl group and γ-methyl group in the circled region). Adapted with permission from (Dragulescu-Andrasi, A.; Rapireddy, S.; Frezza, B. M.; Gayathri, C.; Gil, R. R.; Ly, D. H. *J. Am. Chem. Soc.* **2006**, *128*, 10258-10267). Copyright © (2006) American Chemical Society.

carbonyl oxygen of the PNA backbone points towards the solvent (in trans configuration with γ-Me group) and the backbone-nucleobase linker amide points towards the carboxyl end of backbone.[12] Furthermore, 1D and 2D NMR studies of γ-PNA suggest that γ-Me groups are orientated away from the duplex, but in the edge between minor and major groove.[11]

We envision that γ-substituents could non-covalently interact with the backbone carbonyl group, as pointed out by the arrow in Figure 6.2. Among intra-residue non-covalent interactions, γ-Lys PNA could exhibit favorable hydrogen bonding and electrostatic attractions whereas γ-Asp PNA could induce electrostatic repulsion effects (Figure 6.3). In γ-Lys PNA, favorable electrostatic effects could bring the side chain in close proximity to the backbone but in γ-Asp PNA, unfavorable interactions could point the side chain away from the backbone. We hypothesize that Lys PNA:DNA duplex can accommodate the side chain of Lys in the wide major groove but with RNA, these electrostatic interactions could give rise to unfavorable steric effects due to its narrow major groove. Unfavorable electrostatic effects could interfere with the duplex formation of Asp-PNA with DNA and RNA. However, with RNA these electrostatic effects can be screened more efficiently by counterions than in the case of DNA, as A-form helices are known to recruit a higher density of counter ions than B-form helices.[13] Although our hypothesis provides a possible explanation for the differential binding properties that we observed, exact conclusions cannot be derived from the limited structural data that is currently available for γ-PNA. Thus, in the future, extensive structural information is required to thoroughly understand our results.

Typical A-form and B-form helices have 11 and 10.5 base pairs per turn, respectively. Most of the previous structural studies utilized 10-mer sequences of PNA,[10] presumably due to the sequence length which gives one helical turn. Further studies are required that vary the length of our initial 10-mer sequence to confirm the assumption

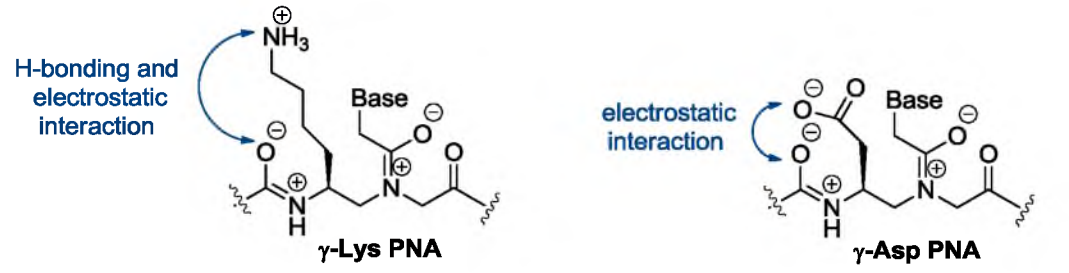

Figure 6.3. Potential noncovalent interactions between PNA backbone and γ-side chain (for clarity: all the potential interactions are not shown).

that the differential binding properties are independent of PNA sequence length. It should be noted that the aspartic acid and lysine monomers used in this initial study have slightly different side chain lengths. Future investigations are needed to explore the effect of side chain length on duplex stability and mismatch discrimination, to confirm that the differential binding properties predominantly arise due to altered charges of side chains rather than the side chain lengths. In addition, further work is necessary to understand the effect of numerous side chains and sequences, and the effect of positioning of the side chains relative to the mismatch site on binding affinity and selectivity.

PNA can bind to DNA and RNA in both parallel and antiparallel orientations because of its achiral backbone, but generally prefers the antiparallel orientation. Introduction of γ-substituents had previously been shown to favor unambiguous antiparallel binding.[10] However, we observed that unmodified PNA discriminates parallel versus antiparallel orientations better than modified PNA. γ-substituted PNAs have a rigid right handed helical structure with less conformational freedom than unmodified PNA. Therefore, in duplex formation, DNA and RNA may undergo conformational changes to accommodate γ-PNA, rather than γ-PNA undergoing changes to bind to DNA and RNA.[14] Thus, we assume that under the salt conditions that we studied, DNA and RNA binding to right handed γ-PNA in the parallel orientation is entropically favorable.

Whereas, unmodified PNA has more conformational flexibility and needs to preorganize into a right handed-helix in binding to DNA and RNA, which imposes a higher entropic penalty in duplex formation in the parallel orientation. Further work must be carried out under different salt conditions to validate the observed orientation selectivity of γ-PNA.

In general, we perceived that the error associated with PNA:RNA duplex data is higher than with DNA. This could be due to the greater instability of RNA than DNA in long cycles of thermal melting (T_m) experiments. However, it is interesting to see whether the error can be minimized by using a new sample of PNA:RNA duplex in each trial of T_m studies. In addition, the simulated physiological buffer used for this initial study mimics the extracellular salt conditions. Therefore, it is desirable to investigate the binding properties in a buffer mimicking intracellular salt conditions. Also, the salt dependent melting properties should be examined with varying concentrations of other monovalent cations including lithium and potassium, instead of sodium.

Our results provide insight into the impact of PNA side chain structure and electrostatics on the binding affinity and selectivity with DNA and RNA in antisense and antigene applications. Since PNA can be negatively charged without sacrificing binding affinity and selectivity, we anticipate that these molecules will show promise as therapeutics that take advantage of both the inherent benefits of PNA and the multitude of charge-based delivery technologies currently being developed for DNA and RNA. Thus, future studies will explore the competence of our negatively charged PNA as an *in vivo* therapeutic agent.

References

(1) Nielsen, P. E.; Egholm, M.; Berg, R. H.; Buchardt, O. Sequence-Selective Recognition of DNA by Strand Displacement with a Thymine-Substituted Polyamide. *Science* **1991**, *254*, 1497-1500.

(2) *Peptide Nucleic Acids: Protocols and Applications*, 2nd ed.; Nielsen, P. E., Ed.; Horizon Bioscience: United Kingdom, 2004.

(3) *Peptide Nucleic Acids, Morpholinos and Related Antisense Biomolecules*; Janson, C. G.; During, M. J., Eds.; Springer: US, 2006.

(4) Egholm, M.; Buchardt, O.; Christensen, L.; Behrens, C.; Freier, S. M.; Driver, D. A.; Berg, R. H.; Kim, S. K.; Norden, B.; Nielsen, P. E. PNA Hybridizes to Complementary Oligonucleotides Obeying the Watson–Crick Hydrogen-Bonding Rules. *Nature* **1993**, *365*, 566-568.

(5) De Costa, N. T. S.; Heemstra, J. M. Evaluating the Effect of Ionic Strength on Duplex Stability for PNA Having Negatively or Positively Charged Side Chains. *PLoS ONE* **2013**, *8*, e58670.

(6) Hyrup, B.; Egholm, M.; Buchardt, O.; Nielsen, P. E. A Flexible and Positively Charged PNA Analogue with an Ethylene-Linker to the Nucleobase: Synthesis and Hybridization Properties. *Bioorg. Med. Chem. Lett.* **1996**, *6*, 1083-1088.

(7) Topham, C. M.; Smith, J. C. Orientation Preferences of Backbone Secondary Amide Functional Groups in Peptide Nucleic Acid Complexes: Quantum Chemical Calculations Reveal an Intrinsic Preference of Cationic D-Amino Acid-Based Chiral PNA Analogues for the P-form. *Biophys. J.* **2007**, *92*, 769-786.

(8) De Costa, N. T. S.; Heemstra, J. M. Differential DNA and RNA Sequence Discrimination by PNA Having Charged Side Chains. *Bioorg. Med. Chem. Lett.* **2014**, *24*, 2360-2363.

(9) Englund, E. A.; Appella, D. H. γ-Substituted Peptide Nucleic Acids Constructed from L-Lysine are a Versatile Scaffold for Multifunctional Display. *Angew. Chem., Int. Ed.* **2007**, *46*, 1414-1418.

(10) Dragulescu-Andrasi, A.; Rapireddy, S.; Frezza, B. M.; Gayathri, C.; Gil, R. R.; Ly, D. H. A Simple γ-Backbone Modification Preorganizes Peptide Nucleic Acid into a Helical Structure. *J. Am. Chem. Soc.* **2006**, *128*, 10258-10267.

(11) He, W.; Crawford, M. J.; Rapireddy, S.; Madrid, M.; Gil, R. R.; Ly, D. H.; Achim, C. The Structure of a γ-Modified Peptide Nucleic Acid Duplex. *Mol. BioSyst.* **2010**, *6*, 1619-1629.

(12) Rasmussen, H.; Kastrup, J. S.; Nielsen, J. N.; Nielsen, J. M.; Nielsen, P. E. Crystal Structure of a Peptide Nucleic Acid (PNA) Duplex at 1.7 Å Resolution. *Nat. Struct. Mol. Biol.* **1997**, *4*, 98-101.

(13) Cheatham, T. E., III; Kollman, P. A. Molecular Dynamics Simulations Highlight the Structural Differences among DNA:DNA, RNA:RNA, and DNA:RNA Hybrid Duplexes. *J. Am. Chem. Soc.* **1997**, *119*, 4805-4825.

(14) Sahu, B.; Sacui, I.; Rapireddy, S.; Zanotti, K. J.; Bahal, R.; Armitage, B. A.; Ly, D. H. Synthesis and Characterization of Conformationally Preorganized, (*R*)-Diethylene Glycol-Containing γ-Peptide Nucleic Acids with Superior Hybridization Properties and Water Solubility. *J. Org. Chem.* **2011**, *76*, 5614-5627.

APPENDIX A

SPECTRAL DATA OF CHAPTER 2: ^{1}H AND ^{13}C NMR, HPLC, MALDI-TOF, UV-MELTING CURVES, AND T_M DATA

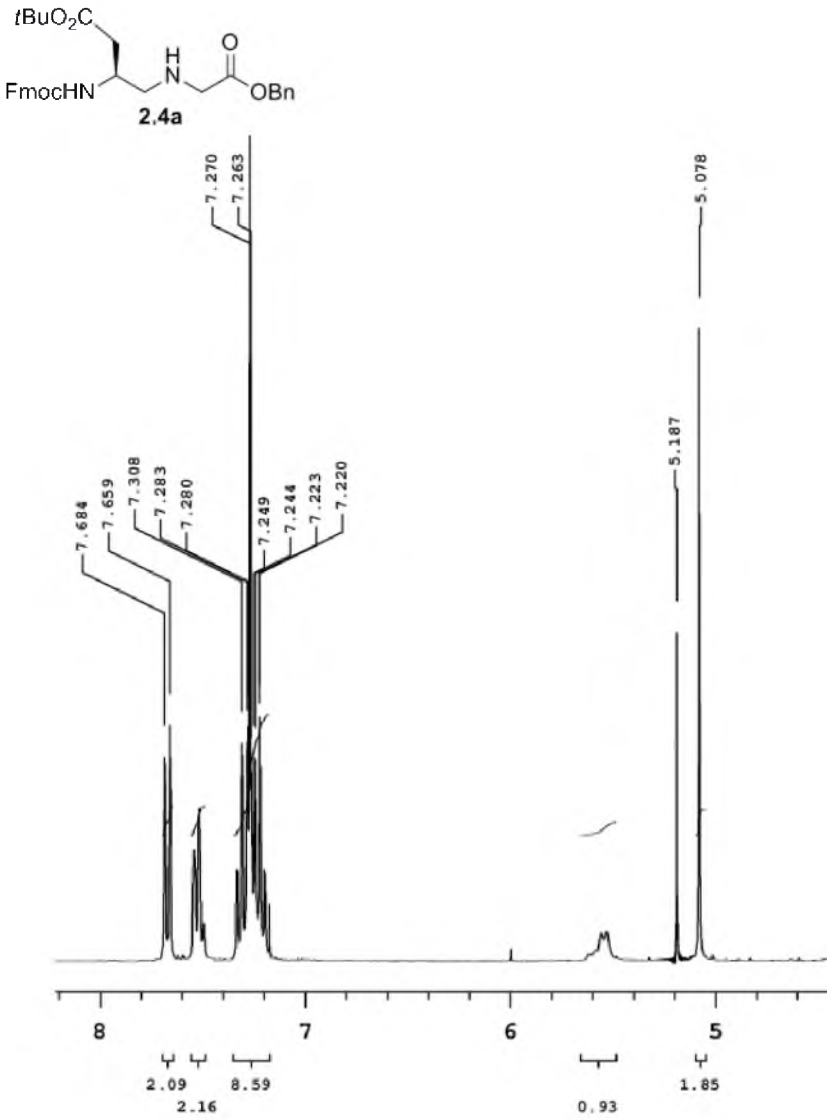
tBuO2C
FmocHN
H
N
O
OBn
2.4a
7.270
7.263
5.078
5.187
7.684
7.659
7.308
7.283
7.280
7.249
7.244
7.223
7.220
8
7
6
5
2.09
2.16
8.59
0.93
1.85

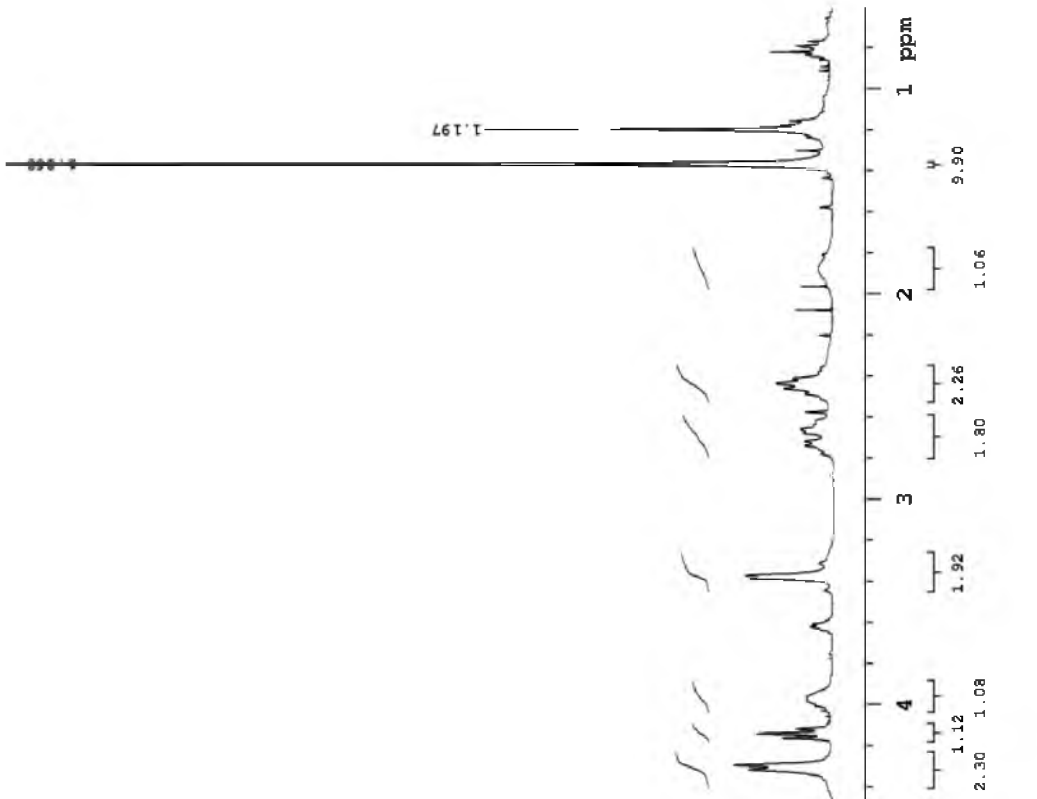
1.197
1 ppm
2
3
4
9.90
1.06
2.26
1.80
1.92
1.12
2.30
1.08

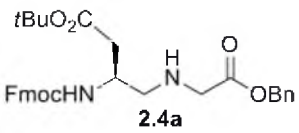
tBuO2C
H
N
O
FmocHN
OBn

2.4a

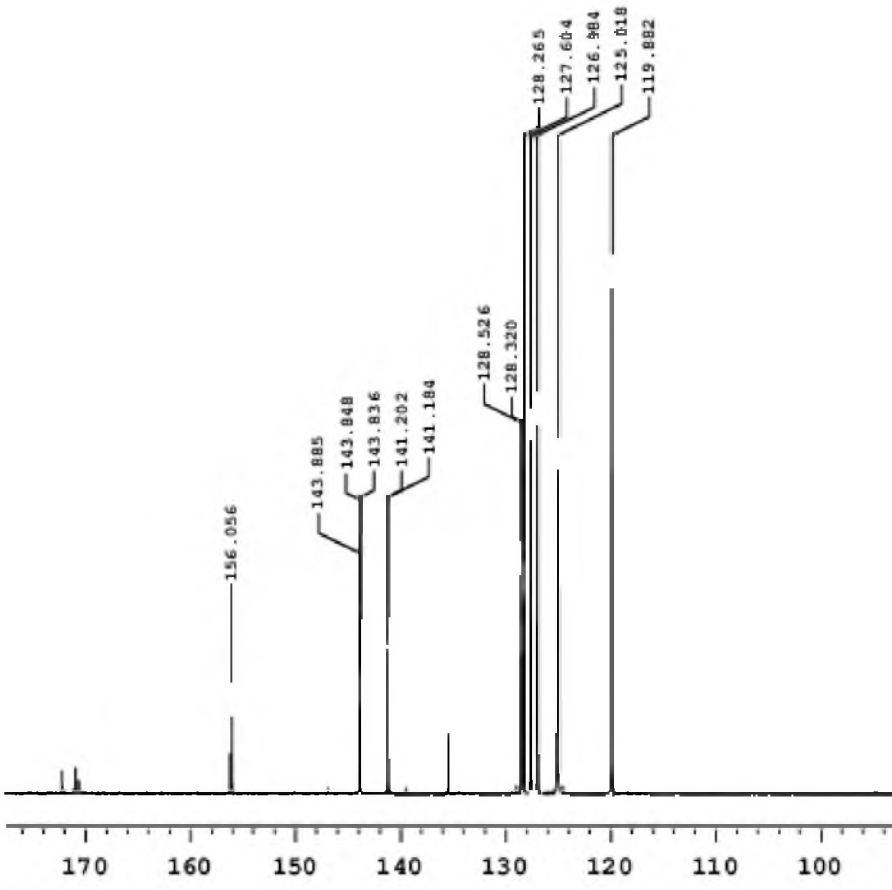
128.265
127.604
126.984
125.018
119.882
128.526
128.320
143.885
143.848
143.836
141.202
141.184
156.056
170
160
150
140
130
120
110
100

66.625
66.479
63.966
52.001
50.538
50.070
47.150
47.096
37.231
27.967
90
80
70
60
50
40
30
ppm

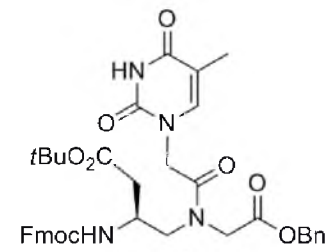
O
HN
O
N
tBuO2C
O
O
FmocHN
N
OBn

2.5a

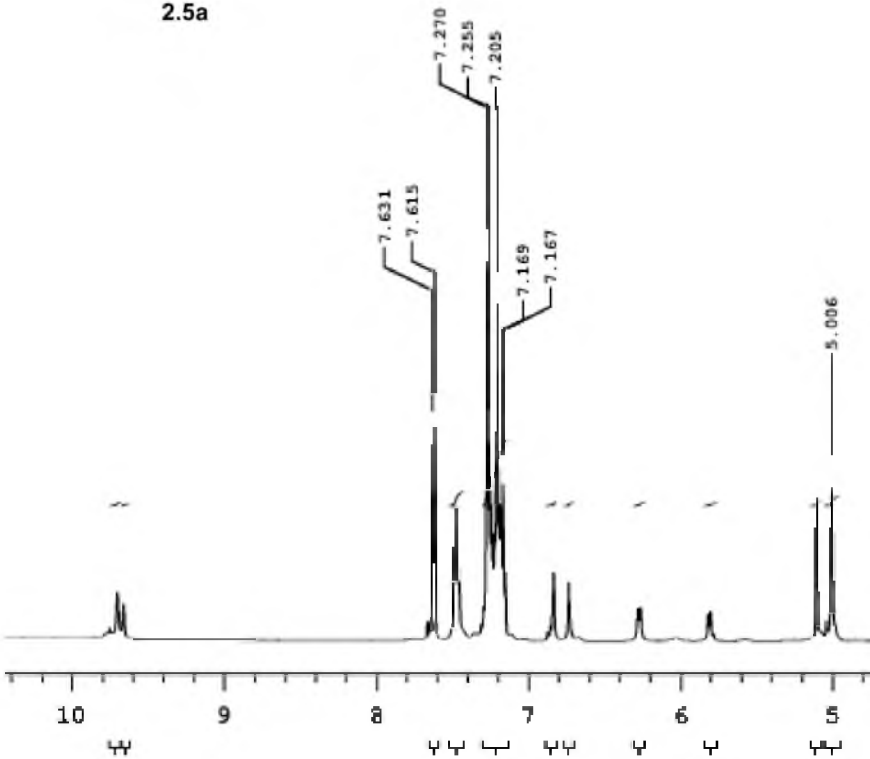
7.270
7.255
7.205
7.631
7.615
7.169
7.167
5.006
10
9
8
7
6
5
0.60
0.32
2.07
2.07
9.30
0.44
0.58
0.48
0.38
1.32
0.81

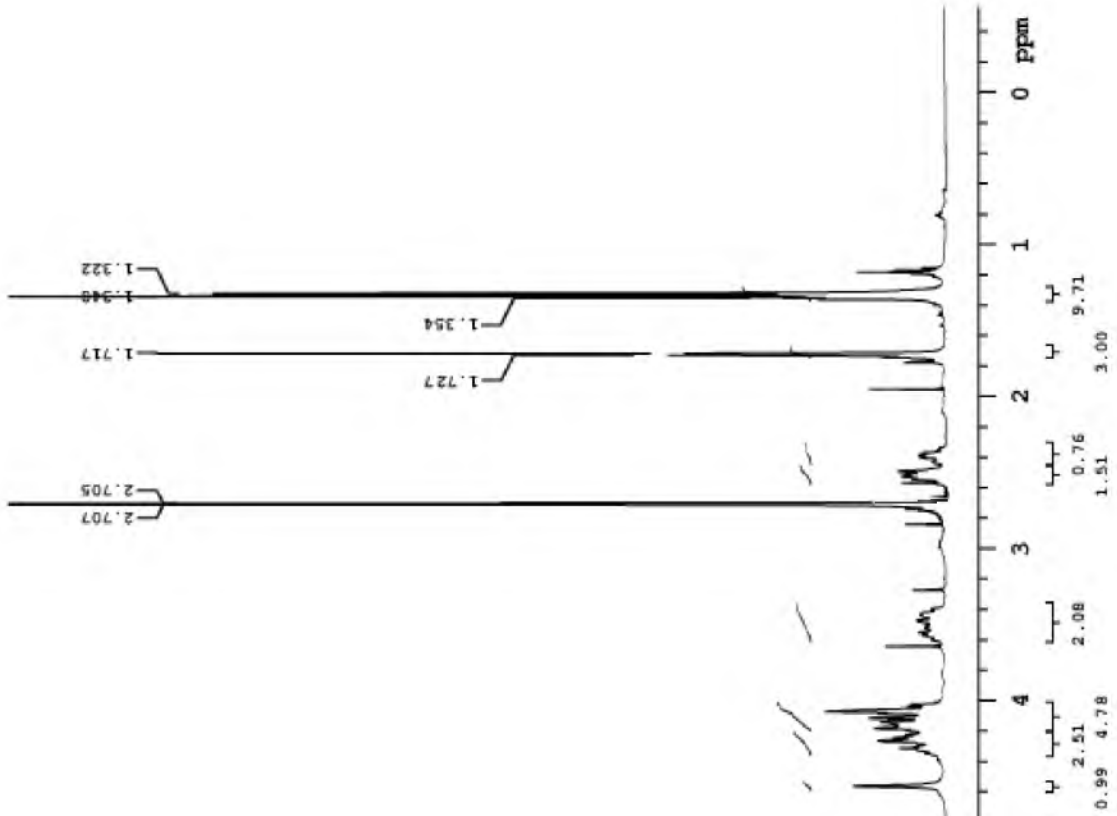
2.707
2.705
1.717
1.727
1.354
1.346
1.322
ppm
0
1
2
3
4
9.71
3.00
0.76
1.51
2.08
2.51
0.99
4.78

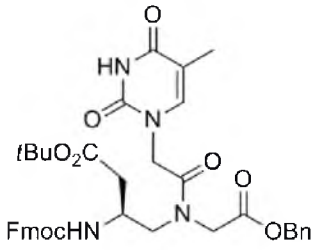
O
HN
O
N
O
tBuO2C
O
O
N
FmocHN
OBn

2.5a

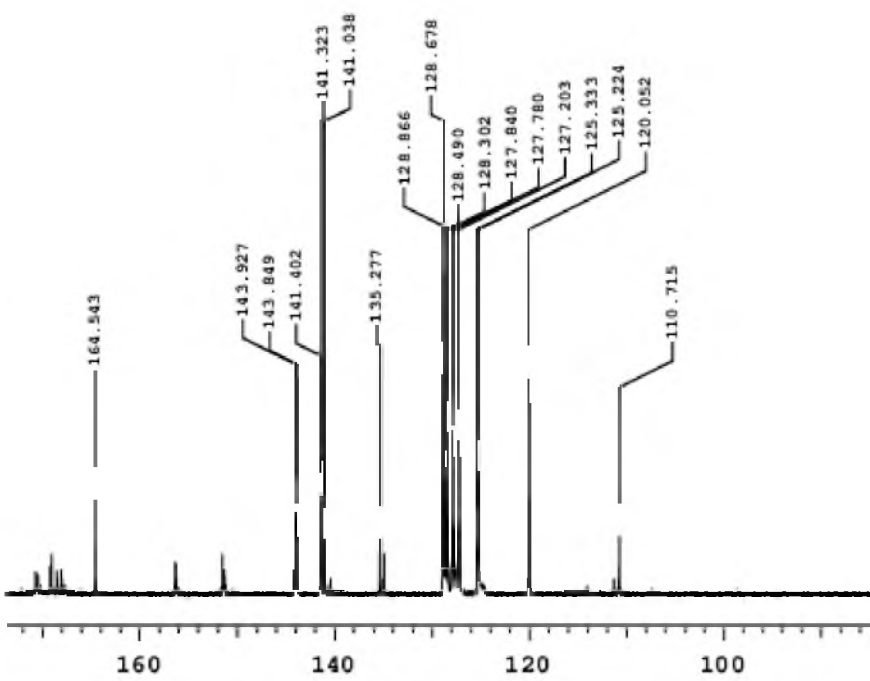
164.543
143.927
143.849
141.402
141.323
141.038
135.277
128.866
128.678
128.490
128.302
127.840
127.780
127.203
125.333
125.224
120.052
110.715
160
140
120
100

77.485
77.230
76.975
67.936
67.262
67.074
66.795
51.011
47.405
47.278
47.169
38.706
37.371
29.795
28.131
12.384
80
60
40
20
ppm

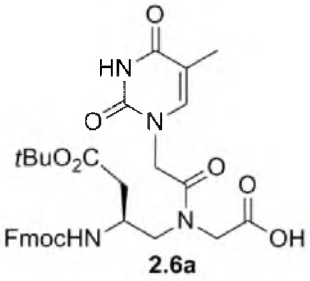
O
HN
O
N
tBuO2C
O
O
FmocHN
N
OH

2.6a

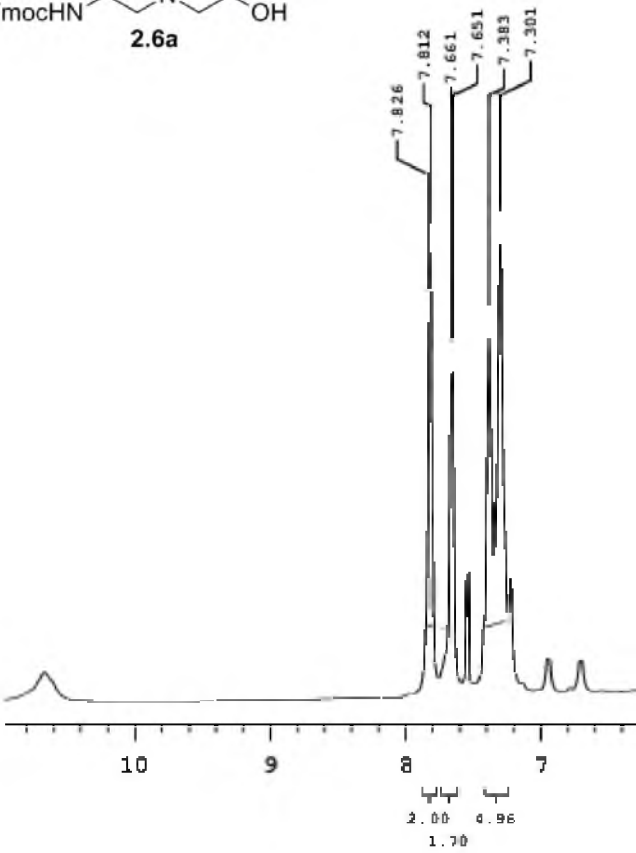
7.826
7.812
7.661
7.651
7.383
7.301
10
9
8
7
2.00
4.96
1.70

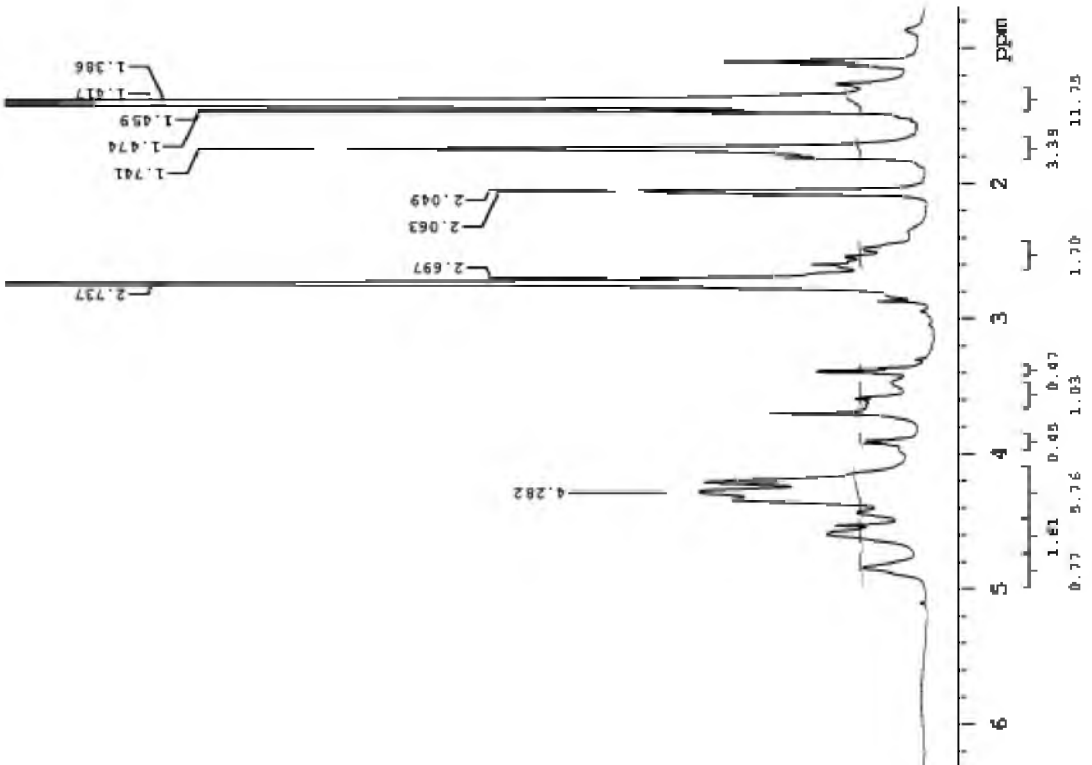
1.386
1.417
1.459
1.474
1.741
2.049
2.063
2.697
2.737
4.282
ppm
1.61
0.77
5.76
0.45
1.03
0.47
1.70
3.39
11.75

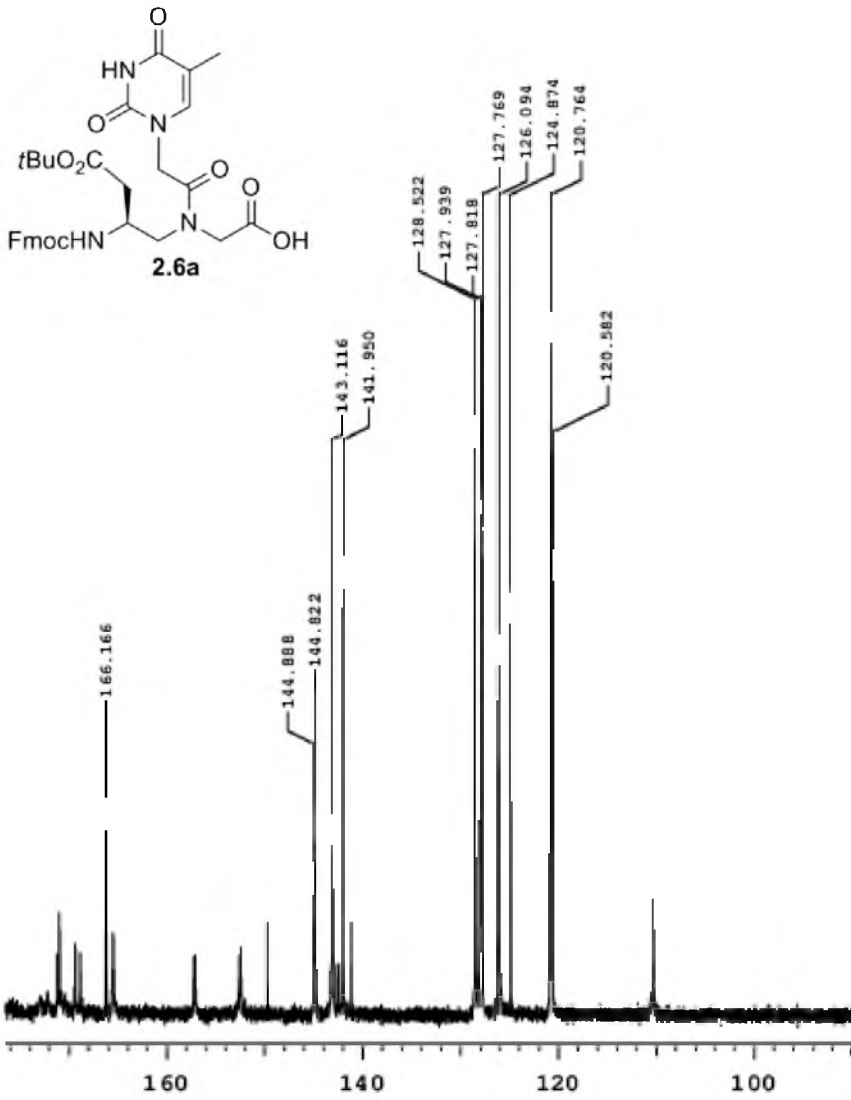
O
HN
O
N
tBuO2C
O
O
FmocHN
N
OH
2.6a
166.166
144.888
144.822
143.116
141.950
128.522
127.939
127.818
127.769
126.094
124.874
120.764
120.582
160
140
120
100

81.518
81.190
67.416
47.863
47.814
43.012
38.751
30.210
30.058
29.900
29.748
29.590
28.218
28.176
28.115
18.554
12.265
80
60
40
20
ppm

Reinjected HPLC traces and MALDI-TOF data for PNA oligomers.

a)

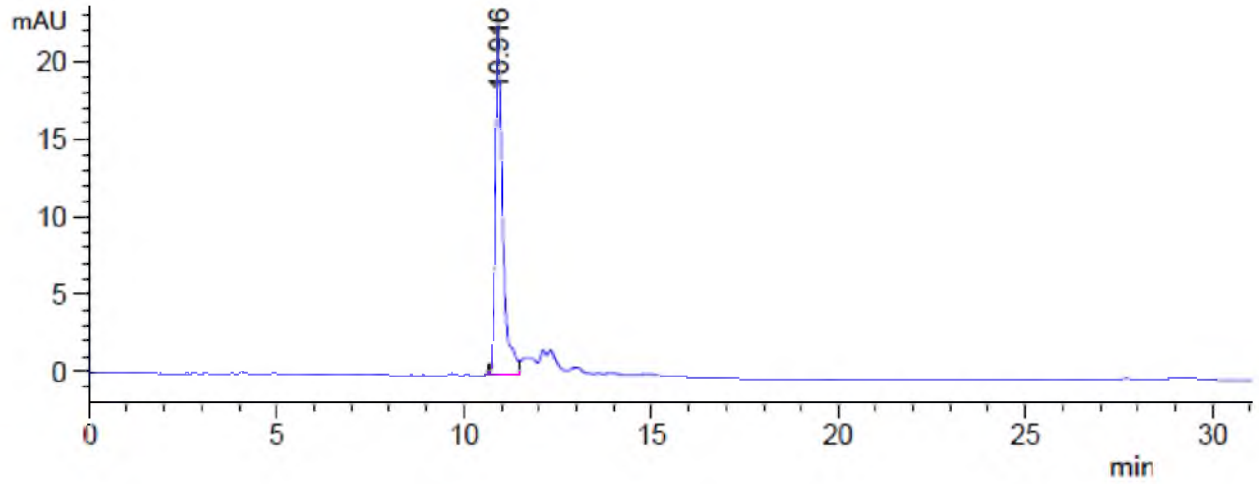

b)

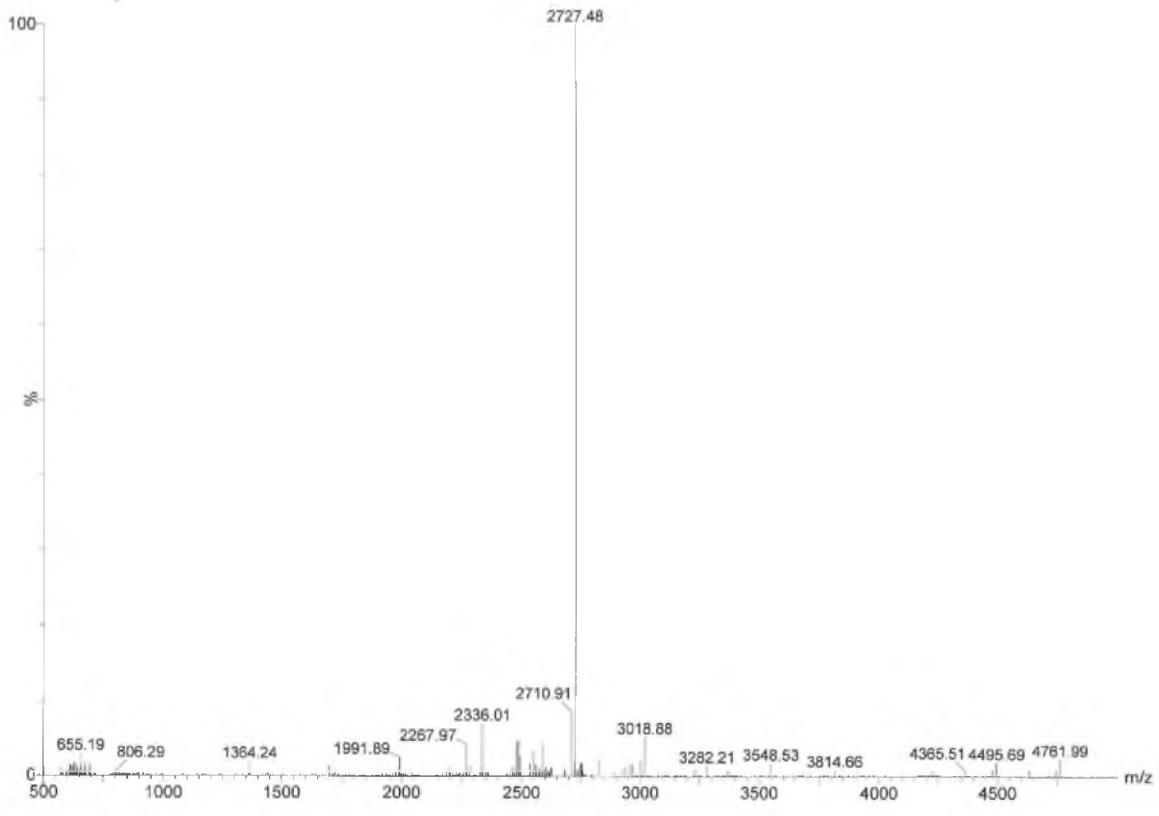

m/z 2727.48 (calcd $[M]^+$ 2727.04).

Figure A.1. HPLC and MALDI-TOF MS of PNA **nf** (H-GTAGATCACT-NH_2).

a)

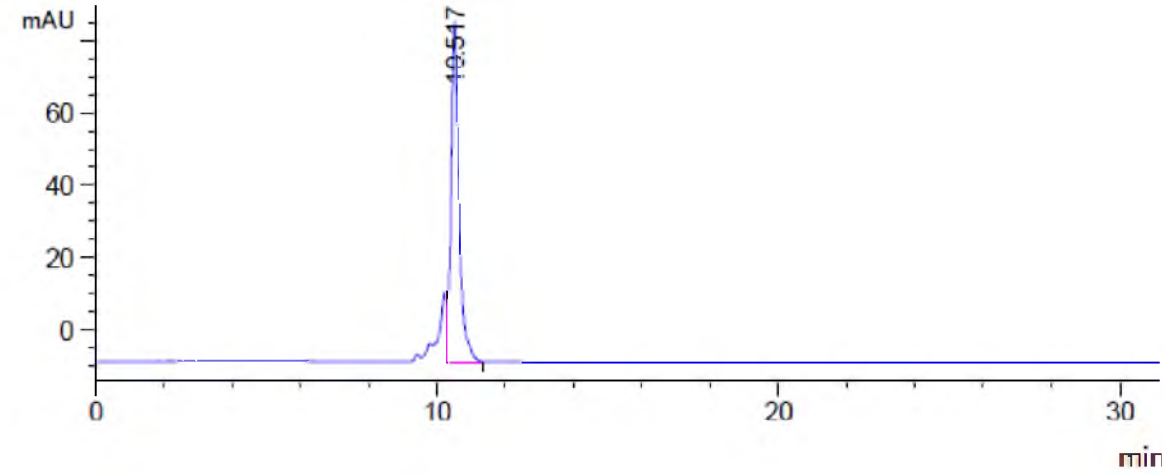

b)

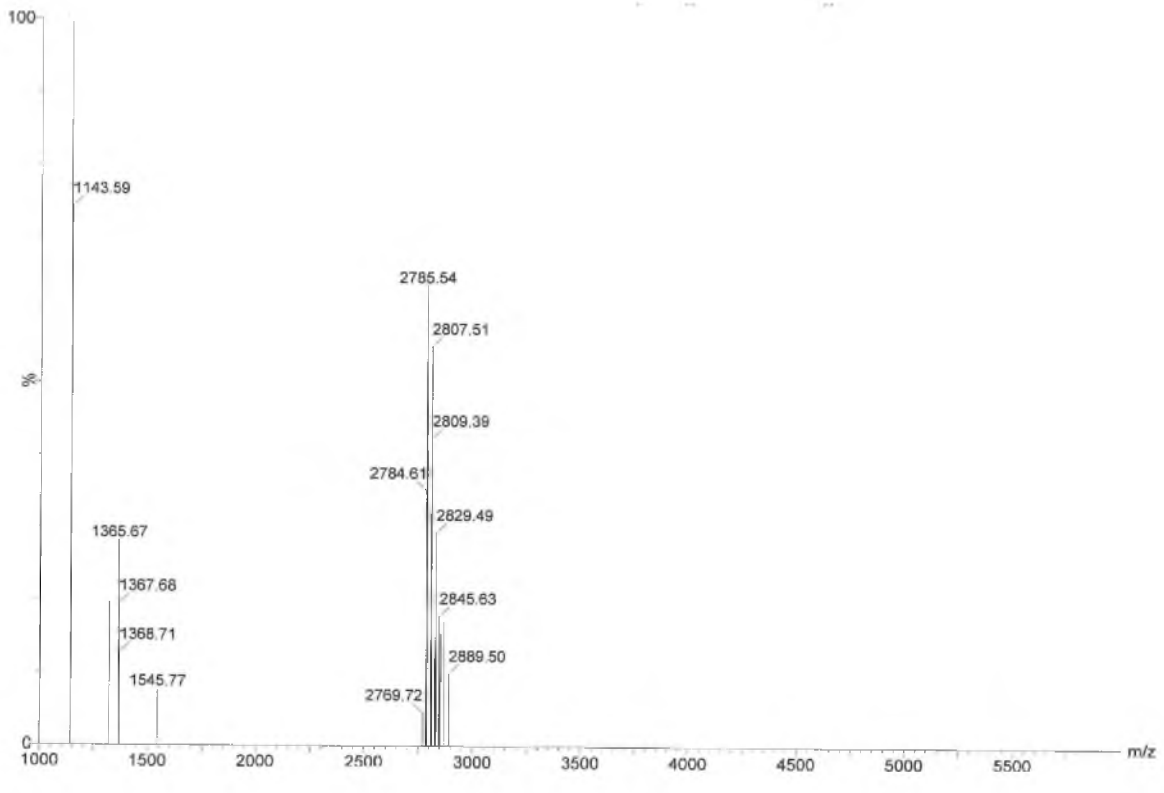

m/z 2785.54 (calcd $[M]^+$ 2785.04).

Figure A.2. HPLC and MALDI-TOF MS of PNA **1neg** (H-GTAGAT$_D$CACT-NH_2).

a)

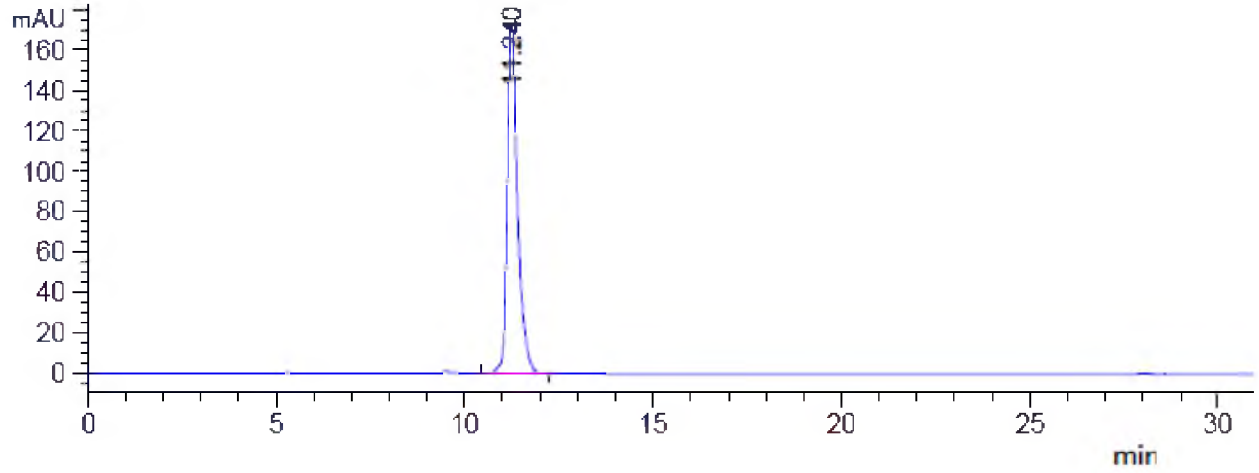

b)

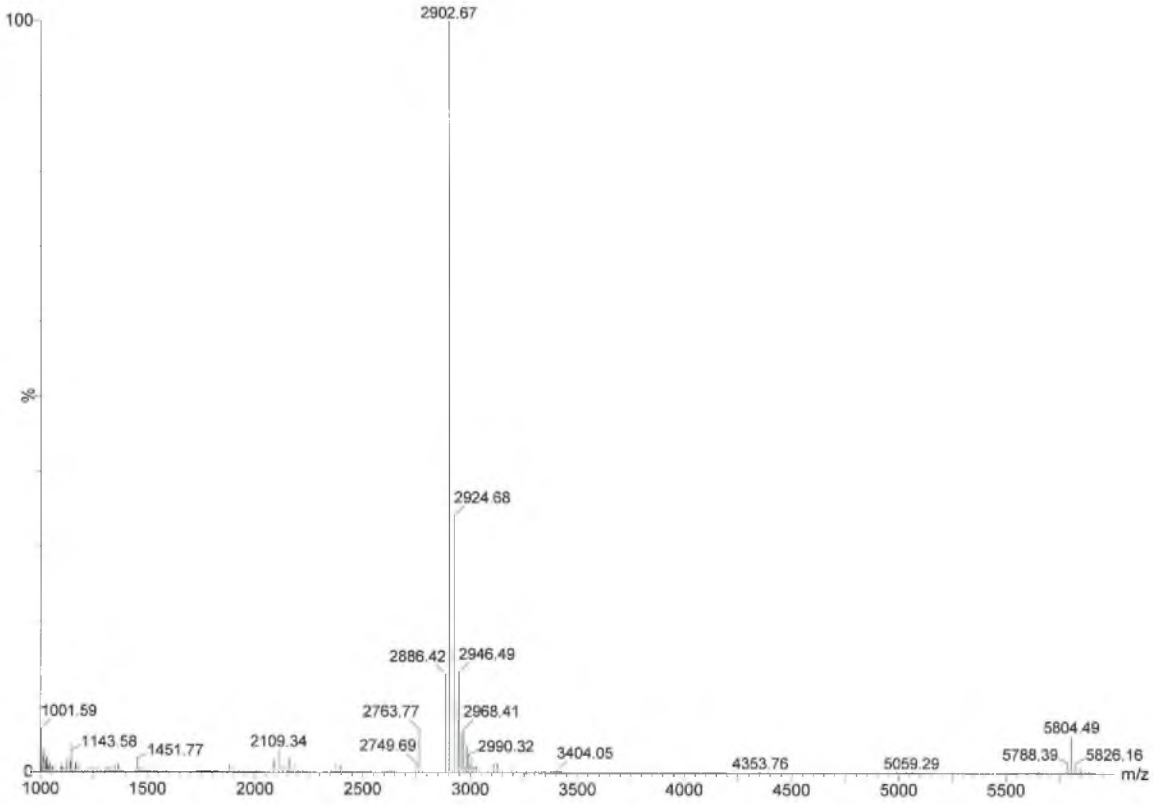

m/z 2902.67 (calcd $[M+H]^+$ 2902.14); 2924.68 (calcd $[M+Na]^+$ 2924.12).

Figure A.3. HPLC and MALDI-TOF MS of PNA **3neg** (H-GT_DAGAT_DCACT_D-NH_2).

a)

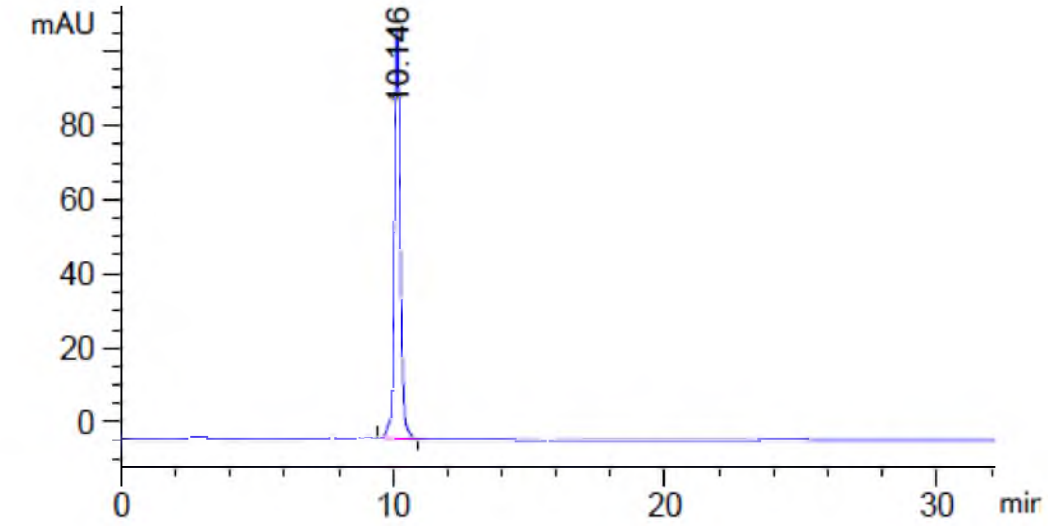

b)

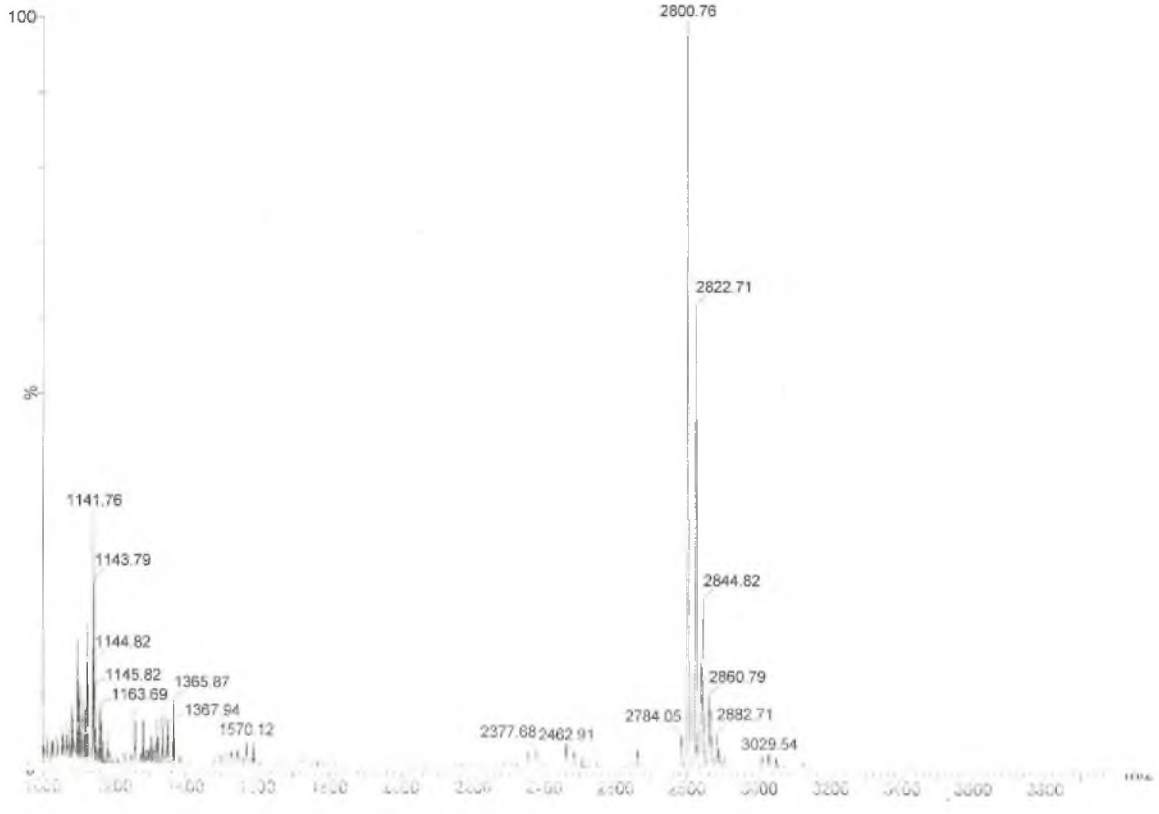

m/z 2800.76 (calcd $[M+H]^+$ 2799.12); 2822.71 (calcd $[M+Na]^+$ 2821.1).

Figure A.4. HPLC and MALDI-TOF MS of PNA **1pos** (H-GTAGAT$_K$CACT-NH$_2$).

a)

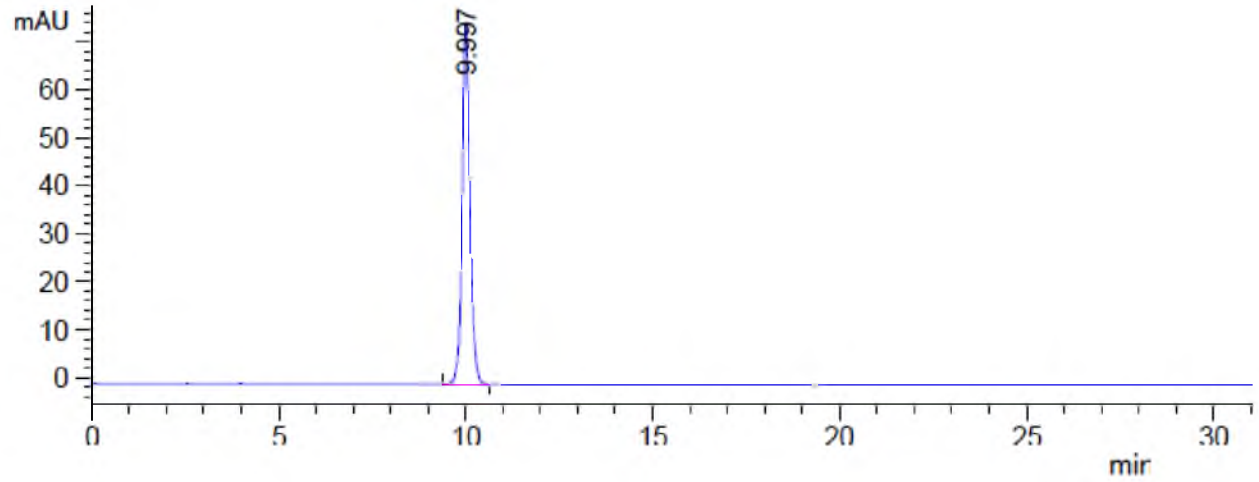

b)

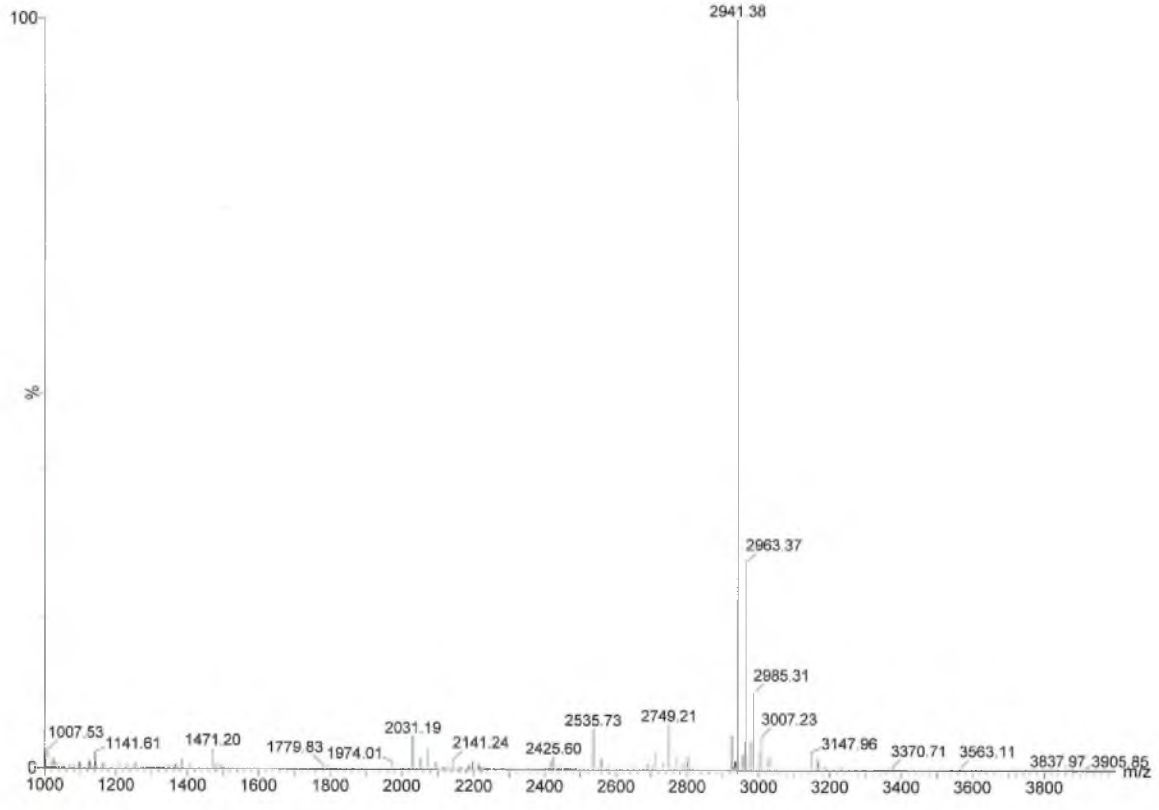

m/z 2941.38 (calcd $[M+H]^+$ 2941.26); 2963.37 (calcd $[M+Na]^+$ 2963.24).

Figure A.5. HPLC and MALDI-TOF MS of **PNA 3pos** (H-$GT_KAGAT_KCACT_K$-NH_2).

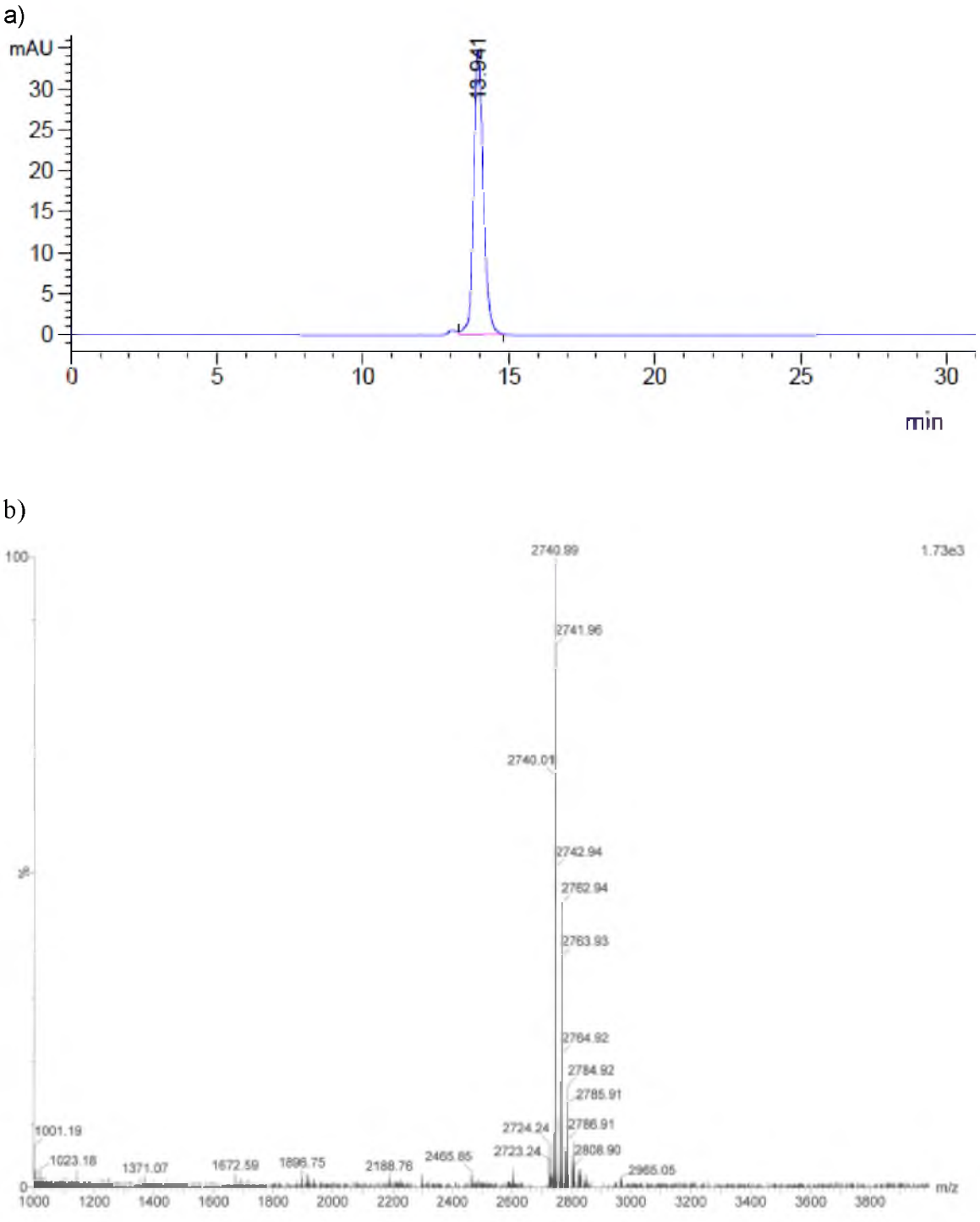

m/z 2740.99 (calcd $[M]^+$ 2741.05); *m/z* 2741.96 (calcd $[M+H]^+$ 2942.06); 2763.93 (calcd $[M+Na]^+$ 2764.04).

Figure A.6. HPLC and MALDI-TOF MS of **PNA 1Me** (H-GTAGAT$_A$CACT-NH_2).

a)

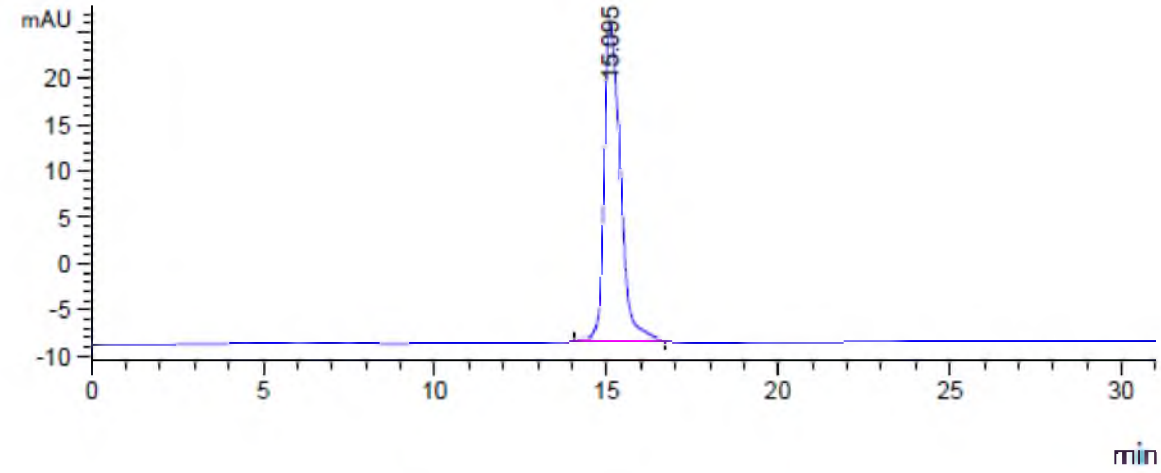

b)

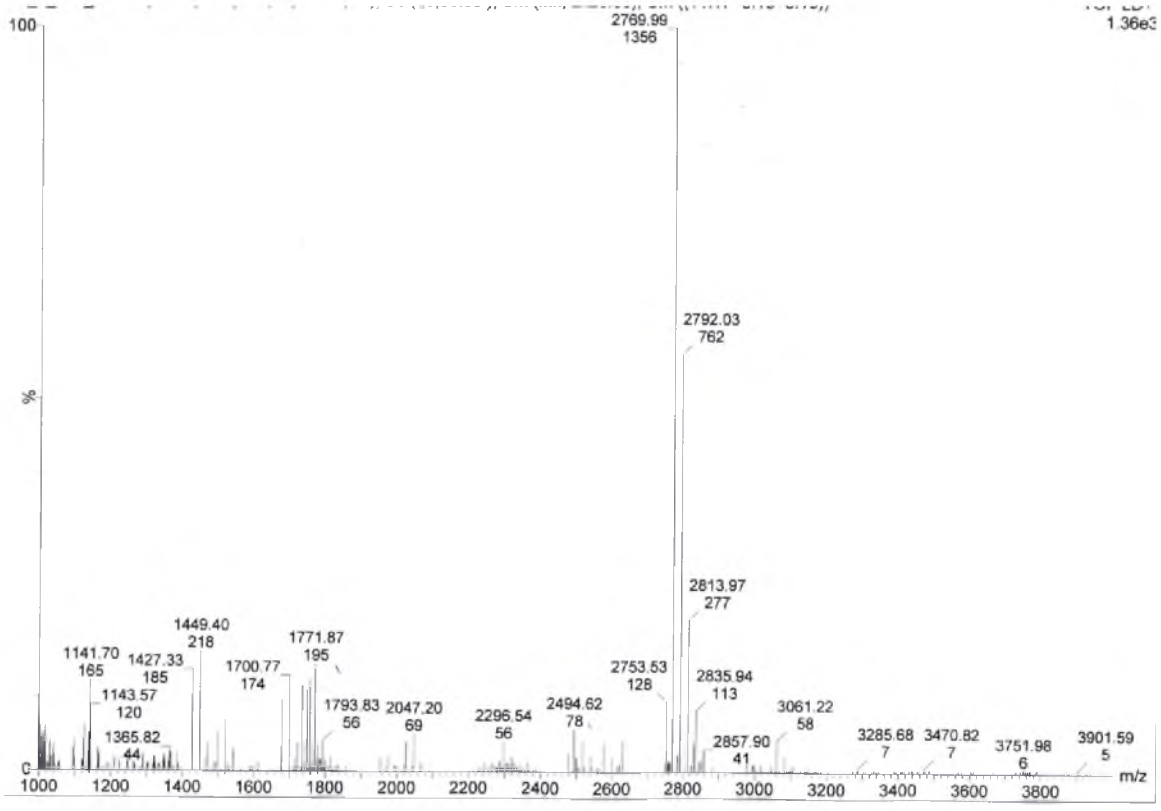

m/z 2769.99 (calcd $[M+H]^+$ 2770.08); 2792.03 (calcd $[M+Na]^+$ 2792.06).

Figure A.7. HPLC and MALDI-TOF MS of **PNA 3Me** (H-GT_AAGAT_ACACT_A-NH_2).

Representative UV-melting curves and T_m data for duplexes under varying salt concentrations.

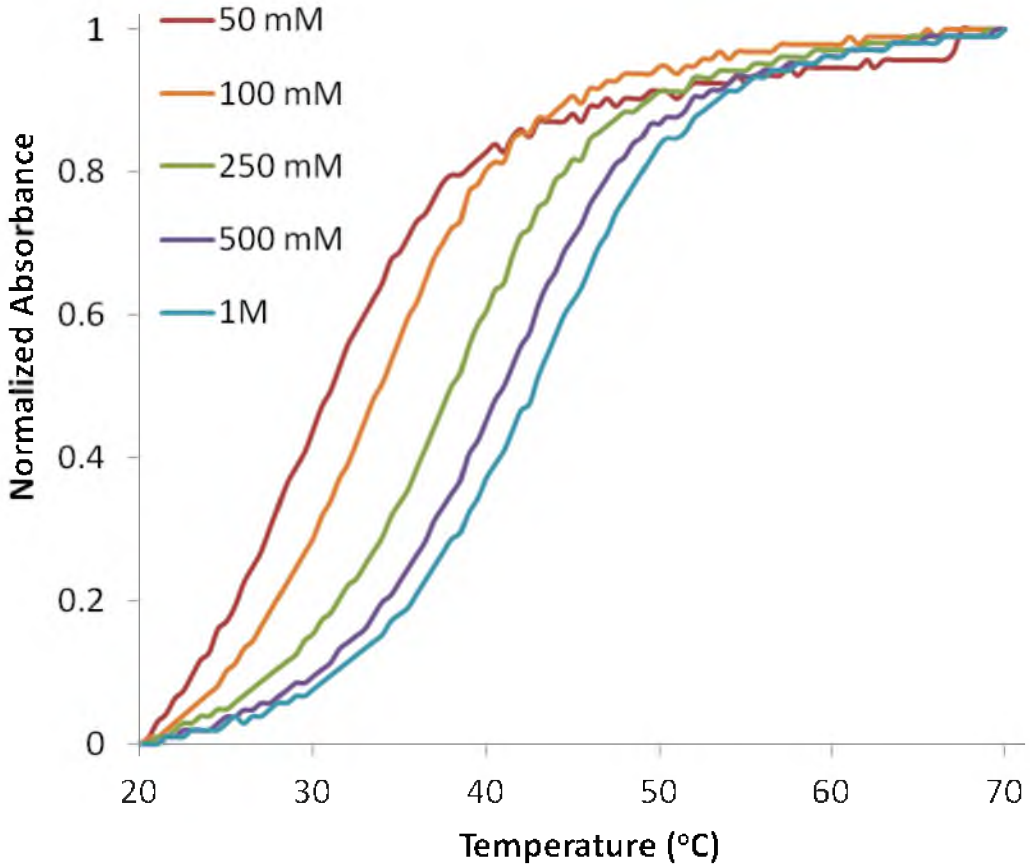

Figure A.8. Representative UV-melting curves of DNA **1**:DNA **2** duplex under varying salt concentrations.

Table A.1. T_m data (°C) for DNA **1**:DNA **2** duplex under varying salt concentrations.

[NaCl] =	0 M	50 mM	100 mM	250 mM	500 mM	1 M
Trial 1	n.d.	28.6	33.1	37.7	40.7	42.7
Trial 2	n.d.	28.6	33.1	37.7	40.7	42.2
Trial 3	n.d.	28.6	33.1	37.7	40.7	42.7
Average	n.d.	28.6 ± 0.1	33.1 ± 0.1	37.7 ± 0.1	40.7 ± 0.1	42.6 ± 0.3

(n.d.- not determined)

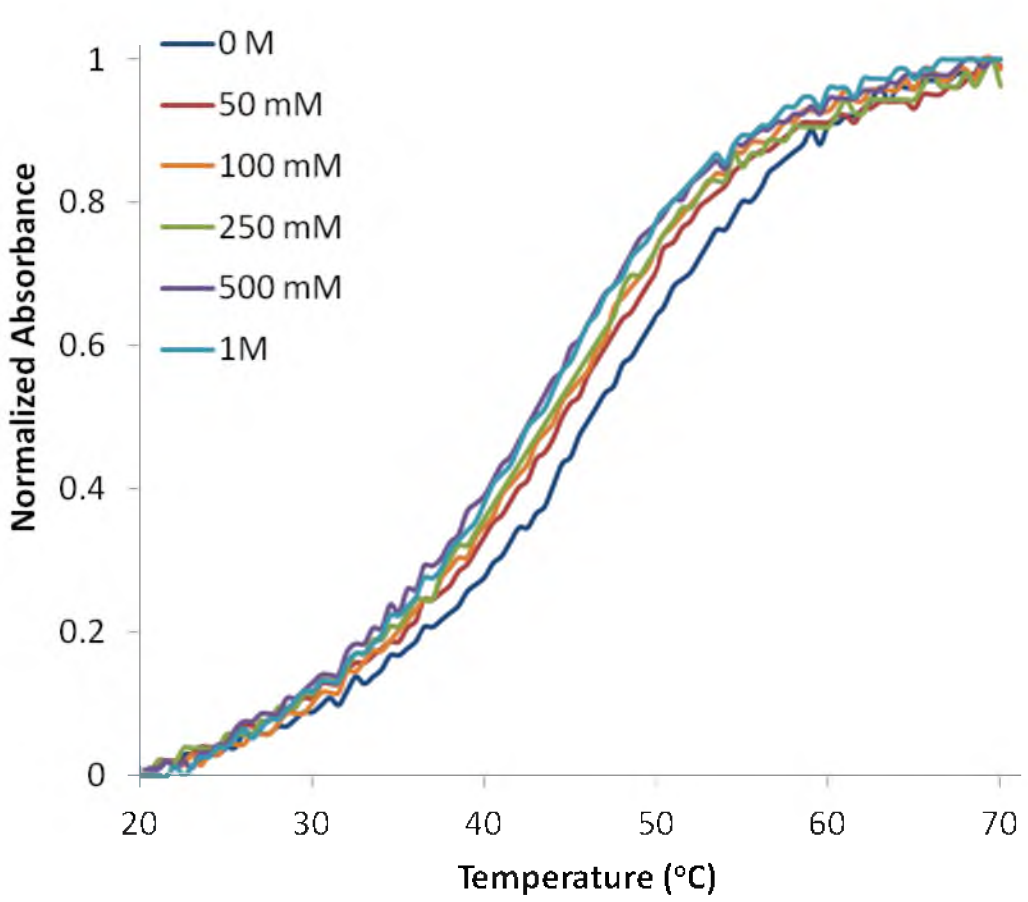

Figure A.9. Representative UV-melting curves of PNA **nf**:DNA **1** duplex under varying salt concentrations.

Table A.2. T_m data (°C) for PNA **nf**:DNA **1** duplex under varying salt concentrations.

[NaCl] =	0 M	50 mM	100 mM	250 mM	500 mM	1 M
Trial 1	47.3	45.2	44.2	43.7	43.2	43.7
Trial 2	46.8	44.2	43.7	43.2	42.2	42.7
Trial 3	44.8	43.7	43.2	43.2	41.7	42.2
Average	46.3 ± 1.3	44.4 ± 0.8	43.7 ± 0.5	43.4 ± 0.3	42.4 ± 0.8	42.9 ± 0.8

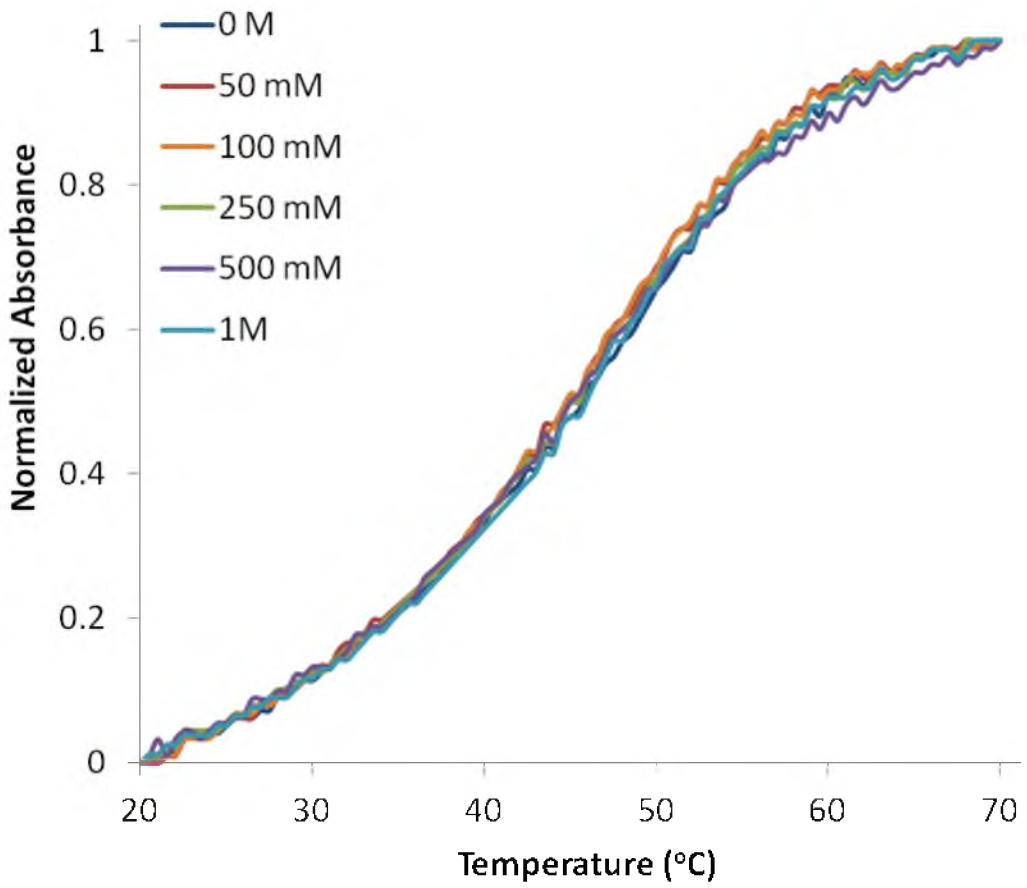

Figure A.10. Representative UV-melting curves of PNA **1neg**:DNA **1** duplex under varying salt concentrations.

Table A.3. T_m data (°C) for PNA **1neg**:DNA **1** duplex under varying salt concentrations.

[NaCl] =	0 M	50 mM	100 mM	250 mM	500 mM	1 M
Trial 1	46.3	45.8	46.3	46.8	46.8	46.8
Trial 2	45.8	44.8	44.8	45.2	45.2	45.8
Trial 3	45.2	44.2	43.7	43.7	44.2	45.2
Average	45.8 ± 0.5	44.9 ± 0.8	44.9 ± 1.3	45.3 ± 1.5	45.4 ± 1.3	45.9 ± 0.8

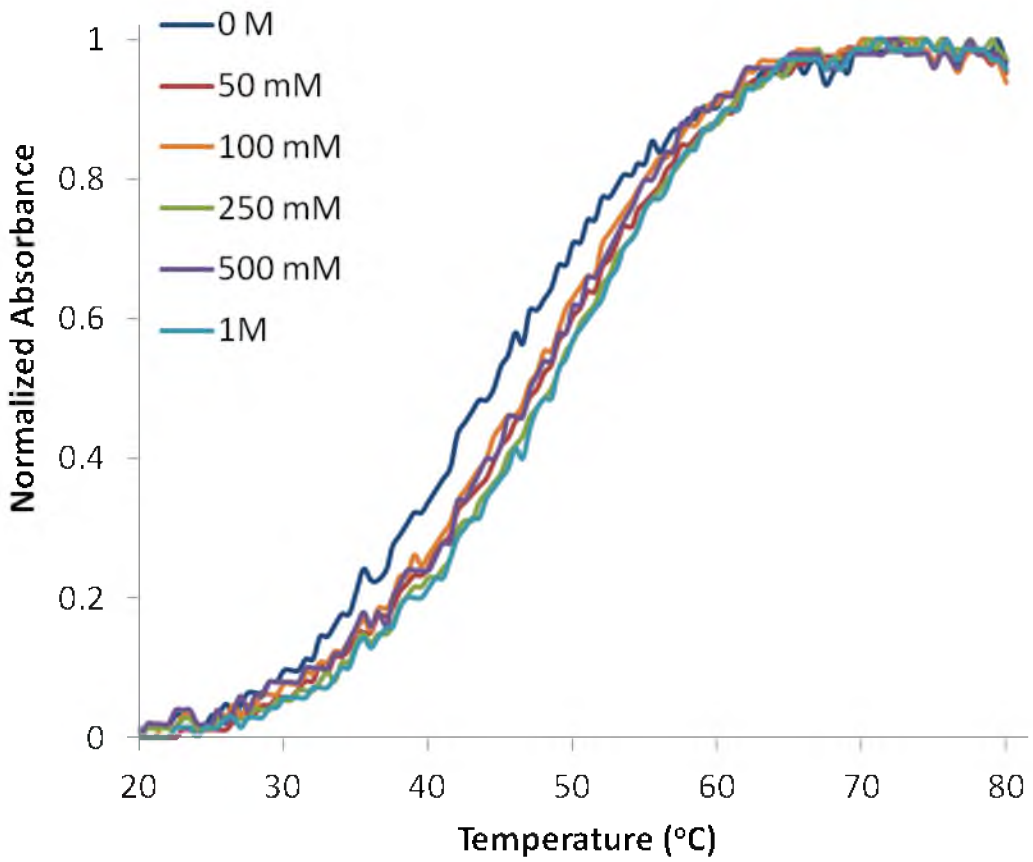

Figure A.11. Representative UV-melting curves of PNA **3neg**:DNA **1** duplex under varying salt concentrations.

Table A.4. T_m data (°C) for PNA **3neg**:DNA **1** duplex under varying salt concentrations.

[NaCl] =	0 M	50 mM	100 mM	250 mM	500 mM	1 M
Trial 1	43.6	48.5	46.7	48.5	49.1	49.7
Trial 2	43.6	47.3	46.7	47.9	47.3	48.5
Trial 3	43.4	46.7	46.1	47.9	47.9	48.5
Average	43.6 ± 0.1	47.5 ± 0.9	46.5 ± 0.4	48.1 ± 0.3	48.1 ± 0.9	48.9 ± 0.7

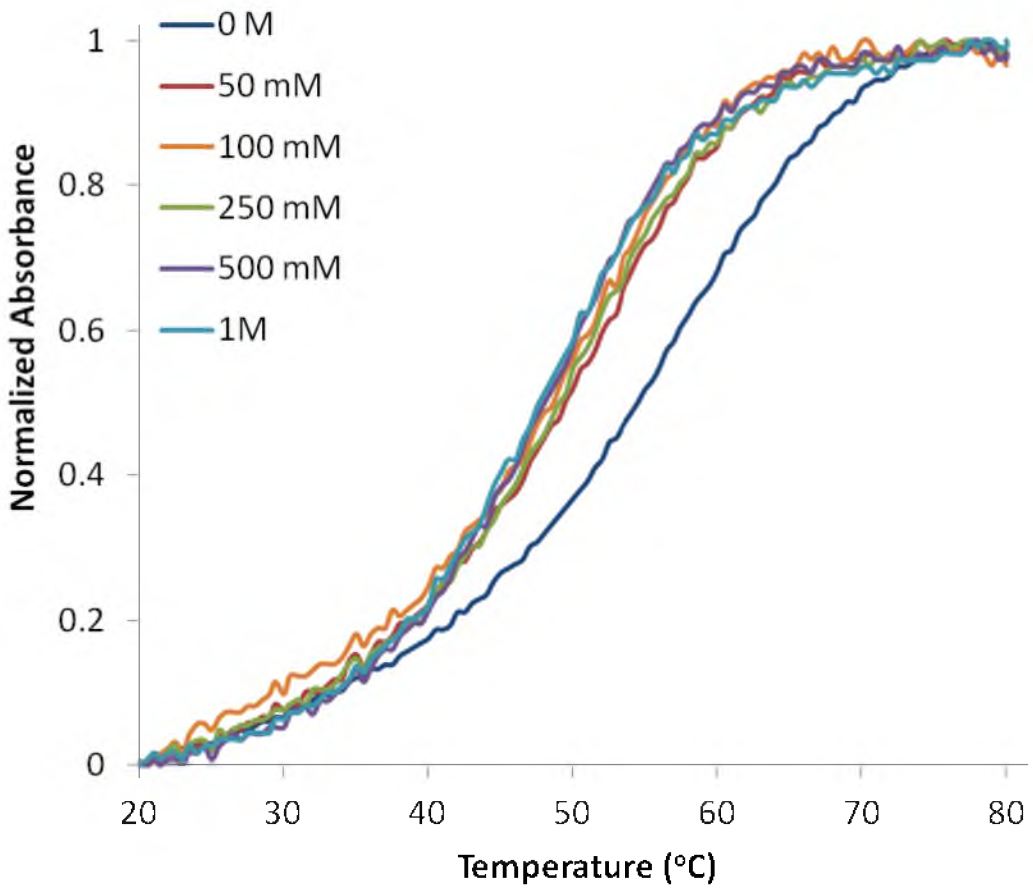

Figure A.12. Representative UV-melting curves of PNA **1pos**:DNA **1** duplex under varying salt concentrations.

Table A.5. T_m data (°C) for PNA **1pos**:DNA **1** duplex under varying salt concentrations.

[NaCl] =	0 M	50 mM	100 mM	250 mM	500 mM	1 M
Trial 1	57.6	50.3	49.7	49.7	48.5	47.9
Trial 2	55.8	49.1	47.9	48.5	47.3	47.3
Trial 3	54.6	48.5	47.9	47.9	47.3	47.3
Average	56.0 ± 1.5	49.3 ± 0.9	48.5 ± 1.1	48.7 ± 0.9	47.7 ± 0.7	47.5 ± 0.4

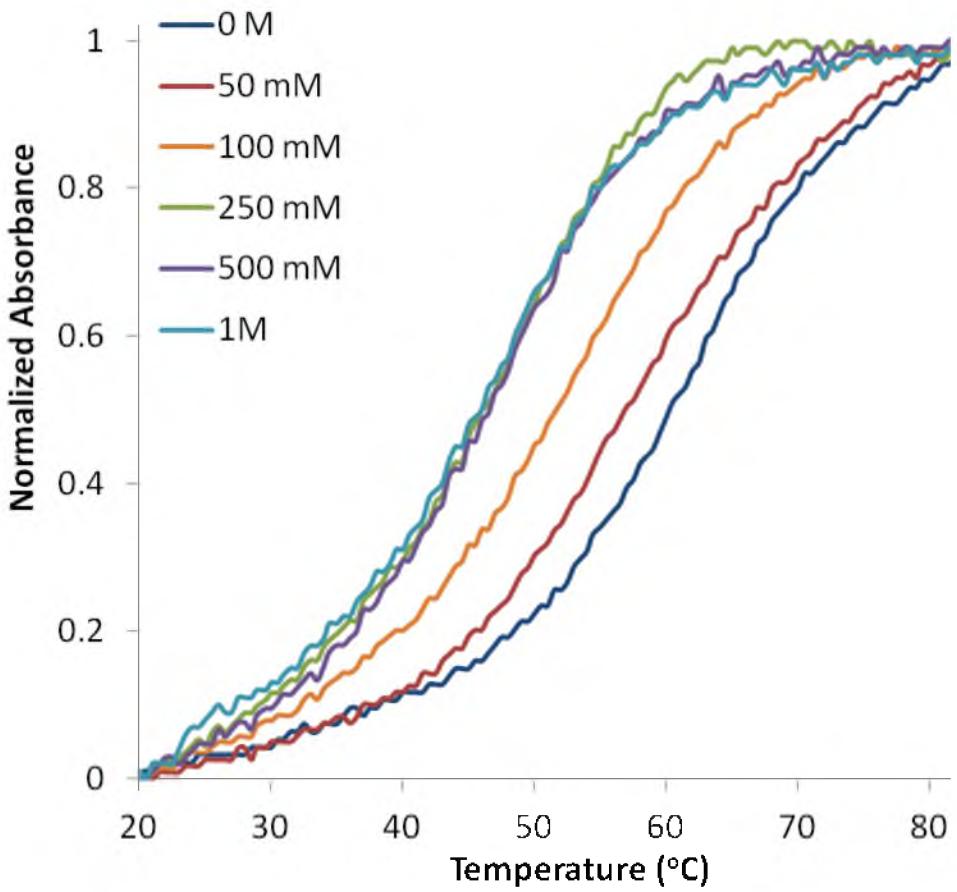

Figure A.13. Representative UV-melting curves of PNA **3pos**:DNA **1** duplex under varying salt concentrations.

Table A.6. T_m data (°C) for PNA **3pos**:DNA **1** duplex under varying salt concentrations.

[NaCl] =	0 M	50 mM	100 mM	250 mM	500 mM	1 M
Trial 1	62.7	58.1	54.1	49.6	48.9	47.6
Trial 2	61.4	58.1	51.5	46.3	46.3	45.6
Trial 3	60.7	57.4	51.5	46.9	46.9	45.0
Trial 4			52.2	48.2	46.3	46.9
Average	61.6 ± 1.0	57.9 ± 0.4	52.3 ± 1.2	47.7 ± 1.5	47.1 ± 1.2	46.3 ± 1.2

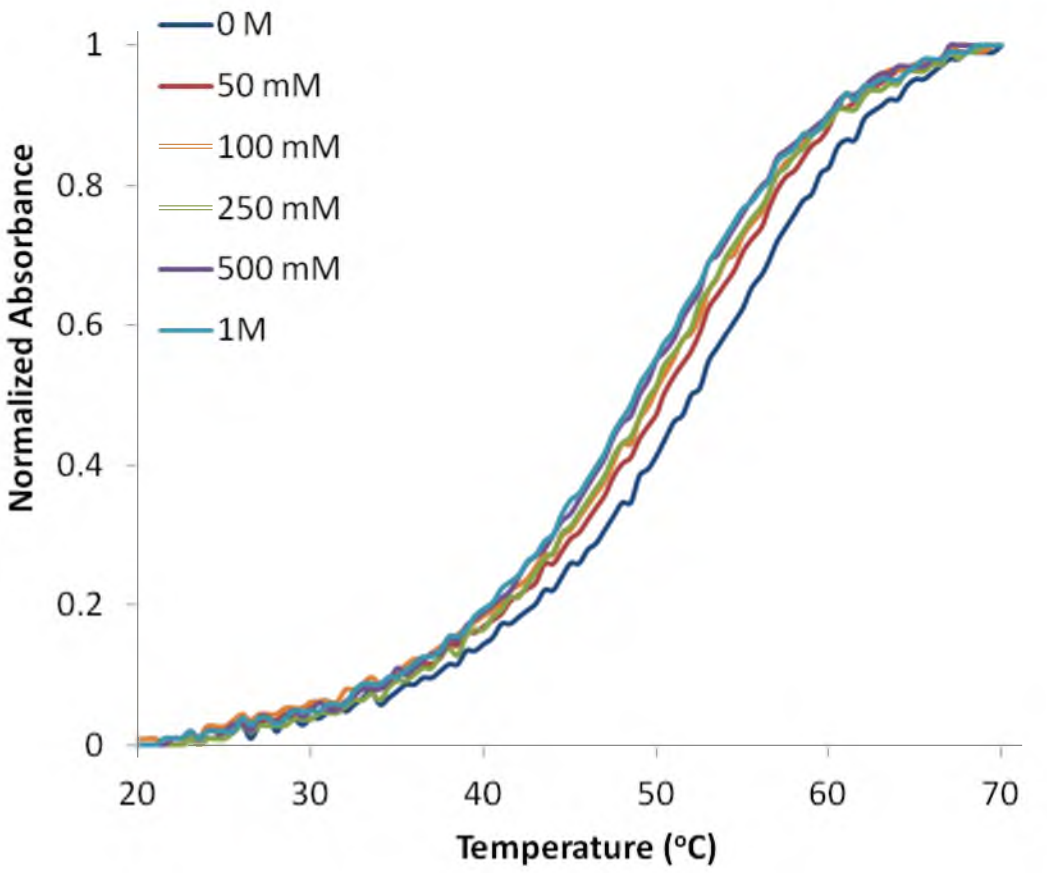

Figure A.14. Representative UV-melting curves of PNA **1Me**:DNA **1** duplex under varying salt concentrations.

Table A.7. T_m data (°C) for PNA **1Me**:DNA **1** duplex under varying salt concentrations.

[NaCl] =	0 M	50 mM	100 mM	250 mM	500 mM	1 M
Trial 1	52.8	51.3	50.3	49.8	49.3	49.3
Trial 2	52.3	50.3	49.8	49.3	48.8	48.8
Trial 3	51.3	49.8	49.3	48.8	48.3	48.8
Average	52.2 ± 0.8	50.5 ± 0.8	49.8 ± 0.5	49.3 ± 0.5	48.8 ± 0.5	49.0 ± 0.3

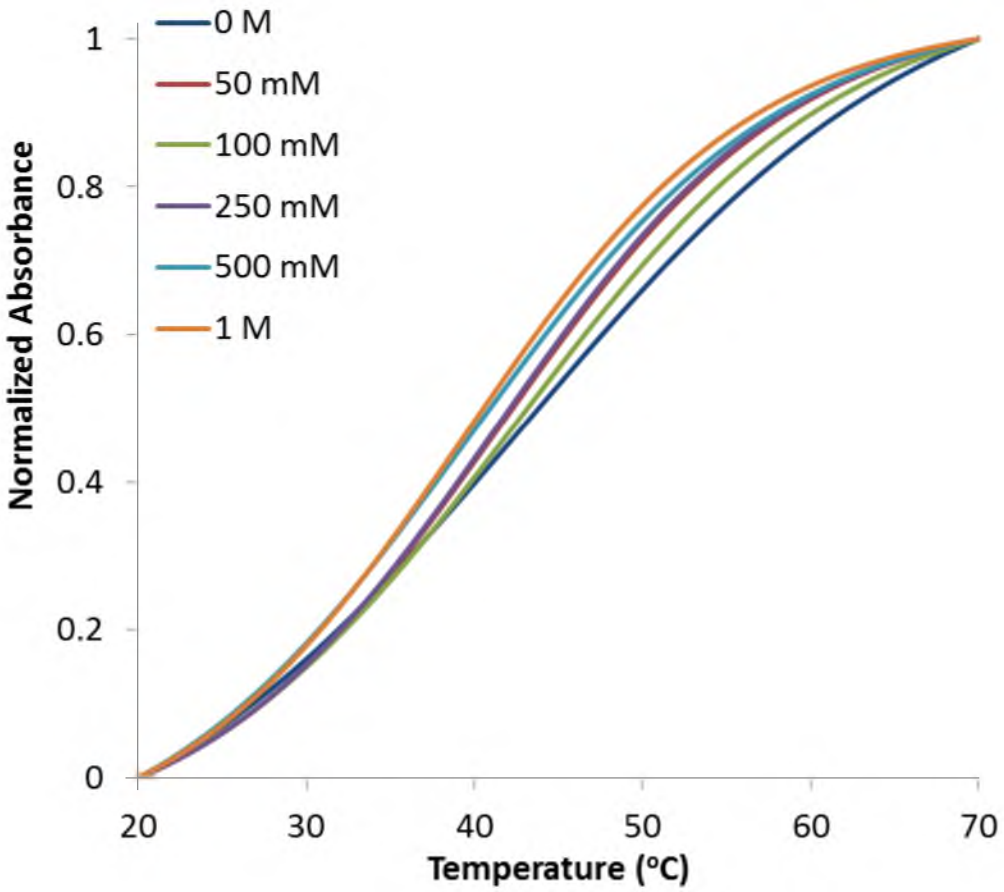

Figure A.15. Representative UV-melting curves of PNA **3Me**:DNA **1** duplex under varying salt concentrations.

Table A.8. T_m data (°C) for PNA **3Me**:DNA **1** duplex under varying salt concentrations.

[NaCl] =	0 M	50 mM	100 mM	250 mM	500 mM	1 M
Trial 1	43.2	41.7	42.2	41.2	39.7	39.2
Trial 2	42.7	42.7	43.2	42.7	40.2	40.7
Trial 3	43.7	42.7	42.7	41.7	41.7	42.2
Average	43.2 ± 0.5	42.4 ± 0.6	42.7 ± 0.5	41.9 ± 0.8	40.5 ± 1.1	40.7 ± 1.5

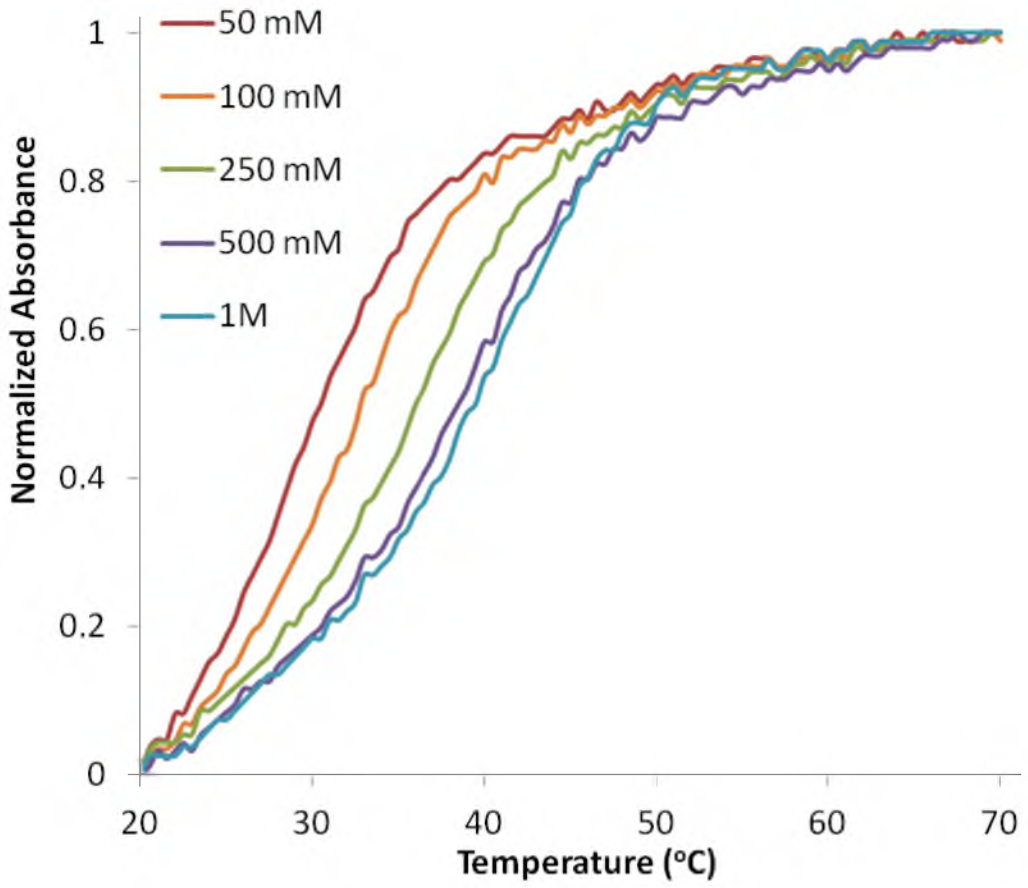

Figure A.16. Representative UV-melting curves of RNA **1**:DNA **2** duplex under varying salt concentrations.

Table A.9. T_m data (°C) data for RNA **1**:DNA **2** duplex under varying salt concentrations.

[NaCl] =	0 M	50 mM	100 mM	250 mM	500 mM	1 M
Trial 1	n.d.	27.6	31.1	35.2	37.7	39.2
Trial 2	n.d.	27.1	31.6	35.7	37.7	39.2
Trial 3	n.d.	28.1	32.1	35.7	38.2	38.7
Average	n.d.	27.6 ± 0.5	31.6 ± 0.5	35.5 ± 0.3	37.8 ± 0.3	39.0 ± 0.3

(n.d.- not determined)

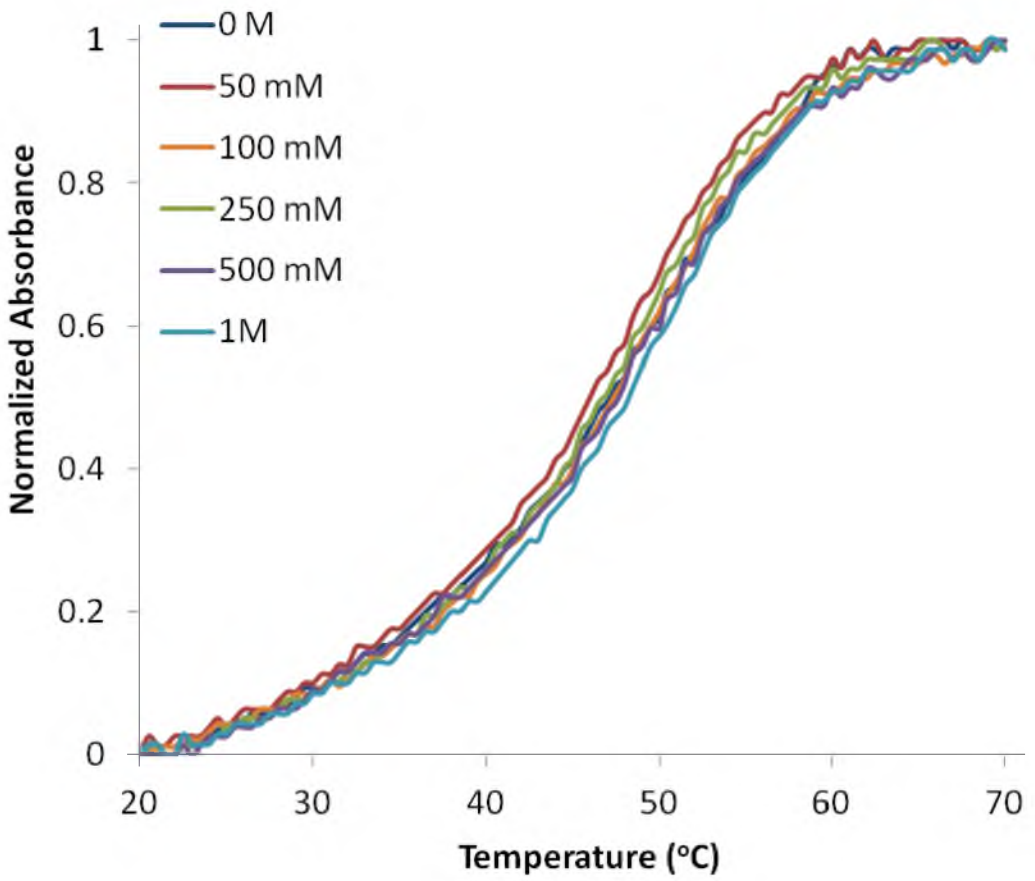

Figure A.17. Representative UV-melting curves of PNA **nf**:RNA **1** duplex under varying salt concentrations.

Table A.10. T_m data (°C) for PNA **nf**:RNA **1** duplex under varying salt concentrations.

[NaCl] =	0 M	50 mM	100 mM	250 mM	500 mM	1 M
Trial 1	47.8	47.3	48.3	48.3	48.8	49.3
Trial 2	47.8	46.3	47.3	46.8	47. 8	48.3
Trial 3	46.8	45.8	46.3	46.3	46.8	47.8
Average	47.4 ± 0.6	46.4 ± 0.8	47.3 ± 1.0	47.1 ± 1.1	47.8 ± 1.0	48.5 ± 0.8

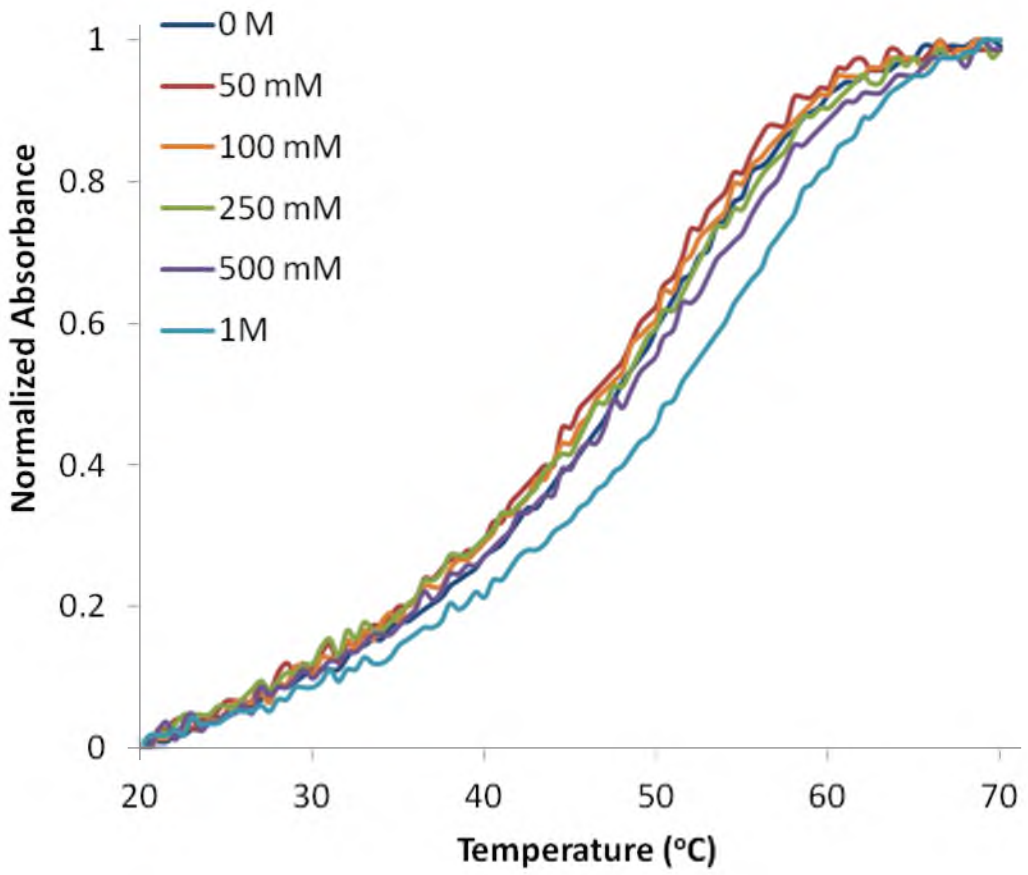

Figure A.18. Representative UV-melting curves of PNA **1neg**:RNA **1** duplex under varying salt concentrations.

Table A.11. T_m data (°C) for PNA **1neg**:RNA **1** duplex under varying salt concentrations.

[NaCl] =	0 M	50 mM	100 mM	250 mM	500 mM	1 M
Trial 1	48.8	48.3	48.8	49.8	50.3	54.8
Trial 2	48.3	46.8	47.3	48.3	49.3	53.3
Trial 3	47.8	45.8	46.3	47.3	47.8	52.3
Average	48.3 ± 0.5	46.9 ± 1.3	47.4 ± 1.3	48.5 ± 1.3	49.1 ± 1.3	53.5 ± 1.3

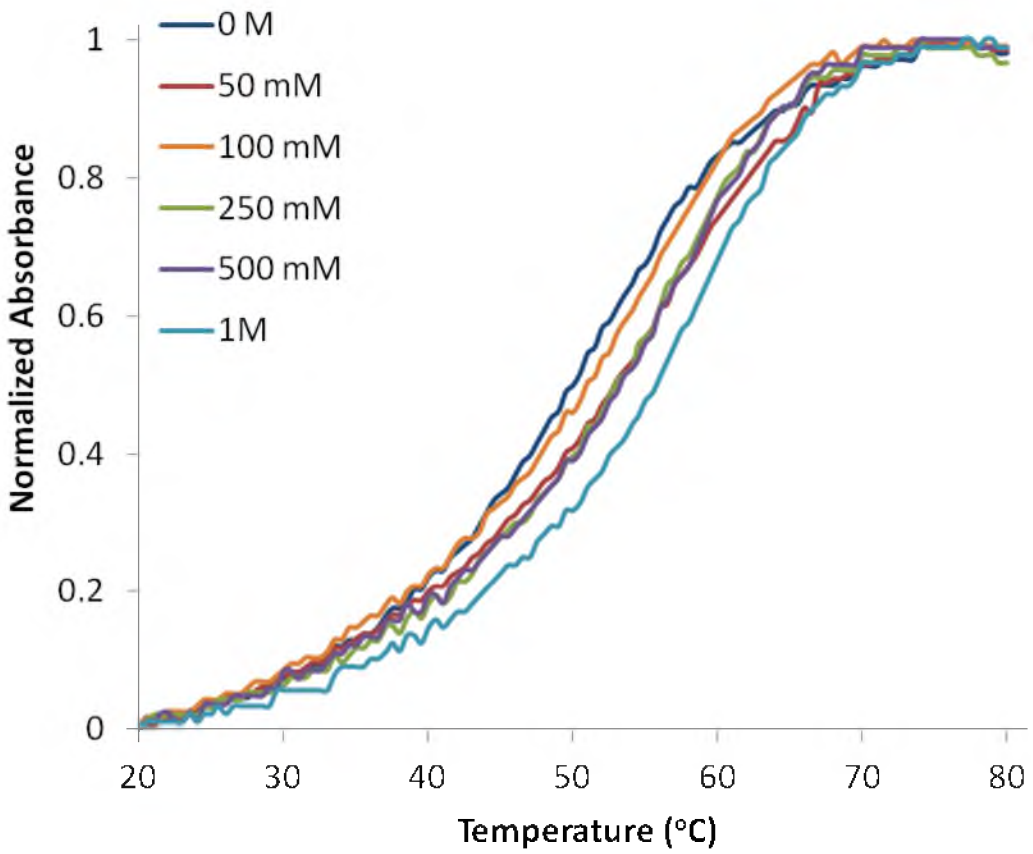

Figure A.19. Representative UV-melting curves of PNA **3neg**:RNA **1** duplex under varying salt concentrations.

Table A.12. T_m data (°C) for PNA **3neg**:RNA **1** duplex under varying salt concentrations.

[NaCl] =	0 M	50 mM	100 mM	250 mM	500 mM	1 M
Trial 1	49.7	52.1	50.9	53.3	55.2	55.8
Trial 2	49.7	53.3	51.5	53.3	53.9	56.4
Trial 3	50.9	52.1	51.5	53.9	53.3	55.2
Average	50.1 ± 0.7	52.5 ± 0.7	51.3 ± 0.4	53.5 ± 0.4	54.1 ± 0.9	55.8 ± 0.6

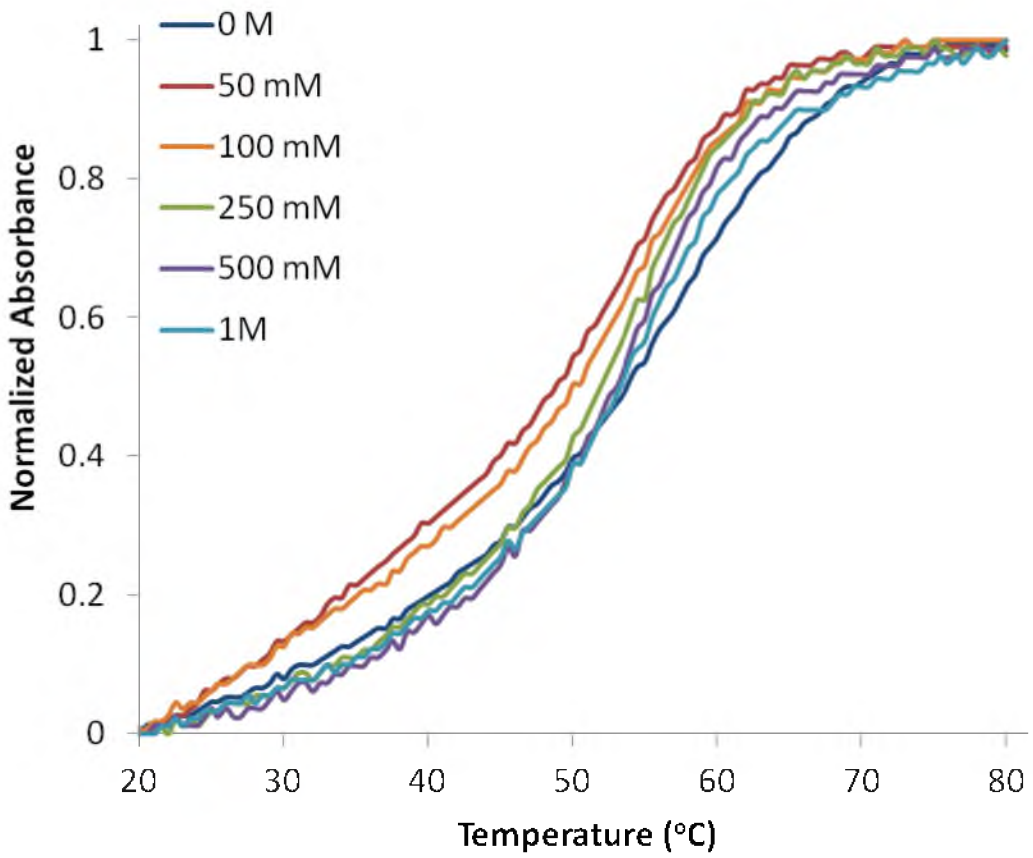

Figure A.20. Representative UV-melting curves of PNA **1pos**:RNA **1** duplex under varying salt concentrations.

Table A.13. T_m data (°C) for PNA **1pos**:RNA **1** duplex under varying salt concentrations.

[NaCl] =	0 M	50 mM	100 mM	250 mM	500 mM	1 M
Trial 1	55.8	48.5	50.3	51.5	52.7	53.3
Trial 2	55.2	46.1	47.9	49.1	50.9	52.1
Trial 3	53.3	46.1	48.5	49.1	50.9	52.1
Trial 4			46.7	48.5	49.7	50.9
Average	54.7 ± 1.3	46.9 ± 1.4	48.3 ± 1.5	49.5 ± 1.3	51.1 ± 1.2	52.1 ± 1.0

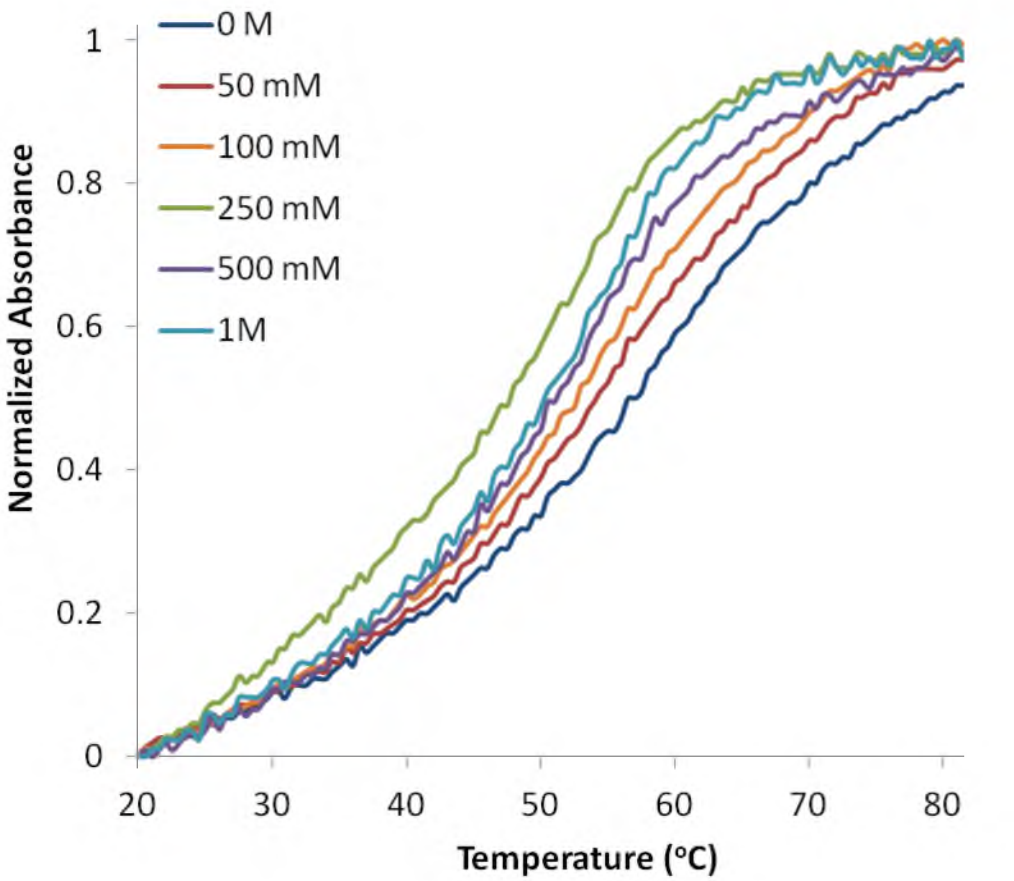

Figure A.21. Representative UV-melting curves of PNA **3pos**:RNA **1** duplex under varying salt concentrations.

Table A.14. T_m data (°C) for PNA **3pos**:RNA **1** duplex under varying salt concentrations.

[NaCl] =	0 M	50 mM	100 mM	250 mM	500 mM	1 M
Trial 1	58.1	54.7	51.8	49.5	51.5	52.5
Trial 2	56.8	54.1	50.4	47.6	49.6	49.7
Trial 3	56.8	54.8	52.5	46.9	50.9	50.4
Average	57.2 ± 0.8	54.6 ± 0.4	51.6 ± 1.1	48.0 ± 1.3	50.6 ± 1.0	50.9 ± 1.5

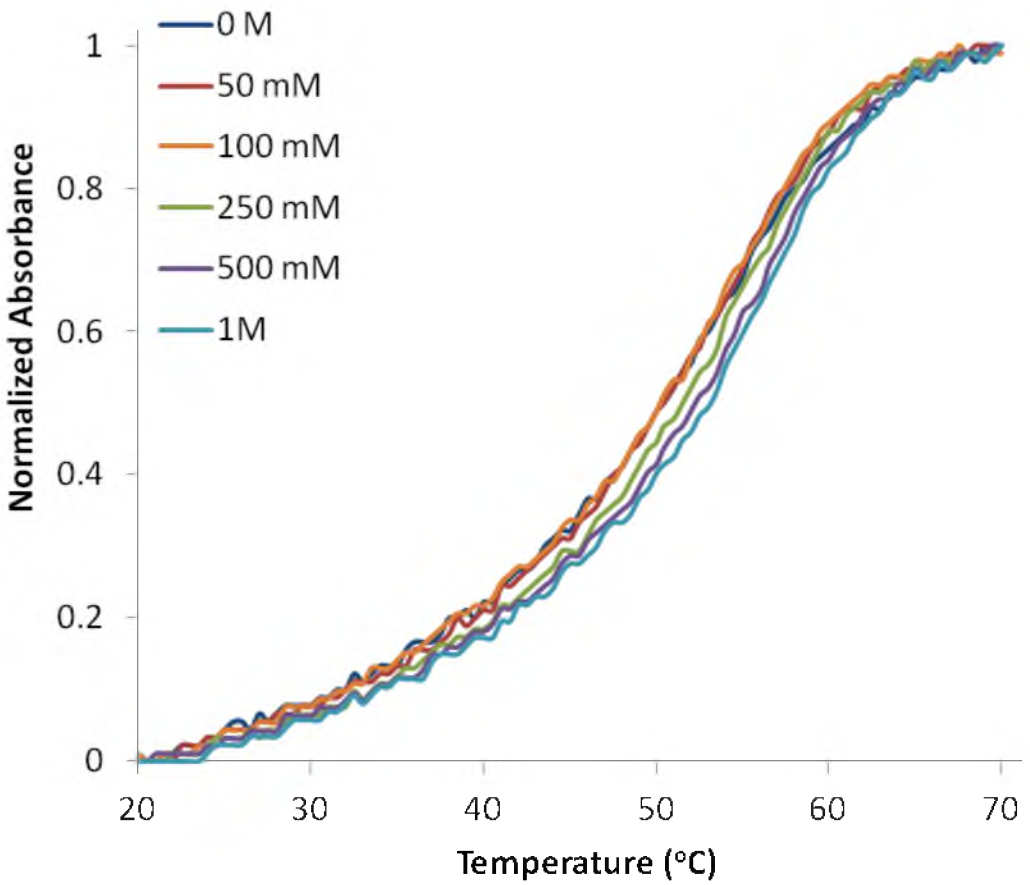

Figure A.22. Representative UV-melting curves of PNA **1Me**:RNA **1** duplex under varying salt concentrations.

Table A.15. T_m data (°C) for PNA **1Me**:RNA **1** duplex under varying salt concentrations.

[NaCl] =	0 M	50 mM	100 mM	250 mM	500 mM	1 M
Trial 1	51.8	51.3	51.3	52.3	53.8	54.3
Trial 2	50.3	49.8	51.2	52.3	53.8	54.8
Trial 3	49.3	49.3	49.3	50.3	52.3	52.8
Average	50.5 ± 1.3	50.1 ± 1.1	50.6 ± 1.1	51.6 ± 1.1	53.3 ± 0.9	54.0 ± 1.0

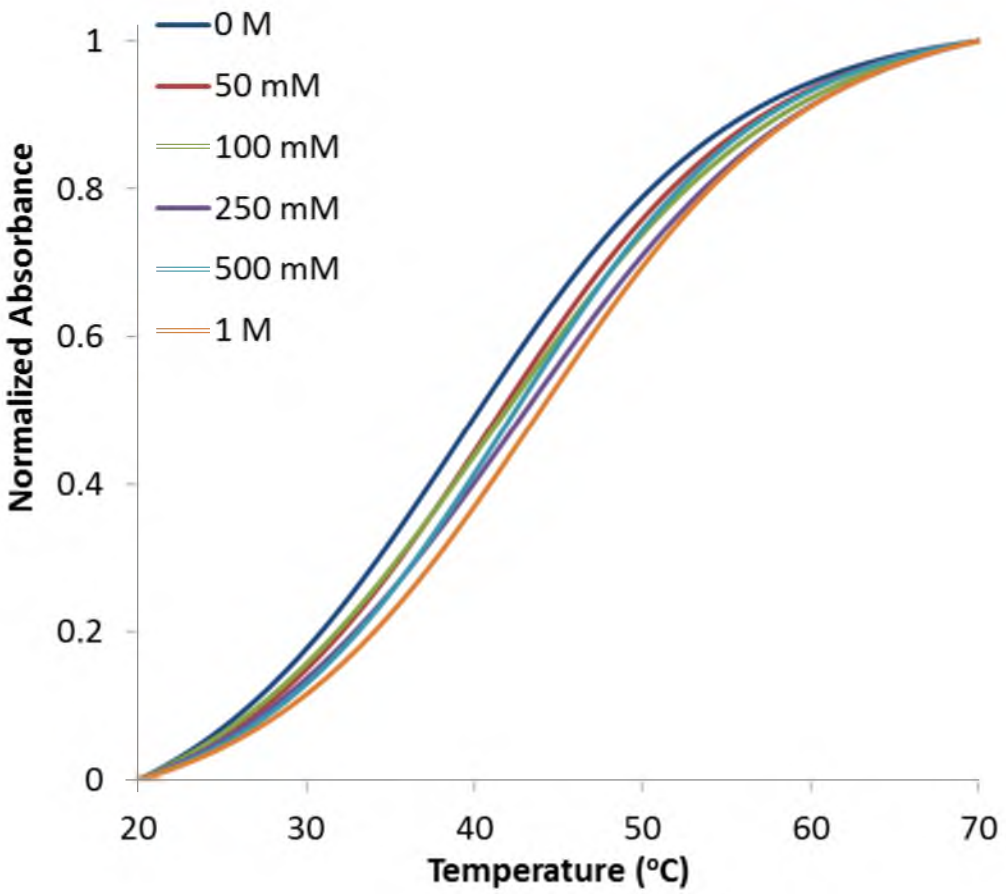

Figure A.23 Representative UV-melting curves of PNA **3Me**:RNA **1** duplex under varying salt concentrations.

Table A.16. T_m data (°C) for PNA **3Me**:RNA **1** duplex under varying salt concentrations.

[NaCl] =	0 M	50 mM	100 mM	250 mM	500 mM	1 M
Trial 1	38.7	40.7	41.2	42.2	42.2	44.2
Trial 2	39.2	40.7	41.2	42.7	42.2	43.7
Trial 3	40.2	41.2	41.2	42.7	43.2	43.7
Average	39.4 ± 0.8	40.9 ± 0.3	41.2 ± 0.1	42.6 ± 0.3	42.6 ± 0.6	43.9 ± 0.3

Representative UV-melting curves and T_m data for duplexes under physiological salt conditions.

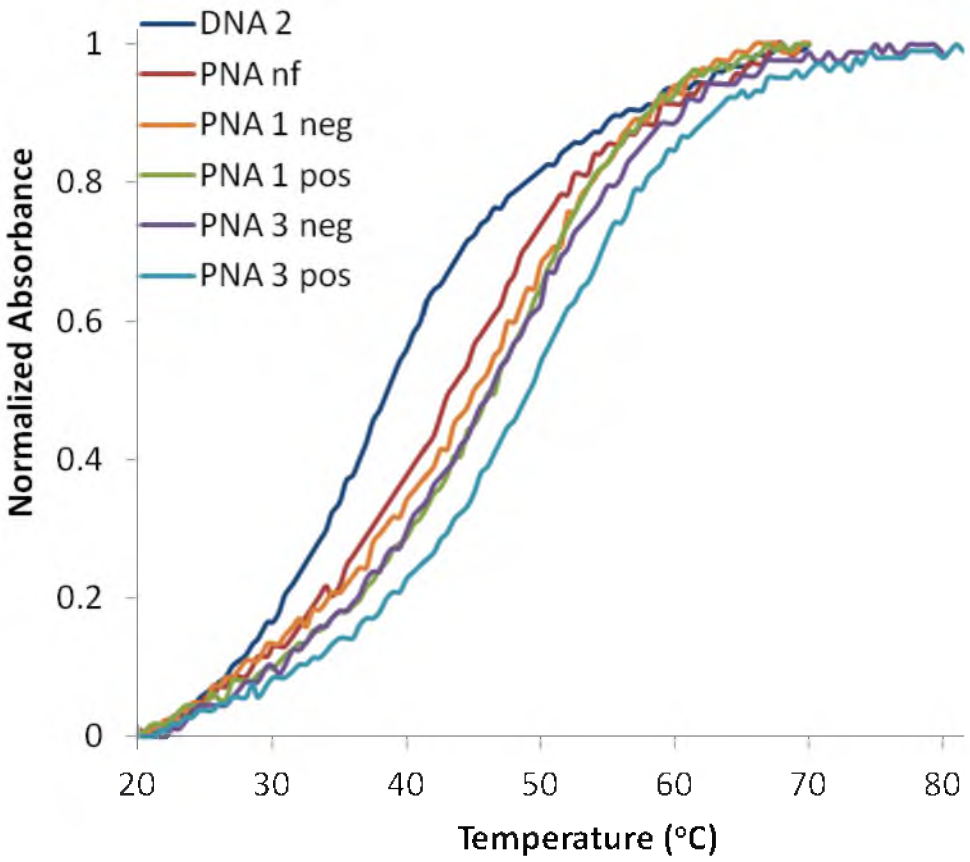

Figure A.24. Representative UV-melting curves of PNA/DNA **2**:DNA **1** duplexes under physiological salt conditions.

Table A.17. T_m data (°C) for PNA/DNA **2**:DNA **1** duplexes under physiological salt conditions.

complement =	DNA **2**	PNA **nf**	PNA **1neg**	PNA **1pos**	PNA **3neg**	PNA **3pos**
Trial 1	37.2	43.7	46.8	47.3	46.7	50.2
Trial 2	37.2	42.7	45.8	46.7	46.1	48.9
Trial 3	37.2	43.2	45.2	46.8	45.4	48.2
Average	37.2 ± 0.1	43.2 ± 0.5	45.9 ± 0.8	46.9 ± 0.3	46.1 ± 0.6	49.1 ± 1.0

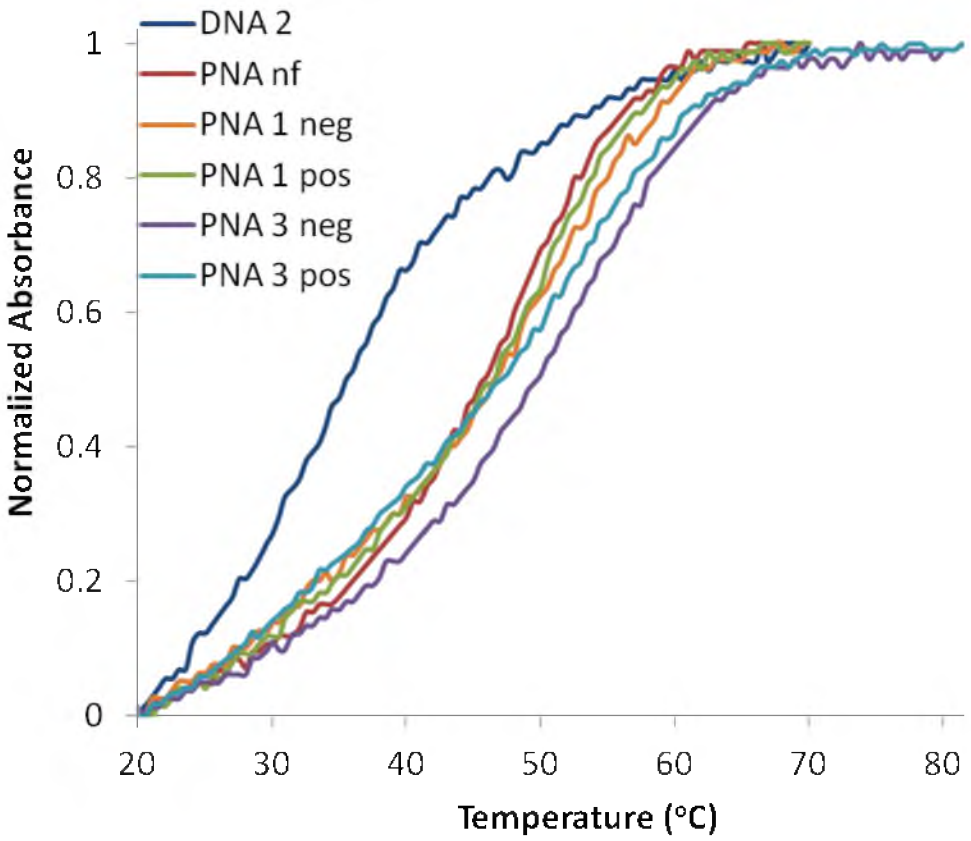

Figure A.25. Representative UV-melting curves of PNA/DNA **2**:RNA **1** duplexes under physiological salt conditions.

Table A.18. T_m data (°C) for PNA/DNA **2**:RNA **1** duplexes under physiological salt conditions.

complement =	DNA **2**	PNA **nf**	PNA **1neg**	PNA **1pos**	PNA **3neg**	PNA **3pos**
Trial 1	33.1	48.3	49.3	47.8	51.5	48.2
Trial 2	32.6	46.8	47.8	46.7	49.7	46.3
Trial 3	31.6	46.3	47.3	46.3	48.5	45.0
Average	32.5 ± 0.8	47.1 ± 1.1	48.1 ± 1.1	46.9 ± 0.8	49.9 ± 1.5	46.5 ± 1.7

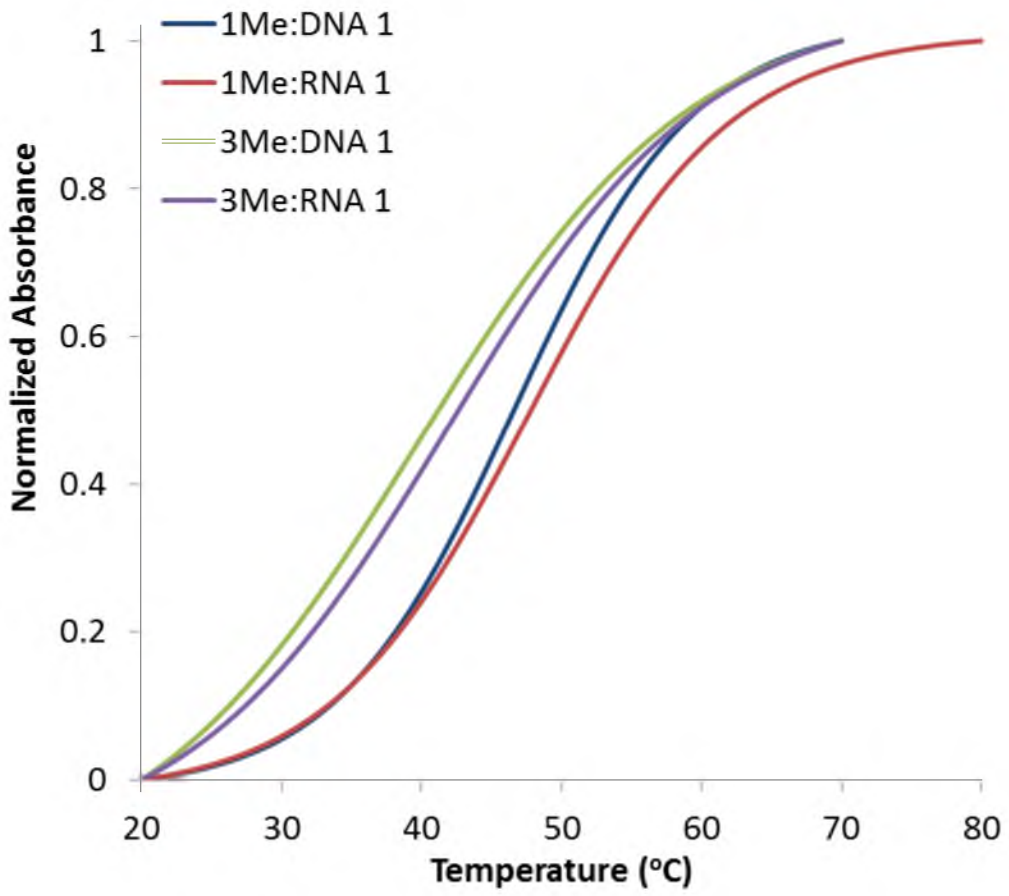

Figure A.26. Representative UV-melting curves of PNA **1Me** and PNA **3Me** duplexes under physiological salt conditions.

Table A.19. T_m data (°C) for PNA **1Me** and PNA **3Me** duplexes under physiological salt conditions.

duplex =	PNA **1Me**: DNA **1**	PNA **3Me**: DNA **1**	PNA **1Me**: RNA **1**	PNA **3Me**: RNA **1**
Trial 1	48.8	39.7	49.7	41.7
Trial 2	46.8	39.7	47.9	41.7
Trial 3	46.3	40.7	46.7	40.7
Average	47.3 ± 1.3	40.0 ± 0.6	48.1 ± 1.5	41.4 ± 0.6

APPENDIX B

SPECTRAL DATA OF CHAPTER 3: UV-MELTING CURVES AND T_M DATA

Representative UV-melting curves and T_m data for duplexes

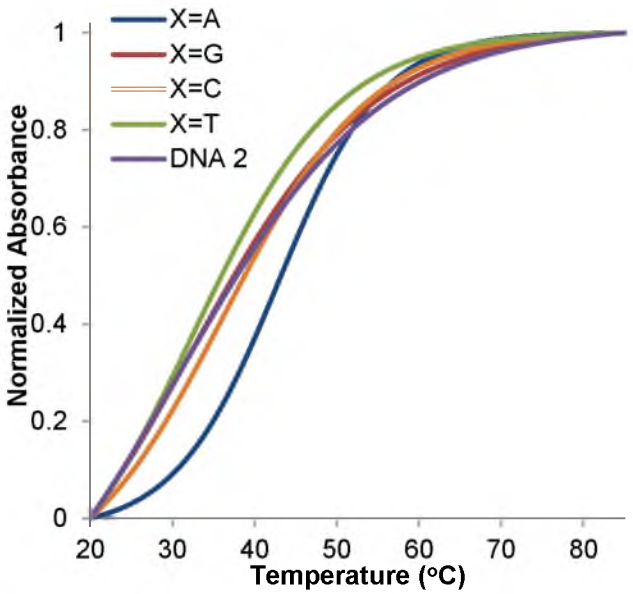

Figure B.1. Representative UV-melting curves of PNA **nf**:DNA duplexes under simulated physiological salt conditions.

Table B.1. T_m data (°C) for PNA **nf**:DNA duplexes under simulated physiological salt conditions.

Complement =	DNA **1** (X = A)	DNA **1** (X = G)	DNA **1** (X = C)	DNA **1** (X = T)	DNA **2**
Trial 1	43.6	32.5	36.4	31.8	33.8
Trial 2	43.0	32.5	35.8	33.1	30.5
Trial 3	42.3	32.5	36.4	32.5	31.2
Trial 4					31.2
Average	43.0 ± 0.7	32.5 ± 0.1	36.2 ± 0.3	32.5 ± 0.7	31.7 ± 1.5

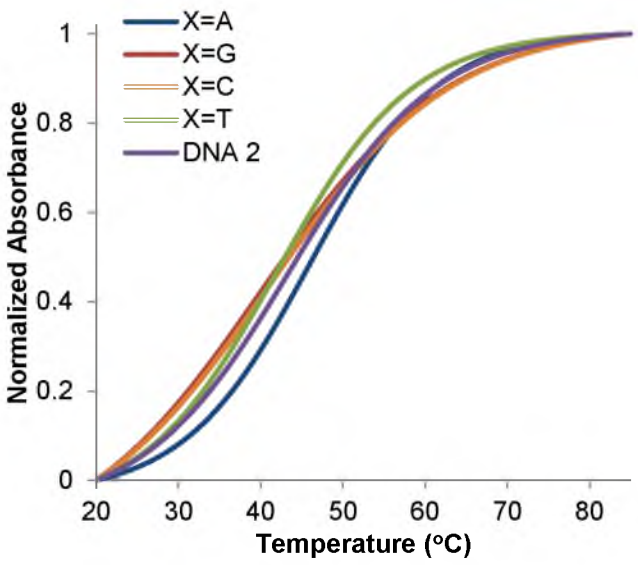

Figure B.2. Representative UV-melting curves of PNA **3neg**:DNA duplexes under simulated physiological salt conditions.

Table B.2. T_m data (°C) for PNA **3neg**:DNA duplexes under simulated physiological salt conditions.

Complement =	DNA **1** (X = A)	DNA **1** (X = G)	DNA **1** (X = C)	DNA **1** (X = T)	DNA **2**
Trial 1	46.9	41.0	41.7	44.3	43.6
Trial 2	46.3	40.4	41.0	41.0	43.6
Trial 3	45.6	40.4	39.7	42.3	42.3
Trial 4				43.0	
Average	46.3 ± 0.7	40.6 ± 0.3	40.8 ± 1.0	42.6 ± 1.4	43.2 ± 0.8

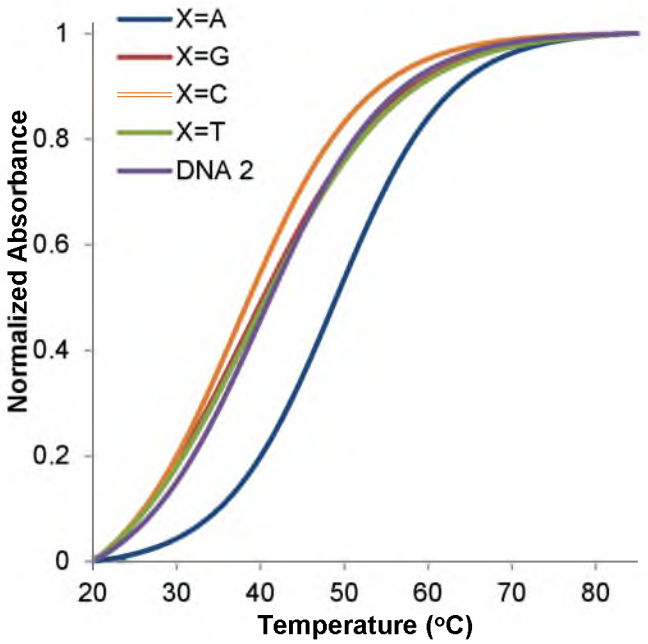

Figure B.3. Representative UV-melting curves of PNA **3pos**:DNA duplexes under simulated physiological salt conditions.

Table B.3. T_m data (°C) for PNA **3pos**:DNA duplexes under simulated physiological salt conditions.

Complement =	DNA **1** (X = A)	DNA **1** (X = G)	DNA **1** (X = C)	DNA **1** (X = T)	DNA **2**
Trial 1	50.2	40.4	38.4	39.7	41.7
Trial 2	48.9	37.7	37.7	38.4	39.0
Trial 3	48.2	38.4	37.7	39.0	40.4
Trial 4		37.7			39.0
Average	49.1 ± 1.0[11]	38.6 ± 1.3	37.9 ± 0.4	39.0 ± 0.7	40.0 ± 1.3

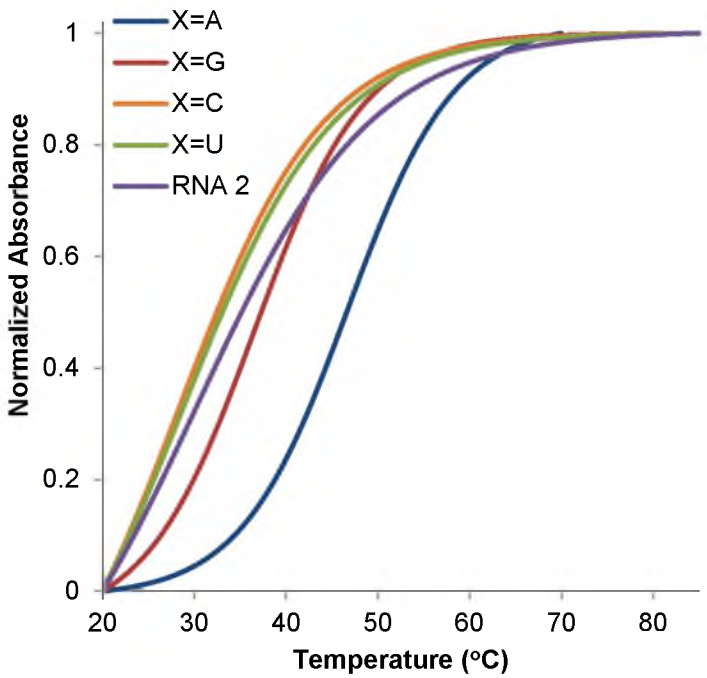

Figure B.4. Representative UV-melting curves of PNA **nf**:RNA duplexes under simulated physiological salt conditions.

Table B.4. T_m data (°C) for PNA **nf**:RNA duplexes under simulated physiological salt conditions.

Complement =	RNA **1** (X = A)	RNA **1** (X = G)	RNA **1** (X = C)	RNA **1** (X = U)	RNA **2**
Trial 1	48.3	37.1	27.9	28.5	30.5
Trial 2	46.8	36.4	28.5	27.9	30.5
Trial 3	46.3	36.4	29.2	29.2	32.5
Average	47.1 ± 1.1[11]	36.6 ± 0.4	28.5 ± 0.7	28.5 ± 0.7	31.2 ± 1.2

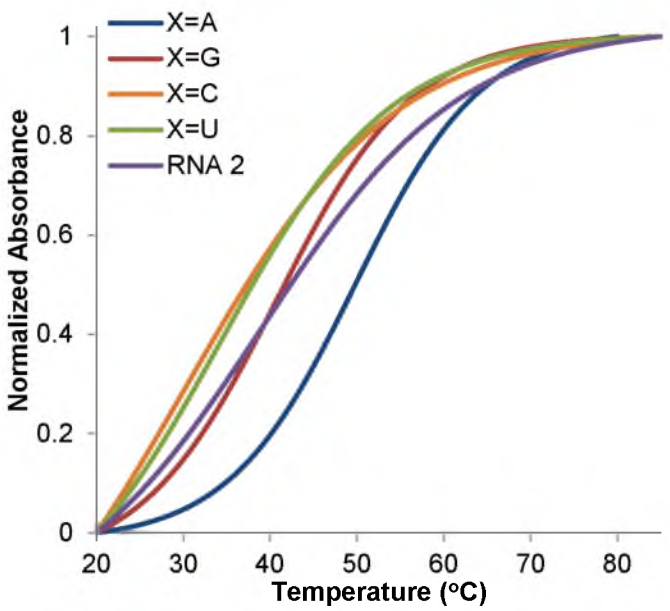

Figure B.5. Representative UV-melting curves of PNA **3neg**:RNA duplexes under simulated physiological salt conditions.

Table B.5. T_m data (°C) for PNA **3neg**:RNA duplexes under simulated physiological salt conditions.

Complement =	RNA **1** (X = A)	RNA **1** (X = G)	RNA **1** (X = C)	RNA **1** (X = U)	RNA **2**
Trial 1	51.5	41.7	30.5	34.4	39.0
Trial 2	49.7	40.4	31.2	34.4	40.4
Trial 3	48.5	39.0	29.2	33.1	37.7
Trial 4		39.0			39.0
Average	49.9 ± 1.5[11]	40.0 ± 1.3	30.3 ± 1.0	34.0 ± 0.8	39.0 ± 1.1

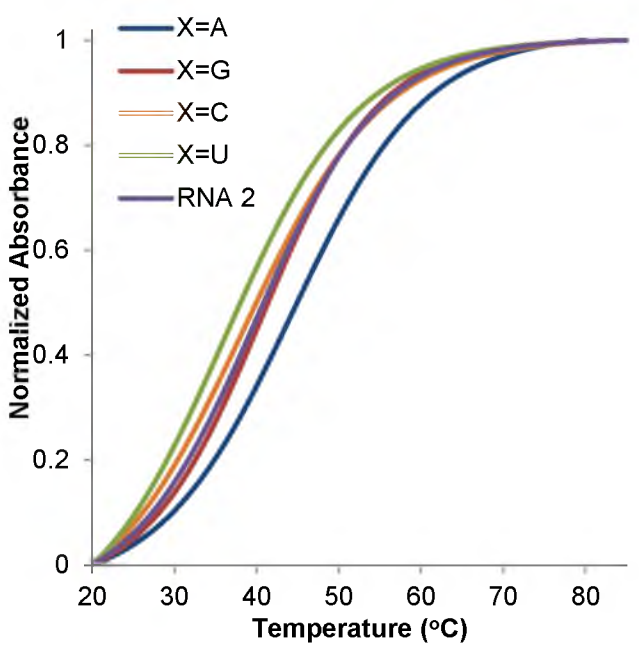

Figure B.6. Representative UV-melting curves of PNA **3pos**:RNA duplexes under simulated physiological salt conditions.

Table B.6. T_m data (°C) for PNA **3pos**:RNA duplexes under simulated physiological salt conditions.

Complement =	RNA **1** (X = A)	RNA **1** (X = G)	RNA **1** (X = C)	RNA **1** (X = U)	RNA **2**
Trial 1	48.2	42.3	39.0	38.4	40.4
Trial 2	46.3	40.4	37.7	36.4	39.0
Trial 3	45.0	39.7	38.4	36.4	39.7
Average	46.5 ± 1.7[11]	40.8 ± 1.3	38.4 ± 0.7	37.1 ± 1.2	39.7 ± 0.7

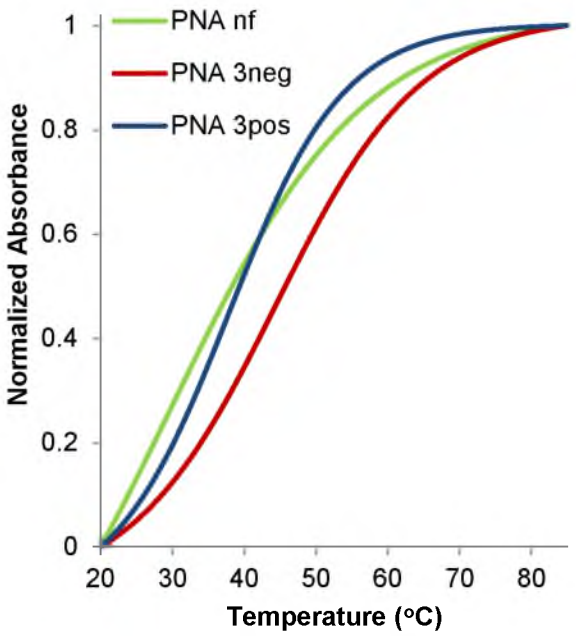

Figure B.7. Representative UV-melting curves of mismatched PNA:DNA **3** duplexes under simulated physiological salt conditions.

Table B.7. T_m data (°C) for mismatched PNA:DNA **3** duplexes under simulated physiological salt conditions.

Duplex =	PNA **nf**: DNA **3** (Y = C)	PNA **3neg**: DNA **3** (Y = C)	PNA **3pos**: DNA **3** (Y = C)
Trial 1	32.5	44.9	39.7
Trial 2	33.8	44.3	37.7
Trial 3	31.8	43.6	37.0
Average	32.7 ± 1.0	44.3 ± 0.7	38.1 ± 1.4

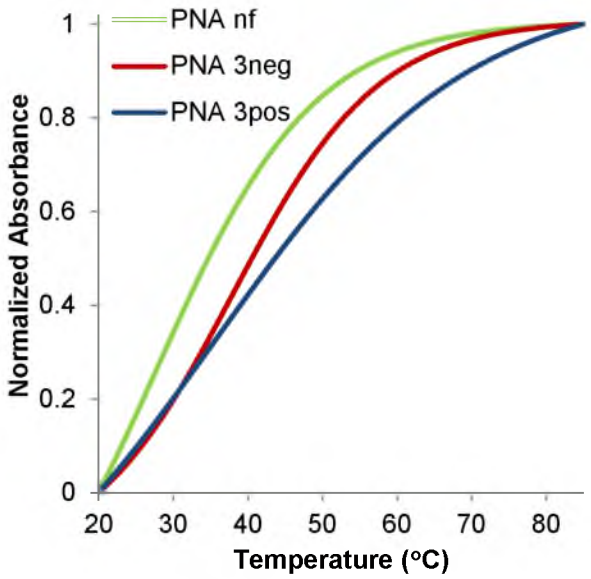

Figure B.8. Representative UV-melting curves of mismatched PNA:RNA **3** duplexes under simulated physiological salt conditions.

Table B.8. T_m data (°C) for mismatched PNA:RNA **3** duplexes under simulated physiological salt conditions.

Duplex =	PNA **nf**: RNA **3** (Y = C)	PNA **3neg**: RNA **3** (Y = C)	PNA **3pos**: RNA **3** (Y = C)
Trial 1	31.2	38.4	36.4
Trial 2	29.8	37.7	35.8
Trial 3	29.2	37.7	35.7
Average	30.1 ± 1.0	37.9 ± 0.4	36.0 ± 0.4

APPENDIX C

SPECTRAL DATA OF CHAPTER 4: ^{1}H AND ^{13}C NMR DATA

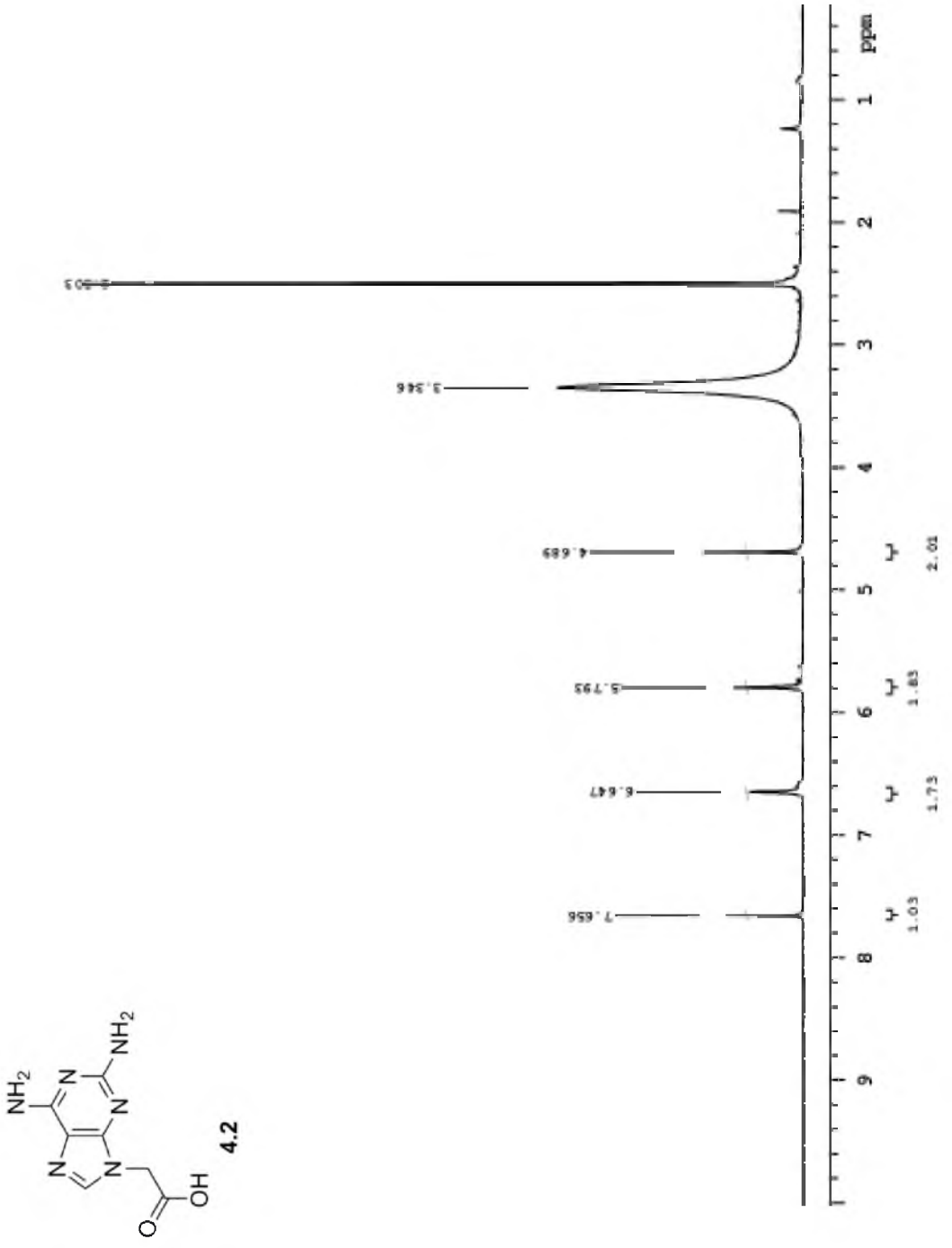
NH2
NH2
N
N
N
N
OH
O
4.2
7.656
6.647
5.795
4.689
3.566
ppm
1
2
3
4
5
6
7
8
9
1.03
1.73
1.83
2.01

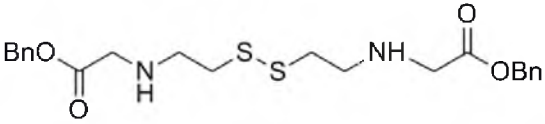

4.10

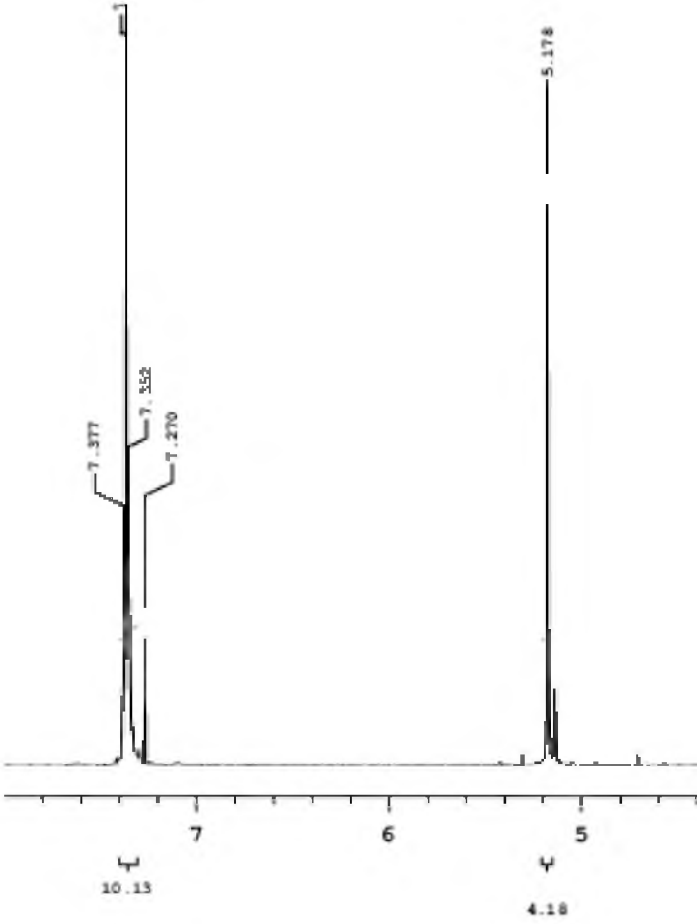

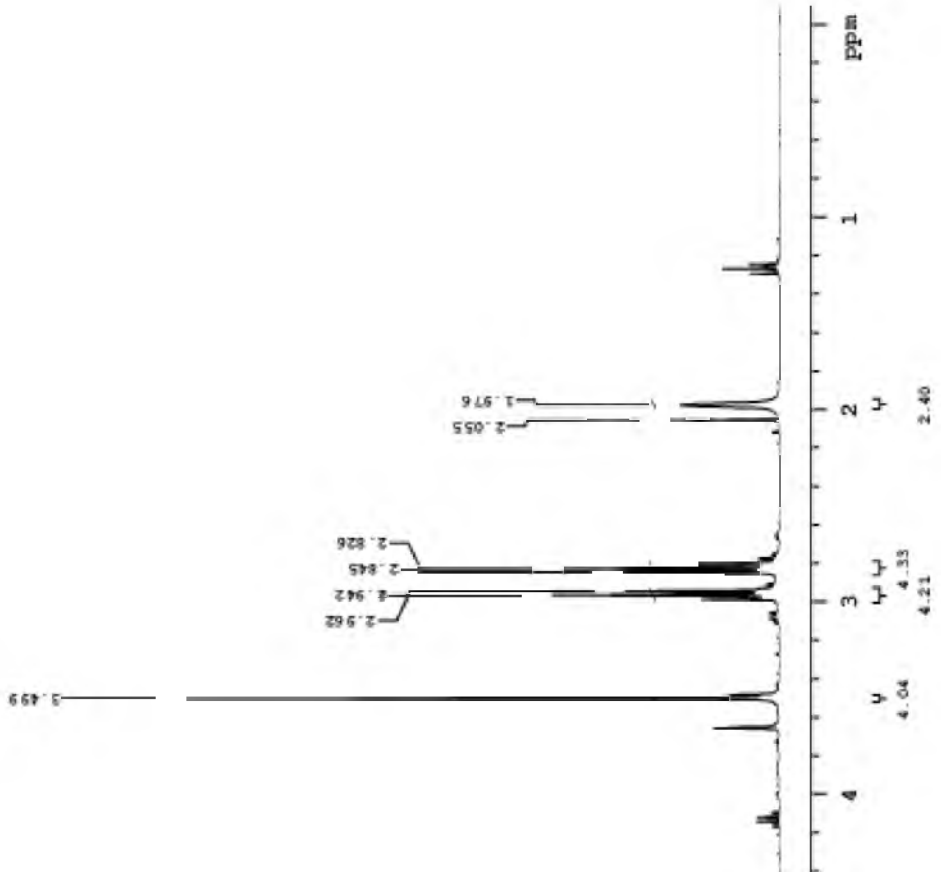
3.499
2.962
2.942
2.845
2.826
2.055
1.976
4.04
4.33
4.21
2.40
ppm

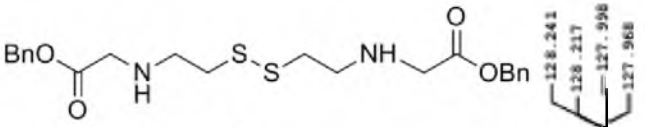
BnO
O
N
H
S
S
NH
O
OBn

4.10

128.241
128.217
127.998
127.968
171.694
171.664
135.380
180
160
140
120
100

66.097
66.042
50.234
50.204
47.533
47.423
38.670
38.615
80
60
40
20
ppm

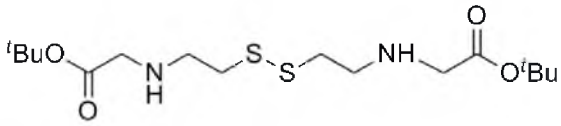

4.12

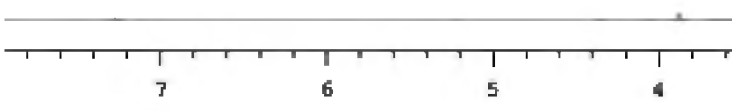

3.198
2.809
2.790
2.725
2.703
2.116
1.333
3
2
1
ppm
3.74
4.00
5.84
1.78
17.88

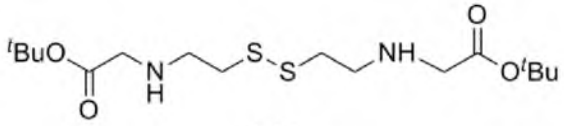

4.12

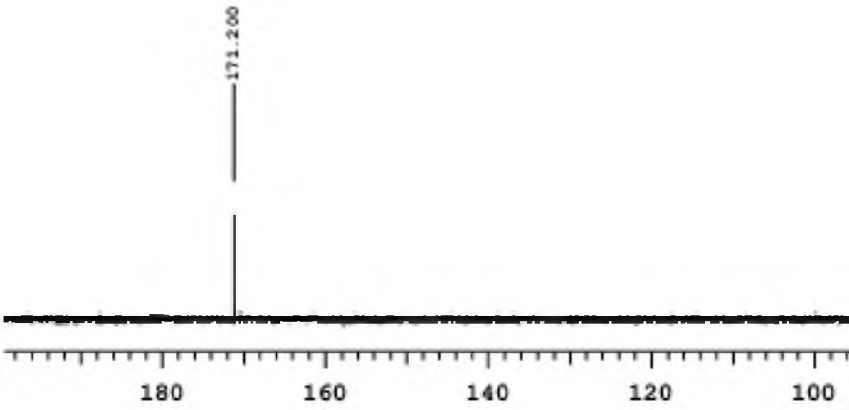

81.308
51.270
47.741
38.752
80
60
40
20
ppm

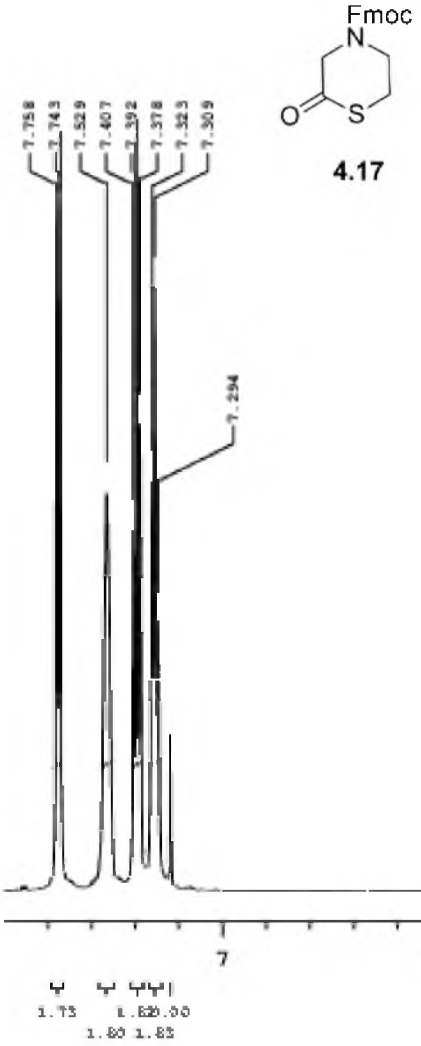
Fmoc
N
O
S
4.17
7.758
7.743
7.529
7.407
7.392
7.378
7.323
7.309
7.294
7
6
5
1.75
1.80
1.83
1.82
0.00

4.560
4.493
4.482
4.269
4.225
4.199
3.823
3.610
3.212
2.981
4
3
2
ppm
2.01
2.86
1.00
0.89
1.02
0.91

77.485
77.230
76.975
68.203
67.766
55.497
55.151
47.567
42.858
42.151
32.101
29.679
28.765
28.671
80
60
40
20
ppm

195.576
154.794
143.836
143.654
141.523
128.053
127.943
125.005
124.860
120.307
120.222
200
180
160
140
120
100

4.17

Fmoc
N
S
O

APPENDIX D

SPECTRAL DATA OF CHAPTER 5: ^{1}H AND ^{13}C NMR DATA

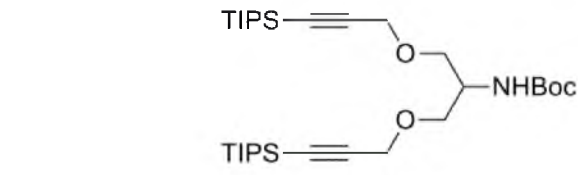

5.14

3.631
3.622
1.473
1.440
1.078
1.056
3
2
1
ppm
4.34
8.46
42.44

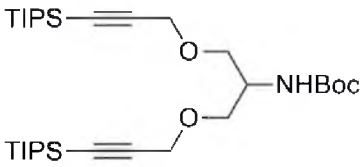

5.14

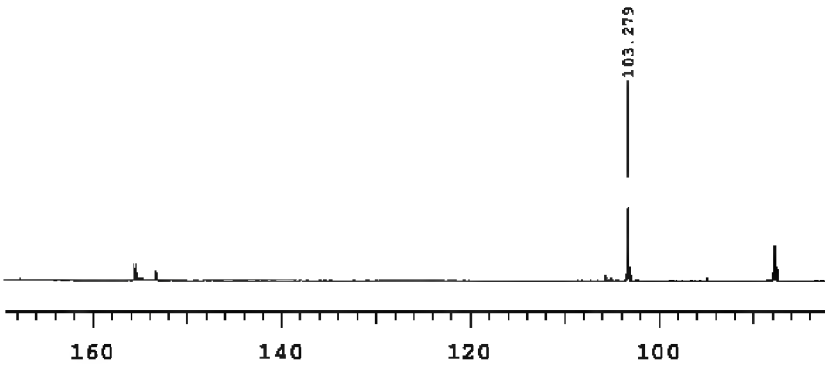

68.331
59.164
28.429
18.697
18.667
17.835
12.487
11.352
11.316
11.261
80
60
40
20
ppm

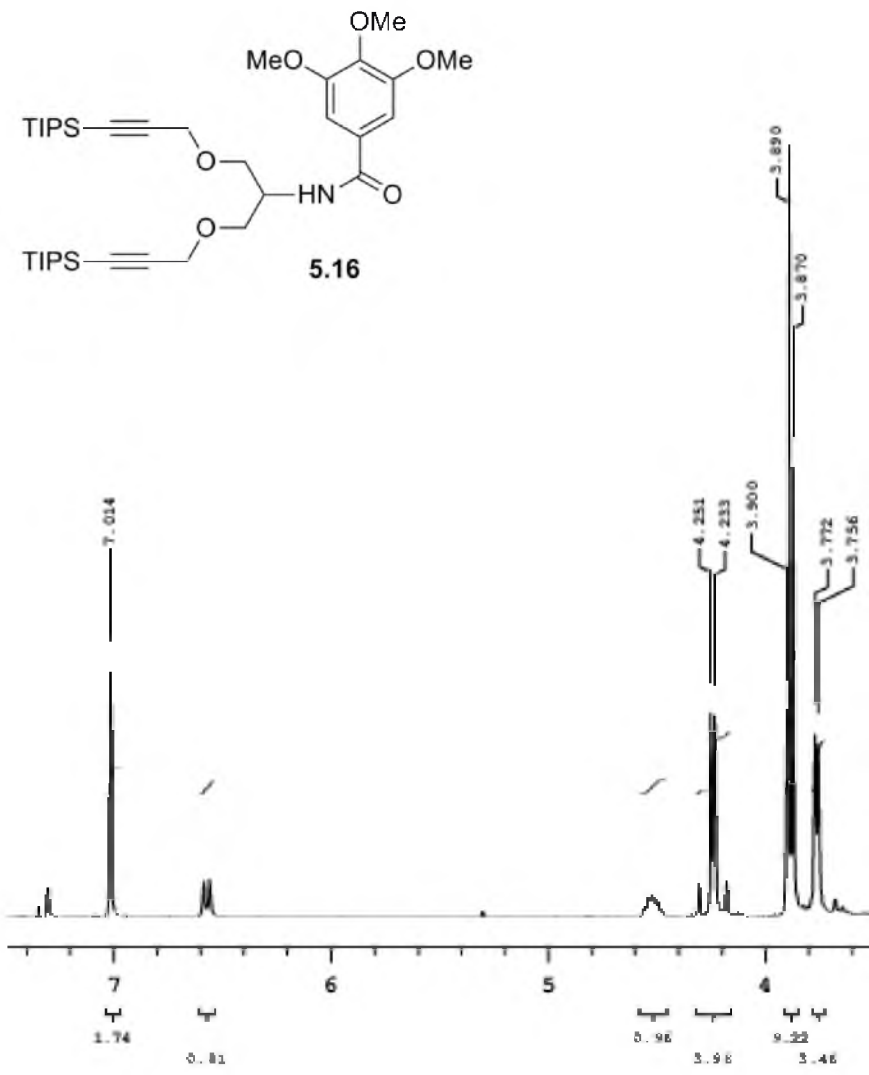
OMe
MeO
OMe
TIPS
O
HN
O
O
TIPS
5.16
7.014
4.251
4.233
3.900
3.890
3.870
3.772
3.756
7
6
5
4
1.74
0.81
0.98
3.98
9.22
3.46

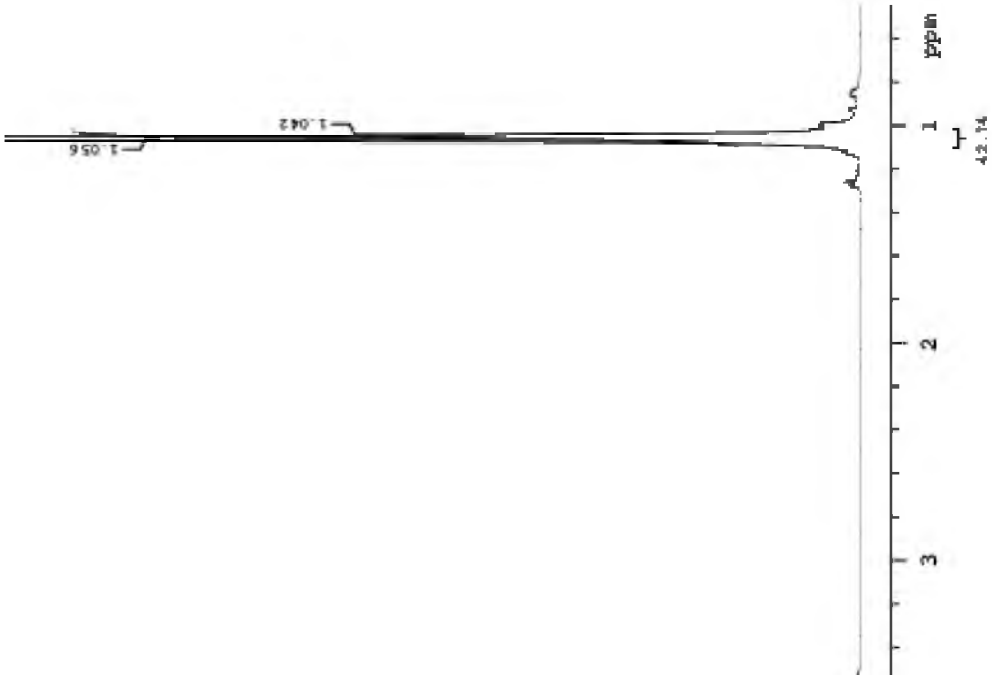
1.042
1.056
ppm
1
2
3
42.74

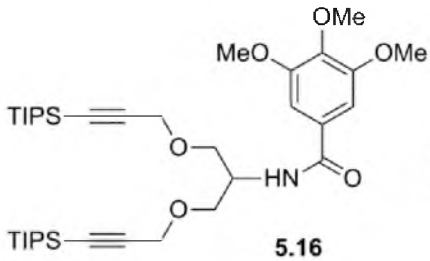
OMe
MeO
OMe
TIPS
O
HN
O
O
TIPS

5.16

166.684
153.105
139.950
104.551
102.983
180
160
140
120
100

87.918
68.110
60.799
59.131
56.269
48.676
80
60
40
20
ppm

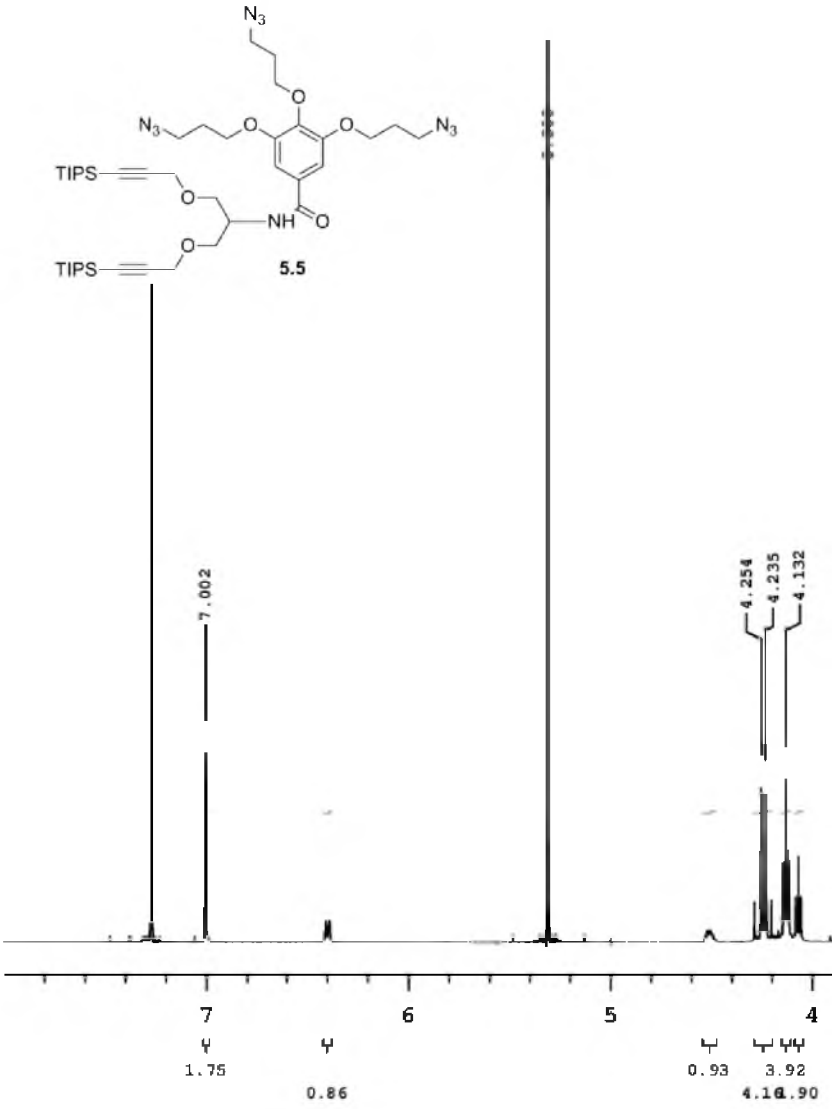
N3
O
N3
O
O
N3
TIPS
O
NH
O
O
TIPS
5.5
7.002
4.254
4.235
4.132
7
6
5
4
1.75
0.86
0.93
3.92
4.16
1.90

3.755
3.552
3.498
2.098
1.274
1.077
1.065
1.060
0.891
0.877
3
2
1
ppm
3.72
3.92
1.86
2.05
3.83
41.45

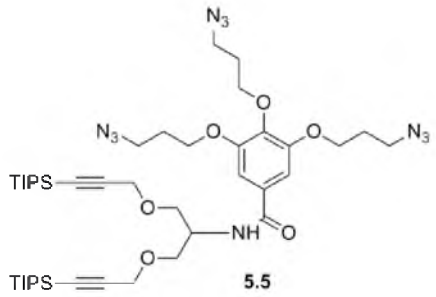
N3
N3
O
O
O
N3
TIPS
O
NH
O
O
TIPS

5.5

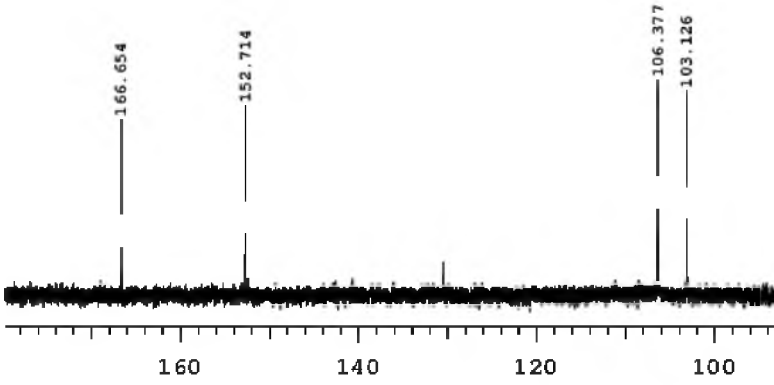
166.654
152.714
106.377
103.126
160
140
120
100

88.271
77.543
76.910
70.172
68.280
66.197
59.429
48.846
48.373
29.931
29.061
11.329
80
60
40
20
ppm